THE ROLE OF PTTG AND PBF IN GENOMIC INSTABILITY AND DNA REPAIR IN THYROID CANCER

By

Jim, Chi Wai Fong

A thesis presented to the College of Medical and Dental Sciences at the University of Birmingham for the Degree of Doctor of Philosophy

Centre for Endocrinology, Diabetes and Metabolism, School of Clinical and Experimental Medicine

March 2015

SUMMARY

Thyroid cancer, the most common endocrine malignancy has a rising incidence worldwide. Radiation damage is a known aetiological factor in thyroid tumourigenesis, particularly in children. Pituitary tumor transforming gene (PTTG) and its binding partner (PTTG binding factor; PBF) are overexpressed in thyroid cancers. Critically, PTTG and PBF have been shown to be independent markers of poor prognosis in thyroid cancer. Both PBF and PTTG have been shown to be tumourigenic in vivo. PTTG, a human securin, has multifunctional roles in mitotic control, DNA repair, apoptosis, cell transformation and genomic instability. PTTG null murine embryogenic fibroblasts demonstrate prolonged G2/M transition and aneuploidy. Overexpression of PTTG in MG63 osteosarcoma, H1299 lung cancer and HeLa cell lines induces aneuploidy. Additionally, PTTG binds and inhibits Ku70, a DNA repair protein involved in double-strand DNA breaks. PBF, which has independent tumourigenic and transforming actions, binds to PTTG, transports it to the nucleus and facilitates its actions within the nucleus. Taken together, the above implicate the functional role of PTTG and PBF in genetic instability.

This thesis describes the generation of a transgenic murine model of thyroid cancer which overexpressed both human PTTG and human PBF in the thyroid gland (BI-Trans). The BI-Trans murine model developed goitres from a young age in both genders. Additionally, they develop thyroid adenomas at a later age, which had a female preponderance. Unexpectedly, this BI-Trans murine model did not develop cancers. We measured the index of genetic instability (GI) in the thyroids of our transgenic murine models with fluorescent inter-simple sequence repeat-PCR (FISSR-PCR). This technique was refined to measure GI with small quantities of DNA obtained from murine thyroids. Additionally, we identified target gene for further evaluation through microarray analysis to elucidate the mechanism by which PBF and PTTG induced genetic instability.

DEDICATION

To my parents and sisters for your continual love and support.

And my research supervisor, Professor Christopher McCabe for your unwavering support, patience and kindness.

ACKNOWLEDGEMENTS

I would like to express my gratitude to Professor John Watkinson for initiating this research project and the Get Ahead charity for the priming grant, without whose support this work would not have been possible. A special thank you to Professors Christopher McCabe and Jayne Franklyn and Kristien Boelaert whose mentoring and support as research supervisors have made completing this thesis possible.

Dr. Martin Read has been a great source inspiration for the countless hours of intellectual discussion. Additionally, Drs. Martin Read, Vicki Smith and Rachel Watkins have been excellent teachers in the multitude of techniques used in experimental molecular biology.

Vital collaborations with Drs. Margaret Eggo, Martin Read, Gregory Lewy, Adrian Warfield and Andrea Bacon have made this line of investigation complete.

The company of Robert Seed, Neil Sharma, Gavin Ryan and Perkin Kwan has made my time in the laboratory both enjoyable and memorable.

Finally, the generous financial support of the Wellcome Trust has made this piece of research a reality.

ABBREVIATIONS

ATM	Ataxia telangiectasia mutated
ATR pathway	Ataxia telangiectasia and Rad3-related pathway
BI-Trans	Homozygote for both PBF and PTTG
qRT-PCR	Quantitative real-time polymerase chain reaction
BSA	Bovine serum albumin
CGH	Comparative Genomic Hybridization
DAPI	4',6-diamidino-2-phenylindole
DSB	Double strand break
DTC	Differentiated thyroid cancer
FGF-2	Fibroblast growth factor 2
FISH	Fluorescent in-situ hybridization
FISSR-PCR	Fluorescent inter-simple sequence repeat PCR
FTC	Follicular thyroid cancer
GI index	Genetic instability index
GI	Genetic instability
HBSS	Hank's Balanced Salt Solution

hPBF	Human PTTG binding factor
hPTTG	Human pituitary tumor transforming gene 1
IR-	No radiation treatment
IR +	Ionising radiation treatment
PBF	human PTTG binding factor
PBFHomo-PTTGHet	PBF homozygote – PTTG1 heterozygote
PBFHET-PTTGHET	PBF heterozygote – PTTG1 heterozygote
PBS	Phosphate buffered saline
PBF-Tg	Homozygote murine model of PBF expression in the thyroid
PCR	Polymerase chain reaction
PMTC	Primary murine thyroid culture
PTC	Papillary thyroid cancer
PTTG +/-	Heterozygote for PTTG1
PTTG +/+	Homozygote for PTTG1
PTTG	Human pituitary tumor transforming gene 1
Cdk	Cyclin dependent kinase
MPF	Maturation promoting factor

SDS	Sodium Dodecyl Sulfate
SSB	Single strand break
Trp53	*p53*
TSH	Thyroid stimulating hormone
MSI	Microsatellite instability
VEGF	Vascular endothelial growth factor

TABLE OF CONTENTS

TABLE OF FIGURES

1 General Introduction

1.1 THE THYROID GLAND

1.1.1 Anatomy and physiology

The thyroid gland, located in the neck is the largest endocrine organ. Embryologically, the thyroid gland originates in the foramen caecum at the junction of the anterior and posterior tongue and descends to its adult position by 7 weeks in the embryo (Kay and Goldsmith, 2010). The thyroid gland measures approximately 10 -30 g in an adult and increases in size during pregnancy (Dorion and Lemaire, 2008). Histologically, the thyroid gland consists of numerous follicles, each of which is comprised of thyroid epithelial cells surrounding a globule of colloid (Krause, 2005).

The main function of the thyroid gland is the production of thyroid hormone which is essential for energy metabolism, growth and maturation of tissue. The secretion of thyroid hormone from the thyroid gland is under the influence of thyroid stimulating hormone (TSH) which is produced in the anterior pituitary gland and secreted into the bloodstream. Circulating levels of TSH is in turn controlled by thyrotropin-releasing hormone (TRH) which is produced in the hypothalamus and transported via the superior hypophyseal artery to the anterior pituitary gland. The secretion of TRH and TSH is negatively regulated by high levels of circulating thyroid hormone (Yen, 2001). See Figure 1-1.

At a molecular level, TSH binds to the TSH receptor on the membrane of thyroid epithelial cells which leads to an increase in the stimulation of several thyroid genes including the sodium-iodide symporter (NIS), thyroglobulin and thyroid peroxidise which promote the biosynthesis of thyroid hormone (Yen, 2001).

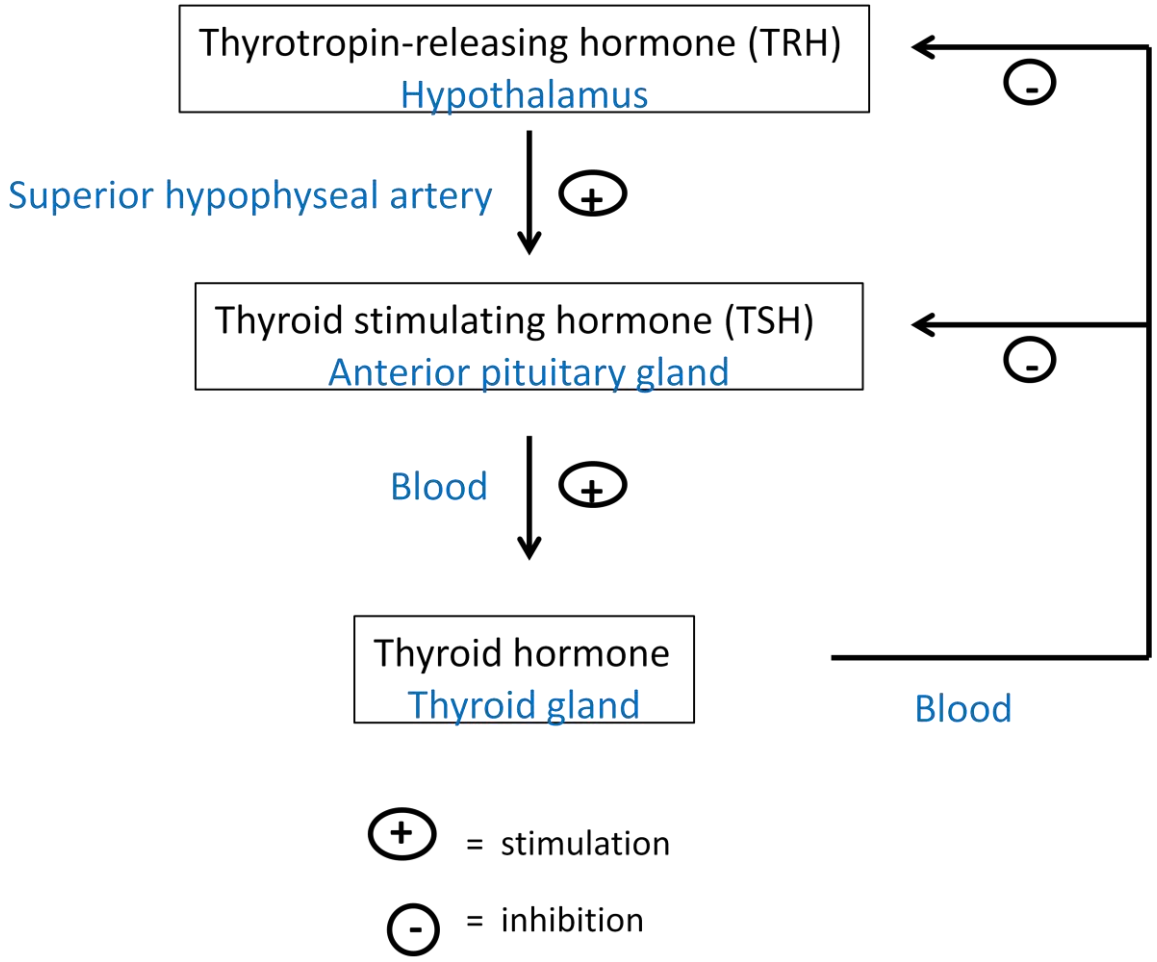

Figure 1-1 Negative feedback loop of thyroid hormone regulation.

1.1.2 **Thyroid hormone biosynthesis**

Iodine, an essential component of thyroid hormone biosynthesis, is concentrated from the bloodstream by the thyroid gland. The ability of thyroid epithelial cells to concentrate iodine lies within the sodium-iodide symporter (NIS) which sits on the basolateral membrane of the thyroid cell (Dohan et al., 2003). NIS is coupled to the Na-ATPase pump which generates the energy required to concentrate iodine against its natural gradient. At the apical part of the thyroid epithelial cell, the transporter pendrin drives iodine from the cytoplasm to the colloid. Iodine subsequently binds to the tyrosine residue of thyroglobulin, a protein found within the colloid, in a reaction catalysed by the enzyme

thyroid peroxidise (TPO). This reaction produces mono-iodothyrosine (MIT) or di-iodothyrosine (DIT). The combination of MIT with DIT results in the active triiodothyronine (T_3) whilst DIT with DIT results in thyroxine (T_4). See Figure 1.2. The products of the reaction catalysed by TPO, MIT, DIT, T_3 and T_4 are stored in the colloid of the thyroid follicle. During the secretion of thyroid hormone, MIT, DIT, T_3 and T_4 are internalised into the thyroid epithelial cell, undergoes proteolytic digestion to recapture MIT and DIT with the release of T_3 and T_4 into the bloodstream (Yen, 2001).

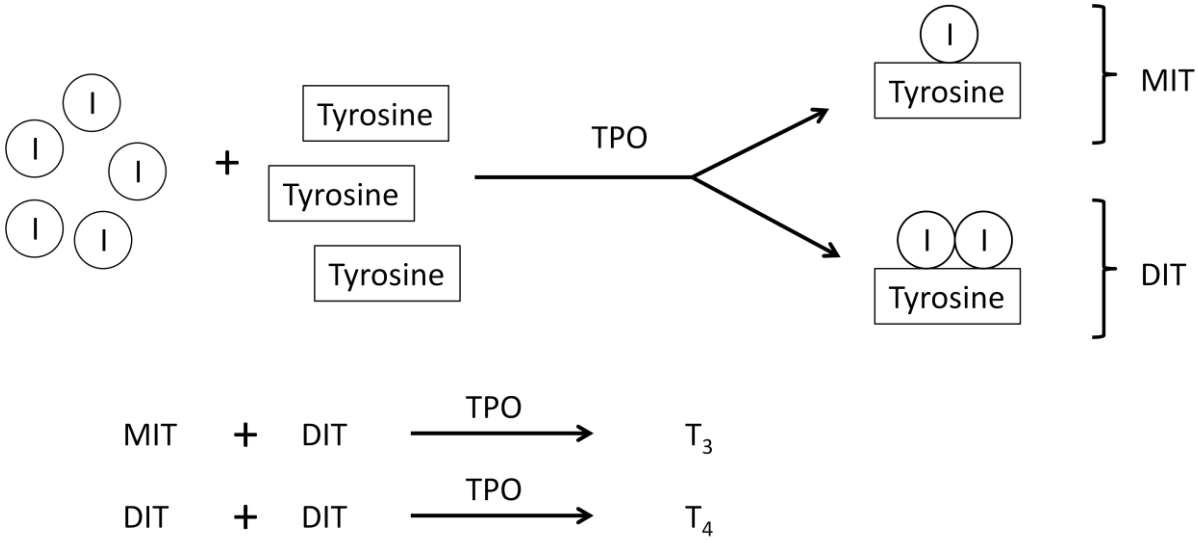

Figure 1-2 The reactions in thyroid hormone biosynthesis catalysed by thyroid peroxidise (TPO).

1.1.3 **Thyroid hormone at the end-organ**

Thyroid hormone in the bloodstream can exist in a free active state or bound to protein such as thyroxine binding globulin (TBG) or albumin. It is the free, unbound T_3 and T_4 that enters target cells and generates a biological response. Overall, the ratio of T_3 to T_4 in the bloodstream is approximately

1:20. The effect of T_3 is about four times more potent at the end-organ compared to T_4. End-organs convert T_4 to the more active T_3 by the enzyme iodothyronine deiodinase and is actively transported across the cell membrane by OATP 1C1, monocarboxylate transporter (MCT) 8 and MCT10 (Visser et al., 2011). T_3 has a short half-life of 2.5 days compared to the half-life of T_4 which is about 6.5 days.

1.2 THYROID CANCER

1.2.1 Classification

The vast majority of thyroid cancers are of the well-differentiated variety which comprises mainly papillary carcinoma (80 %) and follicular carcinoma (10 - 15 %). These well-differentiated tumour types arise from thyroid follicular cells. Poorly differentiated thyroid carcinomas such as anaplastic (ATC) tumours are rare (1 - 3 %) (Nagaiah et al., 2011) and are thought to arise de-novo or be a de-differentiation progression of well-differentiated thyroid carcinoma (Smallridge et al., 2009). Hurtle cell carcinoma, characterized by the presence of oncocytes rich in mitochondria, is considered a subtype of follicular carcinoma of the thyroid gland.

Medullary carcinoma (5%) of the thyroid, a completely separate aetiological entity, arises from the parafollicular C-cells of the thyroid gland. Parafollicular C-cells of the thyroid are involved in the secretion of calcitonin, a hormone related to calcium homeostasis. Calcitonin reduces calcium levels by reducing resorption of calcium in the kidneys, inhibiting the activity of osteoclasts, stimulating osteoblastic activity and inhibits calcium resorption in the intestines. Another type of thyroid cancer, primary lymhoma of the thyroid gland, is not common and is associated with Hashimoto's disease of the thyroid (Kato et al., 1985). The molecular mechanism by which primary lymphoma of the thyroid gland develops in Hashimoto's disease of the thyroid is not understood. Hashimoto's disease is an autoimmune condition causing chronic lymphocytic thyroiditis leading to an underactive thyroid gland. Patients with this condition may have high autoantibody titres to thyroid peroxidise, thyroglobulin or TSH receptor. For the purpose of this thesis, DTC refers to the common papillary and follicular carcinomas of the thyroid.

1.2.2 **Epidemiology**

Thyroid cancer has an incidence of 3.23 cases per 100,000 per year in the the UK. This incidence rate is increasing as shown in Figure 1-3 (Cancer Research UK, 2014). The increasing rate of thyroid cancer, documented over 30 years across 5 continents, showed an average increase of 67% in females and 48% in males (Peterson et al., 2012). This increase has been attributed in part to the early detection of small tumours ("incidentalomas") on neck scanning for other non-thyroid related conditions (Leenhardt et al., 2004, American Thyroid Association Guidelines Taskforce on Thyroid et al., 2009). The increasing trend in the detection of large advanced thyroid tumours (≥4cm; distant spread) does not suggest that the increasing rate of thyroid cancer is solely related to incidentolomas and suggests a true increase in the incidence of thyroid cancer (Chen et al., 2009, Sipos and Mazzaferri, 2010). The main type of thyroid cancer which is on the increase is papillary carcinoma followed by a small increase in follicular carcinoma (Reynolds et al., 2005, Smailyte et al., 2006, Mitchell et al., 2007).

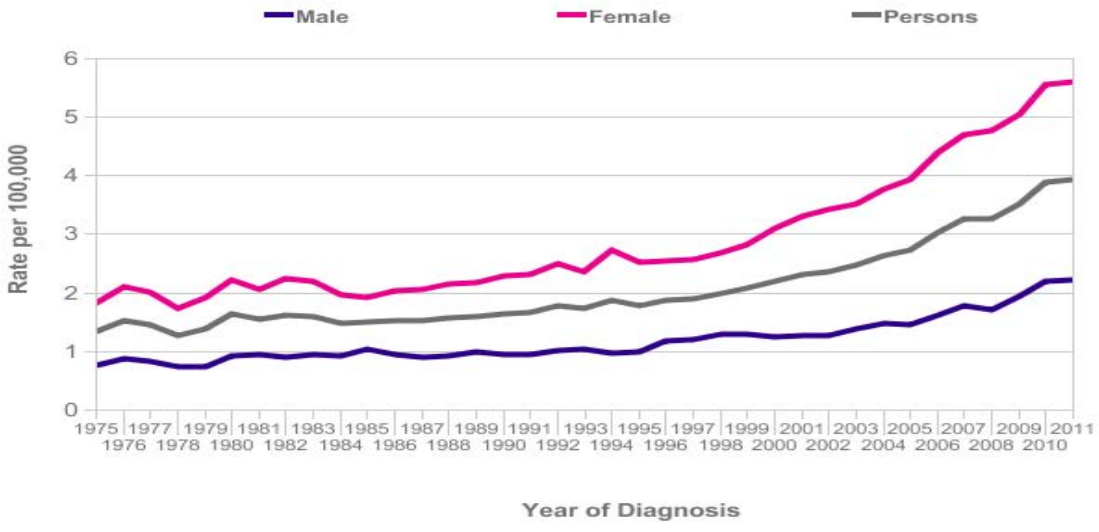

Figure 1-3 The rate of thyroid cancer detected in males and females by year in the UK (Cancer Research UK, 2014).

1.2.3 Risk factors for non-medullary thyroid cancer

1.2.3.1 Female gender

There is a predilection for females to develop thyroid cancer compared to males, seen in Figure 1-4. The ratio of thyroid cancer between male to female is approximately 1:2.5 (Cancer Research UK, 2014). The epidemiological data suggest a link between oestrogen and thyroid cancer. This has been supported by further molecular studies demonstrating the stimulatory effect of oestrogen on thyroid cell proliferation (Santin and Furlanetto, 2011). However, the mortality rates in males is significantly higher compared to females and is largely due to late diagnosis and more advanced disease at the time of initial diagnosis (Sipos and Mazzaferri, 2010).

1.2.3.2 Age

The detection of thyroid cancer peaks in the 4th decade for females and the 6th decade for males in the UK as shown in Figure 1-4 (Cancer Research UK, 2014). The sharp increase in the incidence of thyroid cancer in females from puberty to the end of the 4th decade closely mirrors the fertility period of a female and circulating oestrogen levels.

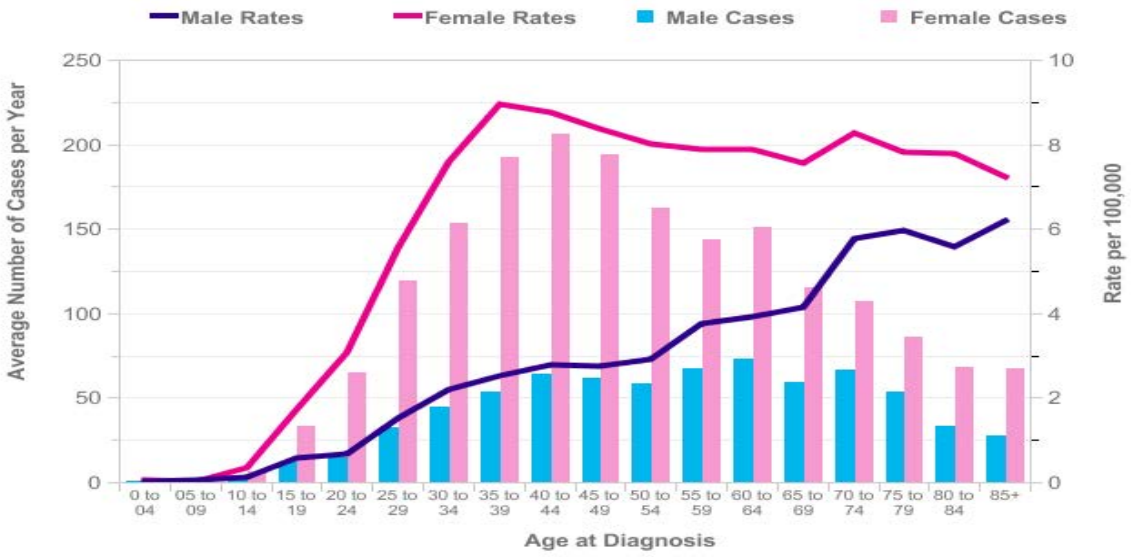

Figure 1-4 Number of cases of thyroid cancer diagnosed per year by age and gender.

1.2.3.3 **Ionising radiation**

Previous exposure to radiation is a well recognised risk factor for the pathogenesis of thyroid cancer. This association was reported in 1950 where 10 out of 28 children with thyroid cancer had received radiation to their thymus gland between the fourth and sixteenth months of life (Duffy and Fitzgerald, 1950). Kaplan et al recently described the historic account between thyroid cancer and medical radiation (Kaplan et al., 2009). The most convincing evidence for thyroid cancer and radiation came following the 1945 nuclear explosion in Hiroshima and Nagasaki. The long term report from the atomic bomb survivors described the risk of thyroid cancer being greatest before the age of 20 years. The magnitude of excess risk decreased with increasing age or time since exposure. The majority of thyroid cancers from the cohort were mainly papillary carcinomas (Furukawa et al., 2013).

The Chernobyl nuclear fallout in 1986 exposed a large population in Russia, Ukraine and Belarus to radiation. It has been estimated that individuals most exposed, including recovery workers, each averaged an effective dose equivalent to 50 years of typical background radiation. This led to a sharp

increase in well differentiated thyroid carcinoma (Stsjazhko et al., 1995). Post-Chernobyl thyroid cancers were characterised by a predominance of papillary carcinomas (93 – 98 %). Aggressive tumour histological characteristics, lymphatic invasion, intrathyroid infiltration and multifocality, were described to be dose-dependent (Zablotska et al., 2015). Known and novel gene rearrangements are thought to be the oncogenic drive for radiation-induced thyroid cancer (Ricarte-Filho et al., 2013). Also, early thyroid cancers that are radiation induced are more likely to have gene rearrangements compared to thyroid tumours that occur after a long latency (9 – 12 years) (Nikiforov, 2006).

1.2.3.4 **Family history of thyroid cancer**

The cumulative lifetime risk of developing non-medullary thyroid cancer in females and males is 3 fold and 1.5 fold respectively compared to the normal population if they had a first-degree relative with thyroid cancer (Fallah et al., 2013).

1.2.3.5 **Other proposed risk factors**

A higher thyroid stimulating hormone (TSH) level, even within the normal range, is associated with thyroid cancer (Boelaert et al., 2006, Haymart et al., 2008, Jonklaas et al., 2008, Polyzos et al., 2008, Boelaert, 2009, Haymart et al., 2009). The thyroid hormone receptor is dependent on transcription factors that regulate apoptosis, cell proliferation and differentiation (Cheng, 2000). The receptor, consisting of four binding components (TRα1, TRα2, TRβ1 and TRβ2) is encoded by two genes, THRA (chromosome 3) and THRB (chromosome 17). Mutation of TRβ1, the PV mutation, results in the inability of the receptor to bind the thyroid hormone T3, causing thyroid hormone resistance syndrome in humans (Kamiya et al., 2003, Kaneshige et al., 2000, Suzuki et al., 2003). The transgenic murine model harbouring this mutation, known as the TRbeta$^{PV/PV}$ mouse, has high levels of thyroid

stimulating hormone and develop follicular thyroid carcinoma (Suzuki et al., 2002) . This murine model supports the observation that TSH has a role in thyroid tumourigenesis.

The association between iodine intake and thyroid cancer in humans is unclear (Blomberg et al., 2012). However, populations with comparative higher iodine intake have a higher proportion of papillary compared to follicular carcinomas of the thyroid. Conversely, there is a higher incidence of follicular carcinoma in populations with low iodine intake (Lind et al., 1998, Feldt-Rasmussen, 2001).

Weight and obesity have been explored by numerous groups as a risk factor for thyroid cancer. Systematic reviews did not however prove definitive causation (Peterson et al., 2012, Zhao et al., 2012).

Female reproductive factors such as pregnancy, number of children, use of prescription hormones, menstrual cycle patterns and menopause were not associated with thyroid cancer in a systematic review (Peterson et al., 2012).

1.2.3.6 **Association with other hereditary disorders**

Gardner syndrome, a subtype of familial adenomatous polyposis (FAP), is associated with a high risk of colon cancer and papillary thyroid cancer. Both conditions are caused by defects in the APC gene and is autosomal dominant. Cowden disease, associated with hamartomas, have an increased risk of thyroid, uterine and breast cancer. This syndrome is commonly caused by defects in the PTEN gene. The Carney complex (Type 1) caused by defects in the PRKAR1A gene have an increased risk of papillary and follicular thyroid cancers. Familial non-medullary thyroid carcinoma, with suspect defective genes on chromosome 19 and 1 is associated with well-differentiated thyroid cancer. Thus, in rare instances, thyroid cancer is associated with other hereditary disorders.

1.2.4 **Management of non-medullary thyroid cancer**

1.2.4.1 **Investigations**

The most common presentation of thyroid cancer to a thyroid specialist is the presence of a lump in the thyroid. The investigations for the assessment of the neck lump include neck ultrasonography (USS) and fine needle aspiration cytology (FNAC). Features suggestive of cancer on ultrasonography include microcalcification, taller rather than wide shape, irregular margins and absence of elasticity of the thyroid lump (Remonti et al., 2015). FNAC is now commonly performed under ultrasound guidance to accurately sample the area in question. The FNAC result is reported using the 5 main categories of the "Thy" classification as shown in Table 1 below. Thyroid cytology reporting can be subjective and thus the decision for further management is dependent on the overall estimated risk of cancer by the clinician based on thyroid USS, FNAC and clinical history. Patient choice is also taken into consideration when the decision is made as to whether further management include repeat USS and FNAC or diagnostic surgery. Presently, studies are underway using biomarkers to improve the diagnostic accuracy of FNAC to aid the clinician's decision-making process.

DIAGNOSTIC CATEGORY	RISK OF MALIGNANCY (%)
Non-diagnostic for cytological diagnosis Thy 1 / Thy 1c	0 - 10
Benign Thy 2	0 - 3
Neoplasm possible / Atypia Thy 3a	5 - 15
Neoplasm possible / Follicular neoplasm Thy 3f	15 - 30
Suspicious for malignancy Thy 4	60 - 75
Malignant Thy 5	97 - 100

Table 1 The Thy classification of thyroid cytology and the associated risk of malignancy (reproduced from the Royal Society of Pathologists, 2009).

1.2.4.2 **Staging**

Differentiated thyroid cancer is staged according to the Tumour, Node and Metastasis (TNM) classification shown in Table 2 below.

STAGE	DESCRIPTION
Tx	Primary tumour cannot be assessed
T0	No evidence of primary tumour
T1a	Tumour ≤ 1 cm in greatest dimension, limited to the thyroid
T1b	Tumour > 1 cm and ≤ 2 cm in greatest dimension, limited to the thyroid
T2	Tumour > 2 cm and ≤ 4 cm in greatest dimension, limited to the thyroid
T3	Tumour > 4 cm in greatest dimension, limited to the thyroid **or** any tumour with minimal extrathyroid extension
T4a	Tumour of any size extending beyond the thyroid capsule **and** invades any of the following: subcutaneous soft tissues, larynx, trachea, oesophagus, recurrent laryngeal nerve
T4b	Tumour invades prevertebral fascia, mediastinal vessels, or encases the carotid artery
Nx	Regional nodes cannot be assessed
N0	No regional lymph node metastases
N1	Regional lymph node metastasis
N1a	Metastasis in Level VI (pretracheal and paratracheal, including prelaryngeal and Delphian lymph nodes)
N1b	Metastasis in other unilateral, bilateral or contralateral cervical or upper/superior mediastinal lymph nodes
cM0	Clinically no distant metastasis
cM1	Distant metastasis clinically

Table 2 TNM staging for differentiated thyroid cancer (reproduced from AJCC Cancer Staging Manual, 7th edition.

1.2.4.3 **Treatment**

The most widely offered treatment options for differentiated thyroid cancer include surgery, radioiodine and TSH suppression with thyroxine. External beam radiotherapy and chemotherapy treatment modalities have largely been reserved for the palliation of thyroid cancer (Perros et al., 2014). The chemotherapy drug Paclitaxel has been used in the treatment of undifferentiated anaplastic thyroid carcinoma (Gomez Saez et al., 2015). Futhermore, targeted therapy with the use of tyrosine kinase inhibitors such as vemurafenib, selumetinib, dabrafenib, sorafenib, sunitinib, pazopanib, cabozantinib, motesanib, axitinib and vandetanib are currently being evaluated for use in patients with advanced or recurrent thyroid cancer refractory to conventional treatments (Ferrari et al., 2015).

1.2.5 **Prognosis of differentiated thyroid cancer**

The prognosis of well managed well differentiated thyroid cancer is excellent, with the majority of patients diagnosed at an early stage of the disease and having a 5 year survival rate in excess of 95 % (Cancer Research UK 2014). Interestingly, mortality rates from thyroid cancer have remained largely unchanged despite the improved detection (Chen et al., 2009).

The worst prognosis arises from anaplastic thyroid tumours. The mortality from anaplastic thyroid tumours contributes 14 – 50 % of the overall mortality rates of thyroid cancer despite being 1- 2 % of all thyroid cancers. The median survival of anaplastic tumours is between 3 to 5 months (Nagaiah et al., 2011).

1.2.6 **Molecular genetics**

The main oncogenic pathways investigated and implicated in the aetiology of differentiated thyroid cancer are the mitogen-activated protein kinase (MAPK) and phosphatidylinositide 3-kinase/Akt pathways (PI3K/Akt) which are frequently dysregulated in thyroid cancer. The MAPK and PI3K

pathways have upstream common points such as Ras and tyrosine kinase receptor (RTK) illustrated in Figure 1-5 below.

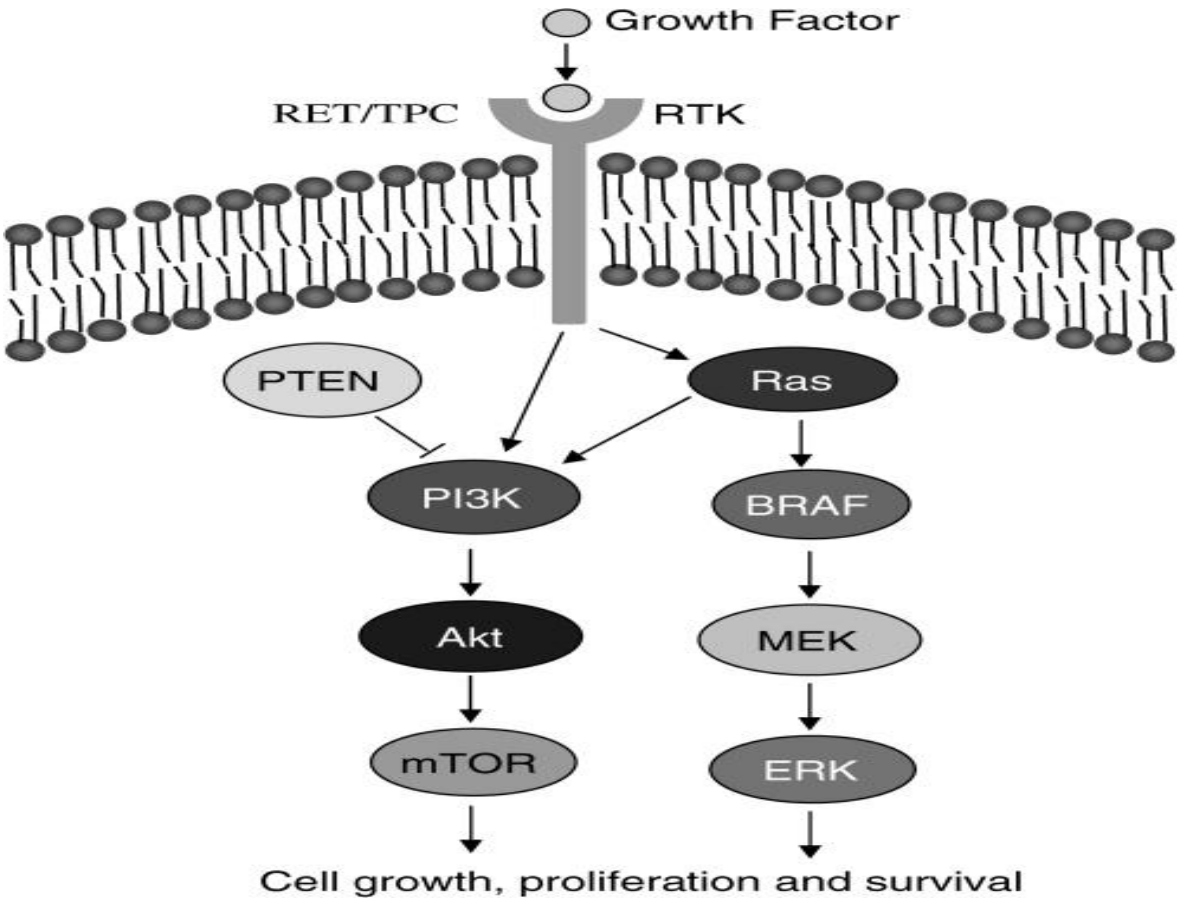

Figure 1-5 Schematic diagram of the upstream interaction between PI3K/Akt and MAPK pathway in thyroid cancer, reproduced from (Xing, 2010). The PI3K/Akt pathway is illustrated on the left and the MAPK pathway on the right. The common points of interaction include the tyrosine kinase receptor (RTK) and Ras. PTEN inhibits the PI3K/Akt signalling pathway.

The most common form of differentiated thyroid cancer, papillary thyroid cancer, is postulated to be largely attributed to dysfunctional MAPK signalling. The PI3K/Akt pathway appears to be mainly involved in the formation of follicular thyroid cancers and adenomas. However, both pathways can act

synergistically in the transformation or dedifferentiation of papillary carcinoma to anaplastic carcinoma, as shown in Figure 1-6 (Xing, 2010).

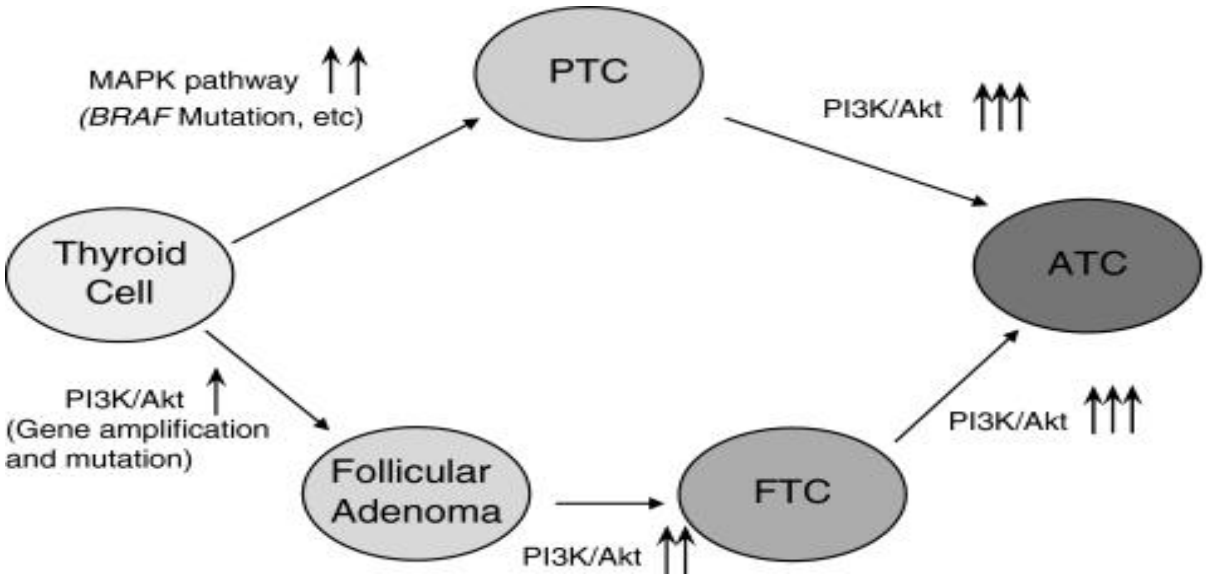

Figure 1-6 The hypothesized pathways involved in the pathophysiology of PTC (papillary thyroid cancer), FTC (follicular thyroid cancer) and ATC (anaplastic thyroid cancer). Reproduced from (Xing, 2010).

The molecular profile of oncogenes causing differentiated thyroid cancer has implications in tumour classification as well as prognosis. For example, currently classified papillary thyroid cancers driven by $BRAF^{V600E}$ or RAS oncogenes have different appearances on histology and response to mitogen-activated protein kinase (MEK) inhibitors (Cancer Genome Atlas Research, 2014, Ho et al., 2013). In PTC, the most frequently encountered gene aberrations include point mutations of BRAF and Ras, and the RET/PTC rearrangement (discussed individually in subsequent sections). The profile of abnormal genes found in FTC is different, with the PAX8/PPARγ featuring in 30 % of follicular carcinomas but not being apparent in papillary thyroid carcinoma (Bhaijee and Nikiforov, 2011). The constituent

mutation proportions found in follicular thyroid cancer is shown in Figure 1-7 and papillary thyroid cancer, Figure 1-8.

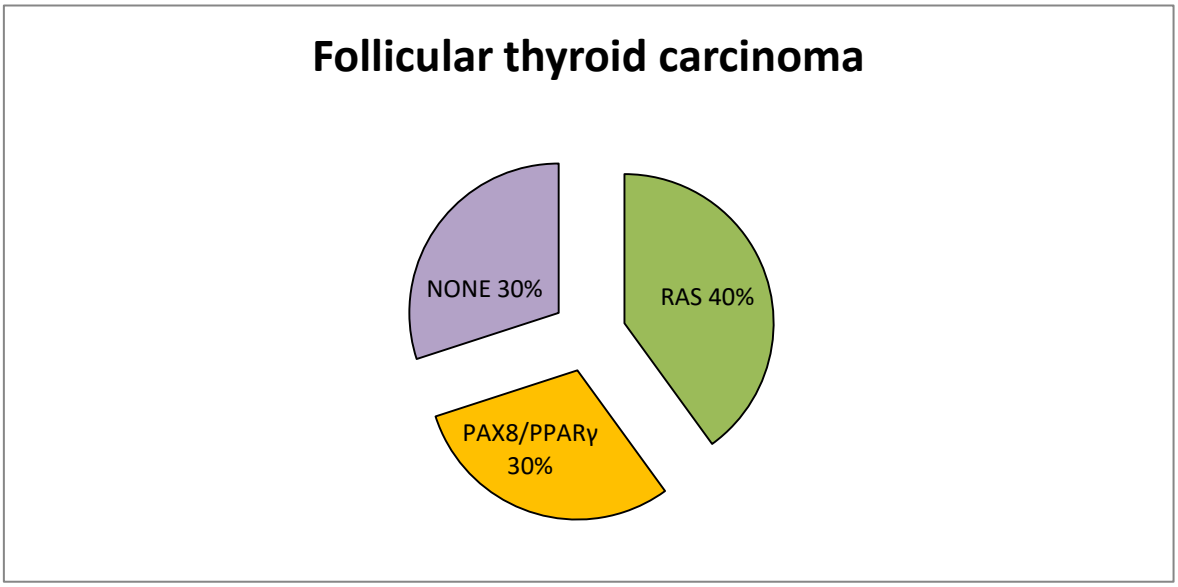

Figure 1-7 Profile of abnormal genes found in follicular thyroid cancer, reproduced from (Bhaijee and Nikiforov, 2011).

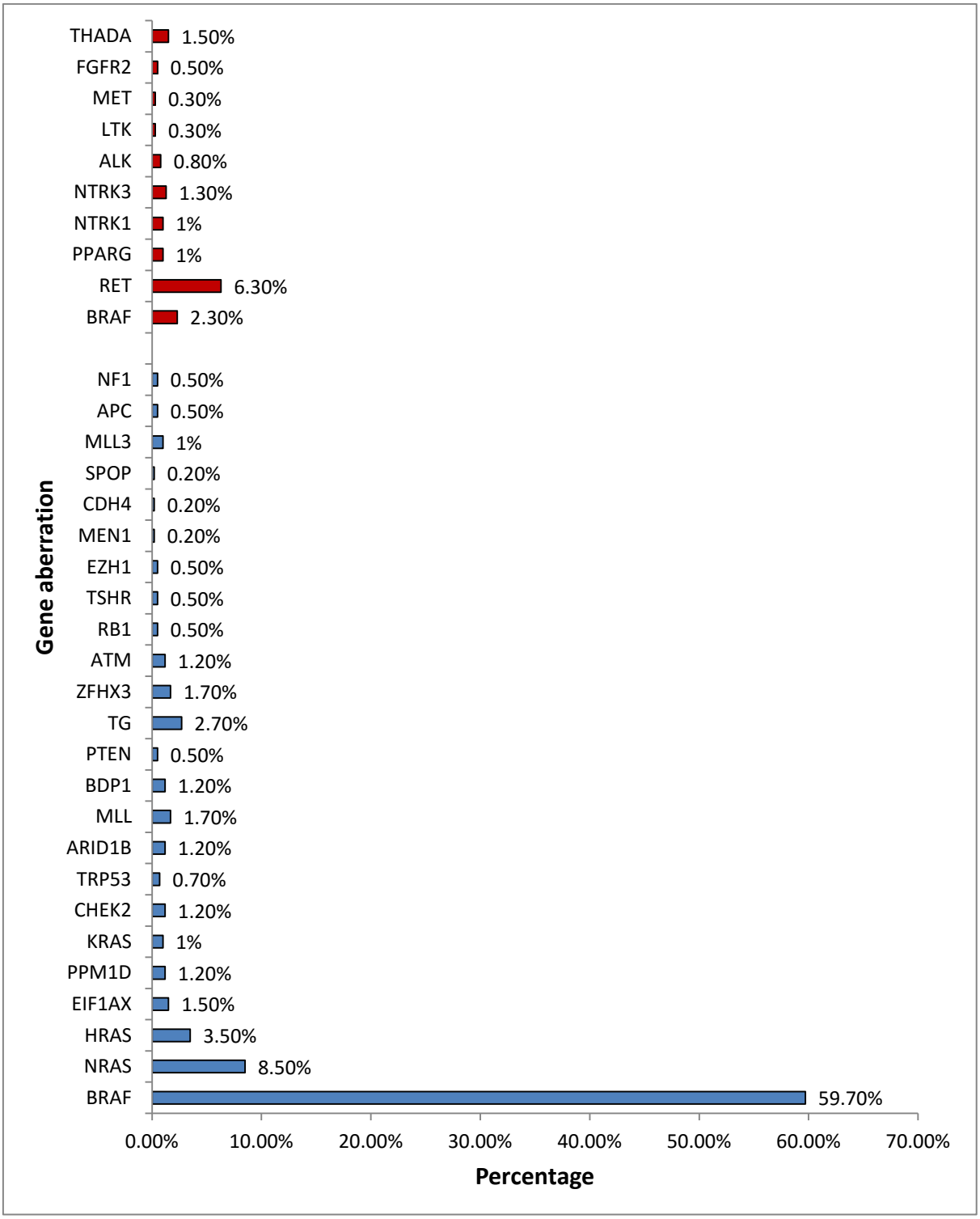

Figure 1-8 Profile of abnormal genes found in papillary thyroid carcinoma adapted from (Cancer Genome Atlas Research, 2014). The bar charts in red denote fusions and in blue, mutations.

1.2.6.1 **Mitogen-activated Protein Kinase Pathway**

The mitogen-activated protein kinase (MAPK) pathway regulates cellular functions of proliferation, differentiation, migration, growth and apoptosis. MAPKs are highly conserved proteins which belong to the serine/threonine family of protein kinases. Conventional MAPK signalling follows a three-tiered kinase cascade of MAPKKK → MAPKK → MAPK. MAPKKK is activated via small GTPases, belonging to the Ras/Rho family. MAPKKK phosphorylates and activates MAPKK which in turn phosphorylates and activates MAPK. Phosphorylated MAPK exerts its effect directly on the nucleus which translates to cellular action(s) (Figure 1-9). Dysregulation of this pathway is critical in the development and progression of thyroid cancer. (Pearson et al., 2001, Dhillon et al., 2007).

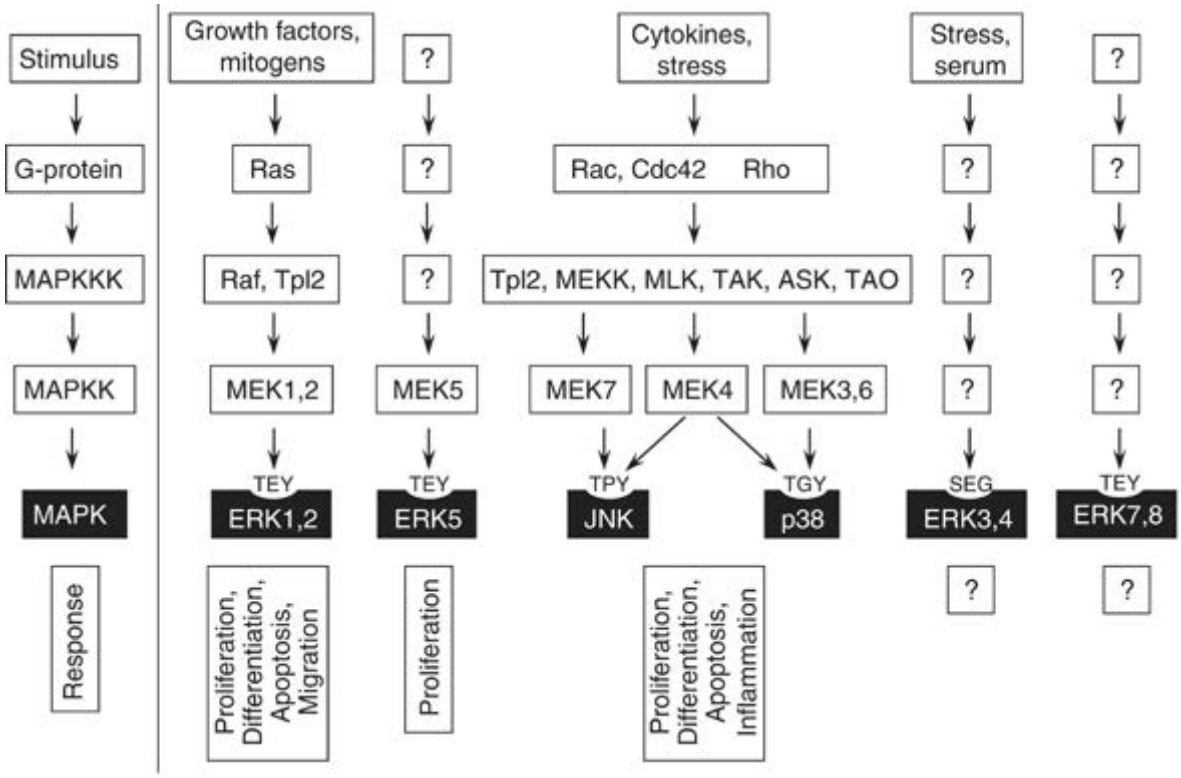

Figure 1-9 Schematic overview of MAPK signalling pathway shown on the extreme left. Various known gene interactions are illustrated to the right of the line. Reproduced from (Dhillon et al., 2007).

1.2.6.2 **Phosphatidylinositide 3-kinase/Akt Pathway**

The lipid kinase phosphoinositide 3-kinase/Akt (PI3K/Akt) pathway is involved in cell growth and metabolism. The central gene Akt is activated by the PI3K complex which in itself interacts with the upstream tyrosine kinase receptor. Activated Akt phosphorylates several downstream targets which lead to cellular actions such as apoptosis, proliferation, DNA repair, growth and survival (Monsalves et al., 2014, Vivanco and Sawyers, 2002). Figure 1-10 describes the PI3K/Akt pathway. Dysregulation of this pathway has been implicated in the development of follicular adenomas and thyroid carcinoma as described above in section 1.2.6.

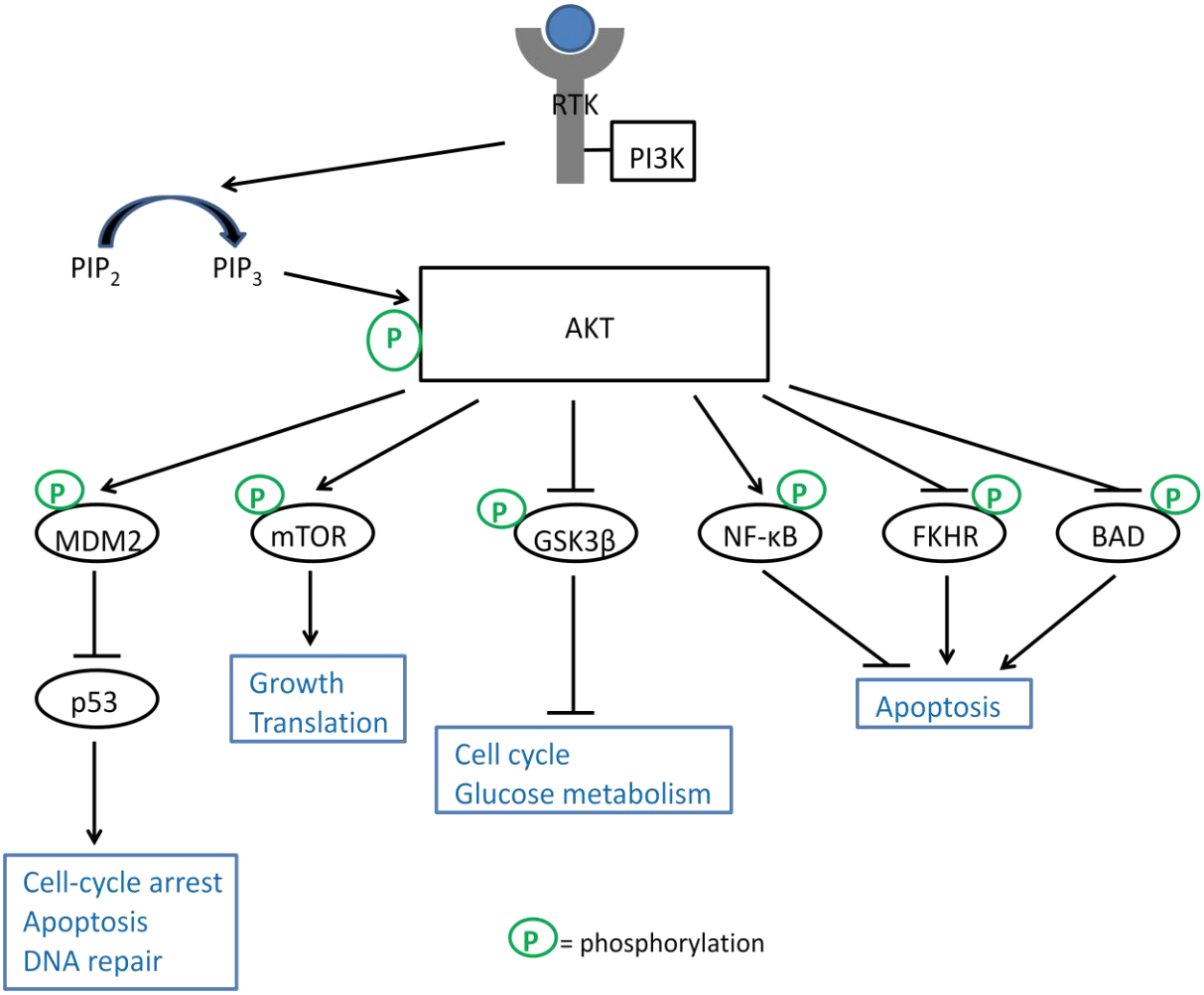

Figure 1-10 PI3K/AKT signalling pathway adapted from (Vivanco and Sawyers, 2002). Activation of class IA phosphatidylinositol 3-kinases (PI3Ks) occurs through stimulation of receptor tyrosine kinases (RTKs) and the concomitant assembly of receptor–PI3K complexes. These complexes localise at the membrane where receptor-PI3K catalyses the conversion of PtdIns(4,5)P_2 (PIP_2) to PtdIns(3,4,5)P_3 (PIP_3). PIP_3 serves as a second messenger that helps activate AKT. Through phosphorylation, activated AKT mediates the activation and inhibition of several targets (GSK3β, glycogen synthase kinase-3β; NF-κB, nuclear factor of κB; MDM2; mTOR; FKHR; BAD) resulting in cellular growth, survival and proliferation through various mechanisms.

1.2.6.3 Point mutations of genes involved in differentiated thyroid cancer

1.2.6.3.1 BRAF

The RAF family of protein kinases is encoded by the BRAF gene and has 3 isoforms; ARAF, BRAF and CRAF. Although all three isoforms play a role in the RAS-RAF cascade, the main activator of the MAPK pathway is BRAF. The most prevalent thyroid oncogene found in papillary thyroid carcinoma, BRAF, is activated by the V600E substitution ($BRAF^{V600E}$) (Krause, 2005). In this mutation the valine (V) amino acid is replaced by glutamic acid (E) at codon 600 and this gene remains active, independent of upstream cues (Davies et al., 2002). Consequently there is excessive downstream signalling of the MAPK pathway, resulting in tumour formation (Hilger et al., 2002, Peyssonnaux and Eychene, 2001).

Papillary thyroid carcinomas with the BRAF V600E mutation are more aggressive tumours as demonstrated by extrathyroidal invasion, lymph node metastases and advanced tumour stage at initial surgery (Xing et al., 2005, Lee et al., 2007). In a multicentre study involving 16 centres and 2099 patients, the hazards ratio of developing recurrence in $BRAF^{V600E}$ positive compared to $BRAF^{V600E}$ negative thyroid cancers is 1.82, after adjusting for clinicopathologic factors (Xing et al., 2015).

Murine models of $BRAF^{V600E}$ thyroid knock-in develop goitres and invasive papillary thyroid carcinoma which later transition to poorly differentiated carcinoma (Knauf et al., 2005). Thyroid cancer initiation via the oncogene $BRAF^{V600E}$ is dependent on TSH signalling (Franco et al., 2011).

1.2.6.3.2 Ras

The Ras gene encodes for 3 isoforms of the protein; H-, K- and N-Ras. The Ras gene belongs to a family of GTP binding proteins that are located in the plasma membrane and has a central role in the transduction of signals from tyrosine kinase and G-protein-coupled receptors to effector genes in the

MAPK and PI3K/Atk pathways (Dhillon et al., 2007, Xing, 2010). Ras possesses intrinsic GTPase activity and in normal cells is mostly in an inactive GDP-bound state. In point mutations of Ras, the gene is active by either having an increased affinity for GTP or has losing its intrinsic GTPase activity (Howell et al., 2013). Consequently, the MAPK or the PI3K/Atk pathways are aberrantly activated, resulting in tumourigenesis.

Mutation of the Ras gene is interesting because it is found in both papillary and follicular thyroid cancers. This probably reflects the ability of mutated Ras to activate both MAPK and PI3K/Akt signalling pathways. Numerous Ras point mutations have been identified but the most common Ras point mutation in follicular neoplasms of the thyroid involves N-Ras at codon 61 (Vasko et al., 2003, Liu et al., 2004).

Ras mutations are also found in follicular adenomas of the thyroid in up to 48 % of cases. This observation suggests that Ras mutations may not be a key oncogene in the malignant transformation of thyroid cells to cancer and that additional mutation or epigenetic insult is required for tumourigenesis.

1.2.6.4 **Tyrosine kinase receptor rearrangements**

1.2.6.4.1 RET/PTC rearrangement

The RET proto-oncogene, implicated in 15 % of papillary thyroid carcinomas, is located on the long arm of chromosome 10 (10q11.2) and encodes a tyrosine kinase receptor (Bhaijee and Nikiforov, 2011, Ishizaka et al., 1989). The RET receptor has extracellular, transmembrane and intracellular domains (Ishizaka et al., 1989, Takahashi et al., 1993). Whilst RET is essential in the development of the urogenital and nervous system, its expression is at very low levels in normal thyroid tissue and is not required in the development of the thyroid gland (Pachnis et al., 1993, Schuchardt et al., 1994, Takaya et al., 1996).

The specific type of RET mutation dictates the phenotype. For example, point mutations in the RET gene produce medullary thyroid cancer, a tumour arising from the parafollicular c-cells of the thyroid. Medullary thyroid cancers with the methionine to threonine substitution at position 918 of the RET gene are most aggressive and the RET mutation with the replacement of serine by alanine at position 891 produces disease less likely to metastasise (Arighi et al., 2005).

Papillary thyroid cancers are associated with the RET/PTC translocation. To date, 13 different oncogenic RET/PTC fusions have been identified. In RET-associated differentiated thyroid cancer, RET/PTC1 accounts for 60 %, RET/PTC3 for 30 % and RET/PTC2 10 % of cases. The other RET/PTC translocations are very rare in papillary carcinoma of the thyroid (Prescott and Zeiger, 2015). In support of the oncogenic nature of RET/PTC fusions, thyroid-specific expression of RET/PTC1 and of RET/PTC3 in transgenic mice results in the development of papillary thyroid cancer (Jhiang et al., 1996, Powell et al., 1998). However, not all RET/PTC fusions result in papillary thyroid carcinoma. RET/PTC fusions are also expressed in benign thyroid adenomas and Hashimotos thyroiditis (Ishizaka et al., 1991, Rhoden et al., 2006).

Thyroid cancers arising from radiation exposure in children in the Chernobyl disaster have a high prevalence of RET/PTC rearrangements which results in the activation of RET kinase, causing papillary carcinomas of the thyroid (Bounacer et al., 1997, Nikiforov et al., 1997, Fugazzola et al., 1995, Mizuno et al., 2000). The gene loci of RET and PTC lie in close proximity to one another within the thyroid nucleus during interphase and are predisposed to recombination after DNA damage from ionising radiation (Nikiforova et al., 2000, Roccato et al., 2005). The finding that 20 % of papillary thyroid carcinomas have the RET/PTC rearrangement in the general non-irradiated population and up to 72 % of papillary thyroid cancers post Chernobyl harboured the RET/PTC fusion suggested that exposure to radiation increases the risk of RET/PTC rearrangement (Unger et al., 2004). The exact molecular pathway from activation of the RET tyrosine kinase receptor to papillary carcinoma tumourigenesis is yet to be fully defined.

1.2.6.4.2 PAX8/PPARγ rearrangement

The PAX8 gene belongs to a family of genes that encode for transcription factors, crucial in the development of the thyroid gland and the production of thyroid hormone. The peroxisome proliferator-activated receptor gamma (PPARγ) encodes for a Type 2 nuclear receptor. Translocational rearrangement of these genes occur between chromosomes 2 and 3 (Wang et al., 2007). The PAX8/PPARγ fusion results in an increased expression of the chimeric protein which inhibits the tumour suppressor activity of PPAR and deregulates PAX8 function (Kroll et al., 2000, Tallini, 2002, Gregory Powell et al., 2004).

The PAX8/PPARγ rearrangement is found in 30 to 35 % of follicular thyroid carcinomas (French et al., 2003, Nikiforova et al., 2003). 2 – 13 % of follicular adenomas and 1 – 5 % of follicular variant of papillary carcinomas have this rearrangement (Marques et al., 2002, Nikiforova et al., 2002, Dwight et al., 2003). Follicular carcinomas with the PAX8/PPARγ translocation affect younger patients, are smaller in size and more likely to exhibit vascular invasion (French et al., 2003, Nikiforova et al., 2003). The detection of the PAX8/PPARγ fusion in fine needle aspiration cytology for distinguishing between benign and malignant follicular lesions has not been particularly helpful (Ferraz et al., 2012, Pauzar et al., 2012).

1.2.6.4.3 TRK rearrangement

The neurotrophic tyrosine kinase receptor Type 1 (NTRK1) gene encodes a protein that is found on the cell surface and has a role in activating other genes or itself through phosphorylation. NTRK1 is located on the long arm of chromosome 1 (1q21 – q22).

Rearrangement of the NTRK1 gene with various activating genes such as TPM3, TPR and TFG in the thyroid results in constitutive activation of tyrosine kinase activity leading to the transformation of thyroid cells. The NTRK1 rearrangements, also known as TRK, commonly found in papillary thyroid cancers are TRK (NTRK1/TPM3 fusion) (Wilton et al., 1995), TRK-T1, TRK-T2 (both

NTRK1/different portions of TPR gene fusion) (Greco et al., 1992, Miranda et al., 1994, Greco et al., 1997) and TRK-T3 (NTRK1/TFG fusion) (Greco et al., 1995). The frequency of TRK rearrangements in papillary thyroid cancers is approximately 3 % (Cancer Genome Atlas Research, 2014). The frequency of TRK rearrangements in papillary thyroid carcinoma in patients previously exposed to radiation was the same as patients who were not exposed to ionising radiation (Rabes et al., 2000). The prognostic significance of the TRK rearrangement in papillary thyroid carcinomas remains unclear, with the numbers involved in various studies being small (Bongarzone et al., 1998, Brzezianska et al., 2006, Musholt et al., 2000). Transgenic murine models expressing TRK-T1 in the thyroid gland develop follicular hyperplasia and papillary carcinoma from 7 months onwards. This provides in vivo evidence that TRK-T1 supports oncogenesis in the thyroid gland. This oncogenic effect on thyroid cells is likely to be downstream in nature because of the incomplete penetrance observed within the cohort with an abnormal phenotype (Russell et al., 2000).

1.2.7 Other genes involved in thyroid cancer

1.2.7.1 Trp53

The Trp53 gene, guardian of the genome, regulates multiple vital cellular functions such as growth, proliferation, apoptosis, cell cycle progression and DNA repair. Mutated Trp53, and hence dysfunctional Trp53, is found in a variety of human cancers. In the Li-Fraumeni syndrome where there is a germline autosomal dominant mutation of Trp53, patients are at high risk of developing sarcomas, breast cancer, glioblastomas, adrenocortical carcinoma and haematopoietic malignancies at a young age (Li et al., 1988, Malkin et al., 1990).

Trp53 mutations are uncommon in differentiated thyroid cancer but found in as many as 83 % of undifferentiated thyroid carcinoma. It is thought that p53 initiates the progression of well

differentiated thyroid cancer to anaplastic cancer (Ito et al., 1992, Dobashi et al., 1993, Donghi et al., 1993, Fagin et al., 1993, Dobashi et al., 1994). Murine models of papillary thyroid cancer, overexpressing RET/PTC1 in the thyroid gland, developed anaplastic tumours of the thyroid gland when crossed with Trp53 null mice suggesting that the lack of functional Trp53 promotes dedifferentiation of papillary thyroid cancer (La Perle et al., 2000).

1.2.7.2 **PTEN**

PTEN is a tumour suppressor that preferentially dephosphorylates phosphoinositide substrates and negatively regulates the PI3K/Akt pathway. In human germline mutations of PTEN, also known as Cowden disease, there is an increased risk of thyroid cancer. In a study of 146 patients with Cowden disease, 74 different mutations were observed. Approximately 70 % of patients with Cowden disease have benign lesions of the thyroid and 17 % develop thyroid cancer. The thyroid cancers observed were papillary carcinomas (59 %), follicular carcinomas (27.5 %), hybrid between follicular and papillary carcinoma (4.5 %), medullary carcinoma (4.5 %) and oxyphil cell tumour (4.5 %) (Bubien et al., 2013).

The loss of PTEN alone in the thyroid gland in murine models induces goitre and follicular adenomas in the presence of normal TSH levels. None of the models developed thyroid cancer by the age of 11 months, strongly suggesting that the persistent activation of the PI3K/Akt pathway alone is not sufficient for malignant transformation within the thyroid gland (Yeager et al., 2007).

1.2.7.3 **Mutations to the thyroid hormone receptor**

The murine model harbouring the PV mutation which results in an abnormality of the TRβ1 component of the thyroid hormone receptor develop follicular thyroid carcinoma with vascular invasion and metastases (Suzuki et al., 2002).

Interestingly, two further novel genes have been discovered to be associated with human thyroid cancer. Both Pituitary Tumor Transforming Gene (PTTG) and PTTG binding factor (PBF) are dysregulated in thyroid cancer (Boelaert et al., 2003, Heaney et al., 2001, Saez et al., 2006, Hsueh et al., 2013, Stratford et al., 2005). The next section describes these two genes, PTTG and PBF, in further detail.

1.3 PITUITARY TUMOR TRANSFORMING GENE (PTTG)

1.3.1 Identification

Pituitary tumor transforming gene (PTTG) was first identified and found to be exclusively highly expressed in rat pituitary tumour cells but not in normal pituitary cells. Subsequently, it was shown that PTTG had transforming abilities where overexpression of PTTG in murine 3T3 fibroblasts injected in athymic nude mice resulted in tumourigenesis (Pei and Melmed, 1997). Human PTTG shares 89 % sequence homology with rat PTTG and lies on chromosome 5q33 (Zhang et al., 1999). Although two further PTTG homologues have been identified (PTTG2 on chromosome 4p12 (Kakar and Jennes, 1999, Prezant et al., 1999) and PTTG3 on chromosome 8q13 (Chen et al., 2000)), PTTG (PTTG1) is most widely expressed in tumours. Hence, it is the most extensively studied and for the purpose of this thesis, PTTG refers to PTTG1.

1.3.2 Structure and function of PTTG

PTTG, shown schematically in Figure 1-11, has an open reading frame containing 609 bp which encodes for 203 amino acids (Zhang et al., 1999). The structure of PTTG can be divided to the basic N-terminal regulatory domain and acidic C-terminal functional domain (Dominguez et al., 1998, Kakar and Jennes, 1999, Zhang et al., 1999).

The regulatory N-terminal domain contain the KEN box (amino acid 9 to 11) and destruction box (amino acid 61 to 68) which are targets for the anaphase promoting complex (APC). APC functions by binding to PTTG, resulting in the degradation of PTTG and consequently allowing the progression from metaphase to anaphase during mitosis. (Zou et al., 1999, Zur and Brandeis, 2001).

PTTG has transcriptional abilities as shown by the presence of a DNA binding domain, from amino acid 61 to 118, and a transactivation domain further downstream, from amino acids 119 to 164 within its structure (Zhang et al., 1999, Pei, 2000, Wang and Melmed, 2000). Although the subcellular

localisation of PTTG, either cytoplasmic or nuclear, is dependent on cell type (Mu et al., 2003), in order for this gene to be functional, it needs to be within the nucleus (Zou et al., 1999). Interestingly, PTTG does not contain a nuclear localisation signal sequence, essential for the ability of a gene to cross the nuclear membrane. This led to the discovery of PTTG binding factor (PBF) which binds to PTTG and translocate it to the nucleus (Chien and Pei, 2000).

The transactivational and transforming capabilities of PTTG is attributed to the proline-rich region in the C-terminal (amino acids 163 to 173). This region contains the highly conserved and putative Src-homology-3 (SH3) interacting domain (Zhang et al., 1999). The only reported phosphorylation site of PTTG, thought to play a role during mitosis, lies at serine residue 165 within the SH3 interacting domain (Pei, 2000, Ramos-Morales et al., 2000, Boelaert et al., 2004).

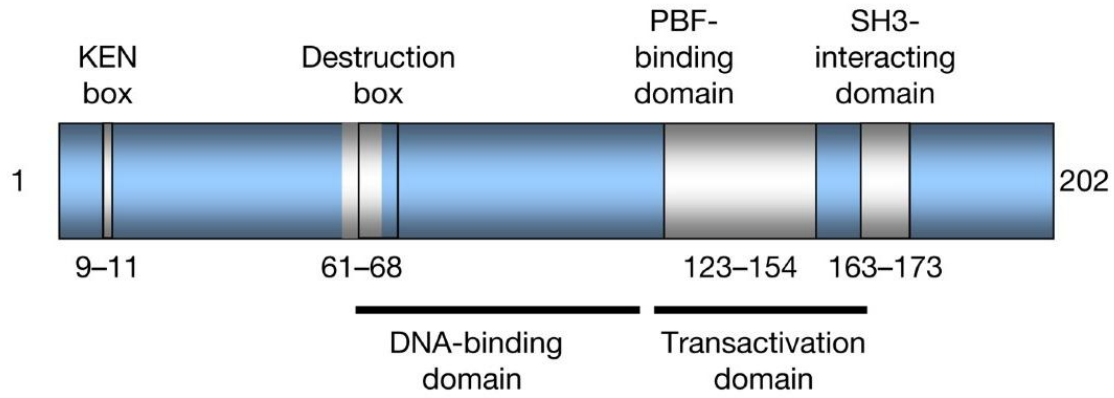

Figure 1-11 Schematic representation of human PTTG protein reproduced from (Smith et al., 2010). The regulatory N-terminal contains the KEN and destruction boxes. The SH3 interacting domain and phosphorylation site lies within the functional C-terminus.

1.3.3 **Regulation of PTTG expression**

The first regulator of PTTG to be identified was the hormone oestrogen. Oestrogen was found to upregulate PTTG expression in pituitary lactotroph tumours in rats (Heaney et al., 1999). Thyroid

stimulating hormone was also found to induce PTTG expression (Heaney et al., 2001). Insulin has been demonstrated to upregulate PTTG expresssion but the effect of insulin differed between malignant and non-malignant astrocytes suggesting that the response of PTTG to insulin is variable depending on tissue type (Chamaon et al., 2005, Thompson and Kakar, 2005).

The basal levels of PTTG transcription is regulated by the transcription factor SP1 (Clem et al., 2003). Oct-1 expression activates the PTTG promoter and increases the expression of PTTG (Zhou et al., 2008). β-catenin was found to increase PTTG expression in oesophageal cancers (Zhou et al., 2005) and colorectal cancers (Hlubek et al., 2006). γ-catenin which exists in conjunction with β-catenin has been shown to increase the transcription of PTTG (Pan et al., 2007). The binding of NF-Y to Trp53 is thought to inhibit the transcription of PTTG (Zhou et al., 2003).

The relationship between PTTG expression and growth factors has been extensively studied. The epidermal growth factor (EGF) receptor, itself regulated by EGF and transforming growth factor alpha (TGF-α), has been demonstrated to upregulate PTTG expression. The promalignant hepatocyte growth factor (HGF) increases the expression of PTTG via the c-Met membrane receptor in astrocytic cells (Tfelt-Hansen et al., 2004). Insulin-like growth factor (IGF-1) has also been shown to enhance transcription of PTTG (Chamaon et al., 2005, Thompson and Kakar, 2005). The relationship between the induction of PTTG by fibroblast growth factor-2 (FGF-2) is well established (Chamaon et al., 2010, Heaney et al., 1999, Tsai et al., 2005).

A small number of studies have investigated the epigenetic mechanisms involved in the control of PTTG expression since no mutations of PTTG and its promoter sequence were found in pituitary neoplasms (Zhang et al., 1999, Kanakis et al., 2003). The overexpression of histone acetyltransferase (HAT) p300, a transcription co-activator, increased PTTG promoter activity, ultimately resulting in increased PTTG mRNA and protein. It was also found that increased PTTG promoter activity with p300 was mediated by NF-YA and NF-YB. (Li et al., 2009).

1.3.4 **Subcellular localisation of PTTG**

The expression of PTTG is cell cycle dependent and increases from low in S-phase, higher in G2-phase and peaks at M-phase in HeLa cells (Zou et al., 1999, Ramos-Morales et al., 2000, Yu et al., 2000b). PTTG was largely localised to the nucleus during interphase, with small amounts in the cytoplasm in JEG-3 cells overexpressing PTTG (Yu et al., 2000b). In contrast, earlier studies have indicated that PTTG was located primarily in the cytoplasm with only partial nuclear expression in Jurkat T lymphoma cells, pituitary adenomas, lung and breast adenocarcinomas (Dominguez et al., 1998, Saez et al., 1999). It is possible that the difference in localisation of PTTG is cell-specific. The function of PTTG requires its presence in the nucleus but it has no nuclear localisation signal within its structure. It is thought that PTTG being a small protein of low molecular weight, has the ability to diffuse freely across the nuclear membrane. Alternatively, PTTG requires a transport protein to facilitate its entry into the nucleus and the discovery of PTTG binding factor (PBF) has supported this hypothesis (Chien and Pei, 2000).

One study observed PTTG expression in the Golgi apparatus and vesicles. Analysis of the culture medium detected the presence of PTTG. It was thus suggested that PTTG is a secretory protein that may have an autocrine and/or paracrine function in murine pituitary tumour cells and human pituitary adenomas (Minematsu et al., 2007).

PTTG has been observed to co-localise with mitotic spindles during mitosis when its concentration within the cell was highest (Yu et al., 2003). These observations are consistent with the role of PTTG as the human securin involved in the regulation of mitosis. Furthermore, the observation that PTTG phosphorylates during mitosis suggests that PTTG is involved in the regulatory pathway controlling cell proliferation (Ramos-Morales et al., 2000).

1.3.5 **Expression in normal human tissue and cancers**

PTTG is expressed at low levels within the spleen, prostate, ovary, heart, brain, liver, skeletal muscle, kidney and pancreas. High levels of PTTG expression are found in the testes, thymus and placenta (Dominguez et al., 1998). It is thought that PTTG plays a role in spermatogenesis (Pei, 1999).

High PTTG expression has been reported in various human cancers including astrocytomas (Tfelt-Hansen et al., 2004), breast (Puri et al., 2001), oesophagus (Shibata et al., 2002), lung (Kakar and Malik, 2006), stomach (Wen et al., 2004), liver (Cho-Rok et al., 2006), colon (Heaney et al., 2000), ovary (Puri et al., 2001) and haematopoietic (Dominguez et al., 1998). Interestingly, promoter mutation was not found to play an important role in PTTG overexpression in pituitary adenomas (Kanakis et al., 2003). Further investigations indicate that neither methylation nor loss of heterozygosity are involved in PTTG overexpression, suggesting that the misregulation of PTTG is a post-transcriptional event (Hidalgo et al., 2008).

1.3.6 **Expression in thyroid cancer**

Of interest to this study is the overexpression of PTTG in thyroid neoplasms (Heaney et al., 2001, Boelaert et al., 2003). Heaney et al initially reported increased PTTG mRNA expression in follicular thyroid neoplasms. Our own group has confirmed that PTTG expression is increased at both an mRNA and protein level in well differentiated thyroid cancers with no difference between papillary or follicular lesions. In addition, thyroids from multinodular goitres or Graves disease did not show a significant increase in PTTG. More importantly, high PTTG expression was an independent prognostic indicator of early recurrence (Boelaert et al., 2003). Saez et al analysed PTTG expression in differentiated thyroid cancers using immunohistochemistry and found a positive association of high PTTG expression with nodal and distant metastases, disease persistence, advanced TNM stage and reduced radioiodine uptake (Saez et al., 2006).

Reduced iodine uptake was observed by Heaney et al in FRTL5 cells overexpressing PTTG (Heaney et al., 2001). Subsequently, PTTG has been shown to repress the sodium-iodide symporter (NIS) responsible for active radioiodine transport into thyroid cells via FGF-2 (Boelaert et al., 2007), discussed in section 1.3.11.4. This observation may account for a poorer prognosis in patients with thyroid cancer overexpressing PTTG.

1.3.7 **Murine models of PTTG overexpression**

To date, there has been a few studies investigating the effect of PTTG overexpression in specific organs. In vivo overexpression of PTTG in murine pituitary cells induced abnormal cell proliferation and adenomas (Abbud et al., 2005). The overexpression of PTTG in the ovarian surface epithelium of transgenic murine models resulted in the formation of pre-cancerous lesions but did not result in ovarian tumourigenesis (El-Naggar et al., 2007). Our group has created a transgenic murine model of targeted PTTG overexpression in the thyroid gland demonstrating small thyroids with reduced cellular proliferation and did not develop thyroid cancer (Lewy et al., 2013).

1.3.8 **PTTG and genetic instability**

PTTG, also known as the human securin, inhibits the separation of sister chromatids (Zou et al., 1999). The ubiquitination of PTTG by APC/C^{Cdc20} is inhibited by Cdk1 which phosphorylates PTTG (Holt et al., 2008). The activation of separase at the metaphase-anaphase transition triggers the release of Cdc14 phosphatase which dephosphorylates PTTG, resulting in its ubiquitination, ultimately allowing the separation of sister chromatids (Queralt et al., 2006, Stegmeier et al., 2002).

Defects in chromatid separation result in aneuploidy (Nasmyth, 2002). Hence, it is not surprising that overexpression of PTTG results in aneuploidy, a histological observation associated with

chromosomal instability (Winnepenninckx et al., 2006, Yu et al., 2000a, Yu et al., 2003, Wang et al., 2001). The measurement of intrachromosomal instability by fluoresecent intersimple sequence repeat PCR in thyroid cancer demonstrated a positive correlation between PTTG expression and genetic instability (Kim et al., 2005).

In keeping with this, PTTG knockout (PTTG -/-) murine embryo fibroblasts had a prolonged G2/M phase and exhibited aneuploidy (Wang et al., 2001). PTTG -/- knockout murine models are surprisingly viable and fertile, with testicular and splenic hypoplasia, thymic hyperplasia and thrombocytopenia (Wang et al., 2001). In addition, PTTG deficient mice developed non autoimmune insulin deficiency with pleiotropic beta islet cells (Wang et al., 2003). This was attributed to a combination of apoptosis and senescence in beta islet cells secondary to DNA damage (Chesnokova et al., 2009). Taken together, the observed PTTG -/- mouse phenotype could be explained by the varying importance of PTTG in different organ development. Also, it appears PTTG plays an important role in cell cycle progression, albeit not being the only mechanism that regulates sister chromatid separation (Mei et al., 2001, Wang et al., 2001). Overall, murine models of both PTTG knockout and overexpression demonstrate that PTTG has a role in genomic stability.

1.3.9 **PTTG, Trp53 and apoptosis**

The functions of Trp53 in apoptosis, cell cycle regulation and DNA repair (Levine, 1997, Vousden, 2000) in response to DNA damage alludes to its importance in the maintenance of genomic stability. The importance of Trp53 in tumourigenesis is demonstrated by the fact that it is mutated in over 50 % of human cancers (Hollstein et al., 1994). The loss of function of or inability to illicit a normal Trp53 response to DNA damage can cause malignant transformation (Vousden, 2006).

PTTG has been demonstrated to cause apoptosis both in a Trp53 dependent and independent manner. The same group found that Trp53 was capable of preventing aneuploidy caused by an overexpression

of PTTG (Yu et al., 2000a, Yu et al., 2000b). These observations suggests that Trp53 exerts a protective effect via apoptosis to ameliorate the chromosomal instability induced by PTTG. PTTG upregulates the transcription of Trp53 through the expression of c-myc. Bax, a pro-apoptotic downstream gene of the Trp53 signalling pathway is upregulated in the presence of PTTG overexpression only when normal functioning Trp53 is present (Hamid and Kakar, 2004). This suggests that PTTG-induction of Trp53-dependent apoptosis is at least partially mediated via Bax.

In vivo and in vitro studies have determined that Trp53 and PTTG interact directly (Bernal et al., 2002). In contrast to the above findings by other groups, Bernal et al reported that the transcriptional ability of Trp53 was inhibited by its interaction with PTTG. In addition, they reported that PTTG inhibited the ability of Trp53 to induce apoptosis (Bernal et al., 2002). Other groups have since also reported that PTTG negatively regulates the apoptotic function of Trp53 (Cho-Rok et al., 2006, Lai et al., 2007).

The DNA damaging drugs doxorubicin and bleomycin suppressed PTTG only in the presence of functional Trp53 with one study proposing that Trp53 suppressed PTTG via the transcription factor NF-Y (Zhou et al., 2003). In the study of apoptosis induced by 5-fluorouracil in HCT116 cells, Trp53 was found to bind directly with the PTTG promoter and repress its expression (Kho et al., 2004).

PTTG is involved in the DNA damage pathway. In eukaryotic cells, ultraviolet (UV) radiation has been found to reduce PTTG protein levels by reducing its synthesis and increasing its degradation, independent of Trp53. PTTG was also found to be required for cell cycle arrest following UV radiation, with its loss resulting in premature entry into mitosis and increased apoptosis (Romero et al., 2004).

1.3.10 **PTTG, DNA damage and repair**

Further evidence for the role of PTTG in the DNA damage response comes from the interaction between PTTG and Ku70 (Romero et al., 2001). Ku70 forms a heterodimer with Ku80 and together

with DNA-PK, this complex facilitates non-homologous DNA end-joining repair of double strand breaks (Smith and Jackson, 1999, Kharbanda et al., 1998). In the presence of double strand breaks, PTTG is phosphorylated by DNA-PK and dissociates from Ku70 allowing for DNA repair to occur (Romero et al., 2001). It has been observed that PTTG overexpression inhibits Ku70 DNA binding and represses double strand break repair (Kim et al., 2007b). Thus, in the presence of high PTTG expression Ku proteins are bound, consequently adversely affecting DNA repair which results in genetic instability.

Overall, the above studies with Trp53 and Ku70 have demonstrated the multifaceted role PTTG plays in the DNA damage response which is complex and not fully understood. Certainly, the role of PTTG in the context of genetic instability and tumourigenesis in the thyroid remains to be elucidated.

1.3.11 Gene interactions with PTTG

The observation that PTTG has a domain for DNA binding, acidic transactivation and partial localisation in the nucleus, suggests PTTG may transactivate other genes. Deletion of amino acids 124 to 202 abolished the transactivational abilities of PTTG, suggesting that the C-terminal end of PTTG is responsible for this function (Dominguez et al., 1998).

The acidic C-terminus of PTTG contains multiple glutamic and proline residues which are characteristic of transactivation domains (Pei, 2000, Wang and Melmed, 2000). Within this region are two PXXP motifs that are SH3-binding sites which are highly conserved regions that govern transduction of intracellular signalling pathways. Point mutations in the PXXP motifs resulted in the abrogation of its transactivational ability and more importantly, in its in vitro transforming and in vivo tumour-inducing activity (Zhang et al., 1999). Furthermore, a point mutation at a key prolene residue disrupted the transactivation and transforming ability of PTTG, suggesting an intrinsic link between its transactivation and transforming functions (Wang and Melmed, 2000).

1.3.11.1 **FGF2, VEGF and PTTG**

PTTG has been shown to interact with growth factors and cytokines that could promote the progression of thyroid neoplasms. The established relationship between PTTG, fibroblast growth factor 2 (FGF-2) and vascular endothelial growth factor (VEGF) appear to be critical in tumour progression through the promotion of growth and angiogenesis. Angiogenesis is an integral part of tumour growth and survival; a blood supply is critical in maintaining tumour viability (Folkman, 1972, Folkman, 1990, Folkman, 1992, Folkman and Shing, 1992, Hanahan and Folkman, 1996). FGF-2 and VEGF act synergistically to modulate tumour angiogenesis and invasion (Bikfalvi et al., 1997, Ferrara and Davis-Smyth, 1997, Gospodarowicz et al., 1987, Fujii et al., 2006, Minematsu et al., 2007, Wang et al., 2004).

Stable overexpression of PTTG in NIH3T3 cells resulted in increased FGF-2 mRNA expression (Zhang et al., 1999). Interestingly, FGF-2 has been shown to induce PTTG expression in NIH3T3 cells (Heaney et al., 1999), suggesting the existence of a regulatory autocrine pathway between FGF-2 and PTTG. The expression of VEGF by PTTG is FGF-2 independent (McCabe et al., 2002).

1.3.11.2 **c-Myc and PTTG**

The transcription factor c-Myc was found to bind to PTTG. c-Myc is involved with the regulation of cellular proliferation and is dysregulated in tumours. PTTG was found to bind to the c-Myc promoter with the upstream stimulatory factor (USF1) (Pei, 2001). Furthermore, the modulation of p53 function by PTTG is mediated through the expression of c-Myc (Hamid and Kakar, 2004).

1.3.11.3 **SP1 and PTTG**

The global transcriptional effect of PTTG was assessed using chromatin immunoprecipitation (ChIP)-on-Chip in JEG-3 cells. PTTG was found to interact with the transcription factor SP1 to induce cyclin D3 expression to promote G1- to S-phase transition, independent of p21 (Tong et al., 2007).

1.3.11.4 **NIS and PTTG**

The sodium-iodide symporter (NIS) is involved in the active transport of iodine into thyroid cells. This has clinical significance in the treatment of thyroid cancers where poor radioiodine uptake correlates to a poor prognosis. Heaney et al demonstrated reduced iodine uptake in rat thyroid FRTL5 cells transfected with PTTG (Heaney et al., 2001). Subsequently, it was shown that PTTG overexpression in thyroid cancers was associated with reduced radioiodine uptake (Saez et al., 2006). Boelaert et al investigated the mechanism by which PTTG repressed NIS. PTTG was found to repress NIS via FGF-2. In addition, it was found that PTTG repressed NIS by binding to the hNUE element within the NIS promoter (Boelaert et al., 2007).

1.3.11.5 **Other interactions**

Pei et al discovered the interaction between the ribosomal protein S10 and the molecular chaperone HSJ2 with PTTG in testicular cells (Pei, 1999). PTTG was also found to inhibit the phosphorylation of Aurora-A and histone H3 Aurora-A substrate which resulted in abnormally condensed chromatin in HCT116 cells (Tong et al., 2008).

1.4 PTTG BINDING FACTOR (PBF)

PTTG binding factor (PBF), mapped to chromosome 21q22.3, contains an open reading frame of 179 amino acids with a predicted molecular mass of 22 kDa and is also known as C21orf3 (Yaspo et al., 1998) or PTTG1IP. As a protein, PBF shares no significant homology with other human proteins but is highly conserved between species, suggesting unique function and evolutionary importance.

1.4.1 Structure, function and localisation of PBF

PBF interacts with PTTG at its transactivating domain between amino acids 123 to 154 (Chien and Pei, 2000). Based on its structure it was speculated that PBF was a protein involved in cell signalling. Initially it was thought PBF was a cell surface protein because of the presence of a N-terminal signal peptide, transmembrane domain, endocytosis motif and N-glycosylation sites (Yaspo et al., 1998). PBF contains a bipartite nuclear localisation signal between amino acids 149 and 166 at the C-terminus suggesting it may be a nuclear protein (Chien and Pei, 2000). Subsequently, the nuclear role of PBF was confirmed when it was demonstrated to facilitate the entry of PTTG into the nucleus. Furthermore, the transcription and hence expression of FGF-2 by PTTG requires the presence of PBF (Chien and Pei, 2000). PBF has also been identified in intracellular vesicles where it co-localised with the late endosomal marker CD63 (Smith et al., 2009).

The structure of PBF contains phosphorylation sites for cyclic AMP- and GMP- protein kinase and casein kinase II (Chien and Pei, 2000). Recently, our group has reported phosphorylation of PBF at residue Y174 by Src, a proto-oncogene tyrosine protein kinase. Phosphorylation of PBF leads to reduced ability to bind NIS (Smith et al., 2013). Also, glycosylation sites for N-linked and O-linked oligosaccharides were identified. Finally, a cleavable N-terminal signal sequence was detected (Chien and Pei, 2000).

Recently, PBF has also been found to be a secretory protein in MCF-7 cells and this function is encoded in the PBF amino acid region of 29 to 93 (Watkins et al., 2010). The schematic representation of PBF is shown in Figure 1-12 below.

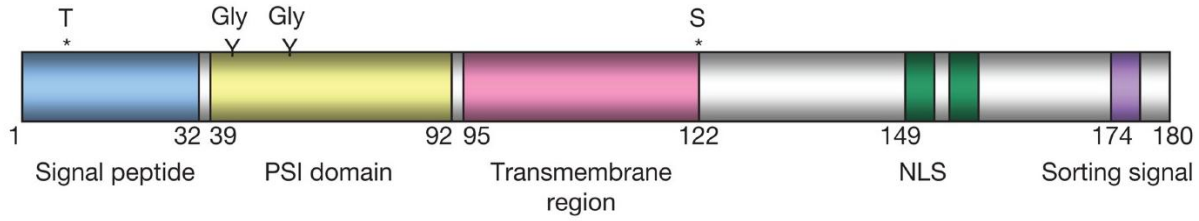

Figure 1-12 Schematic representation of PBF reproduced from (Smith et al., 2010). PBF contains a bipartite nuclear localisation signal sequence and phosphorylation site (residue Y174) at its C-terminus. The N-terminal contains the signal sequence and glycosylation sites denoted by Gly.

1.4.2 **PBF and NIS**

PBF has been shown to repress the expression of the NIS promoter via the upstream enhancer hNUE (Boelaert et al., 2007). Subsequently, it was found that PBF colocalises with NIS, altering its subcellular localisation and affecting the efficacy of radioiodine uptake. In the presence of PBF, NIS translocates from the membrane of COS-7 cells to the cytoplasm. Since the uptake of iodine is dependent on normal NIS function at the membrane, PBF alters the ability of the cell to uptake radioiodine (Smith et al., 2009). Hence, PBF impairs the ability of a thyroid epithelial cell to absorb iodine by directly repressing the expression of NIS and by altering the subcellular localisation of NIS from the membrane to the cytoplasm.

1.4.3 **Expression in human tissue**

PBF is a ubiquitious protein that is expressed in more than one hundred different human tissues with the highest level of expression in the placenta. PBF was also shown to be overexpressed in colon

carcinoma, Wilm's tumour, parathyroid tumours (Chien and Pei, 2000, Yaspo et al., 1998). The finding that PTTG is overexpressed in breast cancer (Ogbagabriel et al., 2005) led to the investigation of PBF in breast cancer. PBF was found to correlate with ER-positive breast cancers (Watkins et al., 2010). Recently PBF was reported to be implicated in the repression of angiogenesis in a mouse model of Down's syndrome (Reynolds et al., 2010).

1.4.4 **Expression of PBF in thyroid cancer**

Stable PBF overexpression in NIH3T3 murine fibroblast cells induced significant colony formation and the injection of nude mice with NIH3T3 cells stably overexpressing PBF led to tumour formation. These observations support the ability of PBF to transform cells in vitro and induce tumours in vivo (Stratford et al., 2005). Unsurprisingly, PBF expression was found to be increased in differentiated thyroid cancers and PBF mRNA expression was independently associated with tumour recurrence (Stratford et al., 2005). A cohort of 153 papillary carcinomas of the thyroid with a follow-up of 11.2 years was studied in the context of PBF expression. It was found that increased PBF expression was an independent predictor of worse prognosis and shorter disease-specific survival. In addition, PBF expression was associated with distant metastases at diagnosis, locoregional recurrence and tumour multicentricity (Hsueh et al., 2013).

1.4.5 **PBF overexpression in murine thyroids**

The human homolog of PBF shares 80 % homology with murine PBF (Chien and Pei, 2000). Our group has generated a transgenic murine model of PBF overexpression in the thyroid gland (PBF-Tg) to study the effects of PBF in thyroid tumourigenesis. The human PBF gene was driven by the bovine thyroglobulin promoter and tagged with haemagglutinin (HA) (Read et al., 2011).

1.4.5.1 **PBF and goitre formation**

The PBF-Tg mouse developed goitres by 6 weeks and more than 65 % of mice developed hyperplastic lesions by 52 weeks of age. These in vivo thyroid changes were not TSH driven and expression of growth factors VEGF, TGFβ, EGF and IGF-1 was unaltered compared to wild-type mice (Read et al., 2011). Further investigation into the aetiology of thyroid pathology revealed dysregulation of TSHR mRNA expression, which was significantly induced by PBF. The mRNA expression of PTTG, throglobulin, transcription factor 1 and paired box gene 8 mRNA was found to be unaltered in the presence of PBF overexpression in the thyroid of PBF-Tg mice (Read et al., 2011).

Interestingly, no cancers were induced although close inspection of the nuclei of the hyperplastic lesions revealed large nuclei consistent with a proliferating cell. Although Akt mRNA expression was normal in PBF-Tg mice, the phosphorylation of Akt was found to be significantly induced by PBF. Furthermore, the expression of cyclin D1, a marker of proliferation and downstream target of activated Akt, showed an upregulation in PBF goitres. Thus, Akt activation, involved in the PI3K/Akt signalling pathway (described in 1.2.6.2), might be involved in inducing goitre and hyperplastic thyroid lesion formation. (Read et al., 2011). The thyroid phenotype observed in the PBF-Tg murine model was very similar to the $Pten^{L/L}$;TPO-Cre mouse in which there is constitutive activation of the PI3K/Akt pathway (Yeager et al., 2007). The $Pten^{L/L}$;TPO-Cre mouse did not develop thyroid cancers but developed metastatic follicular carcinomas when the Kras oncogenic mutation was introduced. On its own, the Kras mutation did not cause thyroid cancer (Miller et al., 2009).

Further to the above finding in PBF-Tg mice thyroids, the expression of PBF in human thyroid goitres was examined. PBF mRNA expression was increased in human multinodular goitres (MNG) but protein expression of PBF in MNGs were similar to normal thyoid tissue. TSHR protein expression was also found to be upregulated in MNGs compared to normal thyroids (Read et al., 2011). The above findings implicate PBF, dysregulated TSHR and the PI3K/Akt pathway in goitrogenesis.

1.4.5.2 **PBF and thyroid hormone**

The absorption of iodine is impaired in the presence of PBF due to reduced expression of the sodium-iodide symporter (NIS) and altered localisation of NIS, discussed in section 1.4.3 above (Boelaert, 2007, Smith, 2009). This observation was confirmed in vivo, in the PBF-Tg murine thyroids where radioiodide uptake was represssed (Read et al., 2011).

Subsequently, Smith et al demonstrated that MCT8, a monocarboxylase transporter which mediates thyroid hormone secretion, binds and co-localises with PBF, resulting in reduced thyroid hormone secretion and an accumulation of thyroid hormone in the thyroid gland of the PBF-Tg mouse (Smith et al., 2012).

1.4.6 **PBF and genetic instability**

PBF has been shown to be overexpressed in differentiated thyroid cancer and is an independent prognostic marker for recurrent disease (Hsueh et al., 2013, Stratford et al., 2005). Genetic instability is a hallmark feature of human cancers and a critical protein that governs genetic instability, Trp53, mediates crucial cellular responses to DNA damage (Petitjean et al., 2007). Although Trp53 is frequently mutated in human cancer, it is rarely mutated in differentiated thyroid cancer. PBF was found to increase the ubiquitination of Trp53 via the E3 ligase, Mdm2 (Read et al., 2014a, Read et al., 2014b). PBF was also found to interfere with the expression of DNA repair genes which may explain the genetic instability induced in thyroid cells overexpressing PBF (Read et al., 2014a).

1.5 GENETIC INSTABILITY

1.5.1 Hypotheses of tumourigenesis

In the 1950s, researchers came to the hypothesis that tumourigenesis is a multistep process (Foulds, 1958). Calculations by Ashley based on gastric cancers estimated that three to eight mutations are required for tumourigenesis (Ashley, 1969). However, a study on retinoblastoma has shown that as few as 2 mutations was required for tumour formation (Knudson, 1971).

It was initially proposed that most neoplasms are monoclonal and that tumour cells are more genetically unstable compared to normal cells (Nowell, 1976). Mutations are a necessary prerequisite for cancer formation and progression because they confer a selective growth or survival advantage. Mutations in genes that are critical in cell cycle control and DNA repair, that play an important role in maintaining genomic stability, play an important role in tumourigenesis, and led to the development of the mutator phenotype hypothesis (Tomlinson and Bodmer, 1999, Loeb, 2001). Negrini et al argues that the low frequency of mutations in caretaker genes in high-throughput sequencing studies of tumours in sporadic cancer does not support the mutator phenotype hypothesis. Furthermore, comparing untreated with treated glioblastomas, the mutations of caretaker genes was higher following treatment, suggesting that caretaker gene mutation is a late event rather than being essential in the initial development of the tumour (Negrini et al., 2010). It was therefore argued that whilst the mutator phenotype hypothesis explained the cause of hereditary tumours, it did not necessarily explain sporadic tumour genesis.

The oncogene-induced DNA replication stress model put forward by Halazonetis et al. attempts to address the issue of genetic instability in tumourigenesis (Halazonetis et al., 2008). In this model, activated oncogenes induce replicative stress resulting in genetic instability and early cancer formation.

Overall, tumourigenesis from a normal to a cancerous cell is a complex process that is not fully understood. However, genetic instability is a consistent feature within cancers and has close association with genes involved in DNA damage and repair.

1.5.2 **Genetic instability and cancer**

The hallmark feature of solid tumours is an unstable genome (Rajagopalan et al., 2002, Loeb and Monnat, 2008). Genetic instability in cancer reflects an increased rate of mutation which may arise either from increased rates of damage or defects in repair ability resulting in reduced genomic integrity within cells (Rajagopalan et al., 2002, Loeb and Monnat, 2008). Loss of genetic stability facilitates tumour development by generating mutants that can undergo clonal selection (Storchova and Pellman, 2004). At a molecular level, the accumulation of extra copies of DNA or chromosomes, chromosomal translocations, chromosomal inversions, chromosomal deletions, single-strand breaks in DNA, double-strand breaks in DNA, the intercalation of foreign substances into the DNA double helix or any abnormal changes in the DNA tertiary structure resulting in the gain or loss of DNA or the misexpression of genes, cause genetic instability. Genetic instability can arise at a nucleotide (microsatellite instability) or chromosomal level (chromosomal instability). Microsatellite instability, characterised by nucleotide base changes that occur preferentially in repeat sequences, is typically caused by a defective repair process whilst chromosomal instability is characterised by aneuploidy caused by deletions or amplification of whole / part chromosomes (Fishel et al., 1993, Ionov et al., 1993, Lengauer et al., 1998). It has been reported that microsatellite instability and chromosomal instability are mutually exclusive, suggesting that instability of one variety alone is sufficient for driving tumourigenesis (Loeb and Loeb, 1999). Previous studies by Lengauer et al (Lengauer et al., 1997) and Willenbucher (Willenbucher et al., 1999) suggested that chromosomal instability is more dominant in driving tumourigenesis than microsatellite instability, at least in the case of colorectal tumours.

The role of genetic instability in thyroid cancer has been described previously (Kim et al., 2005, Mitmaker et al., 2008, Vaish et al., 2004, Lohrer et al., 2001). In addition, benign thyroid lesions have been shown to demonstrate microsatellite instability albeit at a lower level compared to thyroid cancer (Mitmaker et al., 2008). However, other studies did not show this (Bauer et al., 2002).

1.5.3 **Measuring genetic instability**

Chromosomal instability, characterised by abnormal segregation of chromosomes and aneploidy (Rajagopalan et al., 2003), is caused by dysregulation of checkpoint proteins involved in mitosis, resulting in the failure to halt cell cycle progression to allow DNA repair to occur (Roschke et al., 2008). Additionally, apoptosis has an important role to play in removing cells that cannot be repaired following DNA damage. Consequently, apoptotic genes when dysregulated can induce chromosomal instability. This is confirmed by the observation that loss of p53 and p73 is associated with increased aneuploidy in mouse embryonic fibroblasts (Talos et al., 2007, Tomasini et al., 2008).

Chromosomal instability is predominantly quantified using comparative genomic hybridization (CGH) or fluorescent in-situ hybridization (FISH). The FISH technique uses fluorescent probes to detect and localise the presence or absence of specific DNA sequences on chromosomes. In CGH, differences in hybridisation between normal and tumour human DNA can be compared using fluoresecent labelled fragments of normal and tumour on a scaffold of human metaphase chromosomes. This technique is sensitive for deletions or amplifications between 1 – 10 megabases (Bentz et al., 1998). CGH is an improvement of the FISH technique for quantifying chromosomal instability.

Microsatellite (or simple sequence repeats) are repeat sequences scattered throughout the genome and are highly variable from individual to individual. These repeating units consists of 1 to 6 base pairs in length (but can be longer) and most commonly in humans, consist of repeat C and A nucleotides. The technique of measuring microsatellite instability arose when random oligonucleotide primers used to DNA fingerprint colorectal tumours and its adjacent tissue found tumour specific PCR products of

altered length encompassing segments with repetitive nucleotide sequences (Peinado et al., 1992). Basik et al used the $(CA)_8RY$ primer to measure the index of genetic instability in colorectal carcinoma and coined the phrase "Inter-simple sequence repeat PCR" for this technique (Basik et al., 1997). Subsequently, Stoler et al used the same technique of inter-simple sequence repeat PCR to determine genetic instability in colorectal polyps and found that genetic instability is an early event in colorectal tumour progression and is not a consequence of malignancy (Stoler et al., 1999).

Initially, microsatellite instability was shown to be caused by a defective Msh2 gene, involved in mismatch repair, in colorectal carcinoma (Fishel et al., 1993). The mismatch repair family members repair base-base mispairs and larger insertions / deletions (Hakem, 2008). Defective mismatch repair results in increased rates of DNA replication errors within the genome causing microsatellite instability (MSI). Areas within the genome preferentially affected are genes such as TGFβRII, IGF-2R and BAX which contain microsatellites within their coding regions. As such, mismatch repair family defects result in incorrect DNA replication which may consequently cause microsatellite instability preferentially in the above genes (Loeb and Monnat, 2008). Microsatellite instability can also be caused by base excision repair pathway defects (Hakem, 2008, Guo and Loeb, 2003).

1.6 THE CELL CYCLE

Cell cycle dysregulation and consequently genetic instability is found widely in human cancer. Cell duplication begins with synthesis of DNA in the S phase and division in the mitosis (M) phase. In between these two phases are the G1 and G2 gaps where the cell "rests" to recover from the preceding phase. During G1 the cell may enter a special G_0 phase which can last indefinitely. If the cell progresses beyond the end of G1, known as the restriction point, the cell is committed to DNA replication (Alberts et al., 2014).

Cyclins and cyclin-dependent kinases (CDK) determine a cell's progress through the cell cycle. The CDK-cyclin complexes directly involved in driving the cell cycle include the three interphase CDKs (CDK2, CDK4, and CDK6), CDK1 and ten cyclins belonging to 4 different classes (A, B, D and E cyclins) (Malumbres and Barbacid, 2009). DNA damage induces cell cycle arrest via the inhibition of CDK (Bartek et al., 2004) to allow for DNA repair. Unsuccessful DNA repair results in senescence or apoptosis, but if the cell cycle is allowed progress, genetic instability results (Kastan and Bartek, 2004).

1.6.1 CDK and DNA damage

The genes ataxia-telangiectasia mutated (ATM) and ataxia telangiectasia and Rad3 related (ATR) are activated together with checkpoint kinases Chk1 and Chk2 in DNA damage, resulting in increased levels of the CDK inhibitor p21 or inhibition of CDK activators such as Cdc25 phosphatases (Bartek et al., 2004). This results in cell cycle arrest at G1/S and G2/M allowing for DNA repair to occur. Mutations in ATM result in ataxia-telangiectasia and ATR in Seckel syndrome (Cimprich and Cortez, 2008).

There is increasing evidence for the role of CDKs in DNA repair (Yata and Esashi, 2009). Homologous recombination repair during S phase and G2 is mediated by CDK1 and CDK2 phosphorylating Brca2 to modulate its interaction with Rad51 (Esashi et al., 2005).

1.6.2 **CDK and chromosomal instability**

The CDK1-cyclin complex regulates the centrosome cycle and the onset of mitosis. The phosphorylation of downstream targets to the CDK1-cyclin complex during G2 results in centrosome separation, nuclear envelope breakdown and chromosome condensation (Malumbres and Barbacid, 2005). CDK1 activity is repressed at the metaphase-anaphase interface through the activation of separase, to allow sister chromatid separation (Musacchio and Salmon, 2007). Hence, in the dysregulation of CDK1, aneuploidy and chromosomal instability results.

1.7 ATM/ATR signalling pathway

The cell is under constant stress and requires coping mechanisms to respond and maintain its integrity. Genetic instability arises when the appropriate response mechanism fails. As discussed above, genetic instability is related to progressive degeneration, cancer predisposition and sensitivity to various DNA damaging agents (Bensimon et al., 2010, Bhatti et al., 2011, Nam and Cortez, 2011, O'Driscoll et al., 2007, Ruzankina et al., 2007).

The ATM / ATR signalling pathway, which plays a central role in response to DNA damage is shown in Figure 1-13. The ATM (ataxia-telangiectasia mutated) gene belongs to a family of serine/threonine kinases which was first discovered in the ataxia-telangiectasia disorder. This autosomal recessive condition is characterized by progressive cerebellar neurodegeneration and is predisposed to lymphoreticular maliganancies (Lavin, 2008, Perlman et al., 2012). Strikingly, patients with the condition of ataxia-telangiectasia are particularly sensitive to ionising radiation (Perlman et al., 2012).

ATM plays a central role in the coordination of cellular functions such as cell cycle arrest, DNA repair and apoptosis in response to DNA damage (Sancar et al., 2004). The general consensus is that the ATM response occurs in double strand breaks whilst ATR (shown in Figure 1-14) is more pertinent in single strand breaks or stalled replication forks. However there is interplay between the 2 genes where ATM can activate ATR (Shiotani and Zou, 2009) or ATR can phosphorylate ATM, rendering it active (Dodson and Tibbetts, 2006, Stiff et al., 2006, Yajima et al., 2009, Sirbu et al., 2011).

Murine ATM knockout models develop leukaemia, in particular thymic lymphoma and sporadic intestinal cancer (Ejima et al., 2000). ATM has been shown to phosphorylate and activate Trp53, the "guardian of the genome", in response to DNA damage (Banin et al., 1998, Nakagawa et al., 1999).

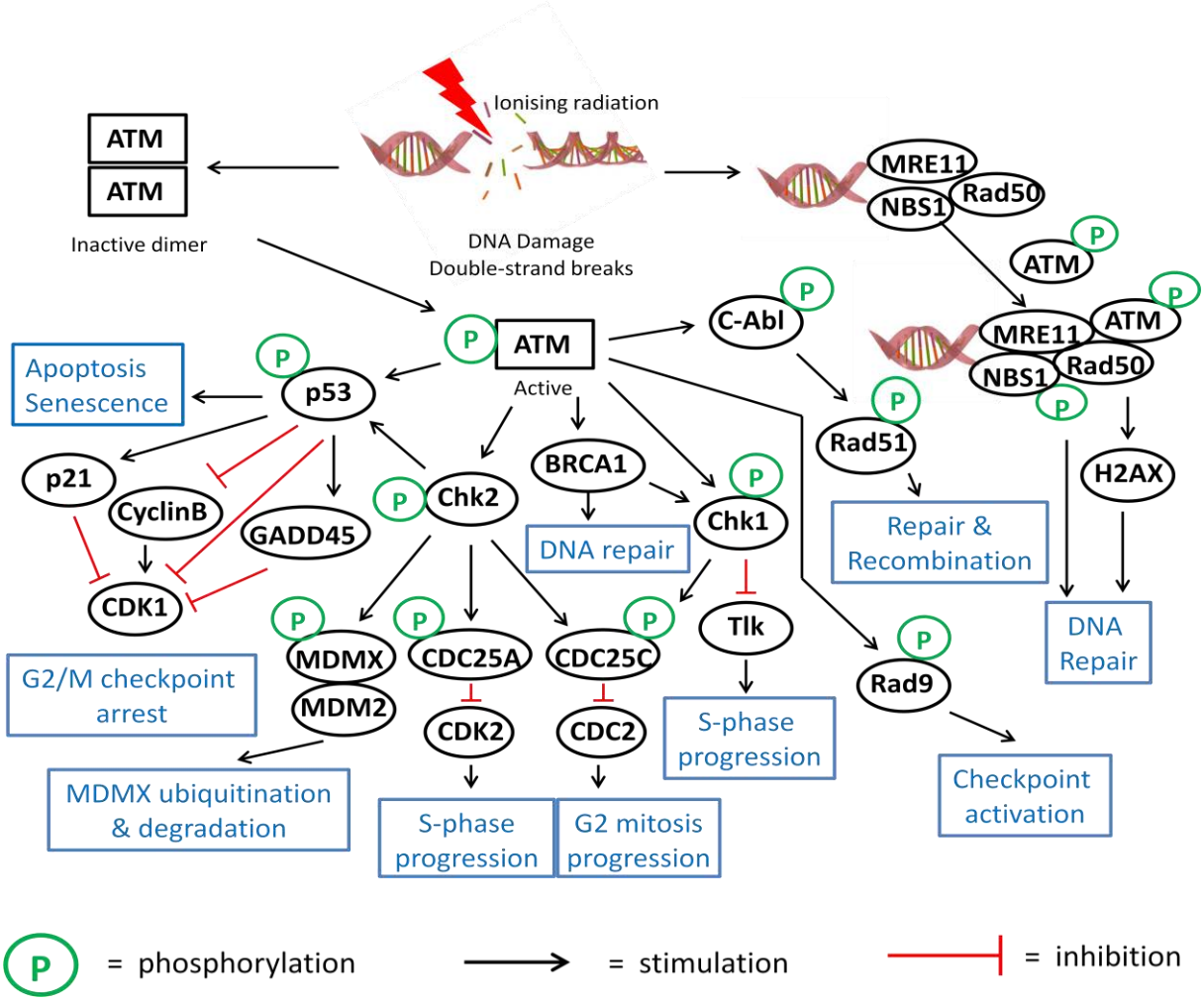

Figure 1-13 An overview of the ATM molecular pathway demonstrating its role in double-strand DNA damage (Adapted from SABiosciences.com). The diagram depicts known genes that interact with ATM and its downstream functions.

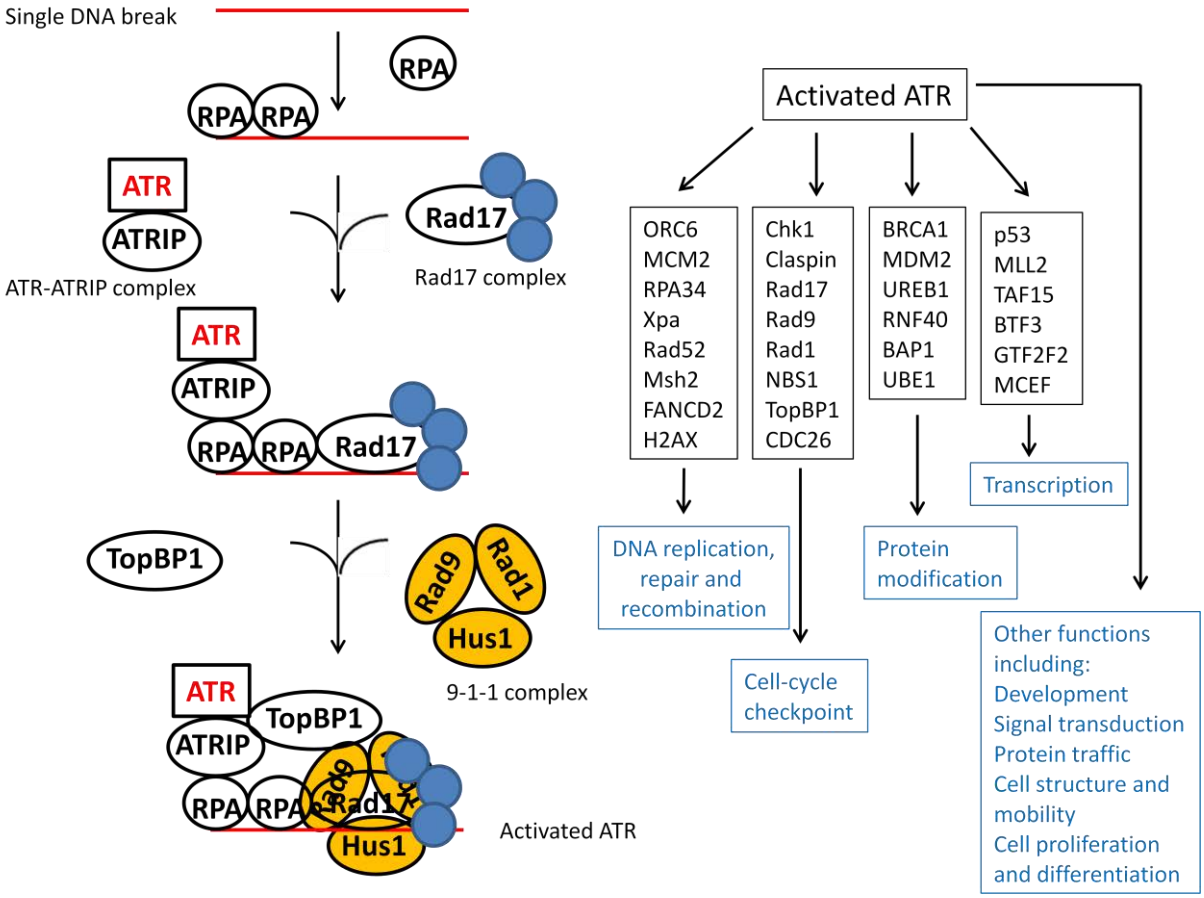

Figure 1-14 ATR signalling pathway adapted from (Shiotani and Zou, 2009).The diagram shows the activation and function of ATR in response to single-strand breaks.

1.8 HYPOTHESIS AND AIMS

PTTG has been shown to have transforming and tumourigenic effects in vitro and in vivo. Additionally, PTTG causes aneuploidy and genetic instability. PTTG is implicated in DNA damage and DNA repair through its known interaction with Trp53 and Ku70. The binding partner of PTTG, PBF, transports PTTG to the nucleus for its transcription and securin function. PBF is independently transforming in vitro and tumourigenic in vivo. PBF is also known to interact with Trp53 which is intimately involved in the response to DNA damage. Important to this investigation is the finding that PBF and PTTG are both overexpressed in human differentiated thyroid cancer.

As both PTTG and PBF are transforming genes which show functional interaction and overexpression in thyroid cancer, we hypothesised that PBF and PTTG have dependent and independent roles in maintaining genomic stability in the thyroid gland.

The aims of this investigation were:

1) *The development of a murine model of simultaneous PBF and PTTG overexpression in the thyroid gland.* Our group had murine models of PTTG or PBF overexpression in the thyroid gland. The observation that murine models of PBF overexpression in the thyroid developed hyperplastic nodules but not cancer and the murine model of PTTG overexpression in the thyroid had small thyroid glands led us to hypothesise that two "hits" might be required for thyroid tumourigenesis. Hence, I aimed to create a bi-transgenic murine model of both PBF and PTTG overexpression in the thyroid gland.

2) *The use of fluorescent inter-simple sequence repeat PCR (FISSR-PCR) for determining genetic instability in our murine models.* FISSR-PCR was modified for measuring genetic instability with small quantities of DNA obtained from our transgenic models and from primary murine thyroid culture.

3) *Establishing key genes involved in the DNA damage / DNA repair pathway in the context of PBF and PTTG expression with ionising radiation*. This part of the study involved the use of a

murine DNA damage PCR microarray to screen for genetic alterations within the DNA damage / DNA repair pathway.

2 Materials and Methods

2.1 MURINE THYROID DISSECTION

Murine models used in the following experiments were euthanized with an intra-peritoneal injection of sodium pentobarbital (0.2 mls of Euthatal; 200mg in 1 ml) and confirmed to be dead prior to harvesting the thyroid gland. The thyroid gland was removed with the aid of a dissecting microscope at 10x magnification. Initially, the mouse was secured to a cork board, exposing the neck. Subsequently, the fur and skin were excised and the strap muscles divided inferiorly. Superior retraction of the strap muscles revealed the thyroid gland sitting on the trachea as shown in Figure 2-1. The thyroid gland was removed with micro forceps and scissors and stored in formalin for histology, RNAlater for RNA analysis, liquid nitrogen for protein analysis or phosphate buffer solution (PBS) for primary cell culture.

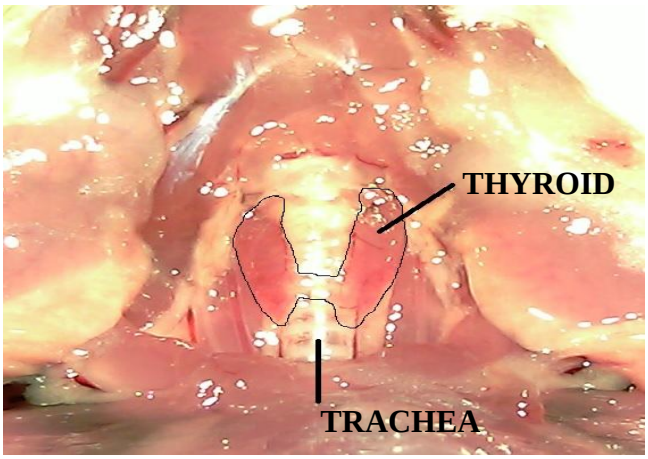

Figure 2-1 View of murine thyroid under 10x magnification during dissection. This view of the thyroid gland was obtained following the removal of fur and strap muscles in the neck.

2.2 PRIMARY MURINE THYROID CULTURE (PMTC)

Murine thyroids were mechanically disrupted in PBS prior to being digested in 0.2 % Type II collagenase (Worthington Biochemicals) at 37 °C for 45 minutes on a rotator. Subsequently, thyroid culture medium described previously by Ambesi-Impiombato *et al* (Ambesi-Impiombato et al.,

1980), was added to inactivate collagenase. The mixture was centrifuged at 700 G for 10 minutes to obtain a pellet comprising of single thyroid follicles. The supernatant was discarded and the pellet resuspended in 1ml of thyroid culture medium. The resuspended thyroid cells were seeded into 12-well plates (2 wells for each hPTTG or WT thyroid; 4 wells for each PBF and Bi-Transgenic thyroid) in thyroid culture medium, supplemented with thyrotrophin (300 mU/l), insulin (10 mg/ml), transferrin (5 mg/ml) [Sigma], hydrocortisone (3.5 ng/ml) [Sigma], somatostatin (10 ng/ml) [Sigma], glycyl-L-histidyl-L-lysine acetate (2 ng/ml) [Sigma], penicillin (105 U/l), streptomycin (100 mg/l) and 5 % fetal calf serum. After 3 days, the thyroid culture medium was changed with calf serum omitted. Experiments were performed at day 10. In experiments involving radiation, primary murine cultures were exposed to 15 Gy of radiation on day 9 and harvested 24 hours later.

2.3 DNA EXTRACTION

DNA was extracted as per the DNA extraction kit protocol (DNeasy 96 Blood & Tissue Kit; Qiagen). Briefly, tissue was dissolved in ATL buffer and Protein K at 56°C for 3 hours. RNAse A was added to the mixture and left to stand for 2 minutes at room temperature to remove RNA contaminants. AL buffer and 100% ethanol were added to the mixture and filtered in a DNeasy Mini spin column. The DNA binds to the filter whilst contaminants wash through. The filter was washed twice to ensure a clean DNA sample. Finally, the DNA was extracted by elution through adding AE buffer to the filter. The amount of DNA was quantified using a spectrophotometer (Nanodrop ND-1000; Thermoscientific).

2.4 RNA EXTRACTION

RNA was extracted using the RNAeasy micro extraction kit protocol (RNeasy Micro; Qiagen). Thyroid tissue was processed using β-Mercaptoethanol to denature RNAses and buffer RLT (proprietary buffer; Qiagen RNAeasy micro extraction kit) to promote RNA binding to the filter. RNA was filtered onto the proprietary filter within the RNeasy MinElute spin column and washed several times to remove contaminants. RNase-free water to dissolve the purified RNA was used in the final step to collect purified RNA. RNA concentration was quantified using spectrophotometry (Nanodrop ND-1000; Thermoscientific). To ensure consistent and good RNA quality, the spectral value of A_{260}:A_{230} ratio was greater than 1.7 and A_{260}:A_{280} ratio, between 1.8 and 2.0. The average amount of total RNA obtained in this manner ranged between 220 to 800 ng.

2.5 REVERSE TRANSCRIPTION

Reverse transcription was carried out using the Promega Reverse Transcription System. Briefly, each reaction consisted of 0.5 µg RNA, 2 µl 25 mM $MgCl_2$, 1 µl 10X reverse transcriptase buffer, 1µl 10mM deoxynucleotide triphosphate, 5 pmol random hexamers, 10 units ribonuclease inhibitor (RNAsin) and 7.5 units avian myeloblastosis virus (AMV) reverse transcriptase, in a total reaction volume of 10 µl. The reaction was incubated for 10 minutes at room temperature followed by 60 minutes at 42 °C to allow primer fixation and extension. The reaction was terminated by heating the sample for 5 minutes at 95 °C.

2.6 QUANTITATIVE REAL-TIME POLYMERASE CHAIN REACTION (qRT-PCR)

Quantitative real-time polymerase chain reaction (qRT-PCR) was performed using TaqMan™ chemistry. In this technique, the target gene of interest is amplified through polymerase chain reaction (PCR). The probe used within the reaction was specially labelled with a 5' reporter dye (FAM 6-carboxy-fluorescein or VIC) and a 3' quencher dye (TAMRA 6-carboxy-tetramethyl-rhodamine). PCR amplification of the target gene released the reporter dye for each cycle of the PCR reaction which was read by a laser and CCD camera. The quantity of gene within the known amount of cDNA or DNA was thus determined. Pre-optimised specific gene-expression assays for qRT-PCR were purchased from Applied Biosystems, UK. All target gene probes were labelled with FAM and housekeeping genes (DS-CAM, 18S or β-actin) labelled with VIC.

These reactions were carried out in 25 µl volumes on 96 well plates. Each reaction comprised of 5 ng DNA, 450 nM each target gene forward and reverse primers, 175 nM target gene probe, 450 nM housekeeping gene forward and reverse primers, 175 nM housekeeping gene probe and 12.5 µl of 1x TaqMan Universal PCR Master Mix (Applied Biosystems). 1x TaqMan Universal PCR Master Mix consisted of 3 mM Magnesium Acetate, 200 µM dNTPs, 1.25 units Ampli-Taq Gold polymerase and 1.25 units AmpErase UNG. The reaction cycle in the ABI 7500 Sequence Detection System was as follows: 50 °C for 2 minutes, 95 °C for 10 minutes followed by 44 cycles of 95 °C for 15 seconds and 60 °C for 1 minute.

The cycle number at which a calculated threshold line bisects the logarithmic PCR plot determined the Ct value. ΔCt values were calculated by subtracting the Ct of the housekeeping gene from Ct of the target gene of interest. The fold change was derived from the following formula: $2^{-(\Delta Ct \text{ of experimental group} - \Delta Ct \text{ of control group})}$.

Reactions were multiplexed where possible. To determine if the reaction could be multiplexed, qRT-PCR was performed with cDNA amounts of 1 ng, 3 ng, 10 ng, 30 ng and 100 ng in a multiplexing experiment using the target gene of interest and housekeeping gene in question. The logarithmic value of cDNA quantity was plotted against the Ct value of each gene in the qRT-PCR experiment (Figure 2-2A). The ΔCt value, obtained by subtracting the target gene Ct value from the β-actin Ct value was plotted in a separate graph shown in Figure 2-2B. The gradient of the best fit linear plot of the logarithmic cDNA quantity against the ΔCt value should be between -0.1 and 0.1 if multiplexing was possible. Figure 2-2 shows the multiplexing experiment between Trp53 and β-actin, used as an example illustrating that these two genes cannot be multiplexed.

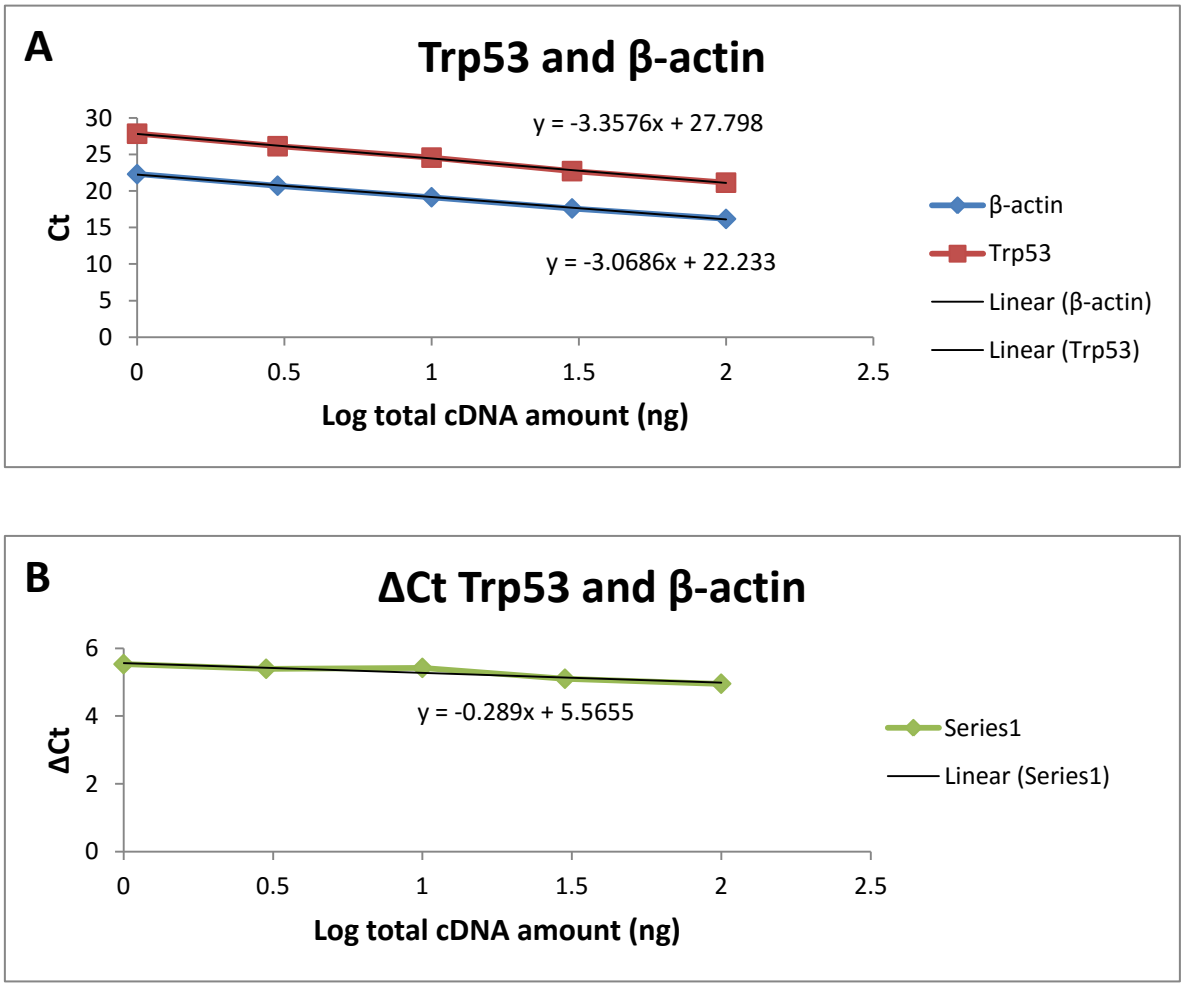

Figure 2-2 Linear plots of logarithmic cDNA against Ct values (A) and Δ Ct values (B).

2.7 PROTEIN EXTRACTION

Tissue and cell culture harvested for protein extraction were homogenized in a tube containing a cocktail of Radio Immuno Precipitation Assay (RIPA) buffer (329 µl) and protease inhibitor (21 µl). Subsequently, the crude lysate was centrifuged at 13,200 rpm for 10 mins at 4 °C. The supernatant was removed and protein concentration quantified using spectrophotometry (Nanodrop ND-1000; Thermoscientific).

2.8 WESTERN BLOT

12 % separating gels were made using 1.875 ml 1.5 M Tris HCl (pH 8.8), 3 mls acrylamide, 75 µl 10 % SDS, 75 µl 10 % APS and 7.5 µl TEMED. Stacking gels were made using 0.625 ml 0.8 M Tris HCl (pH 6.8), 0.3125 ml acrylamide, 50 µl 10 % SDS, 50 µl 10 % APS and 5 µl TEMED. 20 µg of protein in 4X Laemmli buffer (0.1075 g DTT: 1 ml Laemmli buffer) was loaded into each well.

Proteins separated by electrophoresis were transferred to polyvinylidene fluoride (PVDF) membranes, incubated in 5 % non-fat milk in Tris-Bufferred Saline Tween-20 (TBST) and subsequently incubated overnight at 4 °C with a primary monoclonal antibody. After washing in TBST, membranes were incubated in the appropriate secondary antibodies conjugated to horseradish peroxidise. After additional washes, antigen-antibody complexes were visualized by the ECL chemiluminescence detection system on Kodak BioMax Light film. Actin expression (Anti-βactin; 1:10,000; AC-15; Sigma-Aldrich) was also determined to control for differences in protein loading between wells. Western blot films were scanned using the CanoScan Flatbed Photo and Document scanner and relative protein quantification was determined using Image J software.

2.9 IMMUNOFLUORESCENCE

The cells in each well were fixed with 800 µl fixing solution (20 ml of 0.2 M PBS, 0.8g of paraformaldehyde, 0.8 g glucose, 8 ml of 0.1 % sodium azide and 12 ml water) for 20 minutes at room temperature. Following rinsing with PBS, the cells were permeabilised in 800 µl of chilled methanol for 10 minutes. The cells were rinsed again and blocked with 5 % blocking serum for 20 minutes at room temperature diluted in PBS containing 1 % BSA (bovine serum albumin). Subsequently, excess blocking serum is aspirated and cells incubated in primary HA antibody (mouse monoclonal anti-HA.11 (16B12); 1:1000; Covance Research Products) diluted in PBS containing 1% BSA for 1 hour. The cells are rinsed again and incubated for 1 hour in a red fluorescent labelled secondary antibody diluted in PBS containing 1 % BSA and 1.5 % blocking serum. The cells are then visualised using an inverting microscope. DAPI (4',6-diamidino-2-phenylindole; 300 µl of diluted stock solution as per manufacturer's recommendation; ThermoFisher Scientific) staining was used to identify nuclei by staining DNA blue.

2.10 STATISTICAL ANALYSIS

Data was analysed using Sigma Stat and SPSS (SPSS Science Software UK Ltd). The numerical data was determined if it had a normal distribution. Student's t-test was used for comparison between two groups of parametric data. Kaplan-Meier survival analysis was determined using XLSTAT add-on to Microsoft Excel 2007. Two different statistical tests were used to determine the p-value for survival. The p-value derived from the Cox-Mantel or log-rank test is more powerful for detecting late, whilst the Wilcoxon test is more powerful for detecting early differences in probabilities for survival. A p value ≤ 0.05 was taken to be statistically significant.

3 Bi-transgenic murine model of human PTTG and PBF overexpression in the thyroid gland

3.1 INTRODUCTION

The human securin PTTG was first described in rat pituitary tumours (Pei and Melmed, 1997). The role of PTTG in cell transformation and tumourigenesis was subsequently confirmed when murine fibroblast 3T3 cells overexpressing PTTG, injected into nude mice developed tumours (Pei and Melmed, 1997). Further experiments in vitro showed aneuploidy or chromosomal instability when overexpressed (Wang et al., 2001, Winnepenninckx et al., 2006, Yu et al., 2000a, Yu et al., 2003). Further evidence for the role of PTTG in tumourigenesis came from the observation that PTTG was overexpressed in a variety of tumour types (Cho-Rok et al., 2006, Dominguez et al., 1998, Heaney et al., 2000, Kakar and Malik, 2006, Puri et al., 2001, Shibata et al., 2002, Tfelt-Hansen et al., 2004, Wen et al., 2004). More importantly, the link between thyroid cancer and PTTG has been well-established (Liang et al., 2011, Kim et al., 2007a, Kim et al., 2005, Boelaert et al., 2003, Zatelli et al., 2010).

The binding factor for PTTG (PBF) was initially discovered by Yaspo et al and its function as a transport protein for PTTG was described later on (Chien and Pei, 2000, Yaspo et al., 1998). PTTG does not have a nuclear localising signal of its own and yet needs to be within the nucleus for its function. The finding that PTTG requires the presence of PBF to upregulate fibroblast growth factor 2 (FGF-2), a downstream target of PTTG, provides compelling evidence for the need for PBF for its actions (Chien and Pei, 2000). Hence, it was not surprising that the presence of PTTG upregulated the expression of PBF (Stratford et al., 2005). Interestingly, our group has shown that PBF has transforming and tumourigenic actions independent of PTTG (Stratford et al., 2005). Additionally, PBF has been shown to cause genetic instability, is overexpressed in well differentiated thyroid cancer and an independent prognostic marker for tumour recurrence (Hsueh et al., 2013, Stratford et al., 2005).

PBF and PTTG are widely conserved in the eukaryote species. Human PTTG and PBF share 89 % and 93 % homology respectively with murine PBF and PTTG (Zhang et al., 1999, Chien and Pei, 2000). Murine models were generated by our group to study the effects of PTTG or PBF

overexpression in the thyroid gland. Murine models with thyroglobulin driven human PTTG overexpression in the thyroid gland (PTTG +/+) did not demonstrate tumour formation but instead developed small thyroids with reduced cellular proliferation (Lewy et al., 2013). Murine models overexpressing human PBF (PBF-Tg) in the thyroid exhibited hyperplastic and macrofollicular lesions but with no evidence of thyroid tumours (Read et al., 2011). Taken together, PTTG or PBF overexpression individually is inadequate for thyroid tumour formation.

Overall, PBF and PTTG are proto-oncogenes which are overexpressed in human thyroid cancers. PBF binds to PTTG, facilitating its entry into the nucleus, and has independent tumourigenic actions. The observation that murine models overexpressing PBF or PTTG alone in the thyroid do not develop thyroid cancers suggests that PTTG and PBF independently do not induce thyroid tumours in vivo. However, given the strong tumourigenic potential of both PBF and PTTG, and that the genes bind to each other, a murine model overexpressing both PTTG and PBF in the thyroid gland was hypothesised to develop thyroid cancer. Thus, the aim of this chapter is to describe and characterise a transgenic murine model overexpressing both PBF and PTTG in the thyroid gland.

3.2 MATERIALS AND METHODS

3.2.1 Generation of murine model

Two FVB/N murine models of targeted human PBF (hPBF) and PTTG (hPTTG) overexpression in the thyroid gland were generated by Dr. Martin Read and Dr. Gregory Lewy at the University of Birmingham. Very briefly, plasmids containing the gene of interest attached to a bovine thyroglobulin promoter and tag were injected into FVB/N embryos. The tags used for the hPBF gene and hPTTG gene were HA and FLAG respectively. These embryos were implanted into pseudo-pregnant mice and founder lines were obtained from these litters.

The murine model expressing both human PBF and PTTG in the thyroid gland was created by mating the two lines described above. The first pairing between the two different models created a mouse that was heterozygous for both PBF and PTTG (PBFHet-PTTGHet) as depicted in Figure 3-1. The subsequent mating genetics was predictably complicated because of random gene insertion(s) within the genome for the PBF and PTTG murine models. Consequently, mating of the PBF HET-PTTG HET lines had created a colony of transgenic mice with different genotypes, as seen in Figure 3-2. Our plan was to perform all our experiments on the murine model homozygous for both PBF and PTTG in the thyroid gland (BI-Trans). To achieve the objective of producing BI-Trans mice, we aimed to mate BI-Trans with BI-Trans mice, to ensure a continual supply of BI-Trans murine models shown in Figure 3-3.

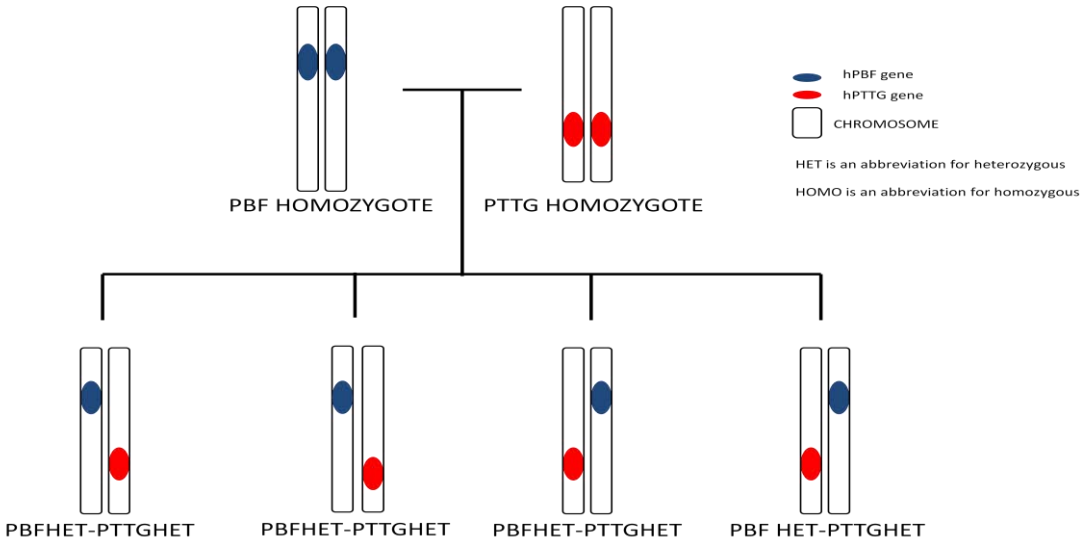

Figure 3-1 Mating genetics of PBF and PTTG homozygotes. Mating a PBF homozygote with a PTTG homozygote created a colony of PBF heterozygote – PTTG heterozygote (PBFHet-PTTGHet).

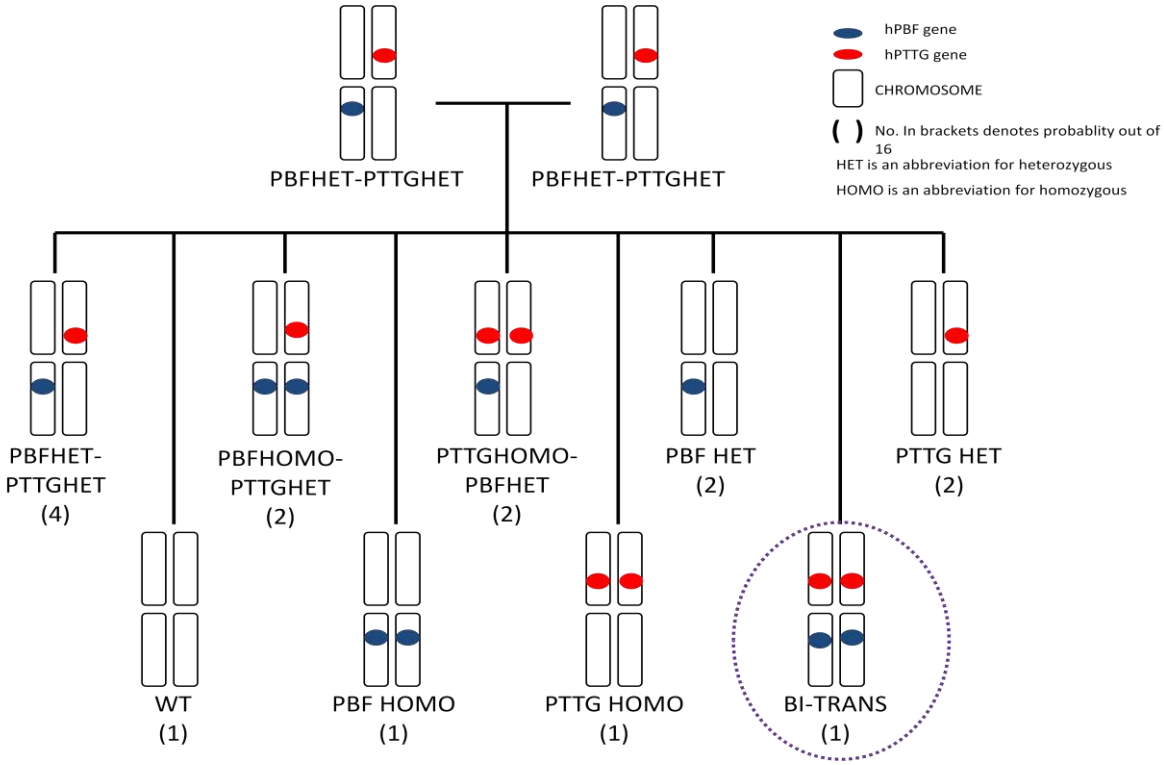

Figure 3-2 Mating genetics of PBFHet-PTTGHet. Mating PBFHet-PTTGHet with PBFHet-PTTGHet yielded a colony of mixed genotypes illustrated above. The offspring genotype pattern is caused by random PBF / PTTG gene insertion in different chromosomes during the creation of the murine models.

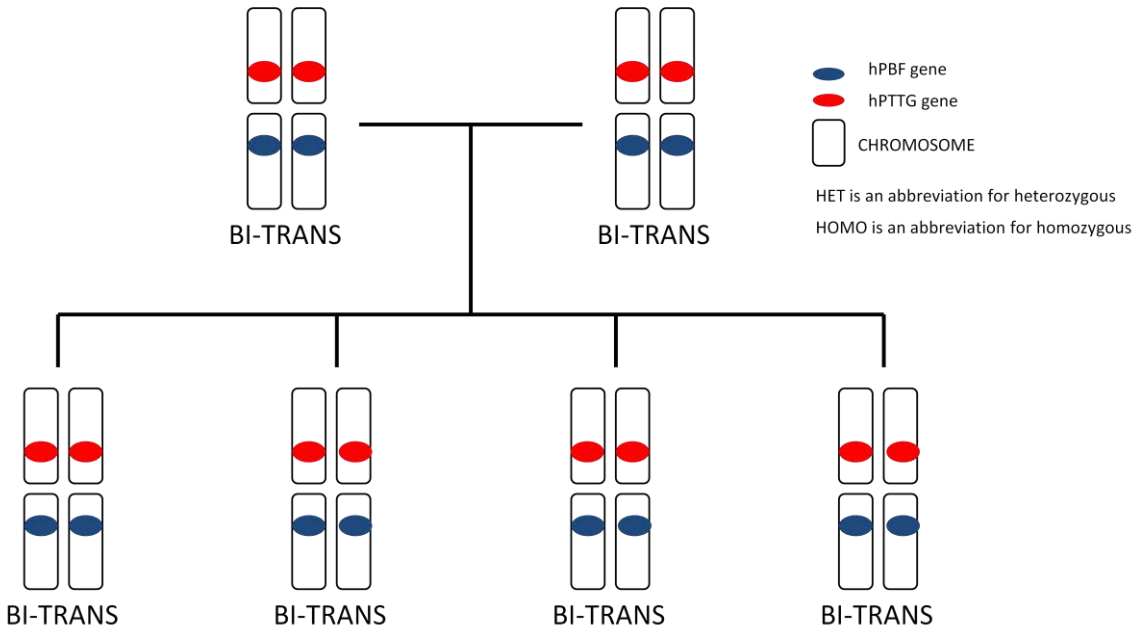

Figure 3-3 Mating genetics of BI-Trans murine models. The mating of BI-Trans models creates a colony comprising exclusively of BI-Trans offspring.

A total of 1271 mice were generate for the above study. Comparison data for the individual hPTTG and hPBF murine models were provided by Dr. Gregory Lewy and Dr. Martin Read respectively (University of Birmingham).

3.2.2 Ageing colony

To study the long term effects of PBF and PTTG overexpression in the thyroid gland, we had a separate colony of mice homozygous for PBF and heterozygous for PTTG (PBFHomo-PTTGHet). The rationale for choosing this model for this aspect of our investigation is discussed in section 3.3.2 and 3.4.2.

3.2.3 Tissue DNA extraction

DNA from ear clippings was obtained from the murine colony and extracted as per protocol described in section 2.3.

3.2.4 Zygosity screening

Zygosity determination was performed using qRT-PCR on the ABI 7500 Sequence Detection System which employs TaqMan™ chemistry for quantification of DNA levels, described previously in section 2.6. In this chapter, the target gene of interest is PBF and PTTG and hence, the appropriate primers and probes were used. The housekeeping gene for the qRT-PCR experiments in this chapter was DSCAM. The zygosity was determined based on the fold change value of the mice of unknown genotype compared to the control mice samples of known genotype.

3.2.5 Murine organ dissection

Following euthanasia of the murine model, the animal was weighed and organs dissected. Harvested organs including the thyroid gland, lungs, heart, kidney, spleen and liver were initially weighed and

stored appropriately. Organs for protein experiments were stored in liquid nitrogen and RNA experiments, in RNAlater. Microdissection for the thyroid gland was described in section 2.1.

3.2.6 **Western blot**

Protein was extracted from harvested murine organs as described in section 2.7 and used for Western blot described in section 2.8. The primary antibodies used were against human PTTG at 2 μg/ml (Invitrogen, UK) and human PBF at 1:1000 (rabbit polyclonal; manufactured in-house Dr. Turnell, University of Birmingham). Subsequent incubation with the appropriate secondary antibody conjugated to horseradish peroxidise (mouse anti-rabbit; Dakocytomation, UK) was performed for 1 hour at room temperature before being developed.

3.2.7 **Cardiac puncture**

The animal was rendered unconscious by an overdose of Sevofluorane. Cardiac puncture was carried out using a 23G needle and approximately 1ml of blood was aspirated. The sample was stored in a 1.5 ml Eppendorf at 4 °C for 24 hours. The sample was then spun at 13,200 rpm for 20 minutes. The extracted supernatant (serum) was transferred to a second 1.5 ml Eppendorf and spun at 13,200 rpm for 10 minutes. The serum was extracted again and transferred to the final Eppendorf which was stored at -80 °C prior to usage.

3.2.8 **Thyroid function test**

Murine thyroid stimulating hormone (TSH) levels were determined by the laboratory of Professor Samuel Refetoff at the University of Chicago. Technical details of this assay has been published previously (Pohlenz et al., 1999).

Total T_3 and T_4 levels were measured using a radioimmunoassay technique (MP Biomedicals thyroid radioimmunoassay kit). Briefly, murine serum and radiolabelled tracer solution were added to tubes coated with either T_3 or T_4 antibodies. The analyte and radiolabelled tracer compete for limited antibody binding sites. Radioactivity level, inversely proportional to analyte concentration, was quantified using a gamma counter. Finally, the concentration of T_3 and T_4 was determined by interpolation from a standard curve of percentage of trace level versus µg/dL T_3 or T_4.

3.2.9 **Histology**

Murine thyroids were fixed in formalin and sent to the Pathology Department at University Hospital Birmingham NHS Trust for processing (courtesy of Dr. Adrian Warfield). Tissue samples were embedded in paraffin and sectioned to produce slides. Slides were stained with Haematoxylin and Eosin (H&E).

3.3 RESULTS

3.3.1 Validation of the murine model

We generated a murine model which was homozygous for both PBF and PTTG in the thyroid gland only (BI-Trans). We confirmed the overexpression of PBF and PTTG in the thyroid gland of the BI-Trans model. We compared the expression of PBF and PTTG in the thyroid gland of the various murine models used in our experiments; wild-type (WT), PBF (homozygous for PBF), PTTG+/+ (homozygous for PTTG) and BI-Trans. The Western blot below (Figure 3-4) confirmed the overexpression of hPBF in the PBF and BI-Trans models and hPTTG in the PTTG+/+ and BI-Trans models (n=4). PBF appeared as a band between 25kDa and 37kDa and PTTG was expressed as a band around 29 kDa. The overexpression of hPBF did not appear to increase PTTG protein. Conversely, the overexpression of hPTTG did not upregulate the protein expression of endogenous PBF as seen in Figure 3.4.

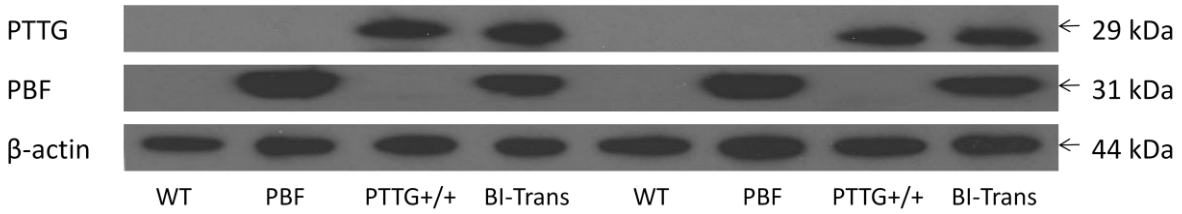

Figure 3-4 Western blot showing the expression of hPBF and hPTTG in WT, PBF, PTTG+/+ and BI-Trans thyroids (n=4 for each genotype; figure shows n=2 for each genotype).

Next, we used the PBFHomo-PTTGHet model (homozygous for PBF and heterozygous for PTTG) to determine the expression of our genes of interest, PBF and PTTG, in the thyroid, heart, lung, liver, spleen and kidney. The reasons for this is discussed in section 3.3.2 and 3.4.2 below. The murine PBFHomo-PTTGHet thyroids overexpressed human PBF and human PTTG in the thyroid gland only and not in the lung, liver, spleen and kidney. A β-actin result in the heart was difficult to obtain as

demonstrated in Figure 3.5 because of its fibrous nature. This was consistent with our previous experience with the heart ~~organ~~ on Western blot (unpublished).

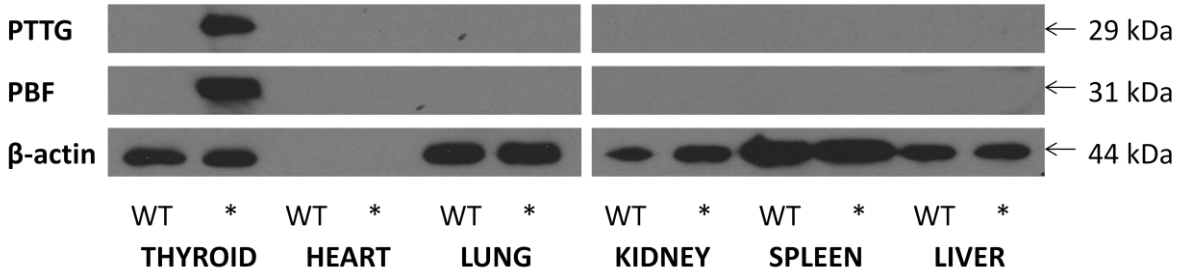

Figure 3-5 Western blot showing the expression of hPBF and hPTTG in PBFHomo-PTTGHet (*) in various organs (n=1) compared to wild type (WT).

3.3.2 **Reduced mortality in founder BI-Trans models**

Seven PBFHet-PTTGHet breeding pairs were set up to create founder lines. Genotype was determined from ear-clippings using qRT-PCR, described above. Offspring genotype followed Mendelian genetic principles as shown in Figure 3-2, in expected ratios. Early bi-transgenic (BI-Trans) founder members homozygous for both PBF and PTTG, were put in breeding pairs.

Interestingly, early BI-Trans founder members had reduced mortality compared to PBFHomo-PTTGHet. In a cohort of breeding pairs over a period of 200 days, 64.3% of Bi-Trans mice died or were culled due to illness (n=27). In comparison, the mortality rate in the PBFHomo-PTTGHet genotype was 17.9 % over the same period of time (n=5). The Bi-Trans murine model had an average lifespan of 150.9 ± 1.0 days (n=53). The average lifespan of a PBFHomo-PTTGHet model was 477.9 ± 2.9 days (n=89). There was a statistically significant difference between the mortality rates of BI-Trans (Wilcoxon and log-rank $p<0.0001$) and PBFHomo-PTTGHet (Wilcoxon $p=0.041$; log-rank $p=0.021$) models compared to wild-type. The Kaplan-Meier survival plot for the different genotypes is

illustrated in Figure 3-6. Post-mortem examination did not reveal any macroscopic cause of death. Histological examination of the thyroid gland did not reveal any obvious tumours.

When comparing the mortality rates between various murine models, PBF and PTTG +/- had similar survival rates to wild-type. The survival of BI-Trans was significantly worse than PTTG +/+ (Wilcoxon p=0.011; log-rank 0.006). PTTG +/+ mortality was worse than PBFHomo-PTTGHet. Hence, for further validation work in this chapter, we used the PBFHomo-PTTGHet model for demographic data collection. Moreover, the PBFHomo-PTTGHet model overexpressed large amounts of both PBF and PTTG in the thyroid gland.

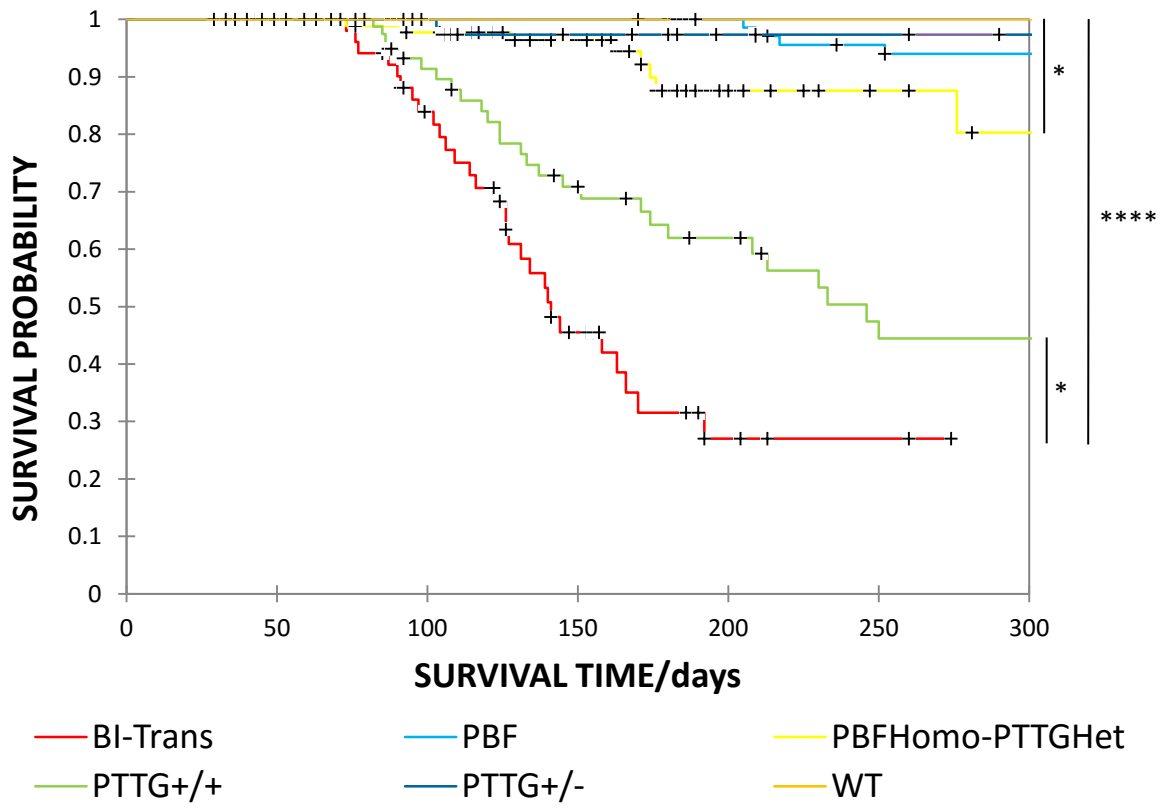

Figure 3-6 Kaplan-Meier survival plot of various murine genotypes according to genotype. If 0.01 < Wilcoxon p-value ≤ 0.05 (*) and Wilcoxon p-value ≤ 0.0001 (****). n=53 (BI-Trans), n=89 (PBFHomo-PTTGHet), n=82 (PBF), n=108 (PTTG+/+), n=129 (PTTG+/-) and n=30 (WT).

3.3.3 Mice overexpressing both PBF and PTTG in the thyroid gland have reduced fertility

A total of 1271 mice of varying genotypes were raised in the colony. We defined fertility by the time to breed, litter size and number of litters. The average mating time for wild-type with wild-type pairings (WT^2) was 173.00 ± 8.40 days (n=9 pairs), PBF with PBF (PBF^2) was 166.17 ± 7.55 days (n=12 pairs), PBFHomo-PTTGHet with PBFHomo-PTTGHet ($PBFHomo\text{-}PTTGHet^2$) was 146.5 ± 10.82 days (n=10 pairs), PBFHomoPTTGHet with BI-Trans (PBFHomo-PTTGHet x BI-Trans) was 142.23 ± 22.62 days (n=41 pairs). There was no statistical difference between the breeding times for the various genotypes compared to the WT^2 apart from the BI-Trans with BI-trans pairing ($BI\text{-}Trans^2$; p=0.003; n=2 pairs) which had a reduced breeding time because of increased mortality. The breeding time for the various genotype breeding pairings are shown in Figure 3-7.

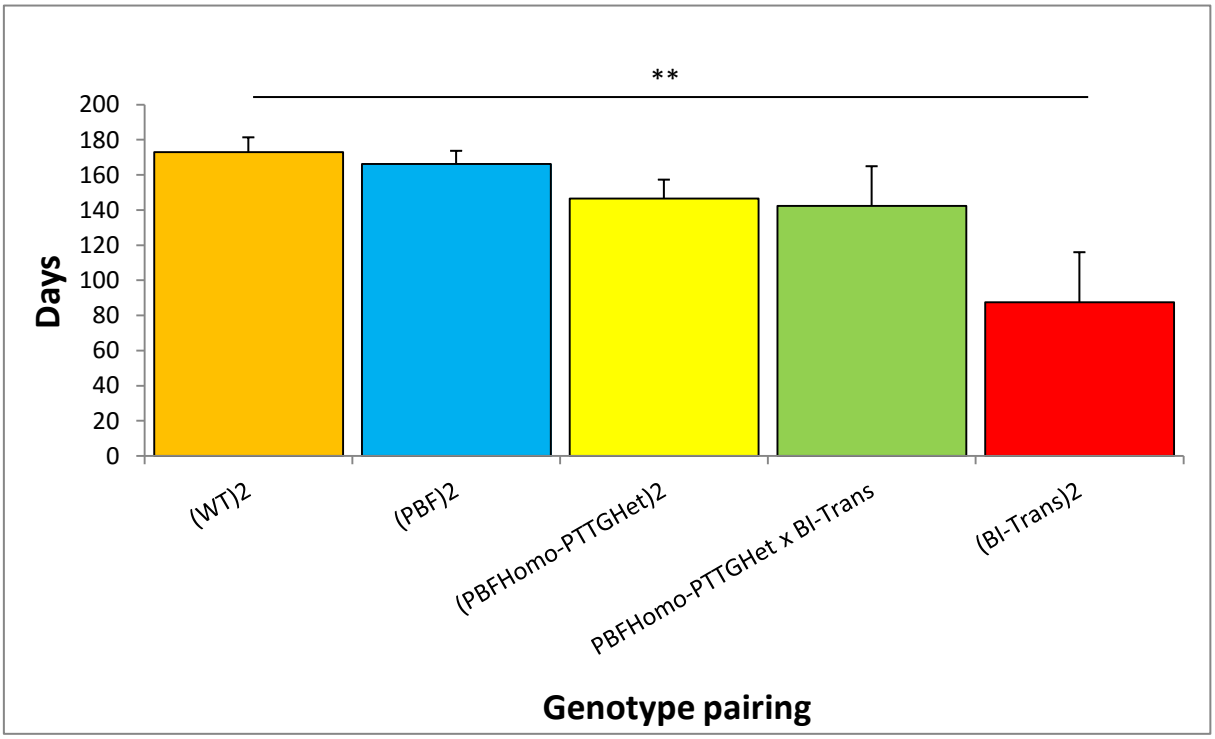

Figure 3-7 Average mating period by genotype pairing. The breeding time between BI-Trans and BI-Trans, ($BI\text{-}Trans^2$) was statistically significant (p=0.003; n=2 pairs). The numbers for each genotype pairing was as follows; n=9 pairs (WT^2), n=12 pairs (PBF^2), n=10 pairs ($PBFHomo\text{-}PTTGHet^2$) and n=41 pairs (PBFHomo-PTTGHet x BI-Trans).

Over the duration of their breeding life, approximately 6 months, mice overexpressing both PBF and PTTG in the thyroid gland, irrespective of homo- or heterozygosity, have a fewer number of litters compared to wild type pairings (WT^2). The PBFHomo-PTTGHet and PBFHomo-PTTGHet pairing ($PBFHomo\text{-}PTTGHet^2$) produced more litters than the PBFHomo-PTTGHet x BI-Trans pairing (1.65 ± 0.20; n=46), shown in Figure 3-8. The average number of litters for the $PBFHomo\text{-}PTTGHet^2$ pairing was 3.39 ± 0.30 (n=23) compared to the wild type-wild type pairing which produced 5.67 ± 0.33 litters (n=9) and this was statistically significant (p=0.0002). The PBF mouse pairing (PBF2) had a similar number of litters as WT^2 producing an average of 5.75 ± 0.30 litters (n=12) over the same period.

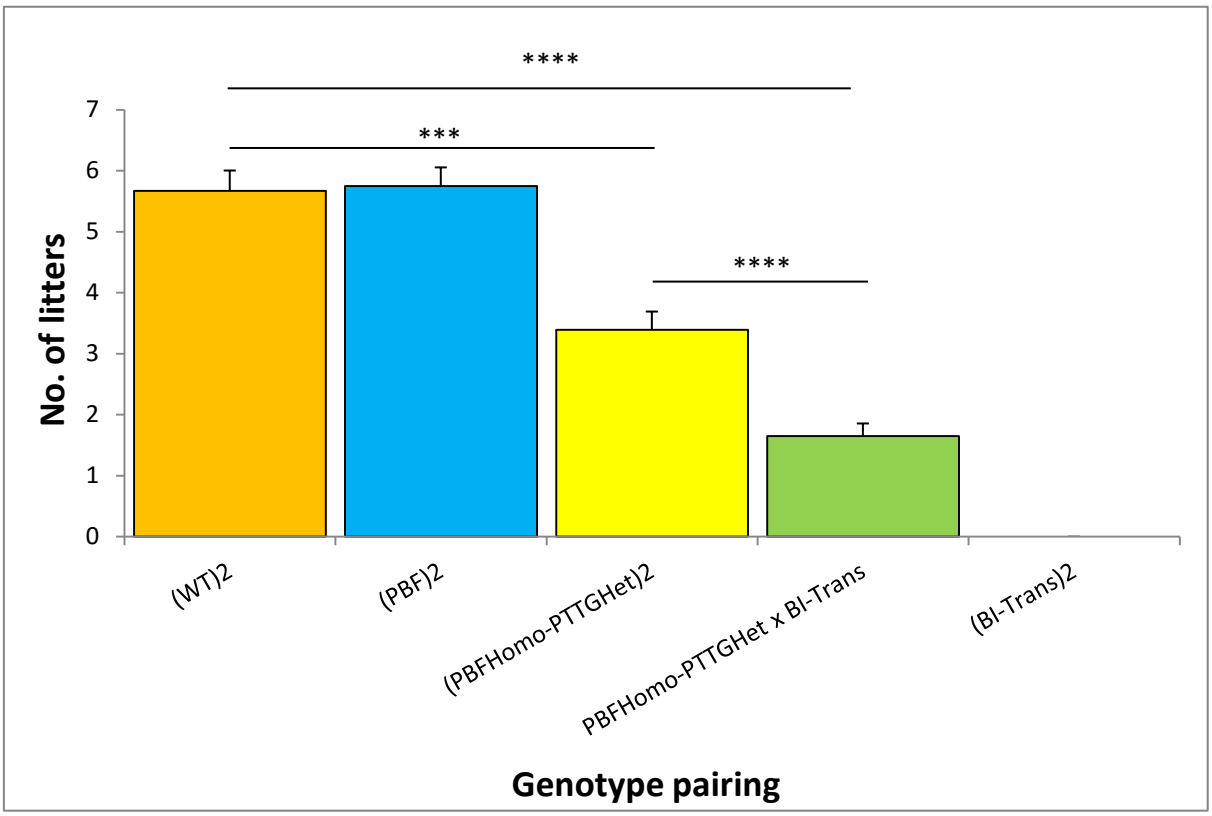

Figure 3-8 Average number of litters by genotype pairing. The WT^2 (n=9) and PBF^2 (n=12) pairing produced similar number of litters over their breeding period. The $PBFHomo\text{-}PTTGHet^2$ pairing (n=23) had fewer number of litters compared WT^2 (p=0.0002) but more than the PBFHomo-PTTGHet x BI-Trans pairing (n=46; p<0.00001).

The average litter size by genotype pairing is illustrated in Fig. 3-9. There was no statistical difference between the size of litter in the WT^2 (9.31 ± 0.36; n=51), PBF^2 (8.91 ± 0.25; n=64) and PBFHomo-$PTTGHet^2$ (8.69 ± 0.34; n=78) pairings. However, when a BI-Trans was introduced into the mating combination (PBFHomo-PTTGHet x BI-Trans), the litter size reduced significantly to 5.53 ± 0.36 ($p<0.00001$ compared to both WT^2 and PBFHomo-$PTTGHet^2$; n=86).

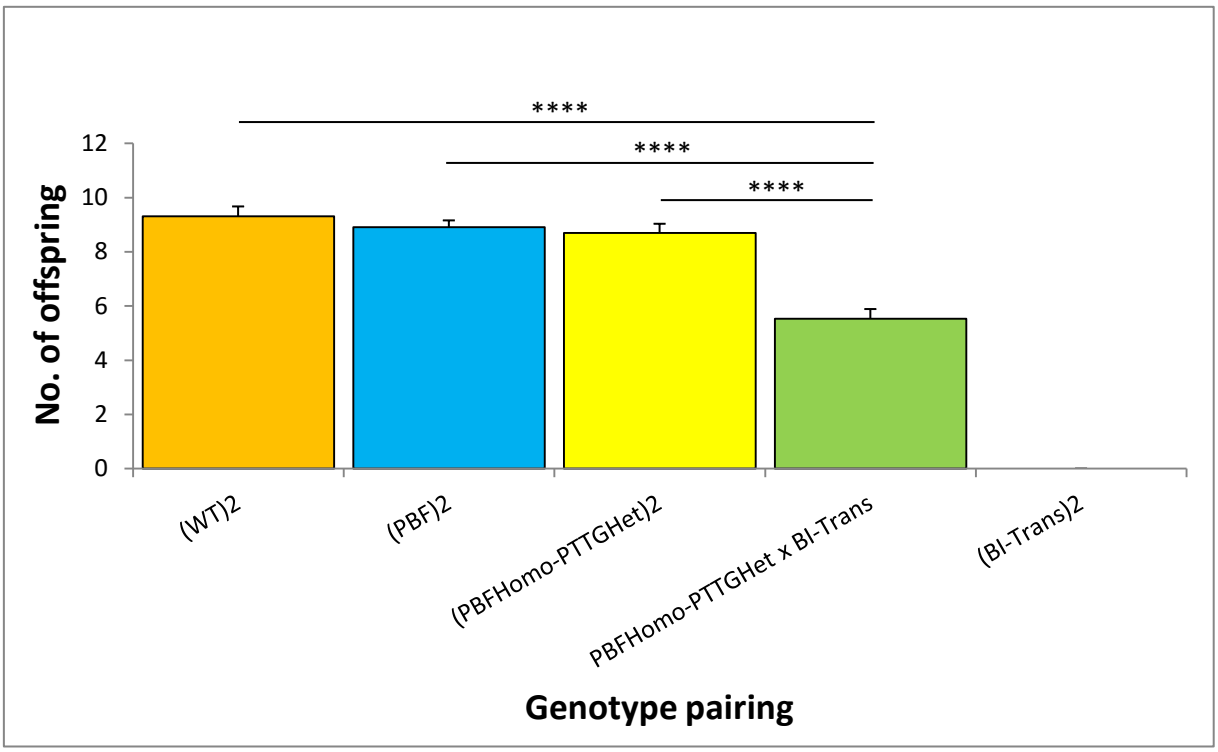

Figure 3-9 Average size of litter by genotype. The litter size for the WT^2 (n=51), PBF^2 (n=64) and PBFHomo-$PTTGHet^2$ (n=78) pairings were comparable. There was a statistically significant difference between the litter size from the PBFHomo-PTTGHet x BI-Trans pairing compared to WT^2 ($p<0.00001$) and PBFHomo-$PTTGHet^2$ pairings.

The average time for the pairing to yield its first litter was 27.22 ± 2.74 days for WT^2 (n=9), 23.58 ± 1.15 days for PBF^2 (n=12), 33.64 ± 4.48 days for PBFHomo-$PTTGHet^2$ (n=22) and 33.86 ± 2.37 days for PBFHomo-PTTGHet x BI-Trans (n=36) as shown in Figure 3-10. There was no statistical difference between WT^2 and PBF^2 (p=0.194), between WT^2 and PBFHomo-$PTTGHet^2$ (p=0.385) and between WT^2 and PBFHomo-PTTGHet x BI-Trans (p=0.187).

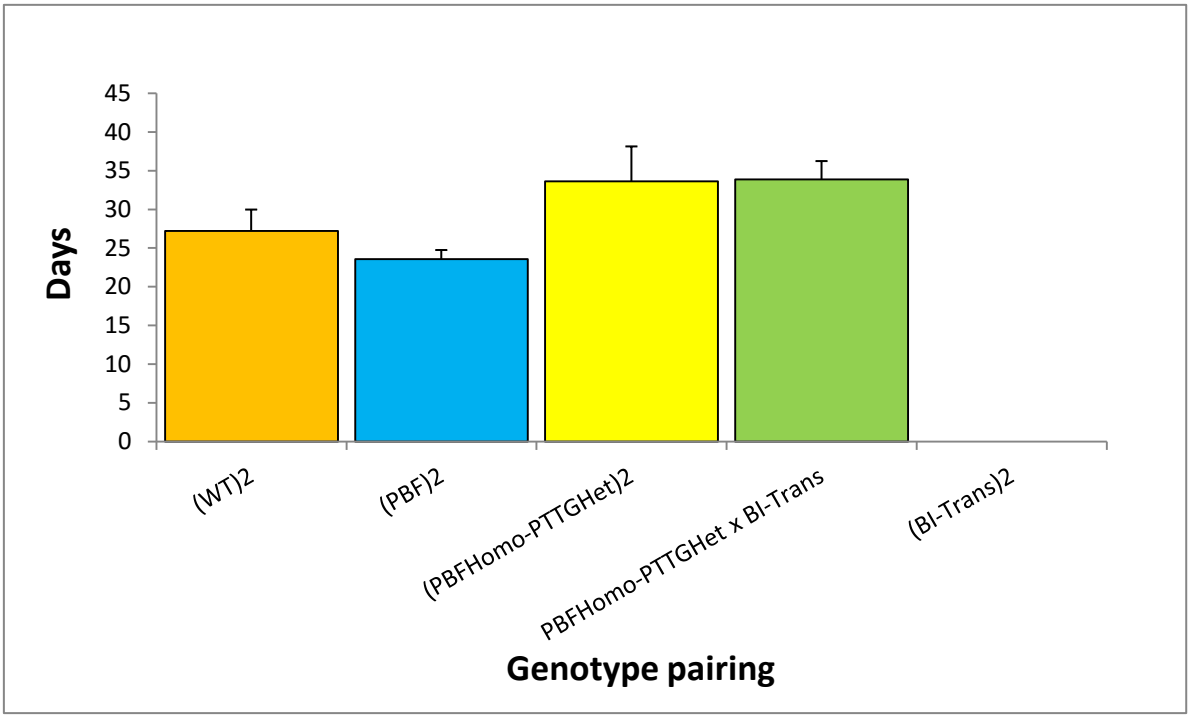

Figure 3-10 Average time to yield first litter by genotype pairing. There was no statistical difference between all genotype pairings. The numbers for each genotype group include n=9 for WT^2, n=12 for PBF^2, n=22 for PBFHomo-$PTTGHet^2$ and n=36 for PBFHomo-PTTGHet x BI-Trans.

Overall, the PBF murine model have similar fertility to wild type (WT). The PBFHomo-$PTTGHet^2$ pairing had reduced litter numbers compared to the WT^2 pairing over the same breeding period. When the PBFHomo-PTTGHet mouse was bred with the BI-Trans mouse, the combination had reduced litter size and number. Interestingly, BI-Trans male and female mating pairs did not produce any offspring

over a mating period of 87.5 ± 28.5 days (n=2 pairs). When BI-Trans mice were mated with PBFHomo-PTTGHet, it was observed that fertility was limited by the presence of a BI-Trans male, suggesting that the BI-Trans male is infertile whilst the BI-Trans female is semifertile. Thus, the main breeding pairs used to maintain the colony and generate BI-Trans mice were PBFHomo-PTTGHet with PBFHomo-PTTGHet (PBFHomo-PTTGHet^2) and male PBFHomo-PTTGHet with female BI-Trans (PBFHomo-PTTGHet x Bi-Trans).

3.3.4 **Bi-Trans and PBFHomo-PTTGHet murine models develop goitres**

We commenced thyroid and body weight data collection from 6 weeks, an age when the transgenic murine models were considered fully grown. The thyroid from the murine model homozygous for PBF and heterozygous for PTTG (PBFHomo-PTTGHet) increased in weight until 12 months, after which, the thyroid weight was essentially stable and in males, atrophied slightly (Figure 3-11A). In the wild-type mice (WT), thyroid weight was essentially stable from 6 weeks as shown in Figure 3-11B. This gradual increase in thyroid weight closely mirrors the trend observed in PBF mice seen in Figure 3-11C. Body weight data revealed an overall increase in murine body weight over time, with males being slightly heavier than their female counterparts up to 6 months. After 12 months, female PBFHomo-PTTGHet and WT mice were heavier than males (Figure 3.11).

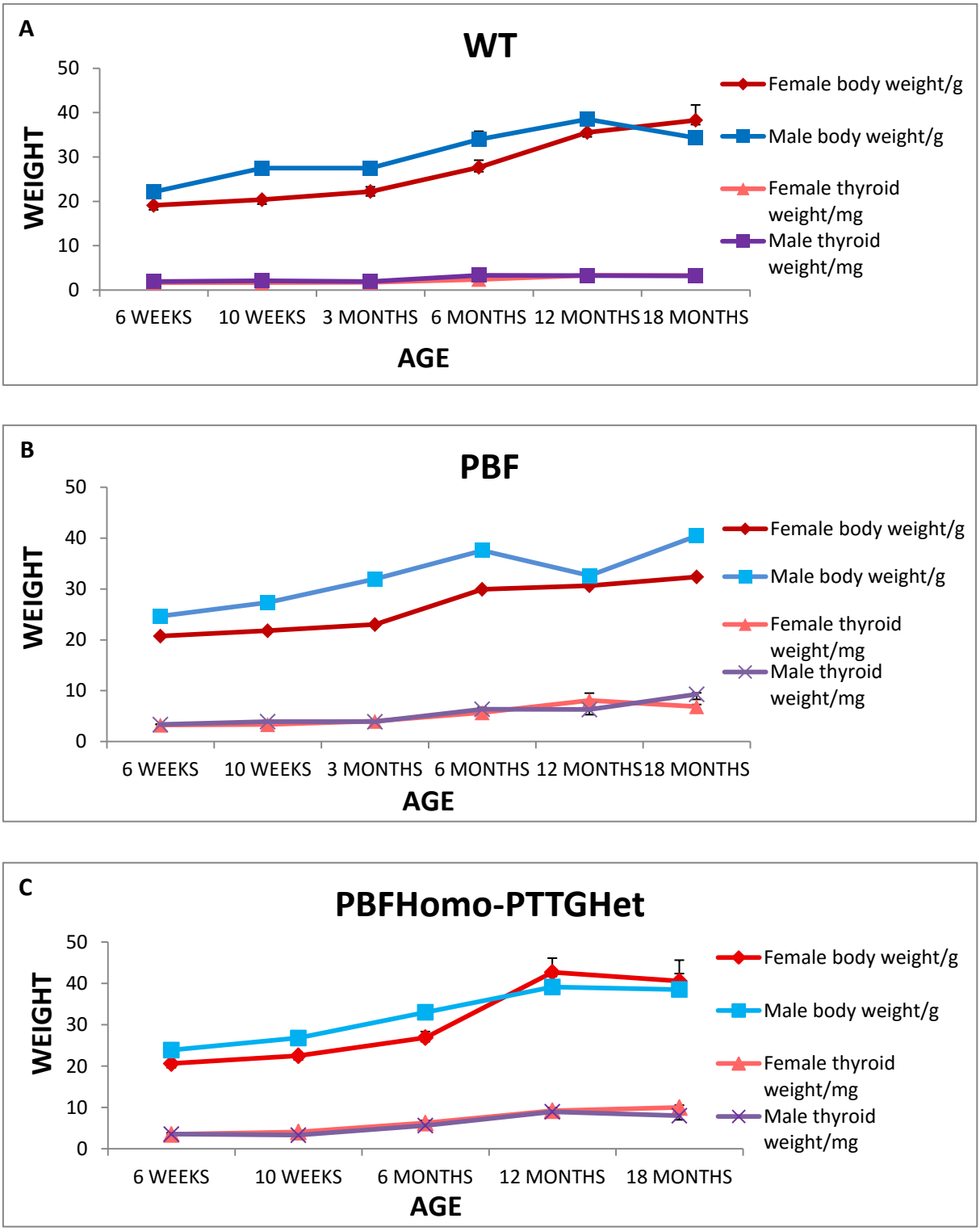

Figure 3-11 Graphs for body and thyroid weight by gender and genotype. The thyroid growth trend of the PBFHomo-PTTGHet model (C) closely follows the thyroid growth trend of the PBF (B) mouse. Body weight data confirmed that male murine models are heavier than their female counterparts up to 6 months in WT (A), PBF and PBFHomo-PTTGHet.

We next compared the thyroid weights by time across the genotypes. At 6 weeks, shown in Figure 3-12, the PBFHomo-PTTGHet ~~mean~~ thyroid weight was 3.5 mg (n=1) in females and 3.58 ± 0.35 mg (n=8) in males. The PBFHomo-PTTGHet thyroid weight was significantly larger than WT mice where the mean thyroid weight was 1.68 ± 0.04 mg (n=42) for females and 1.91 ± 0.06 (n=35) for males ($p<0.0001$ in males) at 6 weeks. The p-value was not calculatable in females because n=1 for PBFHomo-PTTGHet at 6 weeks. There was no significant difference between the thyroid weight of PBF, females (3.24 ± 0.11 mg; n=46) and males (3.35 ± 0.09; n=40) compared to PBFHomo-PTTGHet female (non-calculatable p-value) and males (p=0.38 in males). PTTG heterozygotes (PTTG+/-), thyroid weights at this timepoints were 1.42 ± 0.10 mg (n=5) in females and 1.79 ± 0.09 mg (n=20) in males at 6 weeks.

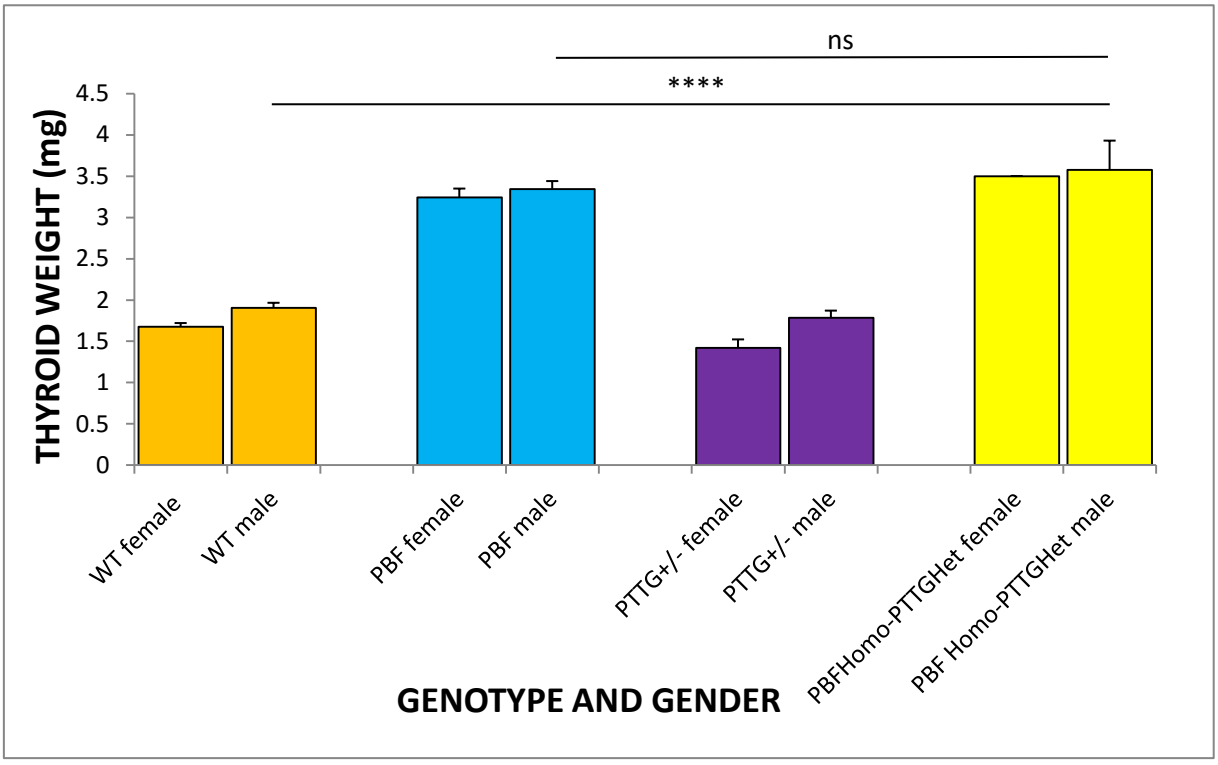

*Figure 3-12 Thyroid weight by gender and genotype at 6 weeks. **** denotes a p-value of <0.0001 and ns denotes p-value > 0.05.*

PBFHomo-PTTGHet thyroid weights were 4.09 ± 0.20 mg (n=12) in females and 3.33 ± 0.28 mg (n=8) in males at 10 weeks (p=0.031 between genders). At 10 weeks, the thyroid weight for WT was 1.68 ± 0.10 mg (n=8) in females and 2.10 ± 0.10 mg (n=9) in males. Again, there was a statistical difference between WT and PBFHomo-PTTGHet thyroid weight at 10 weeks (p<0.0001 females; p=0.0005 males) as shown in Figure 3-13. Comparing PBFHomo-PTTGHet with PBF thyroids, PBF thyroid weight was significantly larger at 3.35 ± 0.18 mg (n=13; p=0.01) in females but not in males (3.93 ± 0.23 mg; n=14; p=0.121) at 10 weeks. No PTTG+/- data was available for this timepoint.

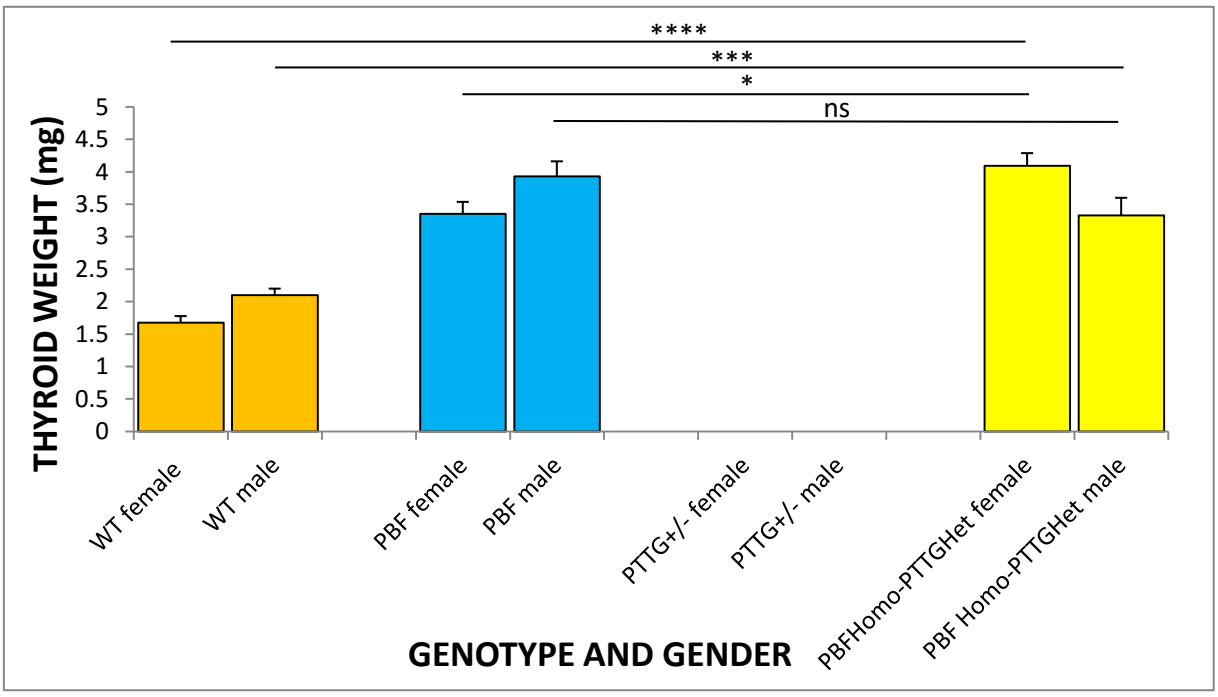

*Figure 3-13 Thyroid weight at 10 weeks by genotype and gender. PTTG+/- data was not available at 10 weeks. p-values are denoted with * if 0.01 < p ≤ 0.05, *** if 0.0001 < p ≤ 0.001, **** if p ≤ 0.0001 and ns if p>0.05.*

The PBFHomo-PTTGHet female (n=6) and male (n=6) thyroid weights were 6.25 ± 0.64 mg and 5.65 ± 1.04 mg respectively at 6 months shown in Figure 3-14. The WT thyroid weight was 2.40 ± 0.15 mg (n=3) in females and 3.33 ± 0.09 mg (n=3) in males. There was a statistical difference between the female PBFHomo-PTTGHet and WT thyroid weight (p=0.004) but no difference in males (p=0.172). PBF thyroid weights were 5.68 ± 0.43 mg (n=6) in females and 6.37 ± 0.35 mg (n=9) in males at 6 months. These were statistically not significant when compared to PBFHomo-PTTGHet (p=0.477 in females and p=0.460 in males). Finally, PTTG+/- thyroid weights at 6 months were 2.4 ± 0.46 mg (n=5) in females and 2.65 ± 0.07 mg (n=8) in males.

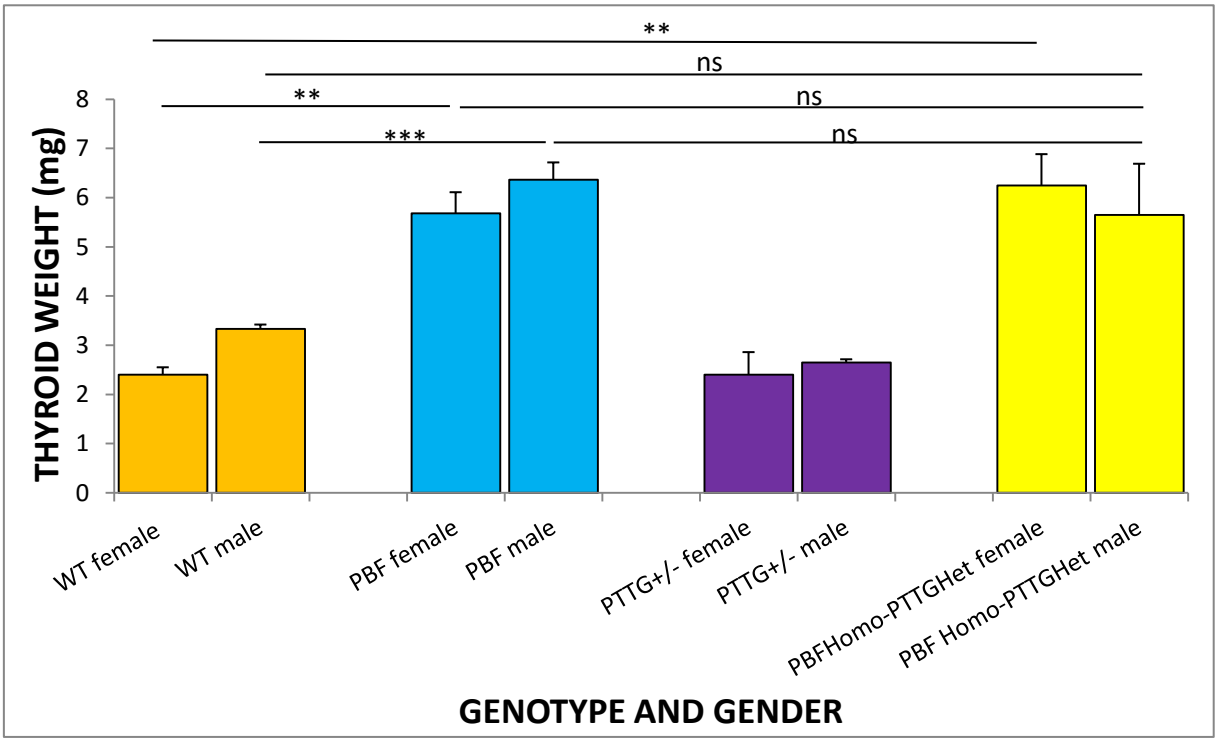

*Figure 3-14 Thyroid weights by genotype and gender at 6 month. p-values are denoted with ** (0.001 < p ≤ 0.01), *** (0.0001 < p ≤ 0.001) and ns (p>0.05).*

Thyroid weights at 12 months is shown in Figure 3-15. At 12 months, female PBFHomo-PTTGHet thyroids were 9.24 ± 0.74 mg (n=5) and male PBFHomo-PTTGHet thyroids were 8.98 ± 0.93 mg (n=6). The PBFHomo-PTTGHet thyroids were significantly larger (p=0.001 females; p<0.0001 males) than their WT counterparts in which the thyroid size was 3.3 ± 0.29 mg (n=3) in females and 3.24 ± 0.17 mg (n=7) in males. PTTG+/- thyroids were 2.9 ± 0.15 mg (n=3) in females and 2.6 mg (n=1; standard deviation not calculable) in males at 12 months. PBFHomo-PTTGHet thyroids were similar in size to wild-type thyroids at 12 months (p=0.687 females; p=0.138 males). Female PBF thyroids at 12 months were 8.1 ± 1.43 mg (n=12) and male PBF thyroids were 6.3 ± 1.08 mg (n=13).

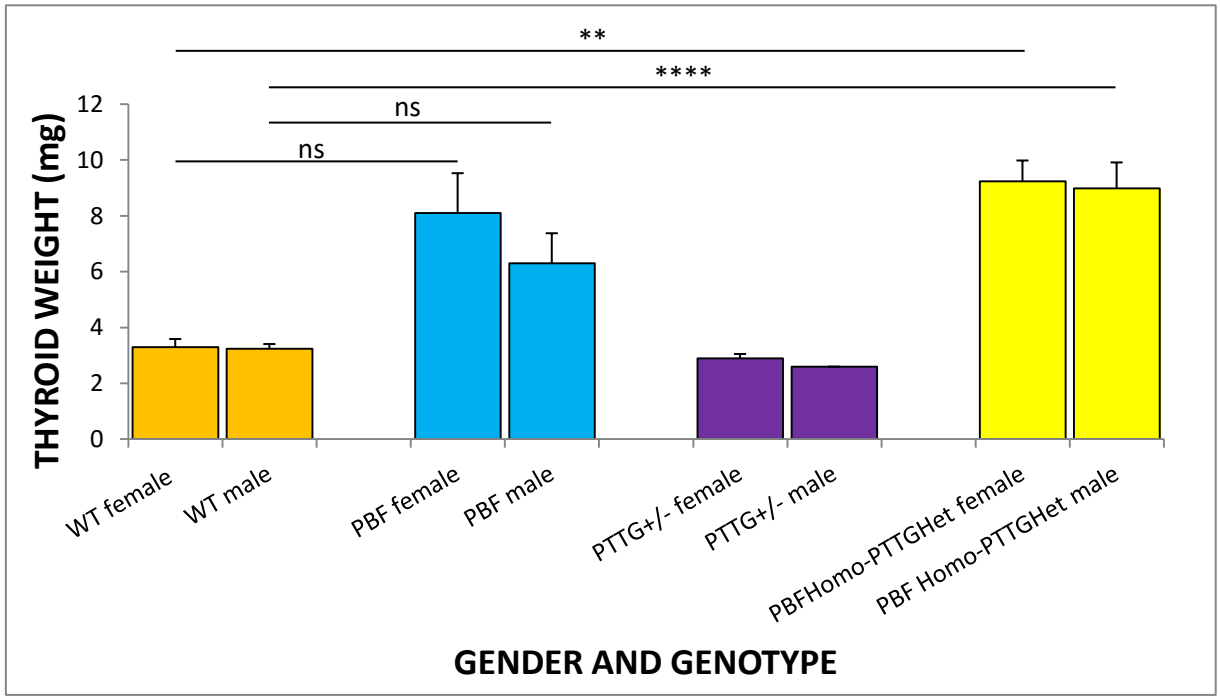

*Figure 3-15 Thyroid weight by gender and genotype at 12 months. p-values are denoted with ** (0.001 < p ≤ 0.01), **** (p ≤ 0.0001) and ns (p>0.05).*

Finally, thyroid weights of the different genotypes at 18 months is shown in Figure 3-16. In comparison with WT thyroids (female, 3.25 ± 0.30 mg, n=4; male, 3.2 ± 0.24 mg, n=4), PBFHomo-PTTGHet thyroids were significantly larger (female 10.00 ± 0.58 mg, $p<0.0001$, n=6; male 8.03 ± 0.37 mg, $p<0.0001$, n=6). The size of PBFHomo-PTTGHet thyroids were larger than PBF thyroids (female 6.87 ± 0.42 mg, n=9; male 9.3 ± 0.29 mg, n=12) at 18 months. PTTG heterozygote (PTTG+/-) thyroids at 18 months were similar in size to WT thyroids, 3.00 mg (n=1; standard error of mean not calculatable) in females and 2.85 ± 0.15 (n=2) in males.

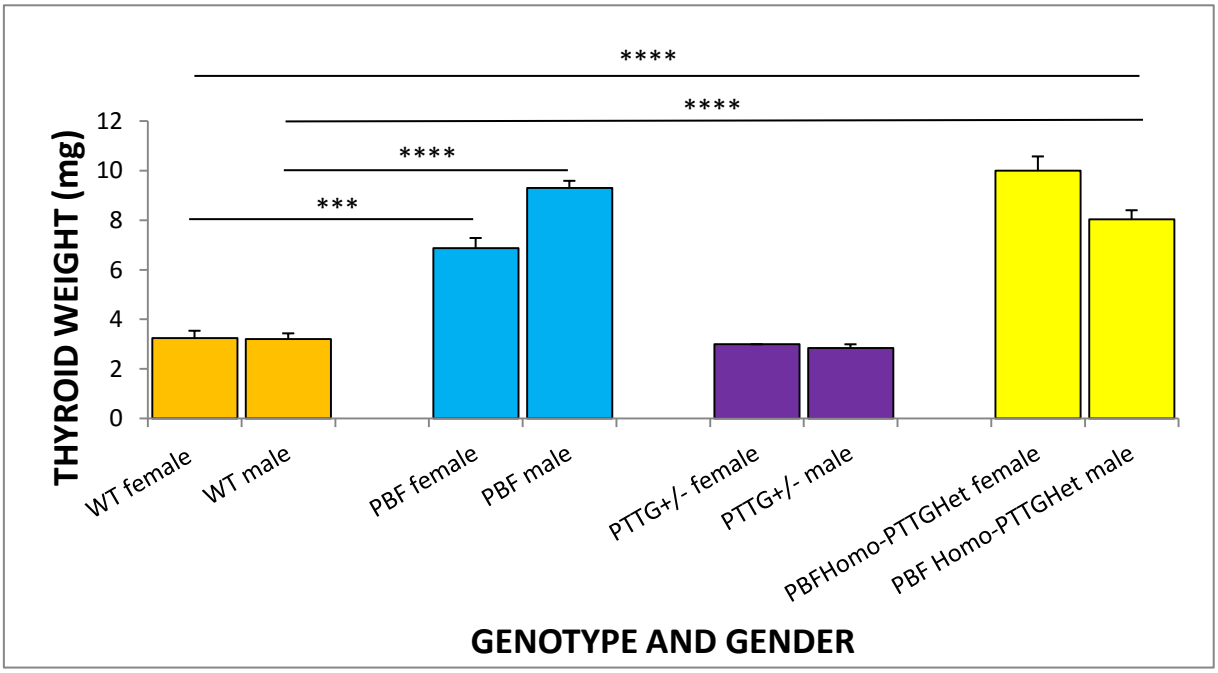

*Figure 3-16 Thyroid weights at 18 months by gender and genotype. p-values are denoted with *** if $0.0001 < p \leq 0.001$ and **** if $p \leq 0.0001$.*

Overall, mice that were homozygous for PBF and heterozygous for PTTG (PBFHomo-PTTGHet) had larger thyroids compared to wild-type (WT) from as early as 6 weeks. This trend of thyroid enlargement was also seen in PBF mice. The PTTG heterozygote mouse (PTTG+/-) had thyroid sizes similar to WT.

3.3.5 Thyroid hormone levels in transgenic murine models

Next, we determined whether large thyroids (goitre) in the murine model homozygous for PBF and heterozygous for PTTG (PBFHomo-PTTGHet) was associated with aberrant thyroid hormone levels. High thyroid stimulating hormone (TSH) levels can stimulate thyroid tissue proliferation. Hence, T3, T4 and TSH levels were determined for the PBFHomo-PTTGHet model at 6 weeks, 6 months, 12 months and 18 months.

T3 levels maintained a constant level throughout the age range, shown in Figure 3-17. Interestingly the mean T3 levels of 6 week PBFHomo-PTTGHet females were 160.19 ± 6.45 ng/dL (n=6) compared to males at 234.66 ± 9.54 ng/dL (n=6). The difference was statistically significant, $p<0.0001$. This statistically significant intergender difference in T3 levels in PBFHomo-PTTGHet was again observed at the 6 month time point; female mice showed a mean T3 of 128.85 ± 5.54 ng/dL (n=6) compared with males, who showed a mean T3 of 162.45 ± 2.99 ng/dL (n=5). Subsequently, at 12 and 18 months there was no significant difference in T3 levels between genders. Overall, there was little variation in T3 levels over a time period of 18 months.

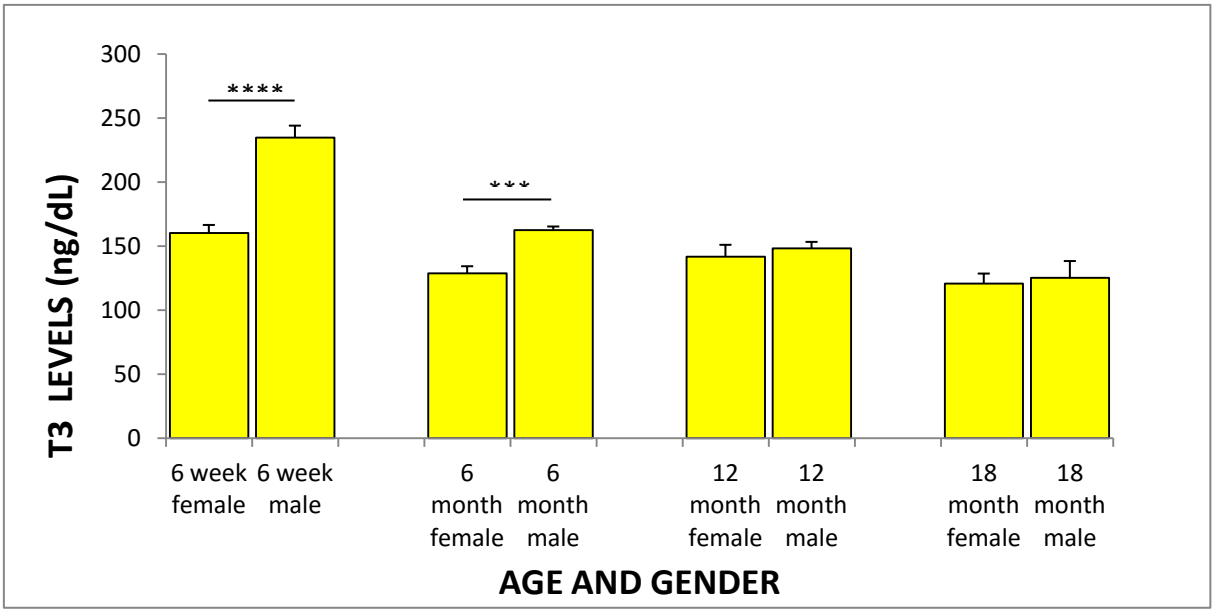

*Figure 3-17 T3 levels in PBFHomo-PTTGHet mice by gender and age. p-values are denoted with *** for $0.0001 < p \leq 0.001$ and **** for $p \leq 0.0001$.*

T4 levels between male and female PBFHomo-PTTGHet mice at 6 weeks, 6 months, 12 months and 18 months were similar and not statistically significant. The PBFHomo-PTTGHet T4 levels demonstrated an overall increase over an 18 month period. The mean T4 level in the PBFHomo-PTTGHet female at 6 weeks was 2.08 ± 0.36 µg/dL (n=5) compared to the 18 month female with a mean of 6.11 ± 1.19 µg/dL (n=4); p=0.009. There was a statistical difference in T4 levels (p=0.0007) between the 6 week and 18 month PBFHomo-PTTGHet male (2.98 ± 0.32 µg/dL (n=6) and 11.20 ± 1.83 µg/dL (n=4) respectively) as shown in Figure 3-18.

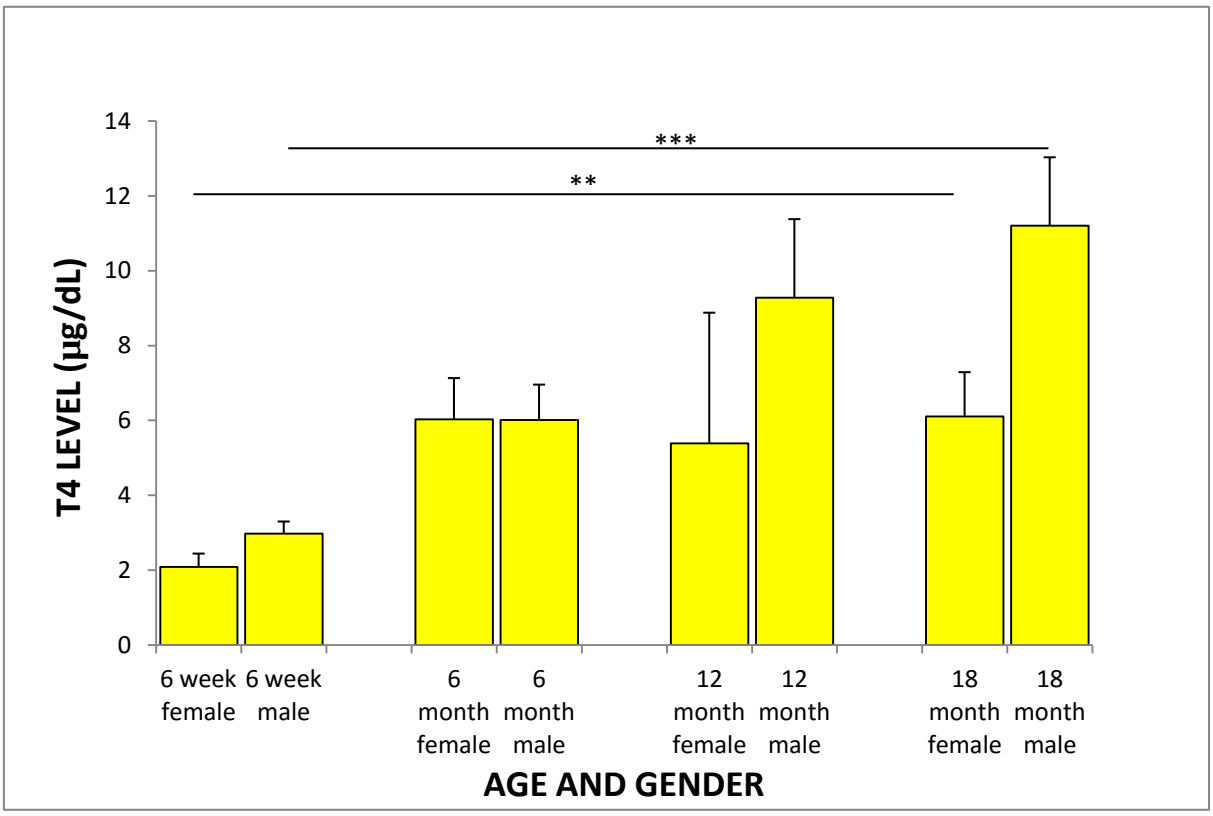

*Figure 3-18 T4 levels PBFHomo-PTTGHet by age and gender. p-values are denoted with ** for $0.001 < p \leq 0.01$ and *** for $0.0001 < p \leq 0.001$.*

We next compared the TSH, T3 and T4 levels across the different genotypes at 6 week and 12 month time points. Mean T3 levels for female PBFHomo-PTTGHet at 6 weeks (160.19 ± 6.45 ng/dL; n=6) were comparable (p=0.23) to wild type (142.34 ± 11.19 ng/dL; n=8. T3 levels in PBFHomo-PTTGHet males at 6 weeks (mean 234.66 ± 9.54 ng/dL; n=6) were significantly higher (p=0.001) than their wild type counterparts (mean 166.32 ± 11.44 ng/dL; n=11), as shown in Figure 3-19.

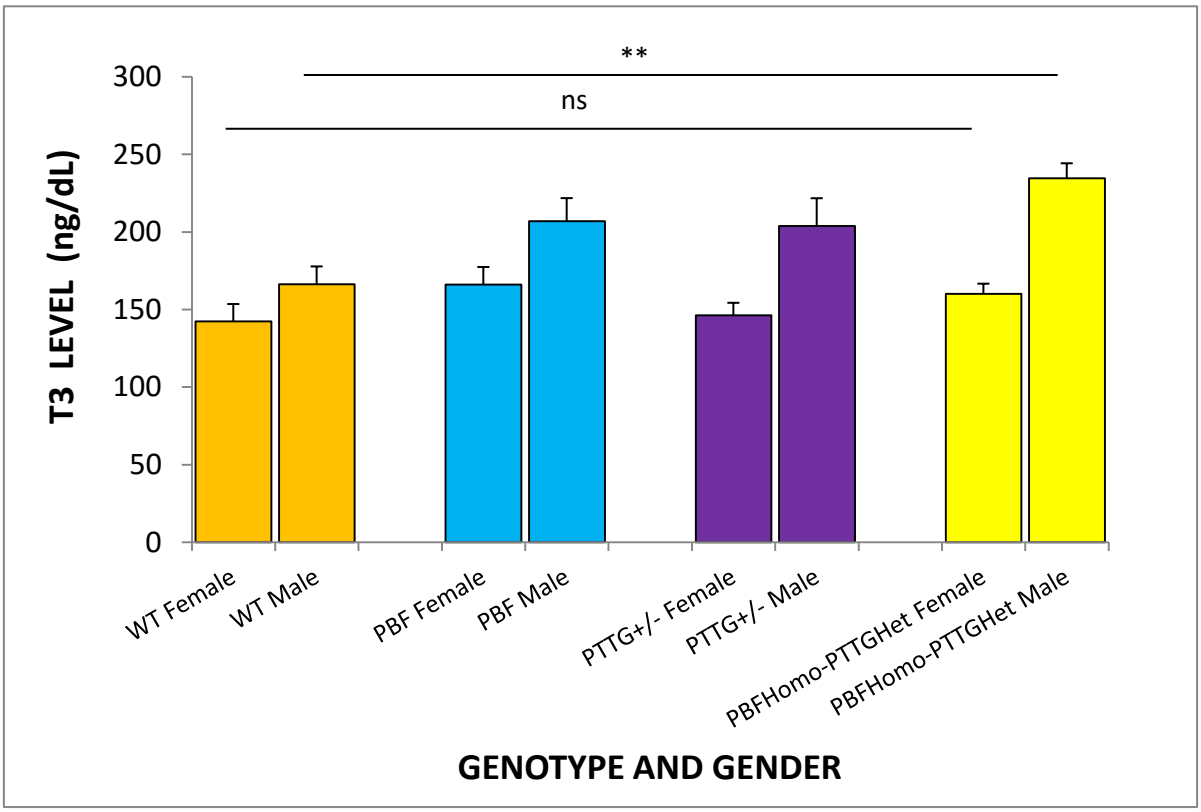

*Figure 3-19 T3 levels by genotype and gender at 6 weeks. p-values are denoted with ** ($0.001 < p \leq 0.01$) and ns ($p > 0.05$).*

PBFHomo-PTTGHet T4 levels (female: 2.96 ± 0.92 mcg/dL, n=6 ; male: 2.98 ± 0.41 mcg/dL, n=6) were comparable to wild type (female: 3.34 ± 0.50 mcg/dL, n=9 ; male: 2.59 ± 0.79 mcg/dL, n=11) at 6 weeks (female p=0.71 ; male p=0.74). However, PTTG heterozygote (PTTG+/-) mice had increased T4 levels at 6 weeks; with mean levels of 5.34 ± 1.45 mcg/dL (n=6) in females and 5.53 ± 0.78 mcg/dL (n=6) in males, as shown in Figure 3.20. In comparing PTTG+/- with PBFHomo-PTTGHet, the p-value in females was 0.197 and in males 0.016.

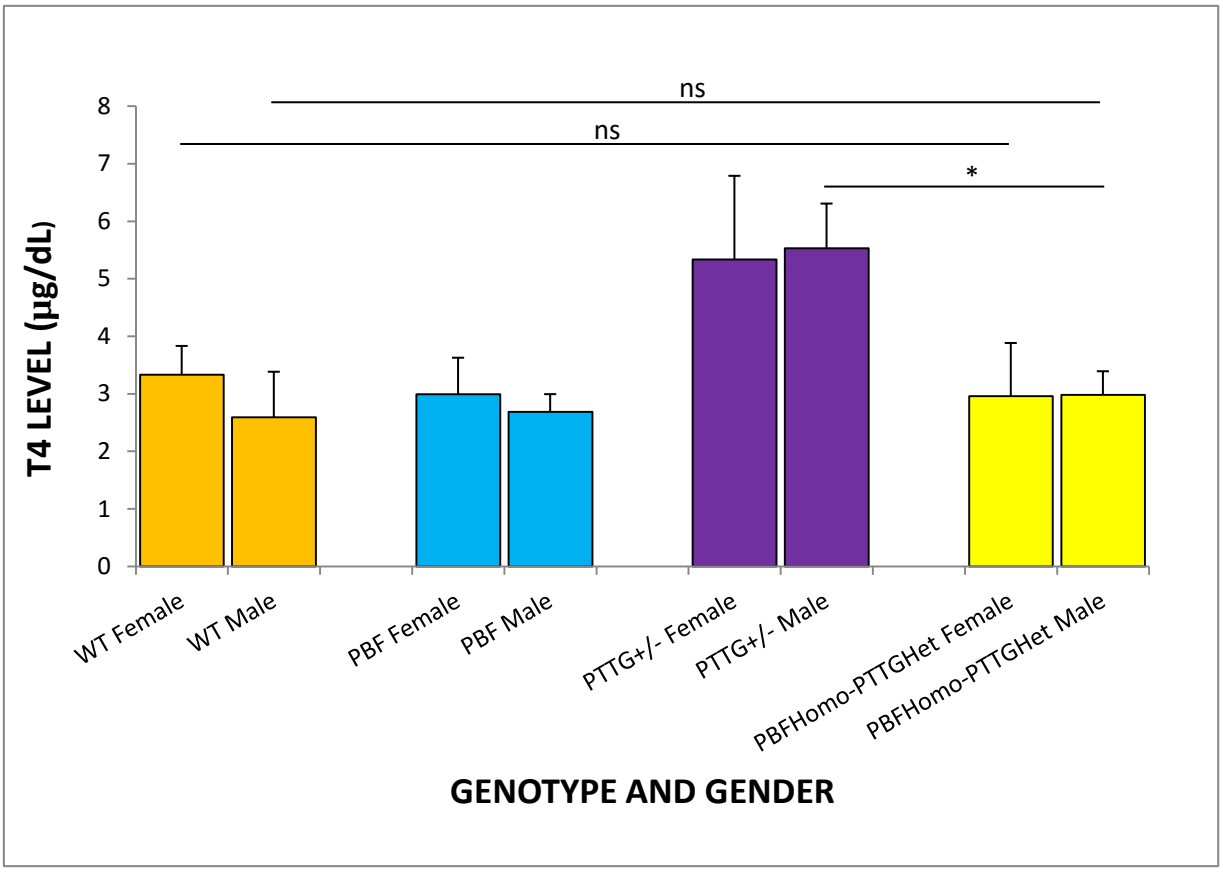

*Figure 3-20 T4 levels at 6 weeks by genotype and gender. p-values are denoted by ns ($p>0.05$) and * ($0.01>p\leq 0.05$).*

The TSH values between PBFHomo-PTTGHet and WT at 6 weeks were no different, seen in Figure 3-21. Female PBFHomo-PTTGHet TSH against WT TSH was 53 ± 20.05 mU/L (n=5) and 24 ± 3.75 mU/L (n=6), respectively, p=0.15. Male PBFHomo-PTTGHet TSH was 78 ± 12.87 mU/L (n=6) compared to male WT TSH 48 ± 13.85 mU/L (n=6), p=0.14.

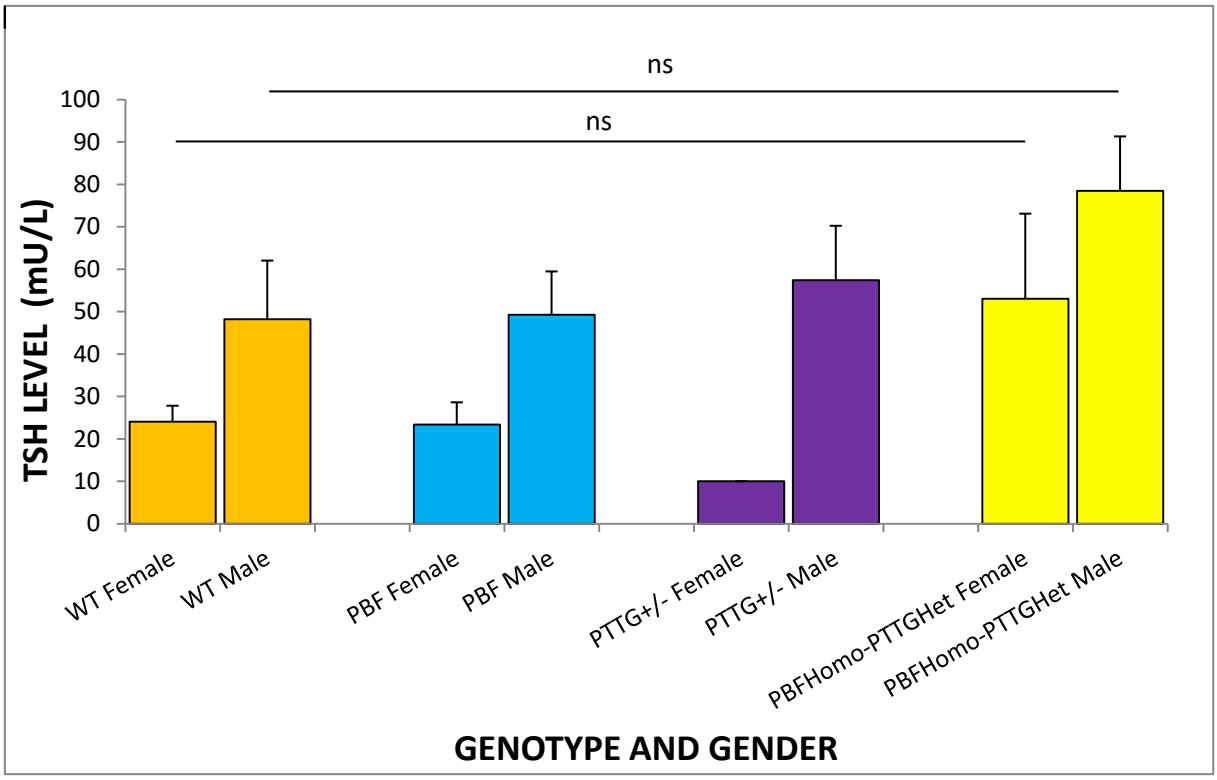

Figure 3-21 TSH levels at 6 weeks by genotype and gender. p>0.05 denoted by ns.

To establish whether thyroid function tests varied with time, we performed thyroid function tests for the different genotypes at a 12 month time point. Similar T3 levels (p=0.14) were observed in PBFHomo-PTTGHet females (141.85 ± 9.28 ng/dL, n=4) compared to wild type females (180.51 ± 22.98 ng/dL, n=3) although there was a slight difference in T3 levels in the male PTTGHomo-PTTGHet (148.34 ± 5.09 ng/dL, n=5) compared to its WT counterpart (173.82 ± 9.05 ng/dL, n=3; p=0.03) shown in Figure 3-22.

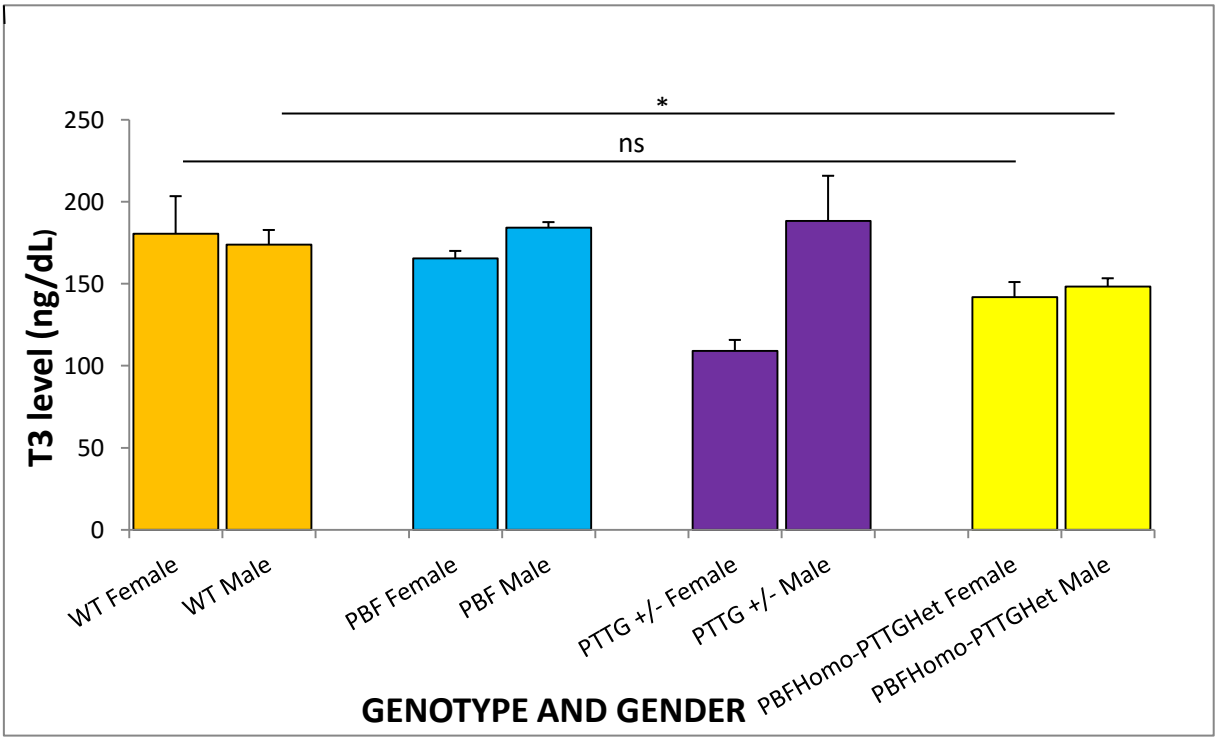

*Figure 3-22 T3 levels at 12 months by genotype and gender. p-values are denoted with * (0.01 < p ≤ 0.05) and ns (p>0.05).*

In contrast, T4 levels at 12 months in the PBFHomo-PTTGHet model were not significantly different from their wild-type counterparts (female p=0.56; male p=0.06) (Fig. 3-23).

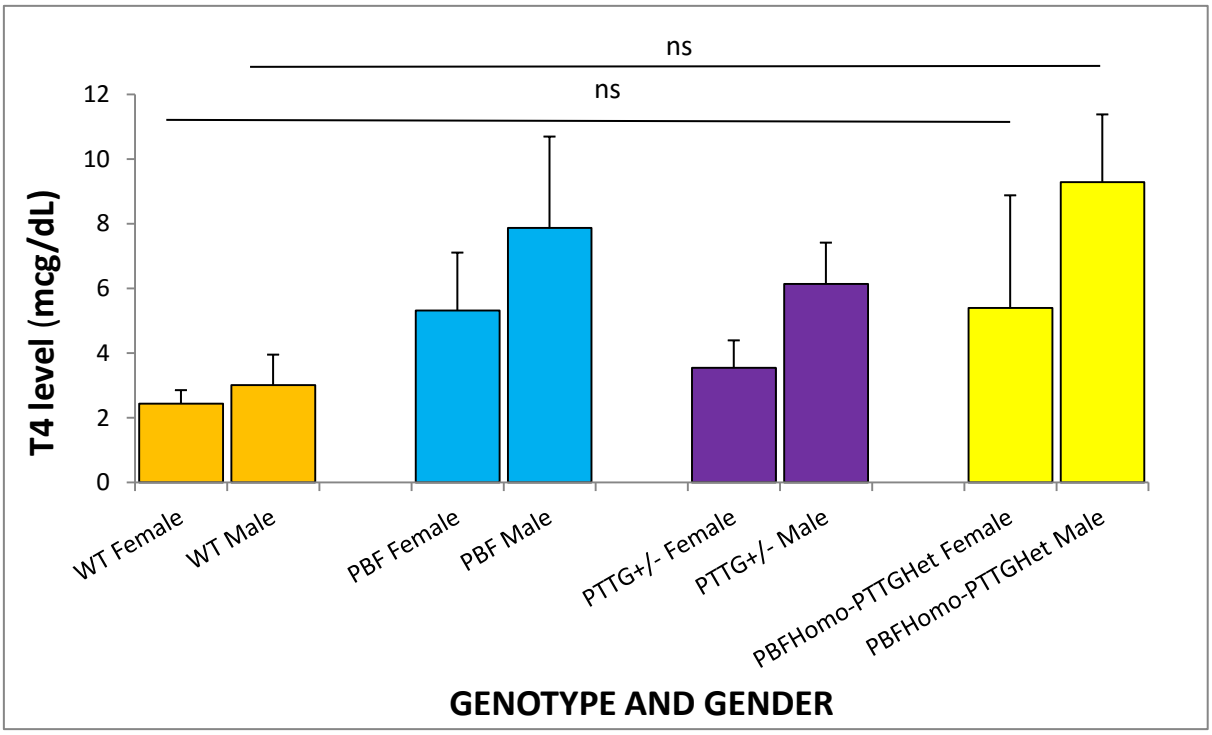

Figure 3-23 T4 levels at 12 months by genotype and gender. p-value >0.05 is denoted by "ns".

Interestingly, TSH levels were significantly different between genders of their various genotypes, shown in Figure 3-24. TSH in WT females (28.00 ± 16.52 mU/L n=3) was significantly reduced compared to males (118.00 ± 7.24 mU/L n=3; p=0.007). Similarly, PBF females (52.00 ± 24.62 mU/L n=4) and PBF males (185 ± 39.11 mU/L n=2) had significantly different TSH values than WT (p=0.039). Finally, there was a significant difference (p=0.026) between PTTG+/- females (25.00 ± 8.07 mU/L n=3) and PTTG+/- males (90 ± 16.75 mU/L n=3). No TSH values at 12 months were available in the PBFHomo-PTTGHet model.

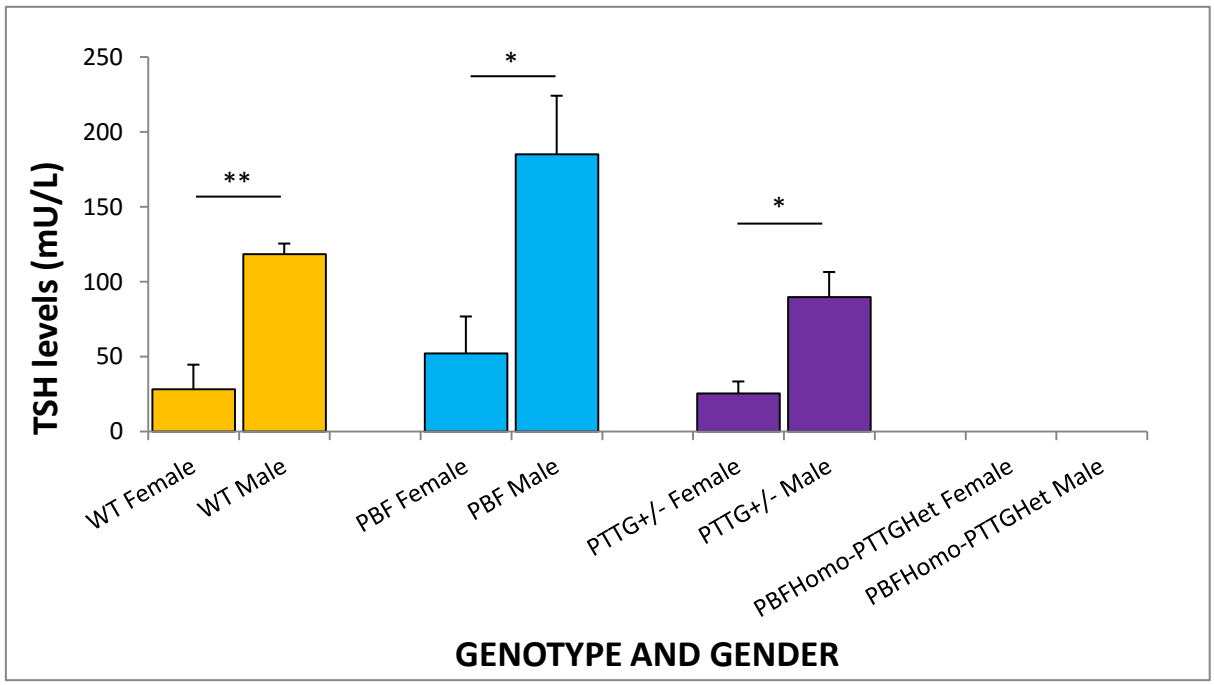

*Figure 3-24 TSH levels at 12 months by genotype and gender. p-values are denoted with * (0.01 < p ≤ 0.05) and ** (0.001 < p ≤ 0.01).*

Overall, there was no clear trend in PBFHomo-PTTGHet thyroid function tests. Moreover, the values of TSH, T4 and T3 did not correlate well to each other despite being taken from the same murine models. Finally, it appears that the goitre observed in the PBF thyroid and reduced thyroid weights in

the PTTG thyroid are not explained by TSH levels. As such, the goitre observed in PBFHomo-PTTGHet is less likely to arise from deranged thyroid function tests.

3.3.6 **PBF Homo-PTTG Het mice develop adenomas**

The goitres found in the PBFHomo-PTTGHet murine models were examined microscopically. Thyroids were rated as normal as depicted in Figure 3-25 or abnormal. Abnormal thyroids had hypercellular areas shown in Figure 3-26 or a distinctive lesion as seen in Figure 3-27.

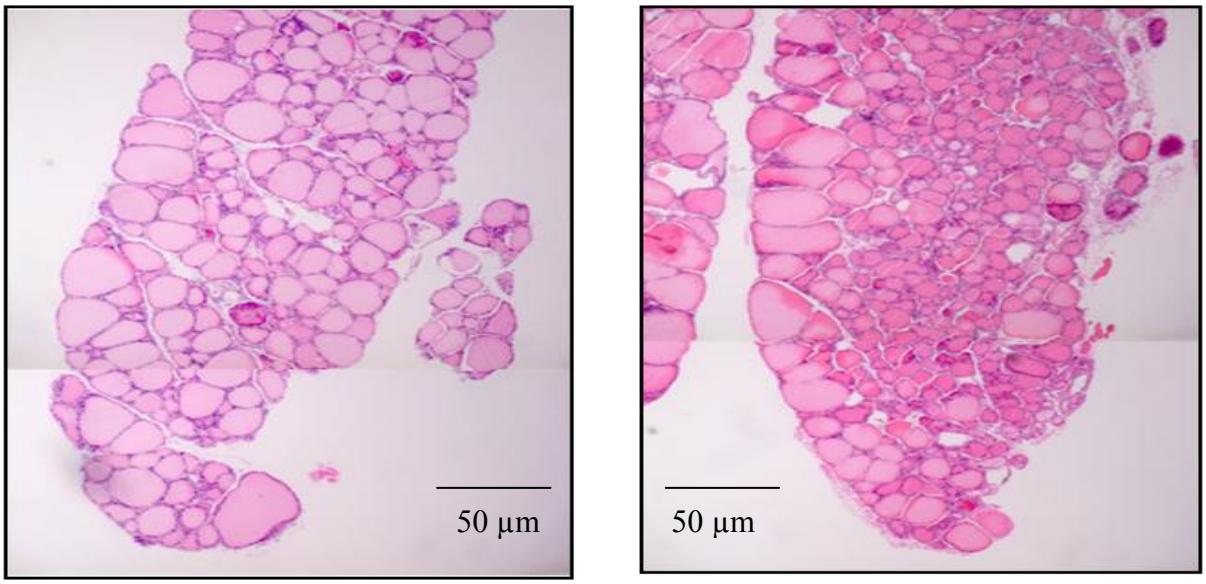

Figure 3-25 PBFHomo-PTTGHet thyroid at 5x magnification.

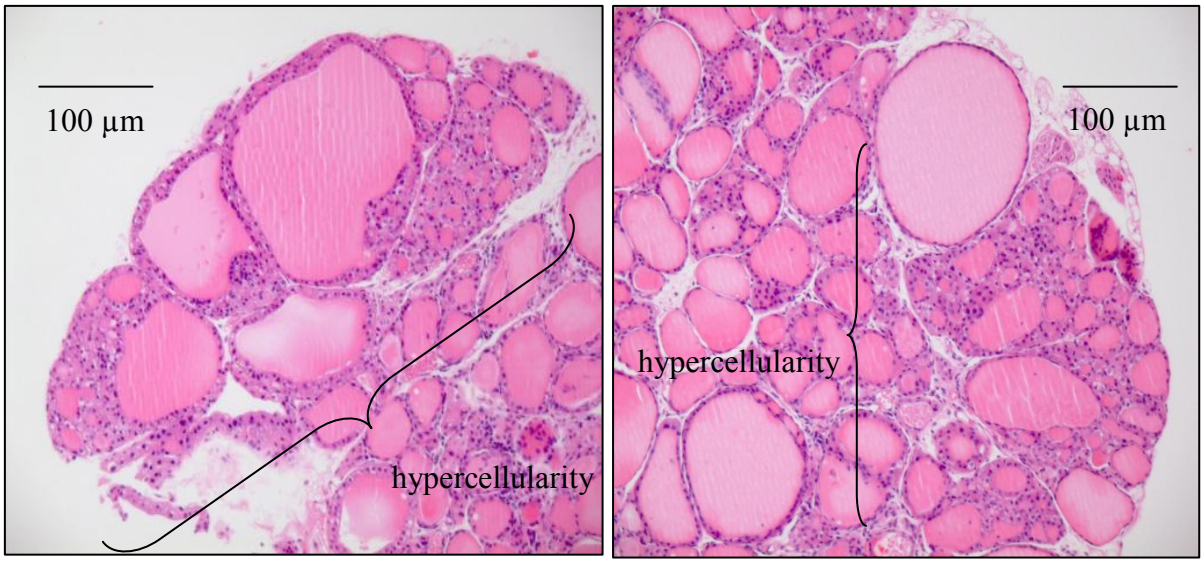

Figure 3-26 PBFHomo-PTTGHet thyroid showing hypercellularity at 10x magnification.

Figure 3-27 PBFHomo-PTTGHet discrete thyroid lesion at 10x magnification.

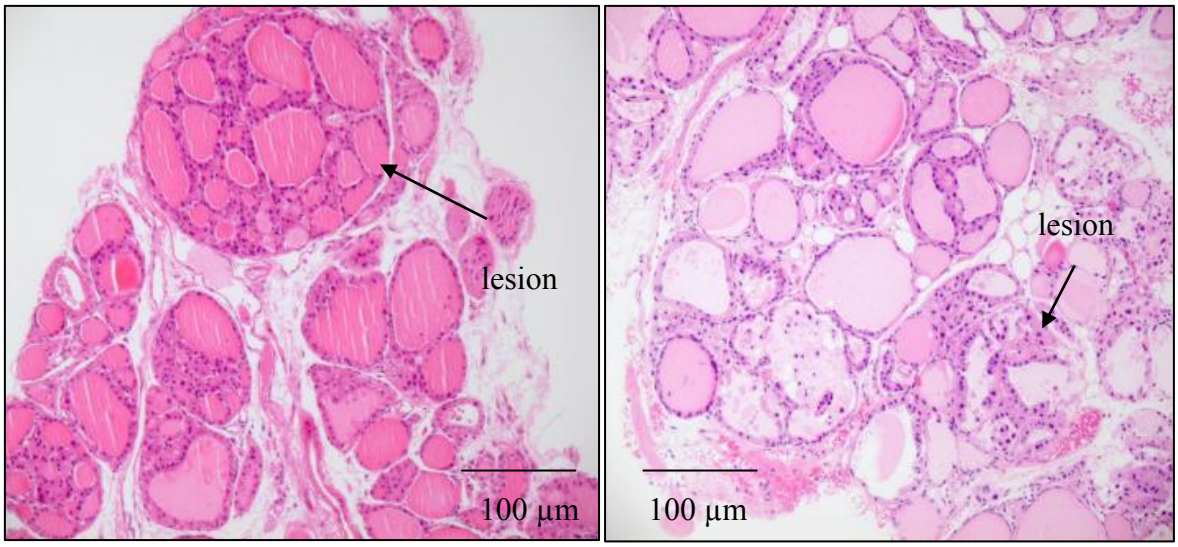

Figure 3-28 Lesion with hypercellularity in PBFHomo-PTTGHet thyroid at 10x magnification.

Overall, microscopic lesions defined above did not develop in the PBFHomo-PTTGHet thyroid gland before 12 months. Although the sample size was small (n=48), 40% of PBFHomo-PTTGHet females developed lesions compared to no lesions in the PBFHomo-PTTGHet males, in the thyroid gland at 12 months. Some thyroids had both lesions and hypercellular areas and this is recorded appropriately in Table 3 below. At 18 months, 83.3 % of PBFHomo-PTTGHet females had an abnormal thyroid gland compared to 14.3 % of PBFHomo-PTTGHet males. Wild-type (WT) mice were not known to develop lesions in the thyroid (Dr. Martin Read, University of Birmingham). The number of PBFHomo-PTTGHet mice that developed lesions. Risk factors for a histologically abnormal PBFHomo-PTTGHet thyroid would seem to include female gender and age of 12 months or more. PBFHomo-PTTGHet thyroids with discrete lesions can co-exist with areas of hypercellularity or not. Hence, hypercellularity may not necessarily precede discrete thyroid lesion formation.

AGE	GENDER	TOTAL NUMBER	NORMAL	HYPERCELLULAR AREAS	LESION
6 WEEKS	FEMALE	6	6	0	0
6 WEEKS	MALE	6	6	0	0
6 MONTHS	FEMALE	6	6	0	0
6 MONTHS	MALE	6	6	0	0
12 MONTHS	FEMALE	5	3	2 (40.0 %)	1 (20.0 %)
12 MONTHS	MALE	6	6	0	0
18 MONTHS	FEMALE	6	1 (16.7 %)	3 (50.0 %)	3 (50.0%)
18 MONTHS	MALE	7	6 (85.7 %)	0	1 (14.3 %)

Table 3 PBFHomo-PTTGHet ageing colony numbers with normal and abnormal thyroids.

3.4 DISCUSSION

The proto-oncogenes PTTG and its binding factor (PBF) have been implicated in thyroid tumourigenesis. Work by other groups and ours have demonstrated the transforming characteristics of PBF and PTTG in vivo (Pei and Melmed, 1997, Stratford et al., 2005). The murine model of PBF overexpression in the thyroid do not develop thyroid cancers but developed goitres and hyperplastic lesions instead (Read et al., 2011), possibly suggesting that thyroid carcinogenesis required a further insult in addition to PBF overexpression. The binding partner of PTTG, PBF, transports PTTG to the nucleus for its actions (Chien and Pei, 2000). Hence, we generated a murine model overexpressing both PBF and PTTG in the thyroid gland to test our hypothesis.

3.4.1 Creation of bi-transgenic model colony

The FVB/N murine model has good reproductive performance and its inbred nature eliminates ambiguity caused by different genetic backgrounds (Taketo et al., 1991). This model is the basis of most scientific experiments involving murine models. We generated a double-hit murine model overexpressing both human PBF (hPBF) and human PTTG (hPTTG) to study the in vivo role of PBF and PTTG on the thyroid gland.

Early in the initial characterisation of the hPTTG model, Dr. Gregory Lewy who constructed the model reported increased death rates in homozygote mice (PTTG +/+). Interestingly, heterozygote hPTTG mice (PTTG +/-) did not exhibit increased mortality compared to wild type. We observed reduced mortality in our BI-Trans model, homozygous for both hPBF and hPTTG. Given that mortality in the PTTG model appeared to be dependent on PTTG zygosity, we hypothesised that a bi-transgenic murine model homozygous for PBF and heterozygous for PTTG (PBFHomo-PTTGHet) would survive for longer. The improved survival of the PBFHomo-PTTGHet compared to BI-Trans was confirmed and shown in section 3.3.2. Hence, we used the PBFHomo-PTTGHet model for our long term characterisation study.

3.4.2 **Reduced mortality**

The reduced mortality observed in the PTTG murine model could be due to one of two reasons or both. Firstly, random gene insertion during the creation of the PTTG model may have disrupted crucial genes which impact mortality, within the genome. Since reduced mortality was not observed in PTTG+/-, it was possible that the organism could cope with a semi disrupted genome. However, in the presence of two copies of genes overexpressing hPTTG, as was in the PTTG+/+ model, the compensatory mechanism failed or was not existent. Secondly, high levels of hPTTG expression in the thyroid might have had a non specific lethal effect. Again, the organism could cope in the presence of limited hPTTG overexpression but not in copious amounts.

The survival probability rank by genotype was observed as follows: WT/PBF/PTTG+/- > PBFHomo-PTTGHet > PTTG+/+ > BI-Trans. The reduced mortality in PBFHomo-PTTGHet compared to PTTG+/- cannot be explained by its PTTG zygosity. Hence, PBF appeared to have a synergistic effect with PTTG in reducing mortality in our model. On its own, however, PBF did not impact on survival rates.

3.4.3 **Fertility issues**

Overall, the PBFHomo-PTTGHet and BI-Trans models had reduced fertility. Breeding pairs consisting of two BI-Transgenic mice did not reproduce. The cause for infertility may lie in the BI-Transgenic male. Pairings between BI-transgenic females and male PBFHomo-PTTGHets led to successful breeding. By contrast, BI-Trans male and PBFHomo-PTTGHet females yielded no offspring.

The PBFHomo-PTTGHet and PBFHomo-PTTGHet pairing yielded more offspring than PBFHomo-PTTGHet and BI-Transgenic. To maximize yield of the PBFHomo-PTTGHet or BI-Trans model, a new breeding strategy was adopted. The pairings and Mendelian genetics shown in Figures 3-29 and 3-30 were adopted to maintain perpetuity of the breeding colony.

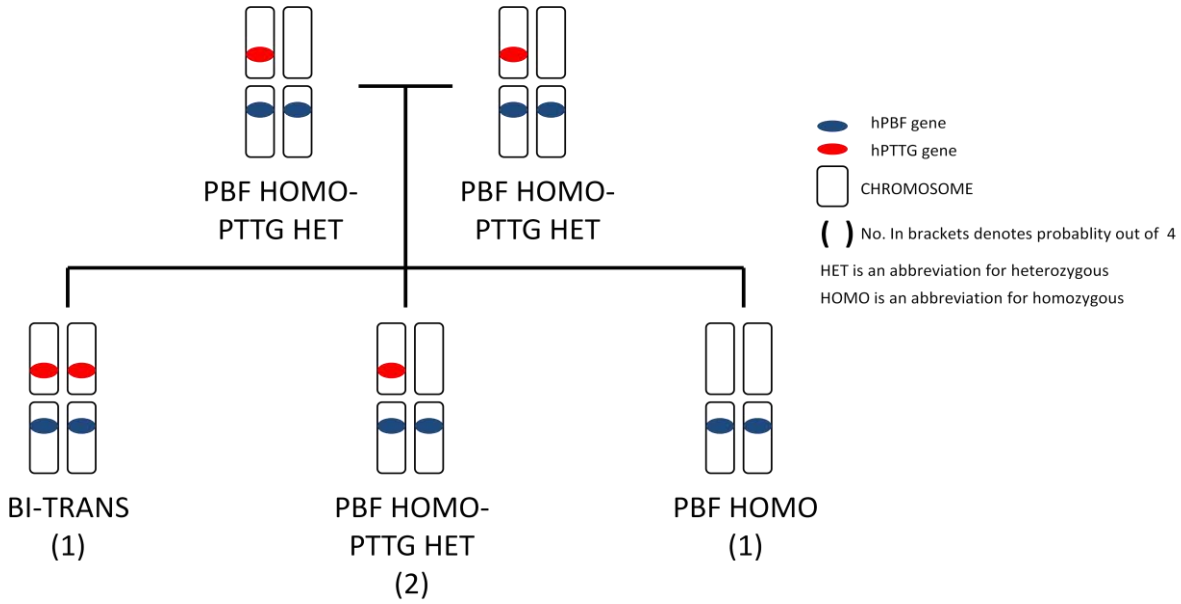

Figure 3-29 Genetics of PBFHomo-PTTGHet x PBFHomo-PTTGHet breeding.

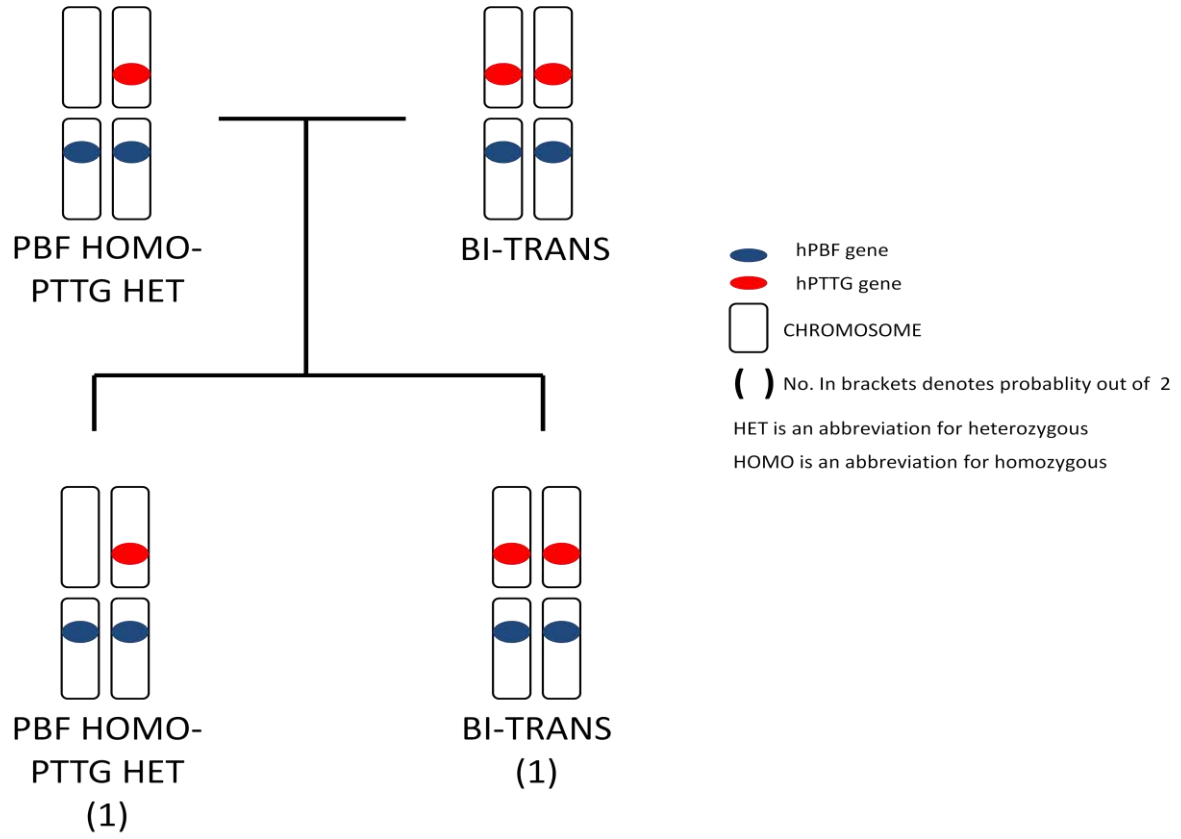

Figure 3-30 Genetics of PBFHomo-PTTGHet and BI-Trans breeding.

3.4.4 Goitre formation in the PBFHomo-PTTGHet murine model

Goitres found in the PBFHomo-PTTGHet model were comparable in size to the PBF model. This suggests that PTTG in the presence of PBF has no additional effect on thyroid size.

PBFHomo-PTTGHet thyroid weights increased over time in a similar fashion to the PBF model. WT and PTTG+/- thyroid weights remained constant over the same period of time. Goitre formation appeared to be PBF dependent, even in the presence of PTTG expression.

There was no gender difference in the corrected thyroid weight of WT and PTTG+/- mice (data not shown). Female thyroid weight adjusted for body weight in both PBGHomo-PTTGHet and PBF murine models was consistently higher than for male counterparts over the study period (data not shown). Hence, it appeared that goitre formation caused by the overexpression of PBF in the thyroid had a greater effect in females than males.

3.4.5 Thyroid function tests

Thyroid function tests are usually interpreted in conjunction with each other. Thyroid hormone biosynthesis operates on a negative feedback loop. Thyroid hormone is produced by the thyroid gland in the form of T4 and T3. The active component T3 is secreted in small amounts relative to T4. The proportion of T4 to T3 in humans is approximately 20:1. High blood thyroid hormone levels inhibit the secretion of thyroid stimulating hormone (TSH) from the anterior pituitary gland. Low TSH results in reduced thyroid hormone secretion from the thyroid gland. Prolonged and high levels of TSH can cause thyroid cell growth in addition to stimulating thyroid production. Hence, the concentration of T3 and T4 should have an inverse relationship to TSH levels.

We performed thyroid function tests on the various genotypes at different time points. There was no observed correlation between TSH, T3 and T4 levels within each genotype suggesting that the study had insufficient power to demonstrate a statistical difference. However, given that we were dealing

with a mutant model where changes should be gross, any effect caused by the overexpression of our genes of interest should be apparent, even in low numbers. Since there was no gross increase in TSH levels, goitre formation in the PBFHomo-PTTGHet and PBF models is not likely to be TSH driven.

3.4.6 Adenoma formation in PBFHomo-PTTGHet

PBFHomo-PTTGHet thyroids demonstrated areas of hypercellularity and lesion formation microscopically. These histological changes were found predominantly in female PBFHomo-PTTGHet from 12 months onwards. Lesions appeared well-circumscribed with no invasive features suggestive of a cancer. The likelihood is that these lesions represent adenomas. Thyroid function tests did not reveal hyperthyroidism in the mice with adenomas suggesting these lesions are non-functional.

It is not possible at this stage to determine if these histological changes are separate entities or progression of the same event. Since the above histological changes were similar to PBF thyroids microscopically, adenoma formation and hypercellularity are likely an effect of PBF overexpression in the thyroid.

3.5 CONCLUSION

In terms of thyroid changes, the PBFHomo-PTTGHet model appeared phenotypically to be a PBF model. The survival characteristics of the PBFHomo-PTTGHet model mirrors the PTTG model. Reduced fertility of the PBFHomo-PTTGHet model is likely a PTTG phenotype because the PBF murine model had normal fertiility. Unfortunately, we did not have any breeding data for the PTTG model to make a direct comparison.

The PBFHomo-PTTGHet model did not produce any cancers as hypothesized. Hence, we next examined whether the PBFHomo-PTTGHet thyroids exhibit genetic instability.

4 Genetic instability in transgenic murine thyroids

4.1 INTRODUCTION

The ability to replicate is a hallmark feature of a living cell. Occasionally, errors of replication result in a mutation. Gene mutations that involve cell cycle regulation, DNA repair and the repair of DNA damage, which is integral to maintaining genomic stability, can result in mutations that lead to the development of tumours. Hence, genetic instability is an integral feature of cancers (Loeb and Monnat, 2008, Rajagopalan et al., 2002). Furthermore, genetic instability has been demonstrated previously in thyroid cancers by multiple groups (Kim et al., 2005, Mitsutake et al., 2005, Saavedra et al., 2000, Ward et al., 1998, Wreesmann et al., Tung et al., 1997).

A technique described by Basik et al, inter-simple sequence repeat PCR (ISSR-PCR), was used for measuring genetic instability in colorectal cancers (Basik et al., 1997). In this technique, a primer to microsatellite sequences was used in the polymerase chain reaction (PCR) to compare normal and tumour samples. Subsequently, Kim et al demonstrated genetic instability in thyroid cancers using the modified technique of fluorescent ISSR-PCR (FISSR-PCR) (Kim et al., 2005).

PBF and PTTG have been shown previously to have independent and dependent effects on tumourigenesis (Stratford et al., 2005). PBF expression is increased in thyroid cancer both at a protein and mRNA level (Stratford et al., 2005). A high level of PBF expression has been shown to be an independent prognostic marker for thyroid cancer recurrence in well-differentiated thyroid cancer (Hsueh et al., 2013). Additionally, PTTG expression has been found to be increased in thyroid cancer (Boelaert et al., 2003) and has been described to cause genetic instability (Kim et al., 2005). Consequently, we aimed to determine if the simultaneous overexpression of PBF and PTTG caused genetic instability in murine thyroids.

Ionising radiation induces DNA damage by causing single and double strand breaks within the DNA. Genetic instability results if the surviving cell cannot be repaired adequately. Additionally, ionising radiation is a recognised cause of thyroid cancer (Nikiforov, 2006, Nikiforov et al., 1996, Nikiforov et al., 1997, Richardson, 2009, Stsjazhko et al., 1995). Since PBF and PTTG overexpression in the

thyroid gland have not been shown to cause thyroid cancers, we aimed to observe the effects of ionising radiation with a background of PBF and PTTG overexpression independently and dependently in the thyroid gland to determine whether our genes of interest affected genomic stability of the thyroid cell following radiation.

4.2 MATERIAL AND METHODS

4.2.1 Primary murine thyroid cultures (PMTC)

Primary murine thyroid culture (PMTC) was developed as a platform for experiments involving radiation. Microdissection on 6 week old murine thyroids is described in section 2.2.

4.2.2 Protein extraction and Western blot

Protein extraction and western blot was performed as described in section 2.7 and 2.8. Primary antibodies used were rabbit anti-human PBF-8 polyclonal and anti-human PTTG (Invitrogen, UK) used in concentrations of 1:1000 and 2 μg/ml respectively. The secondary antibody used was monoclonal anti-β-actin clone AC-15 (Sigma-Aldrich, Poole, UK) in a concentration of 1:10,000.

4.2.3 Immunofluorescence

PMTC was performed in 6-well plates for immunofluorescence. On Day 10, medium was removed from the wells and washed with phosphate buffer solution (PBS). Subsequently, the protocol for immunofluorescence was followed as described in section 2.9.

4.2.4 Radioiodine uptake assays

Murine primary thyrocytes were grown in 12-well plates in 0.5 ml medium. Thyroid function was determined by the ability of the cell to actively absorb ^{125}I from the medium. A solution containing 0.05 μCi ^{125}I (Hartmann Analytic, Germany) and 10^{-9} NaI was added to each well and incubated for 2 hours as previously described (Eggo et al., 1996, Boelaert et al., 2007). Subsequently, the cell layer

was washed with HBSS to remove unincorporated iodide and the cells lysed in 2 % SDS protein lysis buffer. Incorporated radioactivity was estimated in a gamma counter. Relative iodide uptake was corrected for protein concentration measured by the Bradford assay.

4.2.5 **DNA extraction**

DNA was extracted from murine thyroids and primary murine cultures using the same technique described for ear clippings in Chapter 2 (DNeasy 96 Blood & Tissue Kit; Qiagen).

4.2.6 **Polymerase chain reaction (PCR)**

Genomic DNA was subjected to PCR in a Mastercyler® thermal cycler (Eppendorf, Hamburg, Germany). Each reaction comprised 50 ng DNA, 1 µl 10 mM dNTP, 2 µl 50 mM $MgCl_2$, 3 µl of 200 nmol $(CA)_8RG$ (R = a 50:50 mix of the purines adenine and guanine; Y = a 50:50 mix of the pyrimidines cytosine and thymine) primers labelled with FAM fluorophore (Eurogentec), 1x TaqMaster PCR Enhancer (5Prime, Hamburg, Germany), 0.5x NH_2 reaction buffer (Bioline), 2.5 U Biotaq™ DNA polymerase (Bioline) and nuclease-free water to make up a total volume of 50 µl. Initial denaturation of the DNA template took place at 95 °C for 5 minutes before holding at 74 °C. Subsequently, DNA polymerase and NH_2 reaction buffer was added and the reaction subjected to 35 cycles of 94°C for 30 seconds, 50 °C for 30 seconds and 72 °C for 60s. The final extension step for 10 minutes took place at 72 °C.

4.2.7 **Agarose gel electrophoresis**

PCR products were initially electrophoresed in 1 % Agarose (Bioline) gel in 1X TAE (Tris-Acetate-EDTA) buffer (Eppendorf) before being visualized to optimize the PCR reaction for FISSR-PCR experiments.

4.2.8 **Fluorescent inter-simple sequence repeat-PCR (FISSR-PCR)**

This technique involved a polymerase chain reaction (PCR) using primers labelled with a FAM fluorophore targetted to (CA)n microsatellites or simple sequence repeats within the genome. Traditionally, the PCR products or fragments were resolved on a PAGE gel and visualised by autoradiography. The genetic instability index developed by Basik et al and validated by others (Basik, Stoler et al 1997; Viswanathan, Sangiliyandi et al 2003) was determined by dividing the number of

altered fragments in the target tissue by the total number of bands in the corresponding tissue and multiplied by 100 to form a percentage.

The modified technique of FISSR-PCR involved performing the fragment analysis in a DNA sequencer. PCR reaction products were diluted 20 times in nuclease-free water. 1 µl of diluted PCR reaction was added to 8.5 µl Hi-Di Formamide (Applied Biosystems) and 0.5 µl of Genescan™ 1200 LIZ® Size Standard (Applied Biosystems) and aliquoted into a 96-well plate. The whole mixture was denatured at 95ºC for 5 minutes. The sample was analysed using the ABI 3730 automated DNA sequencer (Applied Biosystems) with the microsatellite fragment analysis setting. The "fsa" file obtained was subsequently read using Genemapper v3.5 software (Applied Biosystems). The index of genetic instability was calculated as follows:-

$$\text{GENETIC INSTABILITY INDEX} = \frac{\text{No. of bands lost/gained + No. of different bands}}{\text{No. of expected bands}} \times 100$$

4.3 RESULTS

4.3.1 Primary murine thyroid culture

Primary murine thyroid culture (PMTC) was successfully perfected following several attempts at optimisation. Whole thyroid follicles were observed to be settling on the floor of a 12-well plate under light microscopy, seen in Figure 4-1. Subsequently, the follicles dispersed over several days, creating a sheet of cells with various clusters. Finally, on Day 10 when the cells were ready for experimentation, multiple clusters could be observed, shown in Figure 4-2. The cluster pattern tended to be variable, comprising between 60 – 70 % of the surface area of the well. Overall, the cultures were viable for up to 12 days but were used for experimentation on Day 10.

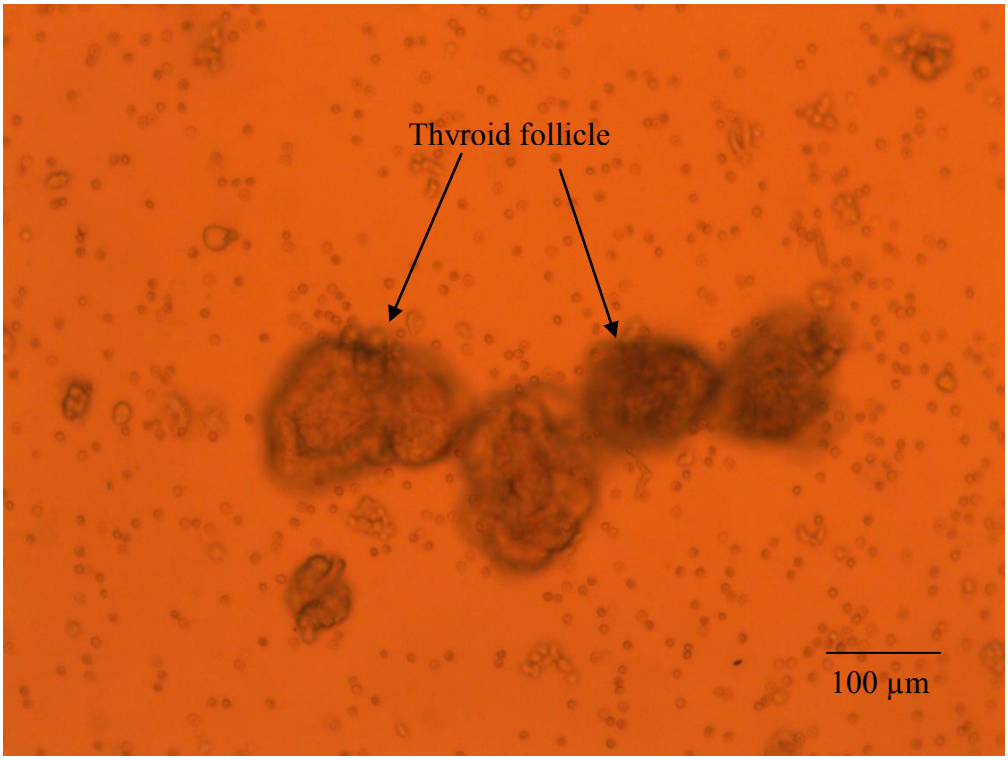

Figure 4-1 Primary murine thyroid culture under light microscopy depicting whole thyroid follicles immediately following processing at Day 0 (10x magnification).

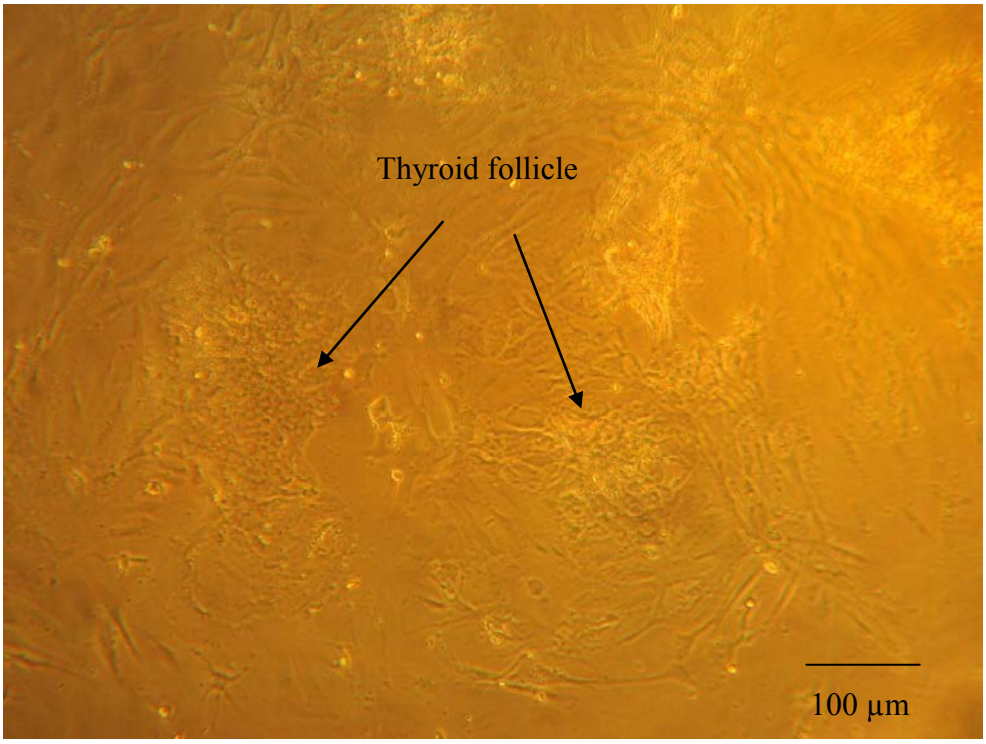

Figure 4-2 Light microscopy of primary murine thyroid culture (10x magnification) showing the formation of clusters in a 12-well plate on Day 10.

4.3.2 Immunofluorescence confirmed the presence of thyroid cells

Having established the technique of PMTC, we next confirmed the purity of our primary cultures. The PBF-Tg murine model overexpressing human PBF tagged to haemagglutinin (PBF-HA) was used for immunofluorescence. DAPI, used to stain nuclei which fluoresced in blue, confirmed the presence of cells in culture. The presence of thyroid cells was confirmed by red fluorescence, detected using a primary HA antibody and a secondary antibody tagged with a red fluorescent dye (Alexa Fluor® 594; Life Technologies). The images obtained from the inverting microscope is shown in Figure 4-3. Interestingly, the presence of HA and hence, thyroid cells, appeared in clusters.

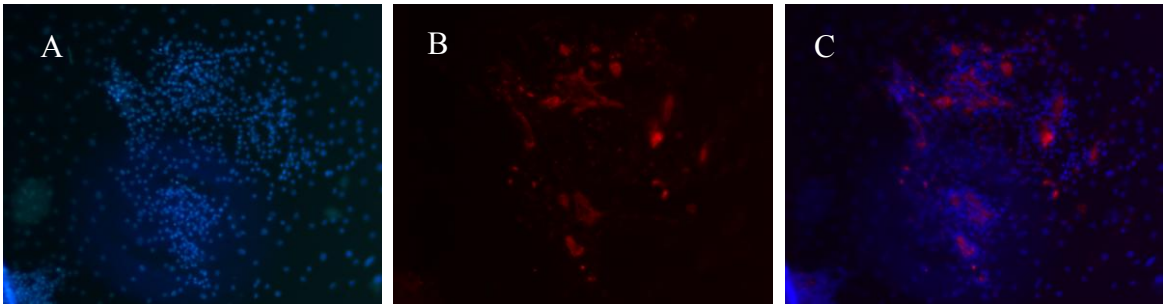

Figure 4-3 Immunofluorescence in PBF-HA primary murine thyroid culture (PMTC) at 10x magnification. The nucleus fluoresced in blue (DAPI) and the HA tag fluoresced in red. Image A depicts the pattern of cellular growth in PMTCs and image B confirmed the presence of PBF-HA thyroid cells. The composite image C depicts the growth of thyroid cells in clusters.

4.3.3 PMTCs overexpress PBF and/or PTTG

Next, we examined the expression of our genes of interest in each of the PMTC genotypes; wild-type (WT; n=4), PBF (n=4), PTTG+/+ (n=4) and BI-Trans (n=4) shown in Figure 4-4 below. The Western blot confirms the overexpression of PBF in both PBF and BI-Trans PMTCs and PTTG in both PTTG+/+ and BI-Trans PMTCs.

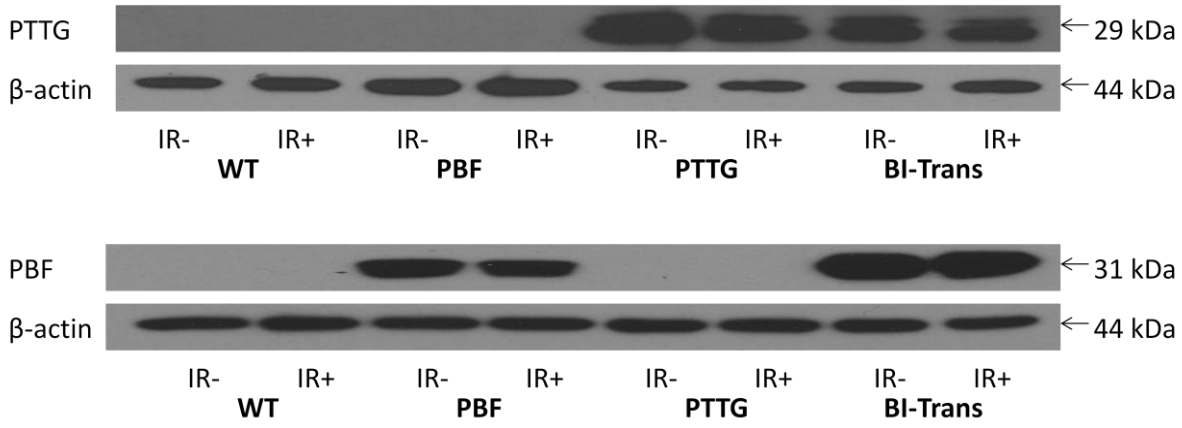

Figure 4-4 Western blot of PMTCs probed with PTTG (top) and PBF (bottom) antibodies. WT, PBF, PTTG and BI-Trans refer to wild-type, PBF, PTTG and BI-Trans PMTCs (n=4 for each genotype).

4.3.4 **Primary murine thyroid cultures were functional**

We next confirmed that the thyroid cells in PMTCs were functional. Previous publications by our group have shown that thyroid cells overexpressing PBF have reduced uptake of ^{125}I (Boelaert et al., 2007, Smith et al., 2009, Read et al., 2011).

A total of 5 WT and 6 PBF thyroids which were age- and sex-matched were used for this study. The average adjusted CPM (counts per minute) for WT was 25,210.4 ± 4,819.99 and for PBF 7,400.29 ± 1,680.58. We observed a 70% reduction of radioiodine uptake in PBF derived cultures compared to WT cultures at 10 days (p=0.0004), as shown in Figure 4-5. Taken together, these data confirmed that primary murine thyroid culture techniques were appropriate, consistent with previous data and functional in that significant reduction in ^{125}I was demonstrated.

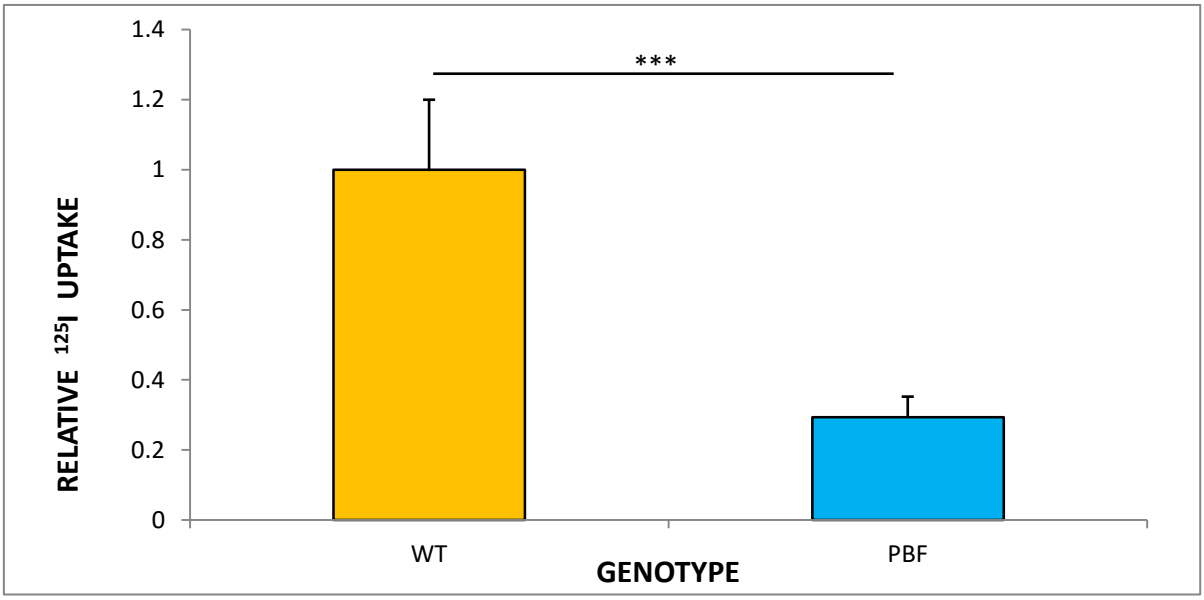

Figure 4-5 Relative ^{125}I uptake in WT and PBF primary murine thyroid cultures. The uptake of ^{125}I is significantly repressed (p=0.0004) in PBF (n=6) compared to WT (n=5).

4.3.5 **PCR optimisation**

The technique of FISSR-PCR used in measuring the index of genetic instability (GI) is dependent on PCR fragments obtained using the $(CA)_8RY$ primer which binds to microsatellite segments within the genome. The quantity of DNA obtained from PMTC is small and hence, it was important to ensure optimal PCR conditions to obtain maximal PCR products that can be subsequently resolved successfully.

Several optimisation experiments were performed to determine the optimal conditions for the PCR reaction for FISSR. The aim of optimisation was to obtain clear fragments from the PCR reaction and to determine the length of products obtained. Initially, we resolved the PCR products on 1 % Agarose gel to compare various PCR reactions. The amount of $MgCl_2$ and NH_4SO_4 buffer in each reaction was altered and the reaction which yielded the optimal number of clear fragments is shown in Figure 4.6 below. Interestingly, the PCR reaction yielded fragments mainly between 200 to 1000 base pairs.

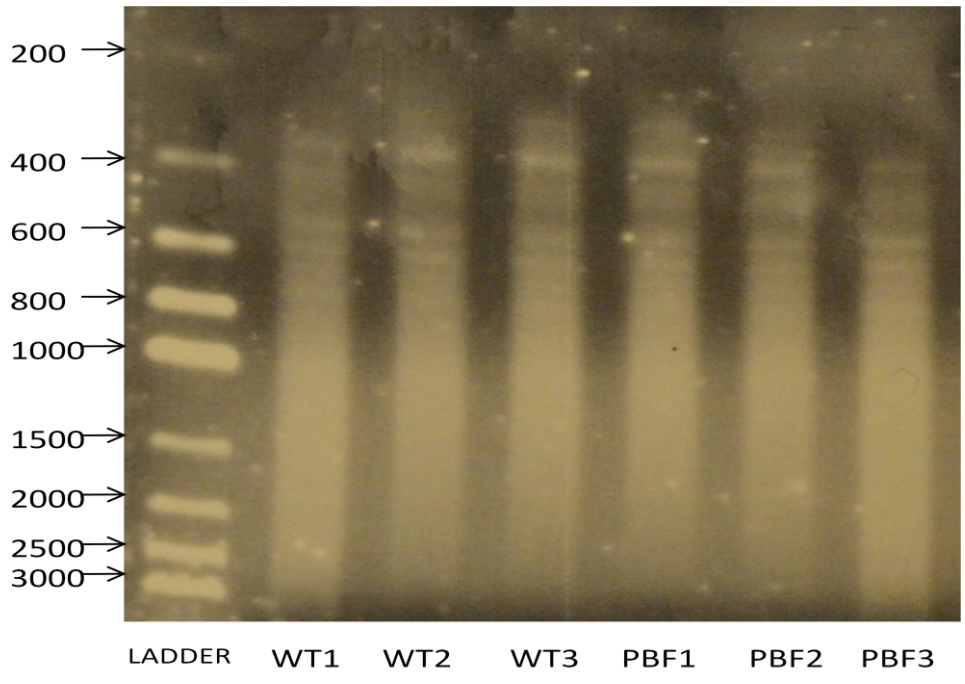

Figure 4-6 DNA PCR products resolved on 1% Agarose gel, extracted from wild type (WT)(n=3) and PBF (n=3) primary murine thyroid cultures. The PCR conditions for this run were deemed optimal and used for subsequent FISSR experiments. PCR products ranged between 200 and 1000 base pairs.

4.3.6 **Modified FISSR-PCR**

The technique of FISSR-PCR described by Kim et al involved the use of PAGE-gel and autoradiography (Kim et al., 2005). This method of resolving PCR products is cumbersome and would require a moderate amount of DNA which our primary murine thyroid cultures do not yield. The DNA sequencer (ABI 3730; Applied Biosystems) is a sensitive and efficient way of resolving PCR products. Hence, the FISSR-PCR technique was modified using the ABI 3730 DNA sequencing machine to resolve PCR products.

Figure 4-7 shows PCR products being resolved within each capillary tube in the ABI 3730 automated DNA sequencer. The files obtained from the sequencer are read using Genemapper software which express data in numerical (shown in Figure 4-8) or graphical format (shown in Figure 4-9).

Interpretation of results was challenging because of the huge volume of data present for each sample. A difference is defined as a change of more than 500 units in peak area and a band height difference of more than 3 fold. The estimated GI index from the same species within the same PCR run had a variation of less than 10 % using these criteria.

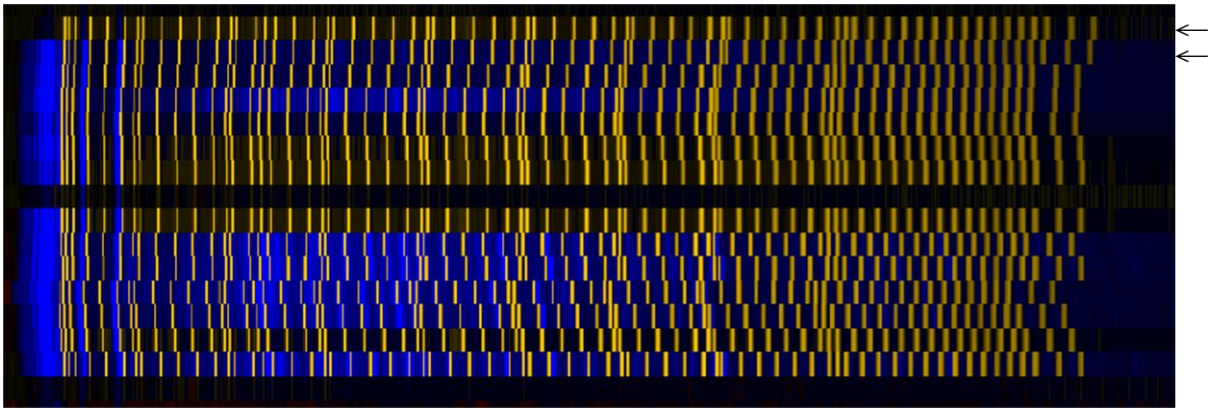

Figure 4-7 An example of PCR products resolved on ABI Genemapper sequencer. Arrows indicate individual sequencing capillaries. Yellow/Orange colour represent the GeneScan LIZ Size Standard (ThermoFisher Scientific). The blue colour arises from the FAM fluorophore attached to the primer used in the polymerase chain reaction (PCR).

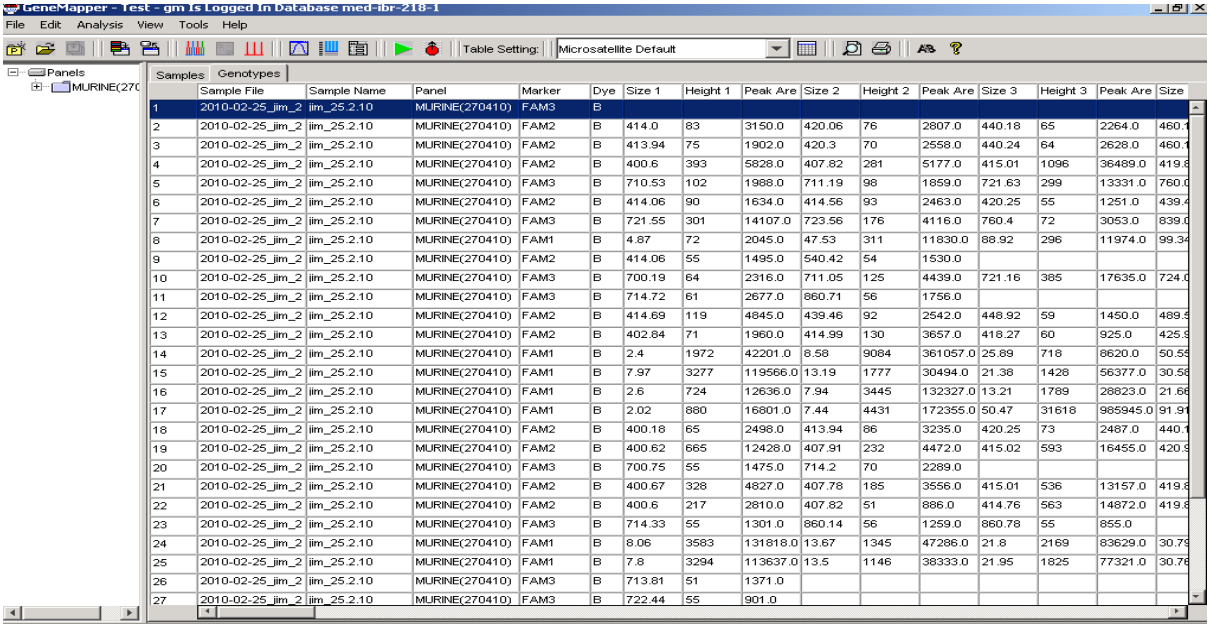

	Sample File	Sample Name	Panel	Marker	Dye	Size 1	Height 1	Peak Are	Size 2	Height 2	Peak Are	Size 3	Height 3	Peak Are	Size
1	2010-02-25_jim_2	jim_25.2.10	MURINE(270410)	FAM3	B										
2	2010-02-25_jim_2	jim_25.2.10	MURINE(270410)	FAM2	B	414.0	83	3150.0	420.06	76	2807.0	440.18	65	2264.0	460.1
3	2010-02-25_jim_2	jim_25.2.10	MURINE(270410)	FAM2	B	413.94	75	1902.0	420.3	70	2558.0	440.24	64	2628.0	460.1
4	2010-02-25_jim_2	jim_25.2.10	MURINE(270410)	FAM2	B	400.6	393	5828.0	407.82	281	5177.0	415.01	1096	36489.0	419.8
5	2010-02-25_jim_2	jim_25.2.10	MURINE(270410)	FAM3	B	710.53	102	1988.0	711.19	98	1859.0	721.63	299	13331.0	760.0
6	2010-02-25_jim_2	jim_25.2.10	MURINE(270410)	FAM2	B	414.06	90	1634.0	414.56	93	2463.0	420.25	55	1251.0	439.4
7	2010-02-25_jim_2	jim_25.2.10	MURINE(270410)	FAM3	B	721.55	301	14107.0	723.56	176	4116.0	760.4	72	3053.0	839.0
8	2010-02-25_jim_2	jim_25.2.10	MURINE(270410)	FAM1	B	4.87	72	2045.0	47.53	311	11830.0	88.92	296	11974.0	99.34
9	2010-02-25_jim_2	jim_25.2.10	MURINE(270410)	FAM2	B	414.06	55	1495.0	540.42	54	1530.0				
10	2010-02-25_jim_2	jim_25.2.10	MURINE(270410)	FAM3	B	700.19	64	2316.0	711.05	125	4439.0	721.16	385	17635.0	724.0
11	2010-02-25_jim_2	jim_25.2.10	MURINE(270410)	FAM3	B	714.72	61	2677.0	860.71	56	1756.0				
12	2010-02-25_jim_2	jim_25.2.10	MURINE(270410)	FAM2	B	414.69	119	4845.0	439.46	92	2542.0	448.92	59	1450.0	489.5
13	2010-02-25_jim_2	jim_25.2.10	MURINE(270410)	FAM2	B	402.84	71	1960.0	414.99	130	3657.0	418.27	60	925.0	425.9
14	2010-02-25_jim_2	jim_25.2.10	MURINE(270410)	FAM1	B	2.4	1972	42201.0	8.58	9084	361057.0	25.89	718	8620.0	50.55
15	2010-02-25_jim_2	jim_25.2.10	MURINE(270410)	FAM1	B	7.97	3277	119566.0	13.19	1777	30494.0	21.38	1428	56377.0	30.58
16	2010-02-25_jim_2	jim_25.2.10	MURINE(270410)	FAM1	B	2.6	724	12636.0	7.94	3445	132327.0	13.21	1789	28823.0	21.66
17	2010-02-25_jim_2	jim_25.2.10	MURINE(270410)	FAM1	B	2.02	880	16801.0	7.44	4431	172355.0	50.47	31618	985945.0	91.91
18	2010-02-25_jim_2	jim_25.2.10	MURINE(270410)	FAM2	B	400.18	65	2498.0	413.94	86	3235.0	420.25	73	2487.0	440.1
19	2010-02-25_jim_2	jim_25.2.10	MURINE(270410)	FAM2	B	400.62	665	12428.0	407.91	232	4472.0	415.02	593	16455.0	420.9
20	2010-02-25_jim_2	jim_25.2.10	MURINE(270410)	FAM3	B	700.75	55	1475.0	714.2	70	2289.0				
21	2010-02-25_jim_2	jim_25.2.10	MURINE(270410)	FAM2	B	400.67	328	4827.0	407.78	185	3556.0	415.01	536	13157.0	419.8
22	2010-02-25_jim_2	jim_25.2.10	MURINE(270410)	FAM2	B	400.6	217	2810.0	407.82	51	886.0	414.76	563	14872.0	419.8
23	2010-02-25_jim_2	jim_25.2.10	MURINE(270410)	FAM3	B	714.33	55	1301.0	860.14	56	1259.0	860.78	55	855.0	
24	2010-02-25_jim_2	jim_25.2.10	MURINE(270410)	FAM1	B	8.06	3583	131818.0	13.67	1345	47286.0	21.8	2169	83629.0	30.79
25	2010-02-25_jim_2	jim_25.2.10	MURINE(270410)	FAM1	B	7.8	3294	113637.0	13.5	1146	38333.0	21.95	1825	77321.0	30.76
26	2010-02-25_jim_2	jim_25.2.10	MURINE(270410)	FAM3	B	713.81	51	1371.0							
27	2010-02-25_jim_2	jim_25.2.10	MURINE(270410)	FAM3	B	722.44	55	901.0							

Figure 4-8 Resolved PCR products in Genemapper (Applied Biosystems) represented in numerical form. The product size for each capillary run is identified. The quantity, defined by height and area, is also provided as illustrated above. The FAM marker refers to the fluorophore attached to the $(CA)_8RG$ primer used in the PCR.

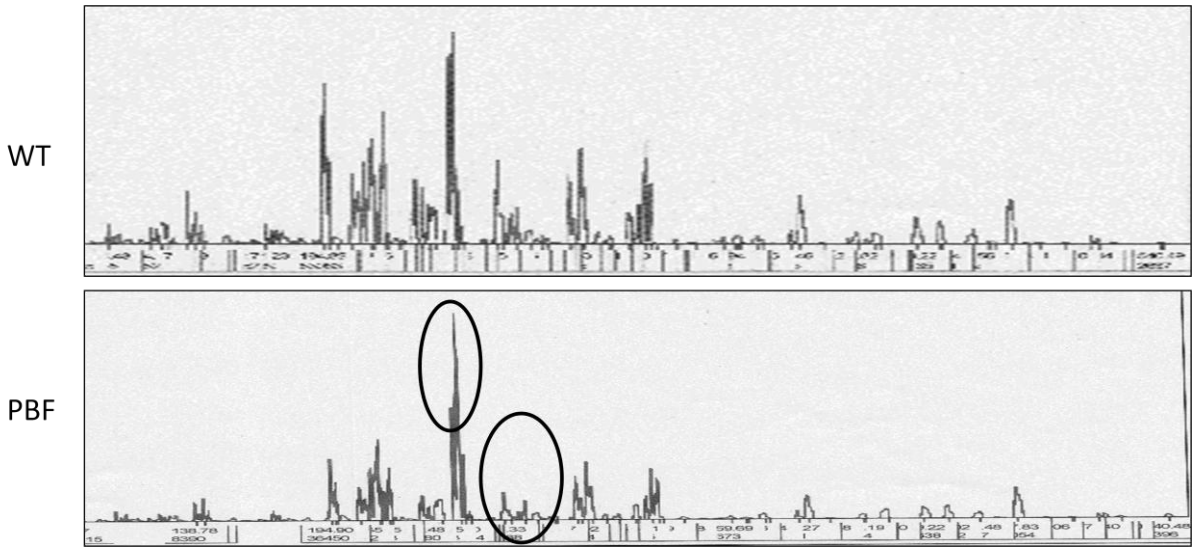

Figure 4-9 Graphical representation of PCR products resolved by sequencing on Genemapper (Applied Biosystems) showing gross differences (encircled) between WT and PBF genotypes, used in calculating the index of genetic instability.

4.3.7 **BI-Trans thyroids demonstrated significant genetic instability**

We compared the 4 different murine thyroid genotypes; wild type (WT), PBF, PTTG+/+ and BI-Trans (homozygous for both PBF and PTTG) using FISSR-PCR. A mean total of 154 unique fragments were found in the WT sample (n=5). PBF (n=5) did not have any unique fragments compared to WT resulting in a GI index of 0.00. PTTG+/+ (n=5) had an average of 3 unique fragments resulting in a genetic instability (GI) index of 1.95 ± 0.96 (p=0.78). Bi-trans (n=4) had a GI index of 3.73 ± 1.28 (p=0.01) as shown in Figure 4-10.

These results suggest that in vivo, PBF or PTTG+/+ overexpression in the thyroid gland independently do not cause genetic instability. However, when PBF and PTTG are overexpressed together within the thyroid gland, the effect is one of increased genetic instability.

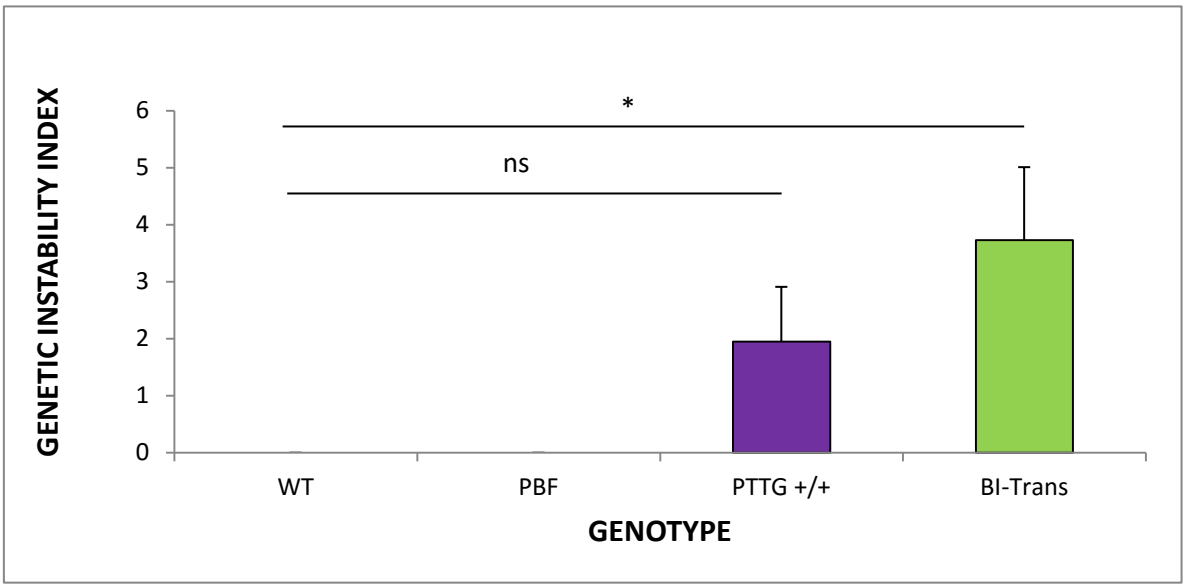

*Figure 4-10 GI index comparison according to genotype in vivo. PBF (n=5) and PTTG+/+ (n=5) thyroids appear to have no statistically significant genetic instability compared to WT (n=5). However, BI-Trans (n=4) thyroids had a GI index which was statistically significant compared to WT (p=0.01, denoted with *).*

4.3.8 **PBF, PTTG and BI-Trans PMTCs exhibited genetic instability**

We next quantified the index of genetic instability (GI) PMTCs for all four genotypes as a control for our experiments with ionising radiation. DNA was extracted from PMTCs on day 10. As shown in Figure 4-11 PBF (n=4), PTTG+/+ (n=5) and BI-Trans (n=5) PMTCs exhibited detectable genetic instability compared to wild type (WT) (n=5). The mean total number of unique fragments in this PCR run for WT was 128. The GI index for PBF, PTTG+/+ and BI-Trans was 18.75 ± 1.78 ($p<0.0001$ compared to WT), 7.19 ± 1.55 ($p=0.002$ compared to WT) and 35.78 ± 2.56 ($p<0.0001$ compared to WT) respectively. Interestingly, PBF PMTC had a higher GI index compared to PTTG+/+ which was statistically significant ($p=0.002$). BI-Trans PMTCs exhibited marked genetic instability compared to PBF ($p=0.001$) or PTTG ($p<0.0001$) PMTC, similar to that observed in murine thyroids.

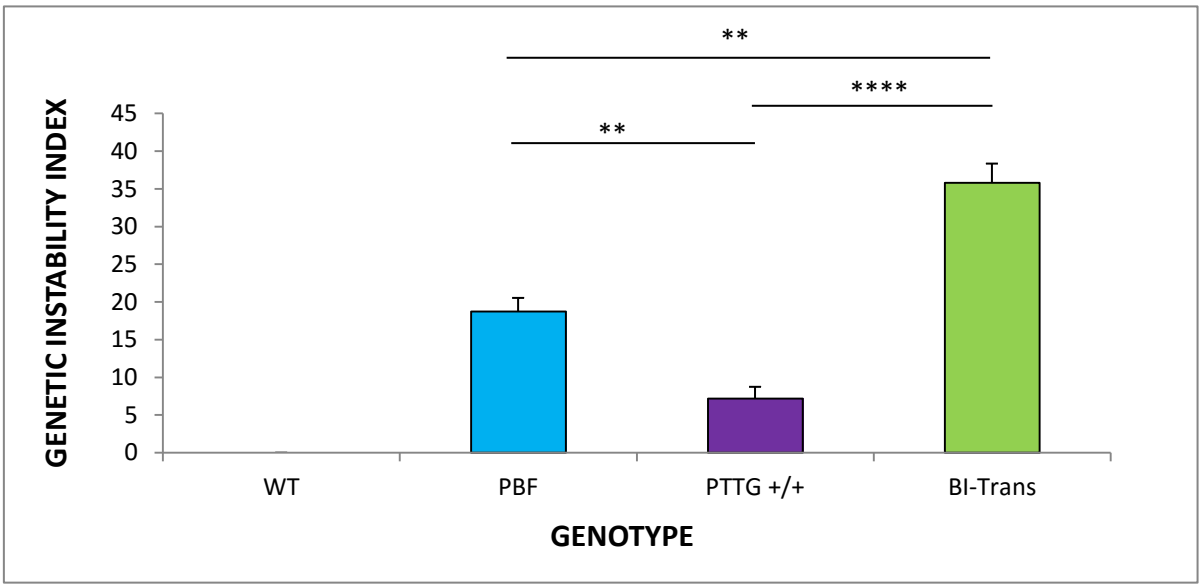

*Figure 4-11 GI index in primary murine thyroid cultures by genotype. All 3 genotypes of PBF (n=4), PTTG+/+ (n=5) and BI-Trans (n=5) exhibit genetic instability compared to WT. p-values are denoted with ** ($0.001 < p \leq 0.01$) and **** ($p \leq 0.0001$).*

4.3.9 PBF is associated with reduced genetic instability in cultured thyroid cells following exposure to ionising radiation

PMTCs which underwent radiation were exposed to ionising radiation (IR+) on day 9 and harvested on day 10. The dose of ionising radiation, 25 Gy was determined to be optimal, without causing cell culture death and sufficient to demonstrate changes (experimental work by Dr. Robert Seed, University of Birmingham). Following irradiation of PMTCs, all genotypes exhibited a statistically significant change in the index of GI as shown in Figure 4-12. In comparison with WT PMTCs without irradiation (WT IR-), WT PMTCs following exposure to ionising radiation (WT IR+) had a GI index of 17.19 ± 2.34 ($p<0.0001$; n=2). Although the GI index of PBF IR+ was significantly increased (7.65 ± 1.63; $p=0.002$; n=5) it had a protective effect on thyroid cells compared to the GI index of WT IR+. PTTG+/+ IR+ (n=5) had a GI index of 29.53 ± 1.51 which was significantly higher than WT ($p<0.0001$) and WT IR+ ($p=0.007$). The GI index for BI-Trans IR+ was significantly elevated (11.09 ± 2.35; $p=0.001$; n=5) but this was not significant when compared to PBF IR+ ($p=0.26$). PTTG+/+ IR+ had a significantly elevated GI index compared to BI-Trans IR+ ($p=0.0002$) and PBF IR+ ($p<0.0001$).

Overall, PBF had a protective effect whilst PTTG+/+ had the opposite effect, augmenting DNA damage following radiation exposure. However, when both PBF and PTTG were overexpressed together in primary murine thyroid cultures, the damaging effects of PTTG appeared to be partially ameliorated by PBF.

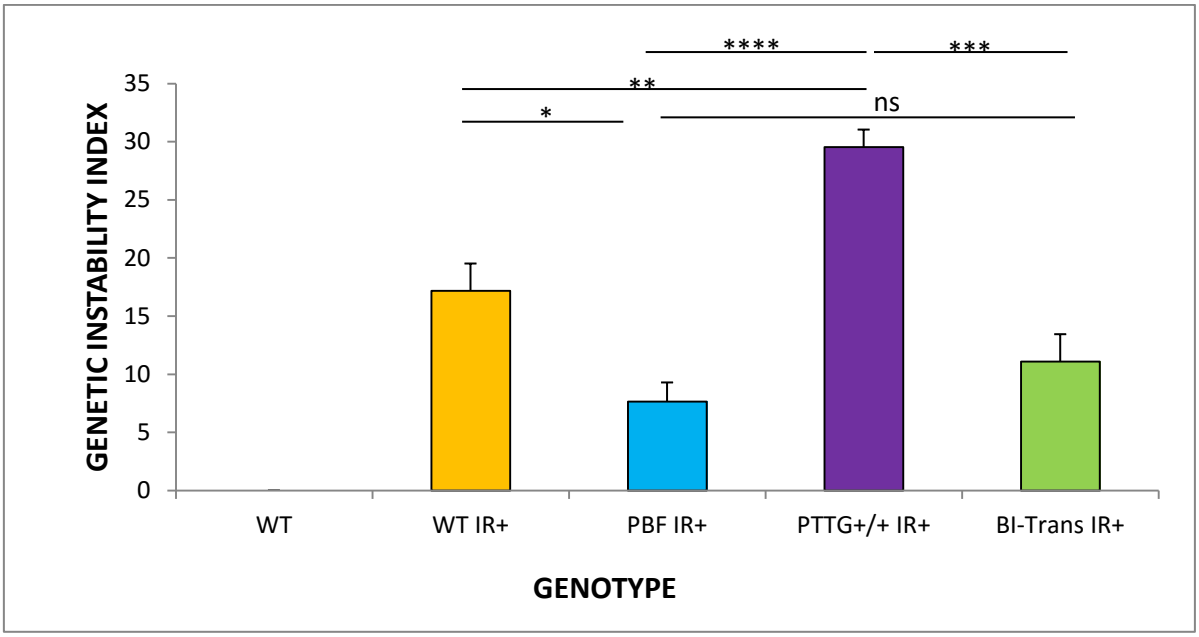

*Figure 4-12 Genetic instability (GI) index of WT, PBF, PTTG+/+ and BI-Trans following ionising radiation. WT IR+ (n=2), PBF IR+ (n=5), PTTG+/+ IR+ (n=5) and BI-Trans IR+ (n=5). p-values are denoted with ns for p>0.05, * (0.01 < p ≤ 0.05), ** (0.001 < p ≤ 0.01), *** (0.0001 < p ≤ 0.001) and **** (p ≤ 0.0001).*

4.3.10 **GI index before and after ionising radiation by genotype**

When the data was assimilated across the treatment groups shown in Figure 4-13, there was a significant change before and after ionising radiation treatment to PMTCs, as expected. Cells overexpressing PTTG after irradiation (PTTG+/+IR+) exhibit more DNA damage than PTTG+/+ without irradiation (p,0.0001). Interestingly, PBF appeared to have a protective effect after exposure to radiation and the difference between PBF IR- and PBF IR+ was statistically significant (p=0.003). This effect was also observed in the BI-Trans model where both PBF and PTTG are overexpressed together (p=0.001). However, PBF independently without radiation appeared to cause more DNA damage than PTTG+/+ in PMTC.

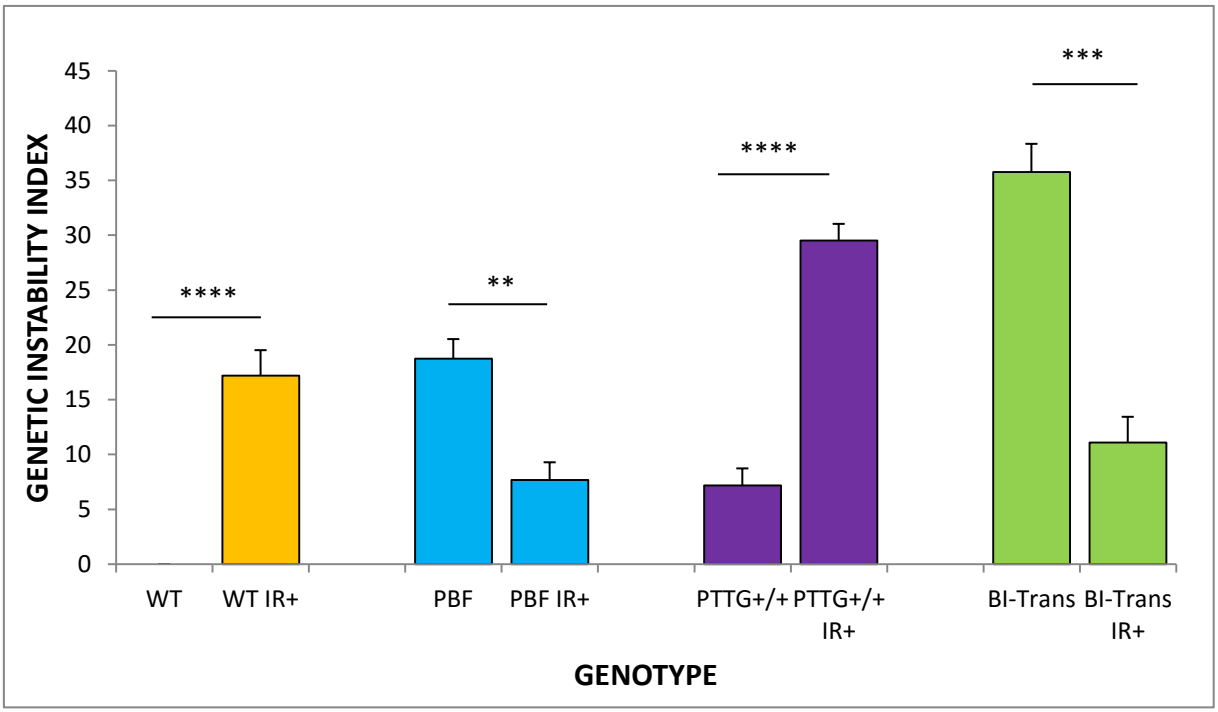

*Figure 4-13 Genetic instability (GI) index with and without ionising radiation by genotype. PMTCs were exposed to 25 Gy of ionising radiation and the GI index measured using FISSR-PCR. p-values are denoted with ** (0.001 < p ≤ 0.01), *** (0.0001 < p ≤ 0.001) and **** (p ≤ 0.0001).*

4.4 DISCUSSION

4.4.1 Primary murine thyroid culture

Human primary thyroid culture has been described and used extensively by various groups previously (Eggo et al., 1996, Boelaert et al., 2007). PMTC has been described much less frequently than human primary thyroid culture and is a technically challenging exercise because of the diminutive size of the murine thyroid gland, which only weighs 2 mg on average. Before the technique was finally optimised and described above, several attempts at the technique were performed.

Growth of murine thyroid cells was confirmed with light microscopy. PMTC was viable for approximately 14 days. However, the optimum period for maximal cell coverage was around 10 days. The cultures were heterogenous in appearance. We established that thyroid epithelial cells arose from follicles and appeared to disperse on the plate resulting in a cluster pattern when viewed under the microscope. Immunofluorescence had revealed a second type of cell which was not typical of a thyroid epithelial cell. These cells were generally one cell thick on the plate, had a fusiform morphology and connected thyroid epithelial cell clusters, and were most likely fibroblast cells arising from murine thyroids. The area of well coverage was approximately 60 – 70 % at day 10 when experimentation occurred. Furthermore, radioiodine uptake studies were useful in confirming that PMTCs were functioning thyroid cells, suitable for experimentation. Overall, we established the technique of PMTC in our laboratory as a functional assay which was suitable for our hypotheses relating to the induction of genetic instability.

4.4.2 FISSR-PCR

An established technique for measuring genetic instability in our group is fluorescent inter-simple sequence repeat PCR (FISSR-PCR) (Kim et al 2005). The modification of the technique using a DNA

sequencer (ABI 3730, Applied Biosystems) to resolve PCR products was necessary for measuring genetic instability in murine thyroids and PMTC.

Several optimisation experiments were carried out. Whilst the sequencing step in FISSR-PCR was consistent and reliable, it appeared that the PCR step was not always consistent in yielding the same result. As such, a control for the base denominator of the GI index equation is required each time the genetic instability index was quantified. Different PCR runs could not therefore be compared with each other.

Unequal loading of sample or reagent during the PCR phase or fragment analysis stage could result in different areas under each peak. To control for this, we determined the total fluorescence of a sample on the ABI 3730 and adjusted it to an arbitrary value of 2,000,000 relative fluorescent units.

Using the sequencer to resolve PCR products yielded a huge volume of data. Typically, PCR products ranged between 80 and 900 base pairs in length. The Genemapper software detects all fragments and quantifies these by using the height or area under each peak. We defined a difference as a change of more than 500 units in peak area and a band height difference of more than 3 fold. The estimated GI index from the same species within the same PCR run had a variation of less than 10 % using these criteria.

The yield of DNA from a whole murine thyroid is far greater than can be obtained from PMTC. This did not prove to be a limiting factor because of the sensitivity of the FISSR sequencing technology.

4.4.3 **Index of genetic instability**

PTTG, the human securin regulates mitosis and is known to be overexpressed in thyroid cancers (Smith et al., 2010). The relationship between PTTG and genetic instability in the thyroid has been reported previously by our group (Kim et al., 2005). The binding factor of PTTG, PBF, shuttles PTTG

to the nucleus for its actions. Furthermore, PBF binds to and negatively regulates Trp53 which has a key role in maintaining genomic stability in a cell (Read et al., 2014a, Read et al., 2014b).

Thyroid cancers have been demonstrated to exhibit genomic instability (Bauer et al., 2002, Kim et al., 2005, Mitsutake et al., 2005, Saavedra et al., 2000, Ward et al., 1998). The relationship between genetic instability and tumour formation is not fully understood. However, ionising radiation which induces DNA damage and causes genetic instability is a recognised cause of thyroid cancer.

In stable thyroid tissue, PBF and PTTG expression independently did not result in genetic instability. However, when both PBF and PTTG (BI-Trans) were overexpressed in murine thyroids, there was an increase in the index of genetic instability suggesting a synergistic effect of PBF and PTTG. PBF independently caused more genetic instability than PTTG in primary murine thyroid cultures (PMTCs). This observation suggests that PBF plays an important role compared to PTTG in causing genetic instability in cells that are growing or being cultured in an environment that encourages proliferation.

Interestingly, it was observed that PBF had a protective effect whilst PTTG had a synergistic effect with ionising radiation in increasing the index of genetic instability. This protective effect was further confirmed when BI-Trans PMTCs following radiation exposure had a lower GI index compared to BI-Trans without irradiation. This observation may be a result of PBF enhancing repair following DNA damage.

4.5 CONCLUSION

The relationship between PBF, PTTG and ionising radiation is complex and we aimed to understand the mechanism by which these two genes cause genetic instability by exploring the expression of genes related to DNA damage and repair pathways next.

5 The effect of genotype on DNA damage and repair genes

5.1 INTRODUCTION

5.1.1 Background

Cancer formation is a result of uncontrolled cellular proliferation. The process of cellular proliferation is a tightly regulated process controlled by a variety of genes. A faulty replication process results in genetic mutation and genetic instability. The association between high levels of PBF and PTTG expression with thyroid cancer has been demonstrated previously (Boelaert et al., 2003, Heaney et al., 2001, Hsueh et al., 2013, Stratford et al., 2005).

PTTG overexpression inhibits Ku70 which facilitates non-homologous DNA end-joining repair of double strand breaks (Kharbanda et al., 1998, Kim et al., 2007b, Romero et al., 2001, Smith and Jackson, 1999). Additionally, PTTG regulates mitosis at the metaphase-anaphase interface.

The binding partner of PTTG, PBF, transports PTTG to the nucleus and facilitates it's action. PBF has been shown to interact with and negatively regulate a critical gene involved in maintaining genomic stability, Trp53 (Read et al., 2014a, Read et al., 2014b). PBF has also been shown to be transforming in vitro and tumourigenic in vivo, independent of PTTG.

Taken together, the above indicate that PBF and PTTG have roles in maintaining genomic stability of a cell dependently and independently. Furthermore, work in this investigation outlined in the previous chapter, demonstrated the effect of PBF and PTTG on the index of genetic instability in thyroid cells. We next studied key genes intimately involved in DNA damage and repair in association with our genes of interest to establish the mechanism by which PBF and PTTG affect genomic stability in a dependent and independent manner. Microarrays based on the key DNA damage and repair pathway, the ATM/ATR signalling pathway, were used for this purpose.

5.2 MATERIALS AND METHODS

5.2.1 Primary murine thyroid cultures

Primary murine thyroid culture (PMTC) was performed on the 4 different genotypes (WT, PBF, PTTG +/+ and BI-Trans), using 3 males in each genotype group as discussed in section 2.2.

5.2.2 RNA extraction

RNA was harvested from PMTCs on day 10 using the micro RNeasy kit (QIAGEN), specifically designed for small samples. PMTCs were harvested using buffer RLT (QIAGEN) to lyse cells. The lysate was subsequently subjected to the QIAshredder homogenizer (QIAGEN) to improve the quality of RNA yield. Next, 70 % ethanol was added to the lysate to provide optimum binding conditions to the silica membrane. The sample was subsequently transferred to a RNeasy MinElute spin column and spun at high speed. This step allowed for binding of the RNA to the silica membrane present in the MinElute spun column. The spin column was washed twice with Buffer RW1 (proprietary solution in RNeasy kit). The third wash was with Buffer RPE to remove traces of salts left by Buffer RW1. The fourth wash was with 80 % ethanol. The final step was the addition of 14 µl of RNAse-free water to dissolve the RNA bound to the silica membrane. The dissolved RNA was collected in an Eppendorf and the RNA concentration measured using the Nanodrop (ThermoScientific).

5.2.3 Reverse transcription

Reverse transcription was performed as described in section 2.5.

5.2.4 RT^2 Profiler™ PCR Arrays

RT^2 Profiler™ PCR Arrays (SABiosciences) were used for gene expression detection. Each array consisted of a panel of 84 genes relevant to the pathway investigated. The array chosen was the mouse DNA Damage Signalling array (PAMM-029E). Each plate contained 384 wells. Measurements were carried out in duplicate for each sample.

Each reaction consisted of 1 µl of cDNA, 5.5 µl of RT^2 qPCR Master Mix (PA-012-8 SABiosciences), containing SYBR Green and ROX, diluted to a total volume of 10 µl in nuclease-free water. The plate was initially heated to 95 °C for 10 minutes. Subsequently, the plate was subjected to 40 cycles of 95 °C for 15 seconds and 60 °C for 1 minute in the ABI 7900HT Real-Time PCR System.

The baseline was manually defined using the log view of the amplification plot. Data were expressed as Ct values and used to determine ΔCt values by subtracting the Ct of the housekeeping gene from the Ct of the target gene. The fold change of mRNA was calculated using the following equation:

$$\text{Fold change} = 2^{-(\Delta Ct \text{ of the experimental group} - \Delta Ct \text{ of the control group})}$$

where the experimental group refers to PMTC genotype e.g. WT, PBF, PTTG+/+, BI-Trans and the control group the housekeeping genes on the array e.g. β-actin. Results were expressed as fold change relative to the standard, wild type PMTC without radiation. Fold changes which were more than twice or less than half the mRNA expression apparent in wild-type (WT) PMTCs were considered significant during data analysis.

5.3 RESULTS

The data from the microarray study in this chapter was analysed initially by identifying the overall pattern of mRNA gene expression on the microarray according to PMTC genotype. Subsequently, mRNA gene expression was analysed by functional grouping as follows: genes involved with apoptosis, cell cycle arrest, cell cycle checkpoint, damaged DNA binding, base excision repair, nucleotide excision repair and double strand break repair.

5.3.1 Expression of DNA damage signalling genes in PBF PMTCs

The overall mRNA gene expression in PBF PMTCs compared with wild type (WT) was predominantly repressive, as shown in Figure 5-1. This pattern suggests an inhibitory effect on genes that might play an important role in DNA repair.

The Transient receptor potential cation channel, subfamily C, member 2 (Trpc2) gene displayed the most suppression in PBF primary murine thyroid cultures (PMTCs), approximately 0.21 fold of WT PMTCs (n=3). Trpc2 is involved in intracellular calcium signalling. The rise of intracellular calcium has been shown to increase apoptosis. It is recognised that the process of apoptosis is intimately related to the influx of Ca^{2+} controlled by Trpc2 and the loss of endoplasmic reticulum Ca^{2+} (Pigozzi et al., 2004).

The expression of X-ray repair complementing defective repair in Chinese hamster cells 3, Xrcc3 was 0.38 fold in PBF PMTCs relative to WT PMTCs (n=3). Xrcc3 is a member of the Rad51 group of genes that maintain chromosome stability and repair DNA damage by participating in homologous recombination.

Both mutYHomolog (Mutyh) and Rad9b had reduced expression at 0.47 fold in PBF PMTC (n=3). Mutyh is involved in oxidative DNA damage repair. This enzyme cleaves adenine bases from the

DNA backbone when adenine is paired incorrectly with guanine, cytosine or 8-oxo-7,8-dihydroguanine. Rad9b is a homolog of DNA Repair Exonuclease Rad9.

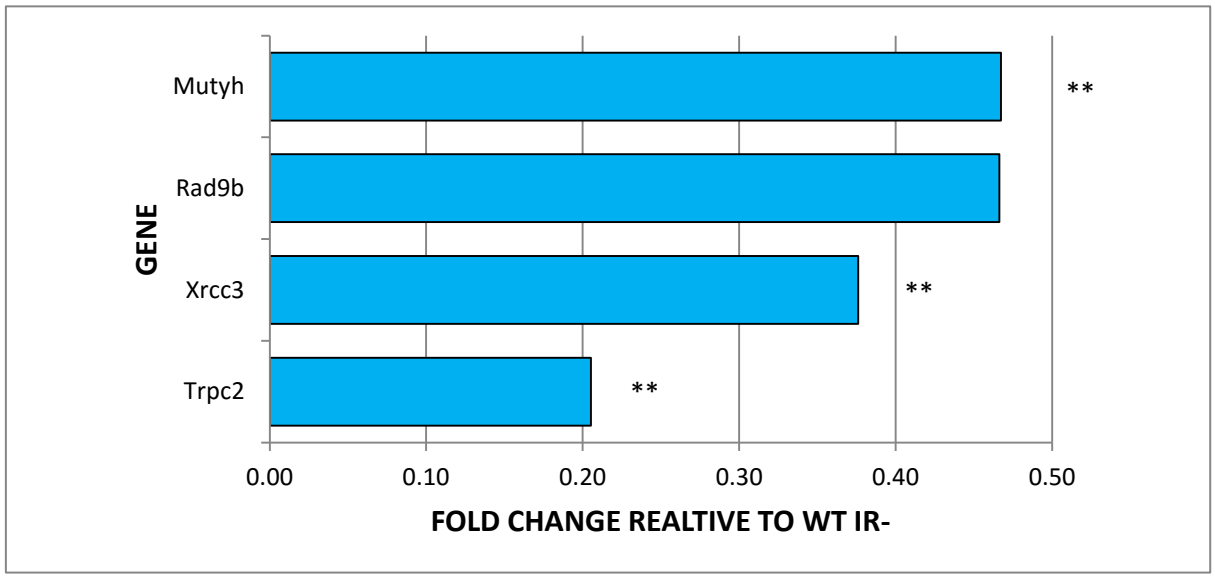

*Figure 5-1 DNA damage gene mRNA expression changes in PBF PMTC compared with wild type (n=3) on the RT^2 Profiler^{TM} PCR Arrays that is less than half. No genes on the array was expressed more than twice. Statistical p-values are represented by ** if $0.001 < p \leq 0.01$. IR- refers to without ionising radiation.*

5.3.2 **Expression of DNA damage signalling genes in PTTG PMTCs**

In contrast to PBF PMTCs, PMTCs from homozygote PTTG mice (PTTG+/+) resulted in significant mRNA expression alterations (defined by an expression of more than twice or less than half) in DNA damage signalling genes compared with wild type (WT) PMTCs as illustrated in Figure 5-2.

The genes most significantly upregulated in the presence of PTTG overexpression in the thyroid were Polk (3.08 x), Rad9 (3.05 x) and Tdg (3.07 x). This was followed by Ube2a (2.24 x), Hus1 (2.12 x), Nthl1 (2.06x) and Pms1 (2.03); (n=3).

Equally, a wide array of DNA damage / DNA repair genes were suppressed in the presence of PTTG. These suppressed genes included Exo1 (0.11 x), Brca1 (0.15 x), Rad51 (0.23 x), Chek1 (0.23 x), Pole (0.29 x), Fen1 (0.31 x) Chaf1a (0.36 x), Rad18 (0.37 x), Fancg (0.38 x), Fancc (0.38 x), Pms2 (0.42 x), Mbd4 (0.43 x), Trex 1 (0.44 x), Xpa (0.46 x) and Rad51l1 (0.47 x); (n=3).

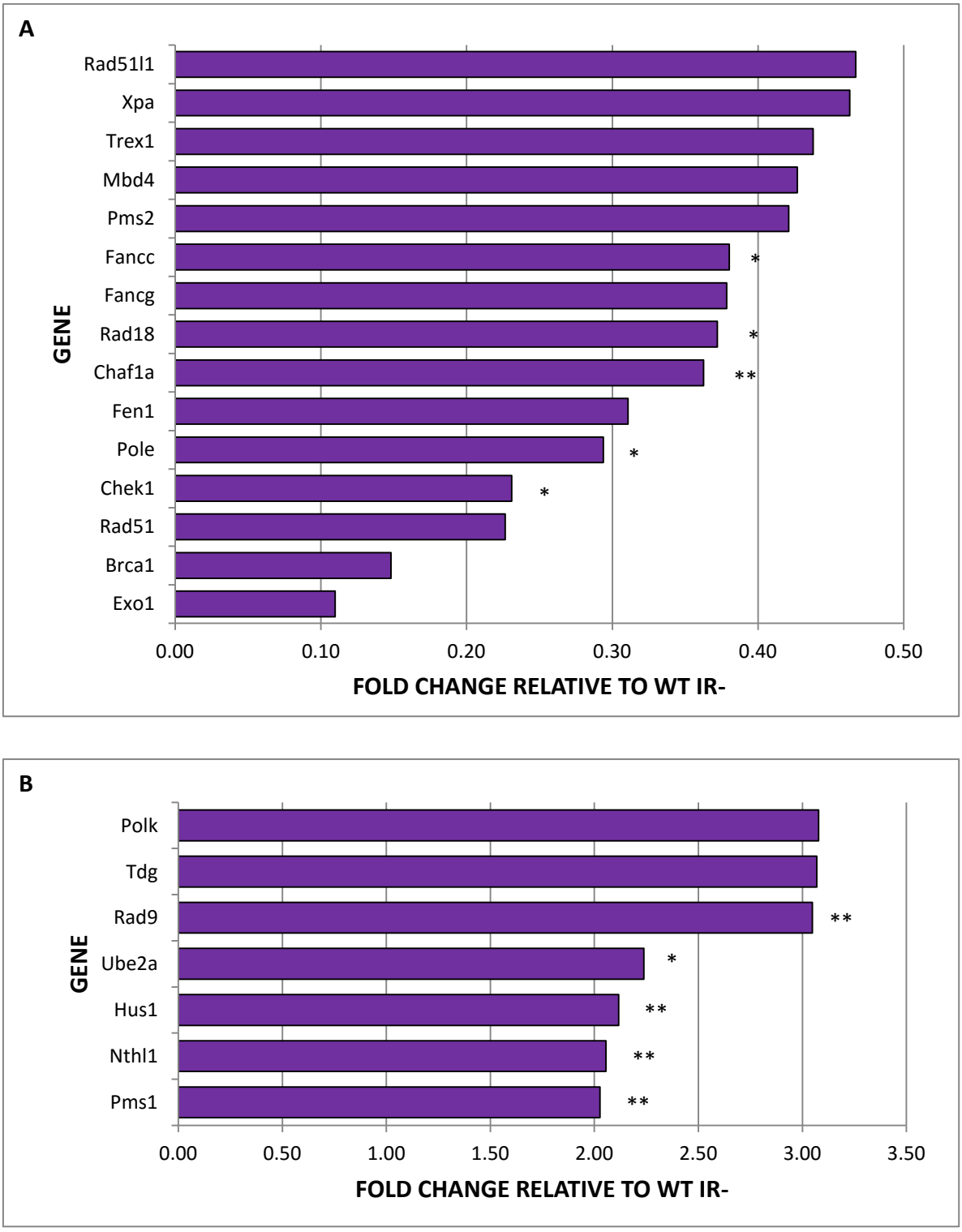

Figure 5-2 DNA damage / DNA repair gene mRNA expression in PTTG+/+ PMTC. The genes that were expressed by more than twice (B) or less than half (A) compared to WT IR- PMTC (n=3) were considered significant. However, statistical p-values are also shown. If $0.01 < p \leq 0.05$ (*) and $0.001 < p \leq 0.01$ (**). IR- refers to without ionising radiation.

5.3.3 **Expression of DNA damage signalling genes in BI-Trans PMTCs**

Targetted overexpression of both PBF and PTTG in transgenic murine thyroids (BI-Trans) resulted in an interesting pattern on the DNA damage signalling pathway microarray seen in Figure 5-3. Genes such as Polk, Rad9, Tdg, Ube2a, Hus1, Nthl1 and Pms1 were no longer stimulated to a significant extent as they have been in PTTG+/+ and PBF transgenic models. The genes inhibited in the BI-Trans PMTCs by more than twice included Trpc2 (0.27 x), Pms2 (0.38 x), Brca1 (0.38 x), Ung (0.38 x), Chek1 (0.39 x), Mbd4 (0.39 x), Exo1 (0.43 x), Fen1 (0.44 x), Fancg (0.45 x), Chaf1a (0.45 x) and Rad51 (0.5 x); (n=3). Genes which were significantly repressed in PTTG PMTCs but not significantly repressed in BI-Trans included Fancc (0.59 x), Pole (0.51 x), Rad18 (0.63 x), Rad51l1 (0.67 x), Trex1 (0.56 x) and Xpa (0.65 x); (n=3). The genes of Muyth, Rad9b and Xrcc3 were significantly repressed in PBF PMTCs but is no longer significantly repressed in cells co-expressing PTTG. Brca1 (0.38 x), Chaf1a (0.45 x), Chek1 (0.39 x), Fen 1 (0.44 x) and Rad51 (0.5 x) repressed in PTTG PMTCs were still suppressed in the presence of PBF but to a lesser extent (n=3). The genes that was repressed in BI-Trans PMTCs, Trpc2 (3.68 x), was not repressed as much in the presence of both PBF and PTTG compared to PBF alone.The only unique gene inhibited when both PBF and PTTG were overexpressed in PMTCs was Ung. The profile of genes repressed in BI-Trans where fewer genes were suppressed compared to PTTG alone, suggests a more stable cell when compared to PTTG but more unstable compared to PBF.

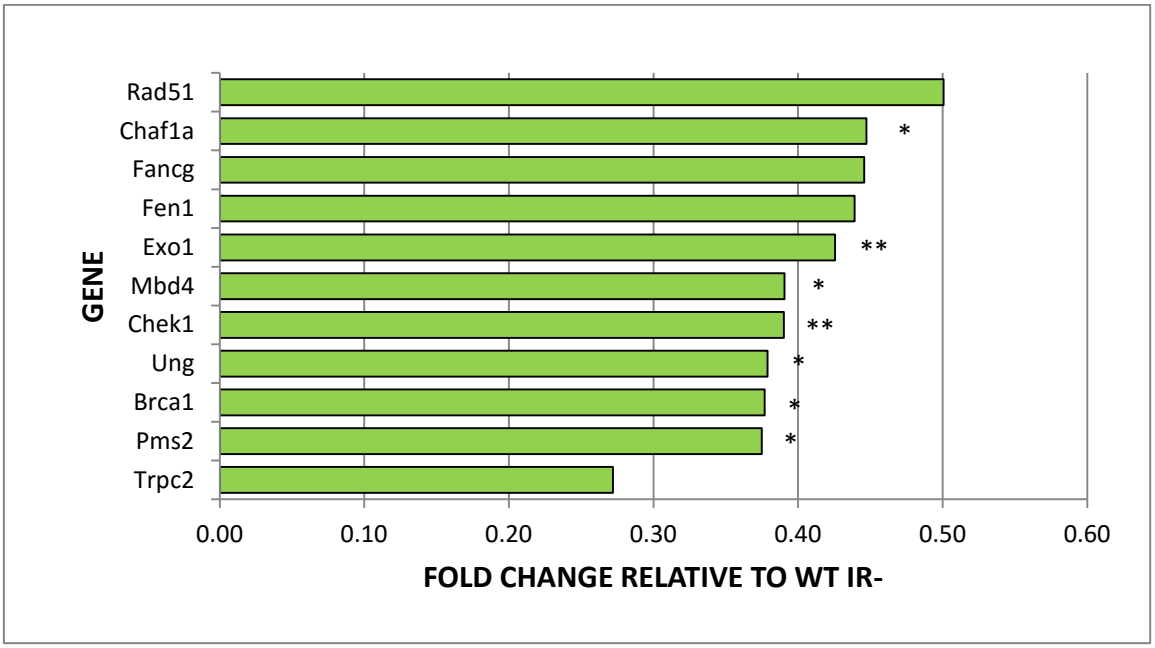

Figure 5-3 DNA damage / DNA repair gene expression in BI-Trans PMTC without irradiation (n=3) compared with wild type without irradiation (WT IR-). If $0.01 < p \leq 0.05$ (*) and $0.001 < p \leq 0.01$ (**). Fold changes were considered significant if expressed by less than half. No genes were expressed by more than twice. IR- refers to without ionising radiation.

5.3.4 **Affect upon apoptotic genes**

We next examined the microarray mRNA gene expression profile by functional grouping. Brca1 (0.15 fold) and Mbd4 (0.43 fold) were repressed by PTTG shown in Figure 5-4. The repression of Brca1 was partially ameliorated by the additional presence of PBF. In BI-Trans, Brca1 expression was 0.38 fold (Figure 4.4). In comparison, Mbd4 repression in BI-Trans remained unaffected by the presence of PBF. Taken together, PTTG suppressed the apoptotic genes Brca1 and Mbd4 but this effect was reduced in the presence of PBF. PBF on its own did not have a significant effect on any of the genes involved with apoptosis in the array.

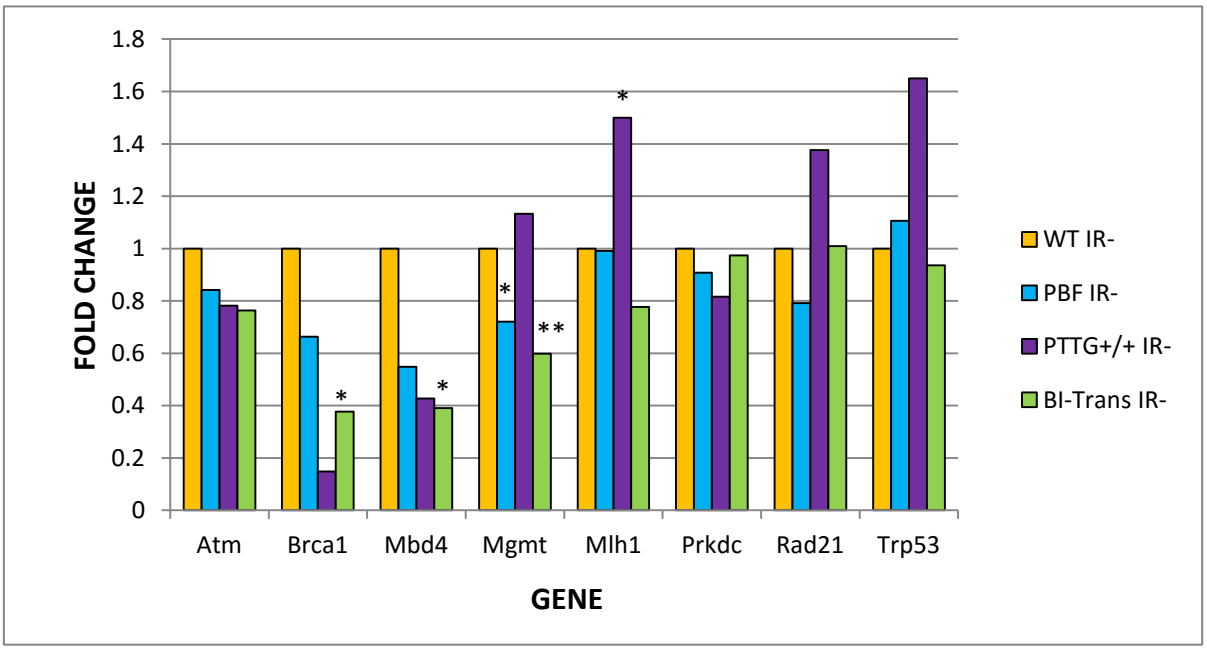

*Figure 5-4 Expression of genes involved in apoptosis according to genotype (n=3). Statistical significance is represented by * if $0.01 < p \leq 0.05$ and ** if $0.001 < p \leq 0.01$.IR- denotes without ionising radiation.*

5.3.5 Affect upon genes involved in cell cycle arrest

PBF did not have any significant effect on the expression of any of the cell cycle arrest genes investigated, illustrated in Figure 5-5. In PTTG+/+ (thyroids homozygous for PTTG) PMTCs, the expression of Hus1 was 2.11 fold and Chek1 0.23 fold relative to wild type (WT) PMTCs (n=3). Hus1 is a gene involved in cell cycle arrest following DNA damage. Interestingly, Chek1, a gene involved in cell cycle arrest in response to DNA damage and serves to integrate signals from ATM and ATR, was suppressed in PTTG+/+ PMTCs. In BI-Trans PMTCs, only Chek1 was suppressed (0.39 fold). Taken together, PTTG overexpression was associated with cell cycle arrest via the overexpression of Hus1, but when PBF was concurrently overexpressed with PTTG, the overexpression of Hus1 was ameliorated.

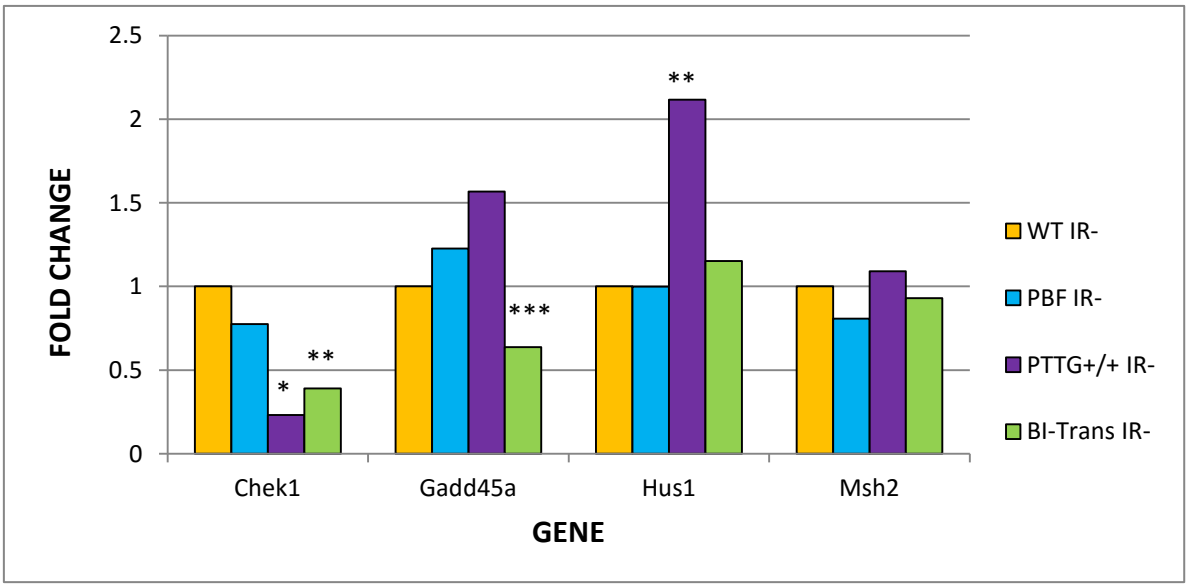

Figure 5-5 Cell cycle arrest gene expression by genotype (n=3). If $0.01 < p \leq 0.05$ (*), $0.001 < p \leq 0.01$ (**) and $0.0001 < p \leq 0.001$ (***). IR- denotes without ionising radiation.

5.3.6 **Affect upon cell cycle checkpoint genes**

PBF PMTCs which overexpressed PBF in thyroid cells did not show any significant expression changes in cell cycle checkpoint genes shown in Figure 5-6. PTTG+/+ PMTCs overexpressed Rad9, a cell cycle checkpoint protein required for cell cycle arrest and DNA damage repair, by 3.05 times. Bi-Trans PMTCs did not show any significant gene expression changes.

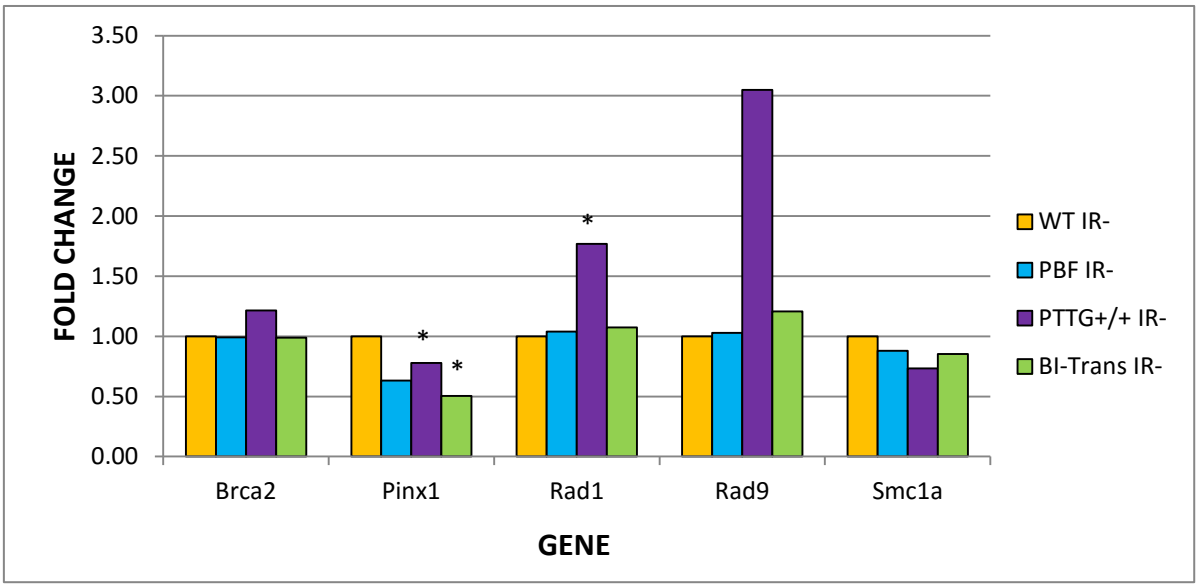

*Figure 5-6 Expression of genes involved in cell cycle checkpoint by genotype (n=3). The p-value is represented by * if $0.01 < p \leq 0.05$. IR- denotes without ionising radiation.*

5.3.7 Affect upon other genes related to the cell cycle

Figure 5-7 shows the affect of our 4 genotypes WT, PTTG+/+, PBF and BI-Trans on further genes related to the cell cycle. PTTG and BI-Trans PMTCs showed a repression of Chaf1a, with expressions of 0.36 and 0.45 fold compared to WT PMTCs, respectively. PBF did not appear to affect the other genes involved in the cell cycle. Chaf1a is a core component of CAF-1 complex, a complex thought to mediate chromatin assembly in DNA repair.

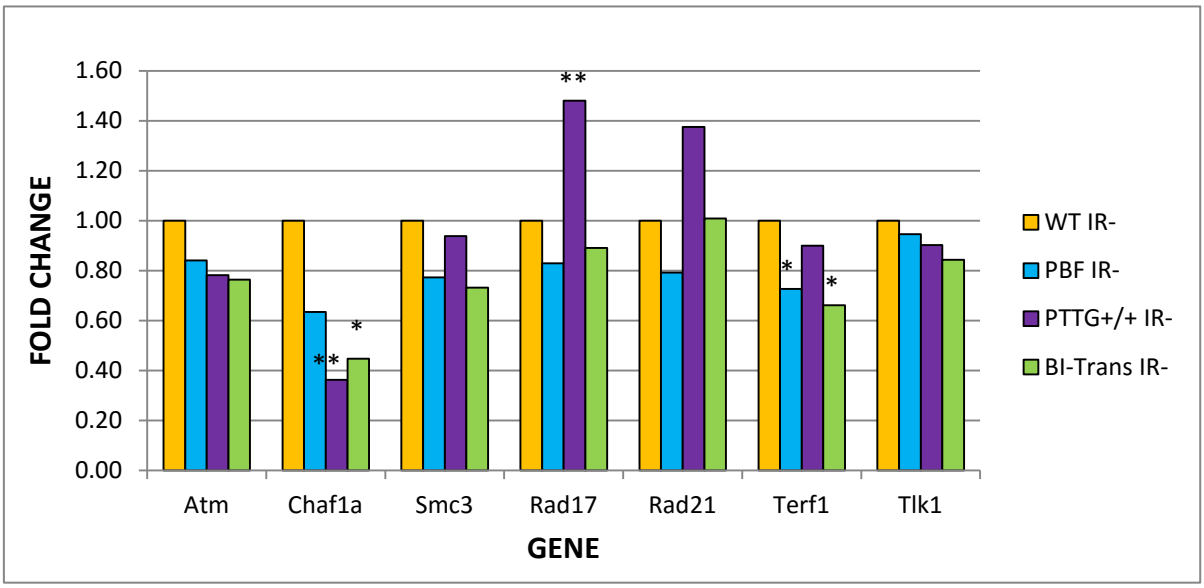

*Figure 5-7 Expression of further genes related to the cell cycle (n=3). p-values are denoted by * if $0.01 < p \leq 0.05$ (*) and ** if $0.001 < p \leq 0.01$ (**). IR- denotes without ionising radiation.*

5.3.8 **Affect upon genes involved in damaged DNA binding**

The expression of Trpc2 and Xrcc3 was reduced in PBF PMTC, with expression levels of 0.21 and 0.38 fold respectively compared to WT PMTCs, seen in Figure 5-8. Trpc2 and Xrcc3 remained suppressed to a lesser extent (0.27 and 0.55 fold respectively) in BI-Trans PMTCs. Additional suppressed genes in BI-Trans included Brca1 (0.38 fold) and Rad51 (0.50 fold). The profile of suppressed genes in PTTG PMTCs were similar to BI-Trans albeit to a more pronounced extent, with the expression of Brca1 0.15 fold and Rad51 0.23 fold relative to WT PMTCs in PTTG PMTCs. Additional genes reduced in PTTG PMTCs include Rad51l1 (0.47 fold) and Xpa (0.46 fold). The results suggest a general suppression of genes involved in DNA damage binding. Although not defined as significant, PTTG PMTCs demonstrated an increase in Rad1 by 1.77 times and Trpc2 by 1.88 times.

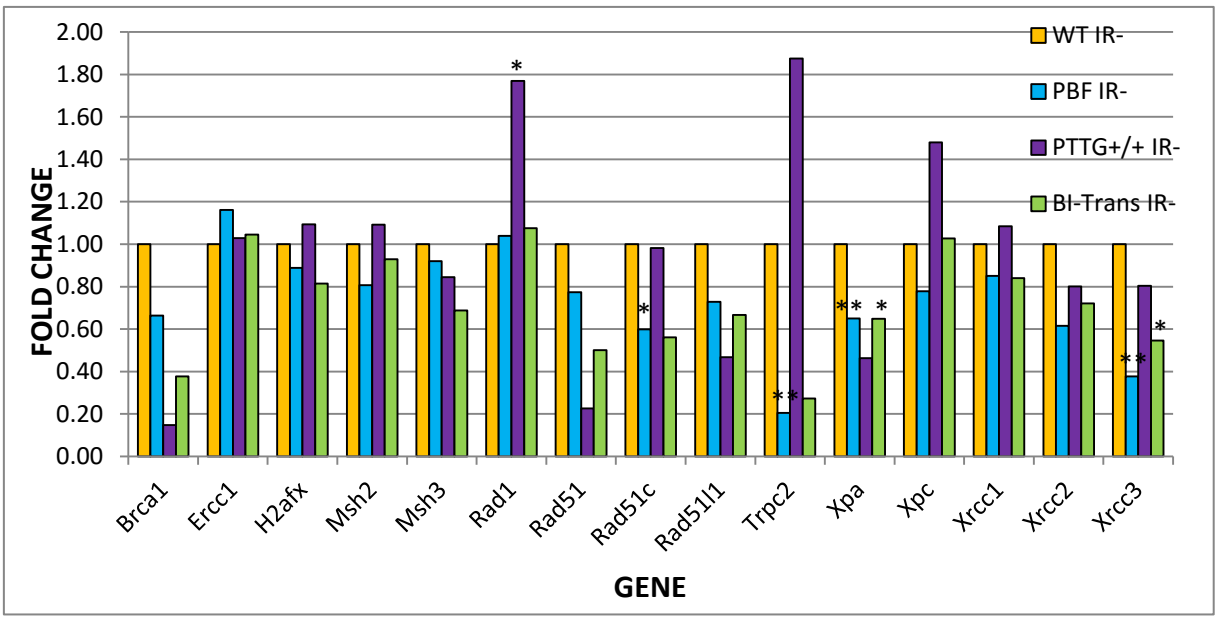

*Figure 5-8 Damaged DNA Binding gene expression by genotype. p-values are denoted by * if 0.01 < p ≤ 0.05 (*) and ** if 0.001 < p ≤ 0.01 (**). IR- denotes without ionising radiation.*

5.3.9 **Affect upon genes involved in base excision repair**

PTTG increased the relative expression of Nthl1 by 2.05 fold and reduced the expression of Mbd4 by 2.34 fold. The expression of Mutyh was 0.77 fold in PBF primary murine thyroid cultures (PMTCs) compared to WT PMTCs. The expression of both PBF and PTTG simultaneously resulted in a relative reduction in Mbd4 at 0.43 fold, shown in Figure 5-9.

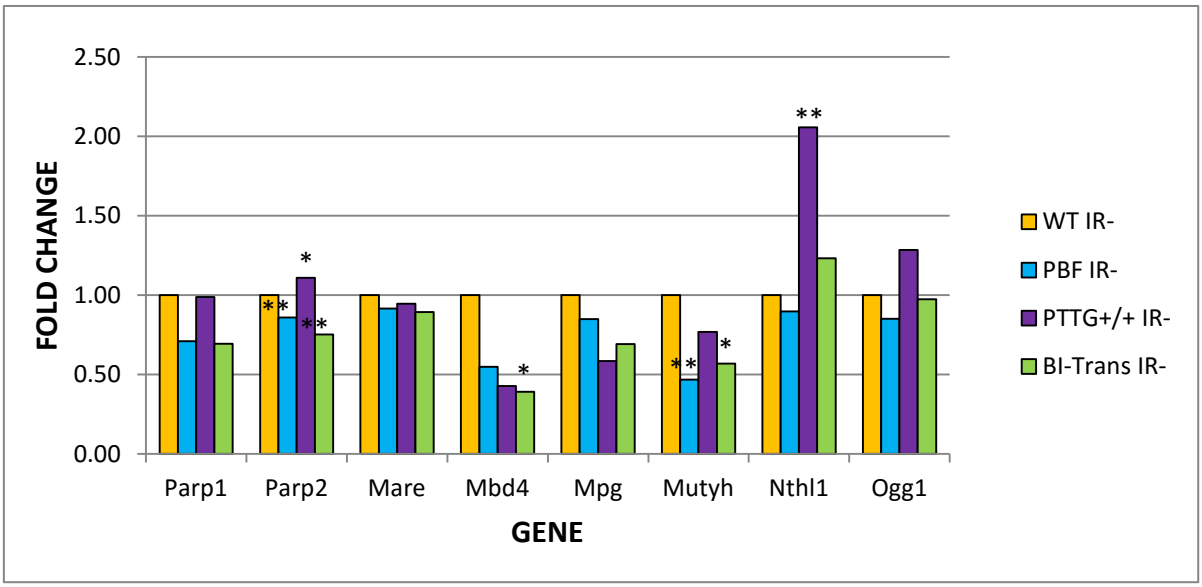

*Figure 5-9 Base excision repair gene expression by genotype (n=3). p-values are denoted by * if 0.01 < p ≤ 0.05 (*) and ** if 0.001 < p ≤ 0.01 (**). IR- denotes without ionising radiation.*

5.3.10 Affect upon genes involved in nucleotide excision repair

Figure 5-10 represents mRNA gene expression involved in nucleotide excision repair. The only gene that appeared to have any effect on genes involved in nucleotide excision repair is PTTG. Targetted thyroid overexpression of PTTG was associated with increased expression of Nthl1 (2.05 fold) and reduced expression of Fancc (0.38 fold) and Xpa (0.46 fold). PBF did not appear to have any effect on investigated genes involved in nucleotide excision repair. However, when both PBF and PTTG were overexpressed together in murine thyroid cells, the effect of PTTG on nucleotide excision repair genes was completely ameliorated.

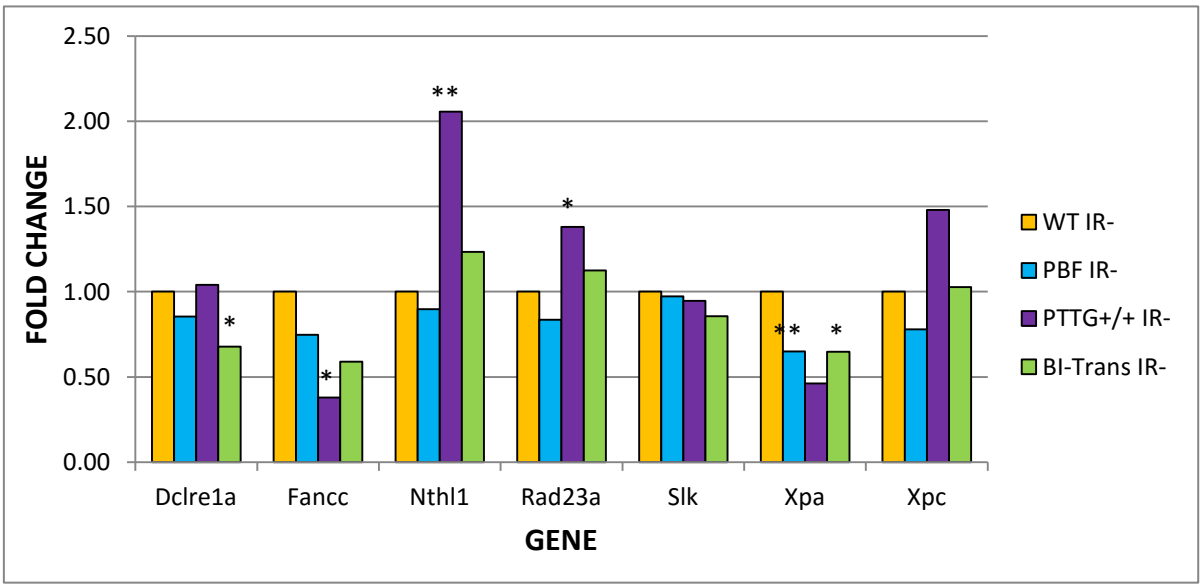

*Figure 5-10 Genes involved with nucleotide excision repair by genotype. p-values are denoted by * if $0.01 < p \leq 0.05$ (*) and ** if $0.001 < p \leq 0.01$ (**). IR- denotes without ionising radiation.*

5.3.11 **Affect upon genes involved in double strand break repair**

The expression of genes involved in double strand break repair was unchanged in PBF, PTTG and BI-Trans PMTCs, shown in Figure 5-11. We defined a significant change in mRNA expression as more than twice or less than half compared with wild type without ionising radiation (WT IR-).

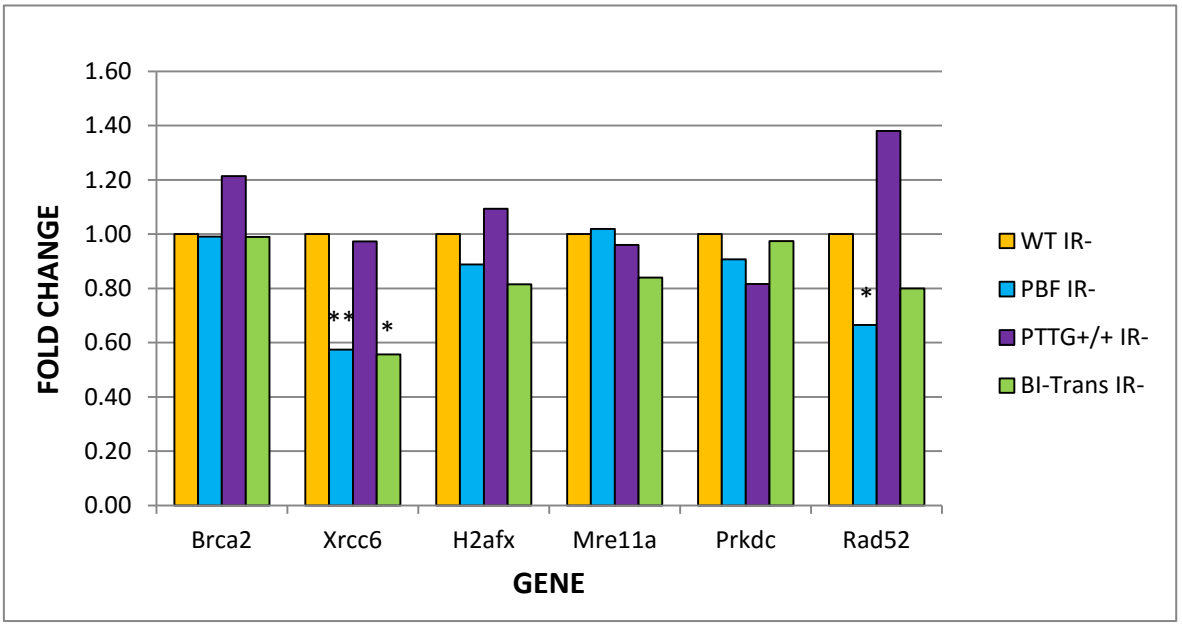

*Figure 5-11 Double strand break repair gene expression by genotype. p-values are denoted by * if $0.01 < p \leq 0.05$ (*) and ** if $0.001 < p \leq 0.01$ (**). IR- denotes without ionising radiation.*

5.3.12 Affect upon genes involved in mismatch repair

PBF did not have discernible effect on the expression of the mismatch repair genes included in the microarray (Figure 5-12). PTTG caused the increased expression of Pms1 (2.03 fold) and the suppression of Pms2 (0.42 fold) and Trex1 (0.44 fold) relative to WT PMTCs. In BI-Trans PMTCs, Pms2 remains suppressed (0.38 fold) but Pms1 is no longer overexpressed and Trex1 not significantly suppressed.

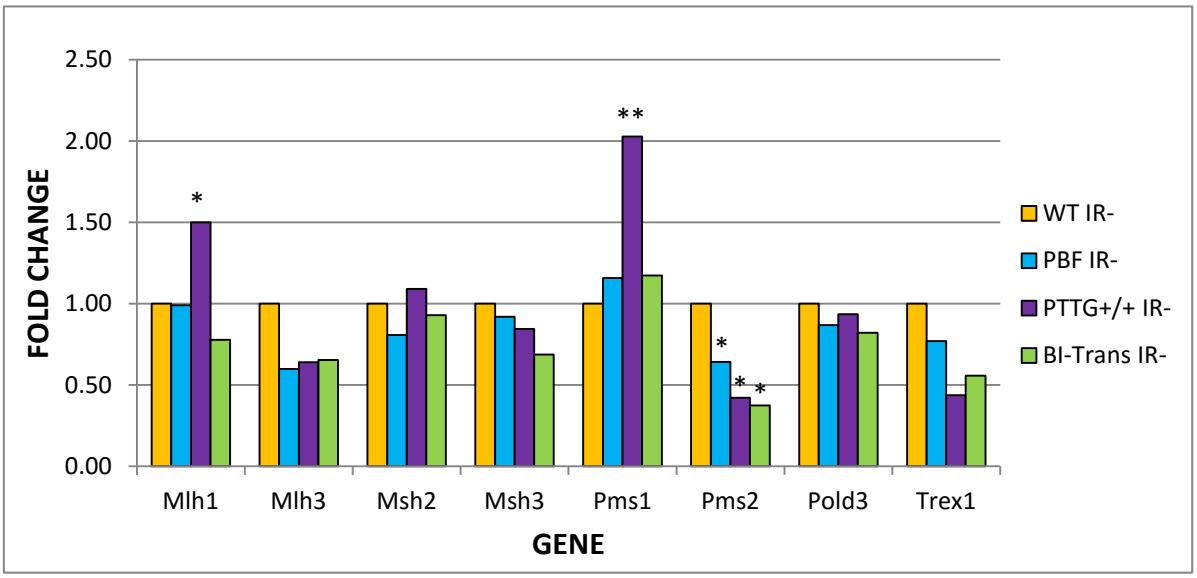

*Figure 5-12 The mRNA expression of genes involved in mismatch repair. p-values are denoted by * if $0.01 < p \leq 0.05$ (*) and ** if $0.001 < p \leq 0.01$ (**). IR- denotes without ionising radiation.*

5.3.13 **Affect on other genes related to DNA repair**

Figure 5-13 is shown in 3 separate bar charts for the same functional grouping of other genes related to DNA repair on the microarray. PBF suppressed the expression of Rad9b (0.47 fold) whilst PTTG increased the expression of Polk (3.08 fold), Tdg (3.07 fold), Rad9 (3.05 fold) and Ube2a (2.24 fold). The expression of Fancg (0.38 fold), Rad18 (0.37 fold), Chaf1a (0.36 fold), Fen1 (0.31 fold), Pole (0.29 fold) and Exo1 (0.11 fold) was reduced in PTTG PMTCs. The genes that are suppressed in BI-Trans included Chaf1a (0.45 fold), Fancg (0.45 fold), Fen1 (0.44 fold), Exo1 (0.43 fold) and Ung (0.38 fold).

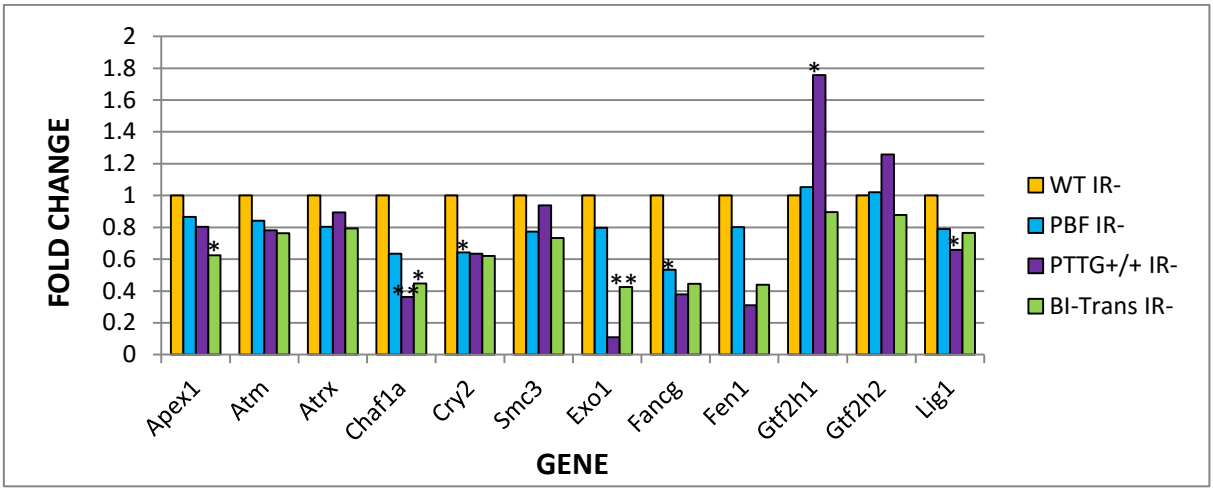

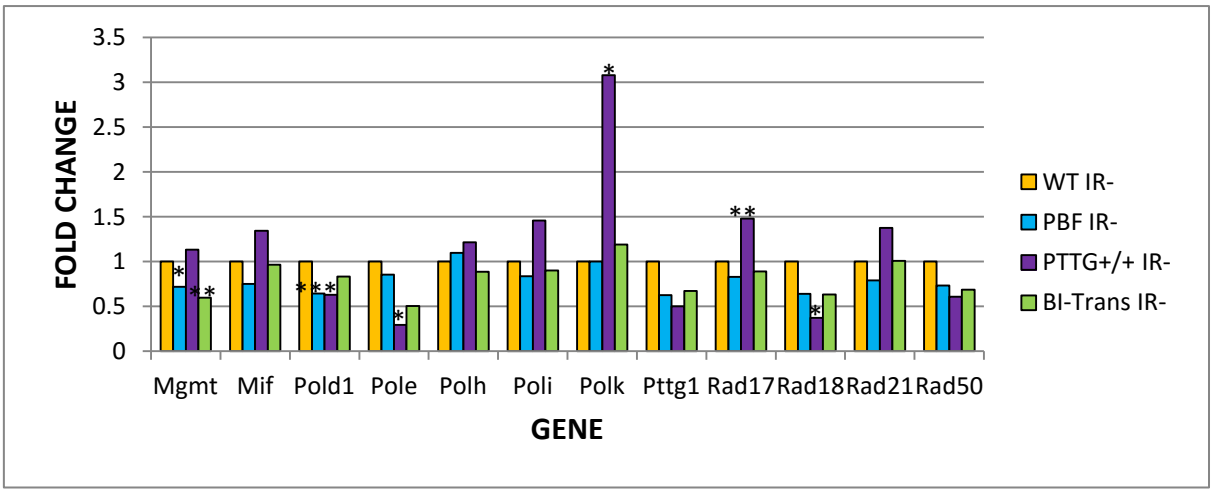

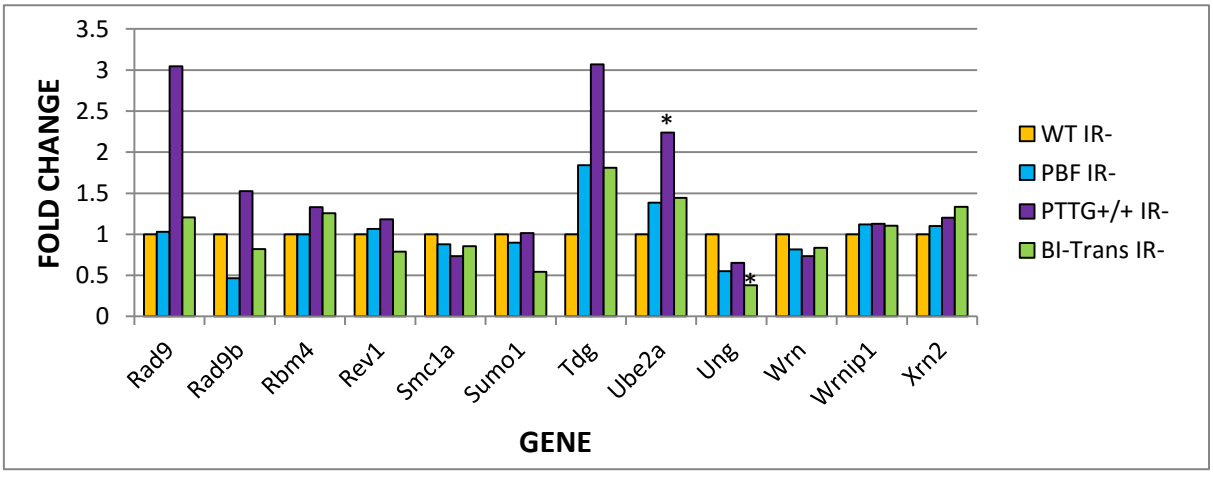

Figure 5-13 Expression of other genes related to DNA repair by genotype (n=3). If $0.01 < p \leq 0.05$ (*), $0.001 < p \leq 0.01$ (**) and $0.0001 < p \leq 0.001$ (***). IR- denotes without ionising radiation.

5.4 DISCUSSION

5.4.1 Murine DNA Damage Signalling Microarray studies

The ability to develop tumours is intimately related to the sophisticated regulation of genes associated with DNA damage and DNA repair.

The Mouse DNA Damage Signalling RT^2 Profiler PCR Array profiles 84 genes involved in murine DNA damage signalling and DNA repair pathways. The featured genes are associated with the ATR/ATM signalling pathways and transcriptional targets of DNA damage response. The ATM pathway is primarily activated by double-strand DNA breaks whereas ATR responds to a much broader spectrum of DNA damage, including DSBs and many types of DNA damage that interfere with DNA replication. ATR stabilises the genome during DNA replication which is essential for maintaining genomic stability.

The interpretation of the microarray data is complex because of the sophisticated gene expression relationships with each other which may or may not have been completely delineated. In order to interpret microarray gene changes, we considered genes which were relatively overexpressed by more than 2 times or genes that were reduced by more than half. Overall, PBF overexpression in the murine thyroid had the effect of gene suppression. In contrast, PTTG had a combination of gene mRNA upregulation and downregulation. The BI-Trans murine thyroid which overexpressed both PBF and PTTG had a gene expression profile similar to PBF.

5.4.2 The effect of PTTG on DNA damage/DNA repair genes

The relationship between Trp53 and PTTG is complex and ill-defined. Apoptosis involving PTTG can be Trp53 dependent and independent (Yu et al., 2000a, Yu et al., 2000b). Interestingly, the transgenic overexpression of PTTG was associated with the suppression of the genes Brca1 and Mbd4 involved in apoptosis but had no significant effect on Trp53.

Previous studies have shown the interaction between PTTG overexpression and the inhibition of Ku70 involved in non-homologous end-joining DNA repair (Kim et al., 2007b), leading to our hypothesis that PTTG has an effect on DNA repair. Using the microarray, we have screened for genes involved in DNA damage and DNA repair. PTTG increased the expression of Hus1 and Rad9 but simultaneously reduced the expression of Chek1 and Chaf1a. Hus1, Rad9 and Rad1 form the 9-1-1 ring-shaped trimeric complex which is formed in response to DNA damage. Together with Rad17, they act as a checkpoint sensor to activate ATM or ATR (ATM and Rad3 related protein) protein kinase. The 9-1-1 complex interacts and stimulates DNA repair enzymes involved in base excision repair, nucleotide excision repair and mismatch repair. Expression changes in PTTG PMTCs may have encouraged the production of 9-1-1 complex which then caused a plethora of changes in gene groups on the microarray representing suppression of damaged DNA binding (suggesting no damaged DNA involved), equivocal changes in base excision repair, nucleotide excision repair and mismatch repair and no change in double strand break repair. There was a variety of suppression and enhancement of the expression of genes involved more widely in DNA repair. It is conceivable that PTTG affects the DNA repair pathway by way of encouraging the formation of the 9-1-1 complex.

In contrast, a marked suppression was observed in Chek1, a serine/threonine protein kinase, required for checkpoint-mediated cell cycle arrest and activation of DNA repair in response to the presence of DNA damage or unreplicated DNA. Chek1 also binds to and phosphorylates RAD51 at Thr-309 which promotes the release of Rad51 from BRCA2 and enhances the association of Rad51 with chromatin, thereby promoting DNA repair by homologous recombination. The PTTG suppression of Chek1 suggests cells may be allowed to progress in the cell cycle.

Apoptosis is discouraged by the suppression of Brca1 and Mbd4. The expression of Trp53 was not significantly increased. Chek1 is known to phosphorylate multiple sites within the C-terminus of Trp53, promoting cell cycle arrest and suppression of cellular proliferation. Hence, although the expression of Trp53 was not significantly enhanced, it is still possible to that Trp53 is activated by phosphorylation via Chek1, in the presence of PTTG. This hypothesis needs to be investigated further

at a protein level. The above would strongly suggest that PTTG suppresses apoptosis, preferring to repair the defect within the genome. Further studies are required to delineate the action of PTTG and p53 dependent apoptosis.

The above suggests that the presence of PTTG caused more cellular stress from a DNA damage and DNA repair perspective, necessitating the stimulation and suppression of various genes in order to maintain genomic stability.

5.4.3 The effect of PBF on DNA damage/DNA repair genes

The overexpression of PBF in PMTCs did not appear to increase the expression of DNA damage genes in the microarray. PBF appeared to suppress the genes Trpc2 and Xrcc3 involved in DNA damage binding and Mutyh in base excision repair to a significant extent, defined by our criteria. The other gene suppressed is Rad9b which again is involved in DNA repair. Overall, it appeared that PBF predominantly suppressed several genes associated with DNA repair but the effect is not entirely clear.

PBF is recognised to bind to and negatively regulate Trp53 (Read et al., 2014a, Read et al., 2014b). The mRNA expression of Trp53 in murine thyroids overexpressing PBF was not significantly altered on the microarray suggesting that the interaction between PBF and Trp53 mostly occurred at a protein level in our models.

5.4.4 The effect of both PBF and PTTG on DNA damage/DNA repair genes

Most genes involved in DNA repair were inhibited in BI-Trans PMTCs with the exception of nucleotide excision repair and double strand break genes, which remain unaffected. When both PBF and PTTG were co-expressed in PMTCs, the general trend observed was the amelioration of over or under expression of DNA damage / DNA repair genes observed in PTTG PMTCs. This effect is interesting because PBF is a protein that transports the mainly cytoplasmic PTTG to the nucleus. This

microarray observation is in contrast to the hypothesis that PBF enhances the genetic instability caused by PTTG. However, further studies are required to establish this.

5.5 CONCLUSION

The changes observed in the microarray show that PTTG caused more disruption to the DNA damage/ DNA repair gene expression profile than PBF alone. The study of both genes being expressed together suggested that PBF partially ameliorates the instability introduced by PTTG. Ultimately, the gene expression profile is important in establishing a background of genes affected by genotype before we study the effect of genotype following real DNA damage.

6 The effect of radiation on genotype in DNA damage and repair genes

6.1 INTRODUCTION

6.1.1 Background

PBF and PTTG have been shown independently to alter genomic stability (Read et al., 2014a, Kim et al., 2005). Thyroid cancers, particularly of the variety with poor prognosis overexpress PTTG and PBF (Stratford et al., 2005, Boelaert et al., 2003, Hsueh et al., 2013). Moreover, ionising radiation which induces DNA damage is a known aetiological factor for thyroid carcinoma. PTTG has roles in mitosis and can impair DNA repair via the inhibition of Ku70, involved in double strand break repair (Kim et al., 2007b). PTTG has a binding partner PBF which facilitates its entry into the nucleus for its functions (Chien and Pei, 2000).

To study the effects of PBF and PTTG in the context of thyroid cancer, we have created transgenic murine models that overexpress our genes of interest in the thyroid gland. To study the effects of ionising radiation, we established the technique of primary murine thyroid culture (PMTC) which overexpress PBF and/or PTTG in a uniform manner in a Petri dish.

We previously studied the expression of genes associated with the DNA damage and repair pathways in the context of PBF and PTTG overexpression in the thyroid gland, described in the last chapter. We next investigated the effect of external genomic stress, in the form of ionising radiation to determine the expression of the same gene before, in a background of PBF and PTTG overexpression. We hypothesised that thyroid cells overexpressing PBF and PTTG will respond differently in the presence of DNA damage, resulting in reduced genomic stability compared to wild type PMTCs.

6.2 MATERIALS AND METHODS

6.2.1 Primary murine thyroid cultures

Primary murine thyroid culture (PMTC) was performed on the 4 different genotypes, WT, PBF, PTTG +/+ and BI-Trans, using 3 males in each genotype group. Details of the technique can be found in section 2.2.

6.2.2 RNA extraction

RNA was harvested from PMTCs on day 10 using the micro RNeasy kit (QIAGEN) as described in section 2.4.

6.2.3 Reverse transcription

Reverse transcription was performed using the Promega Reverse Transcription system as described in section 2.5.

6.2.4 RT^2 Profiler™ PCR Arrays

The RT^2 Profiler™ PCR Arrays (SABiosciences) were used for gene expression detection as described in Chapter 5. Interpretation of data was based arbitrarily on a fold change relative to WT IR- of more than 2 or less than 0.5. Values between 0.5 and 2 were deemed as insignificant for the purpose of this analysis. The n value for each genotype category was 3 (e.g. WT IR- (n=3) and WT IR+ (n=3)). Although p values were calculated and incorporated within the chapter, the emphasis was more on trend rather than the actual p-values because the sample size was small for each genotype, and the aim was to identify robust gene expression changes which could be further investigated in subsequent chapters.

6.3 RESULTS

6.3.1 The effect of radiation on WT PMTCs

Gene expression changes in wild type primary murine thyroid cultures of less than 0.5 fold and more than two fold following ionising radiation (WT IR+ PMTCs) is shown in Figure 6-1. The most striking change affected by radiation in the WT IR+ PMTC is a reduction of Brca1 to 0.35 fold (p=0.004; n=3) relative to WT IR-. Brca1 together with Rad51 and γ-H2AX, is usually recruited to areas requiring repair following damage (Krum et al., 2010, Feng and Zhang, 2012). Expression of Mgmt, associated with alkalyting injuries (Aquilina et al., 1992, Xiao and Samson, 1993, Hegi et al., 2005), was noted to be increased by 2.05 fold (p=0.003; n=3). The expression of genes involved with DNA repair such as Brca1, Mbd4 (0.50 fold, p=0.072, n=3), Exo1 (0.30 fold, p=0.006, n=3), Pole (0.37 fold, p=0.002, n=3), Lig1 (0.43 fold, p=0.013, n=3) and Ung (0.50 fold, p=0.085, n=3) were reduced on the microarray compared to WT IR-. Interestingly, endogenous PTTG was reduced at 0.41 fold in WT IR+ PMTCs (p=0.162, n=3).

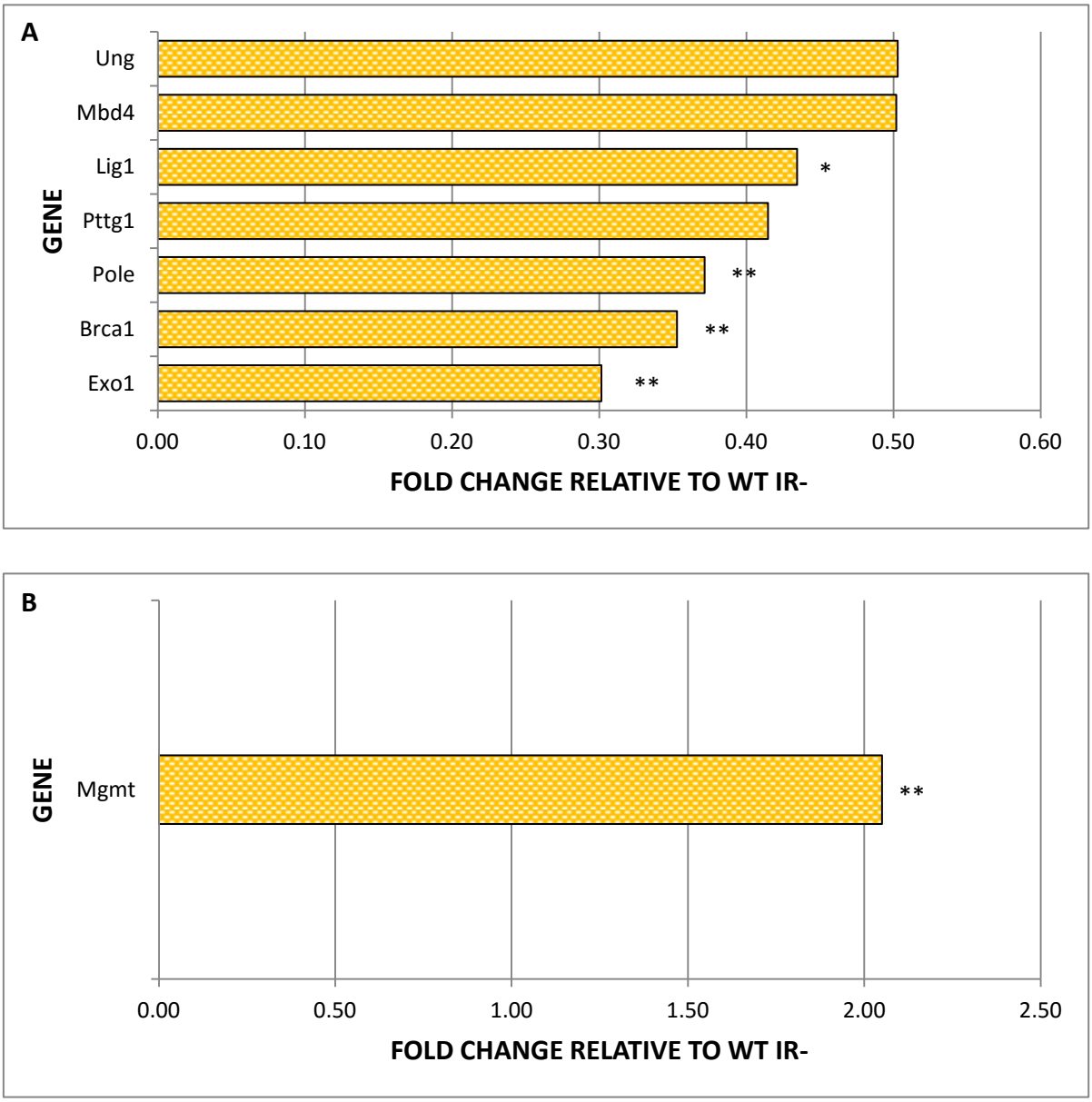

*Figure 6-1 Gene expression changes in WT PMTC following irradiation (WT IR+) that were less than 0.5 fold (A) and more than 2 fold (B). Fold changes are expressed relative to WT PMTC without irradiation (WT IR-). p-values are denoted with * ($0.01 < p \leq 0.05$) and ** ($0.001 < p \leq 0.01$).*

6.3.2 **The effect of radiation on PBF PMTCs**

Significant gene expression changes found on the microarray for PBF primary murine thyroid cultures (PMTC) following ionising irradiation (PBF IR+) is shown in Figure 6-2. In PBF IR+ PMTCs, the observed pattern was primarily gene suppression on the microarray relative to WT IR-. The observed suppression of Exo1 (0.15 fold, p=0.098, n=3), Brca1 (0.23 fold, p=0.130, n=3), Pole (0.26 fold, p=0.512, n=3), Pttg1 (0.28 fold, p=0.386, n=3), Ung (0.41 fold, p=0.142, n=3) and Mbd4 (0.45 fold, p=0.056, n=3) probably reflected the effect of radiation as a similar pattern of suppression in the same genes was observed in WT IR+ (Figure 6-1A). The expression changes in the genes Xrcc3 (0.31 fold, p=0.009, n=3), Mutyh (0.36 fold, p=0.003, n=3), Rad9b (0.46 fold, p=0.052, n=3) and Trpc2 (0.49 fold, p=0.004) observed in PBF IR+ were also observed to be expressed less than 0.5 fold in PBF IR- PMTCs (Figure 5-1), suggesting that the reduced expression of these genes were likely the effect of the PBF genotype. The gene expression in PBF IR+, Chaf1a (0.39 fold, p=0.064, n=3), Chek1 (0.18 fold, p=0.077, n=3), Terf1 (0.35 fold, p=0.032, n=3), Rad51 (0.10 fold, p=0.658, n=3), Rad51l1 (0.32 fold, p=0.336, n=3), Rad51c (0.35 fold, p=0.015, n=3), Lig1 (0.36 fold, p=0.129, n=3), Parp1 (0.46 fold, p=0.149, n=3) and Xrcc2 (0.49 fold, p=0.167, n=3) were exclusively the effect of radiation on PBF PMTCs because these gene expression changes were not found in PBF IR- or WT IR+ PMTCs.

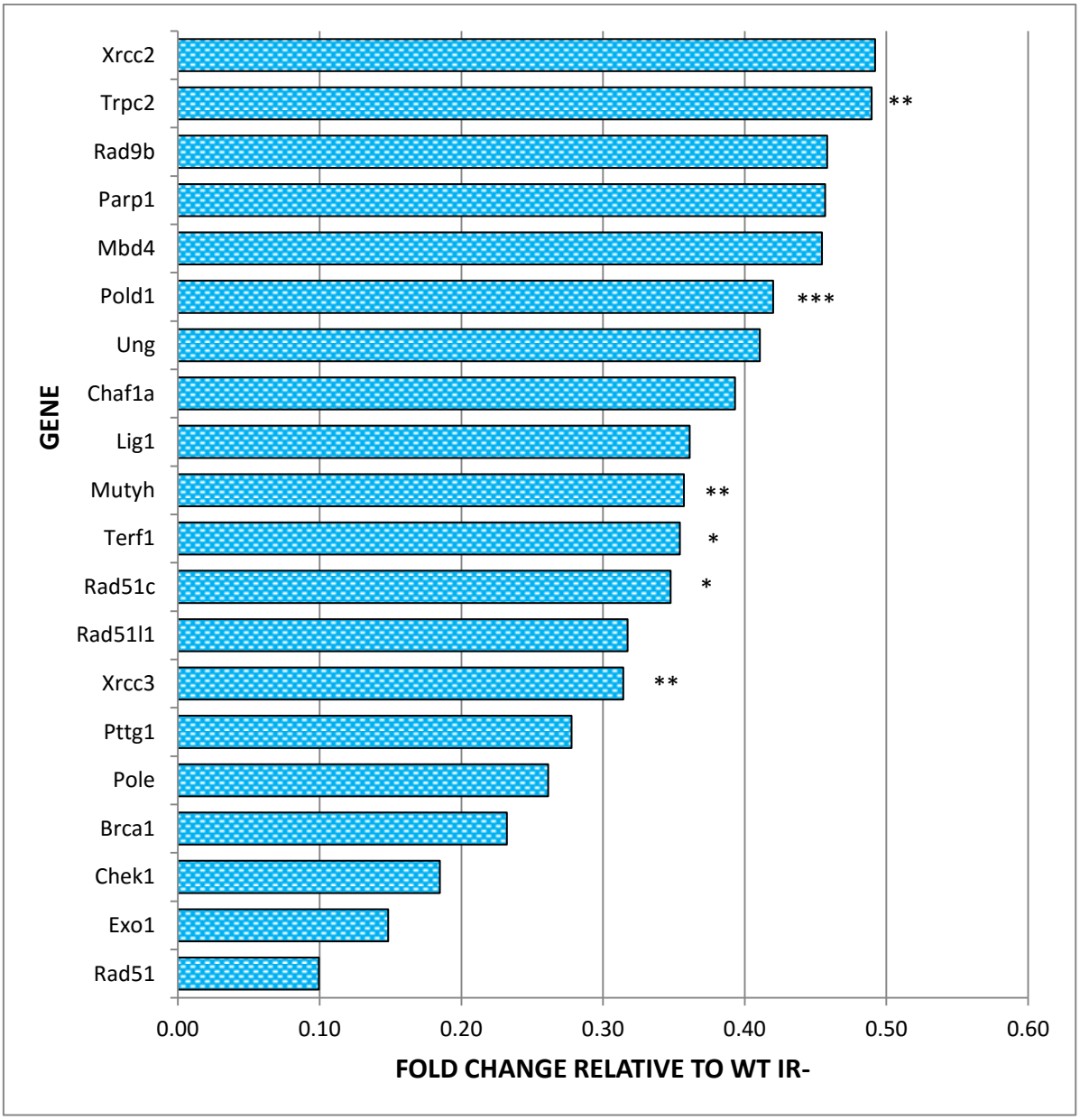

*Figure 6-2 DNA damage / DNA repair gene expression changes in PBF PMTC following exposure to radiation. All values are relative to WT IR-. p-values are denoted with * ($0.01 < p \leq 0.05$), ** ($0.001 < p \leq 0.01$) and *** ($0.0001 < p \leq 0.001$). There were no genes on the RT2 Profiler™ PCR Array that were expressed more than twice in PBF IR+ PMTCs.*

6.3.3 The effect of radiation on PTTG+/+ IR+ PMTCs

The significant gene expression changes on the microarray for PTTG primary murine thyroid cultures (PMTCs) with ionising radiation (PTTG+/+ IR+) is shown in Figure 6-3. The genes suppressed in PTTG+/+ IR+ PMTCs, also observed in WT IR+ PMTCs were as follows; Exo1 (0.13 fold, p=0.010, n=3), Brca1 (0.16 fold, p=0.003, n=3), Pole (0.19 fold, p=0.003, n=3) and Mbd4 (0.39 fold, p=0.058, n=3). The genes which were suppressed in WT IR+ but not in PTTG IR+ were Lig1, Pttg1 and Ung. The gene Mgmt increased by 2.05 in WT IR+ but was not elevated by more than 2 fold in PTTG+/+ IR+. The genes suppressed to less than 0.5 fold compared to WT IR- in both PTTG+/+ IR- and PTTG+/+ IR+ included Chek1 (0.14 fold, p=0.013, n=3), Rad51 (0.15 fold, p=0.036, n=3), Fen1 (0.22 fold, p=0.002, n=3), Chaf1a (0.30 fold, p=0.022, n=3), Rad18 (0.31 fold, p=0.001, n=3), Fancc (0.31 fold, p=0.023, n=3), Trex1 (0.37 fold, p=0.012, n=3), Fancg (0.40 fold, p=0.032, n=3), Pms2 (0.48 fold, p=0.071, n=3) and Xpa (0.48 fold, p=0.060, n=3). The genes expressed by more than 2 fold in PTTG+/+ IR+ were Hus1 (2.04 fold, p=0.011, n=3), Nthl1 (2.10 fold, p=0.020, n=3), Ube2a (2.46 fold, p=0.018, n=3), Trpc2 (2.79 fold, p=0.025, n=3), Tdg (2.81 fold, p=0.090, n=3), Rad9 (3.23 fold, p=0.011, n=3) and Polk (4.97 fold, p=0.004, n=3), were also expressed by more than twice in PTTG+/+ IR-. The genes that were significantly altered in PTTG+/+ IR- but not in PTTG+/+ IR+ were Rad51l1, Pttg1 and Pms1. The genes exclusively suppressed in PTTG+/+ IR+ but not in PTTG+/+ IR- were Pold1 (0.44 fold, p=0.004, n=3) and Wrn (0.48 fold, p=0.264, n=3).

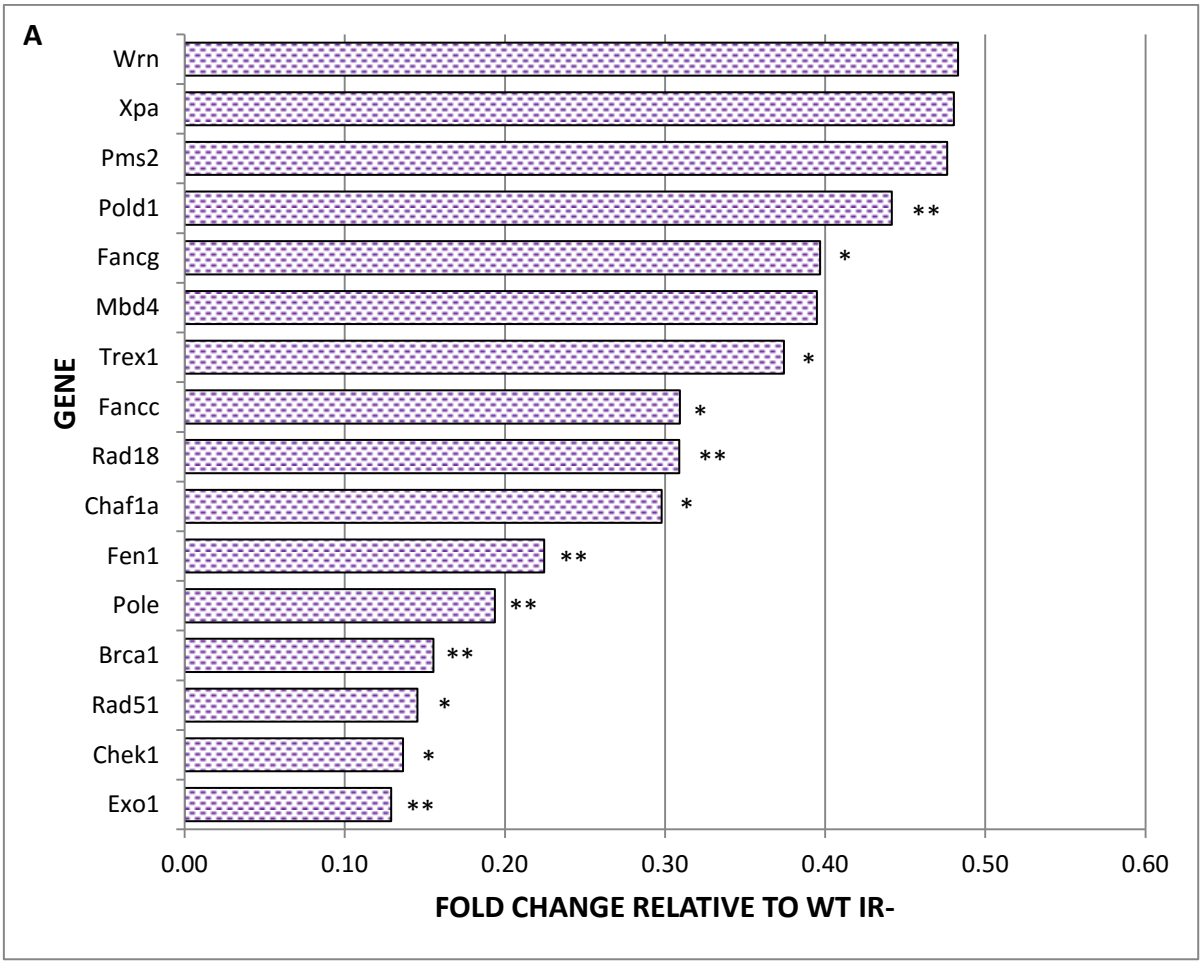

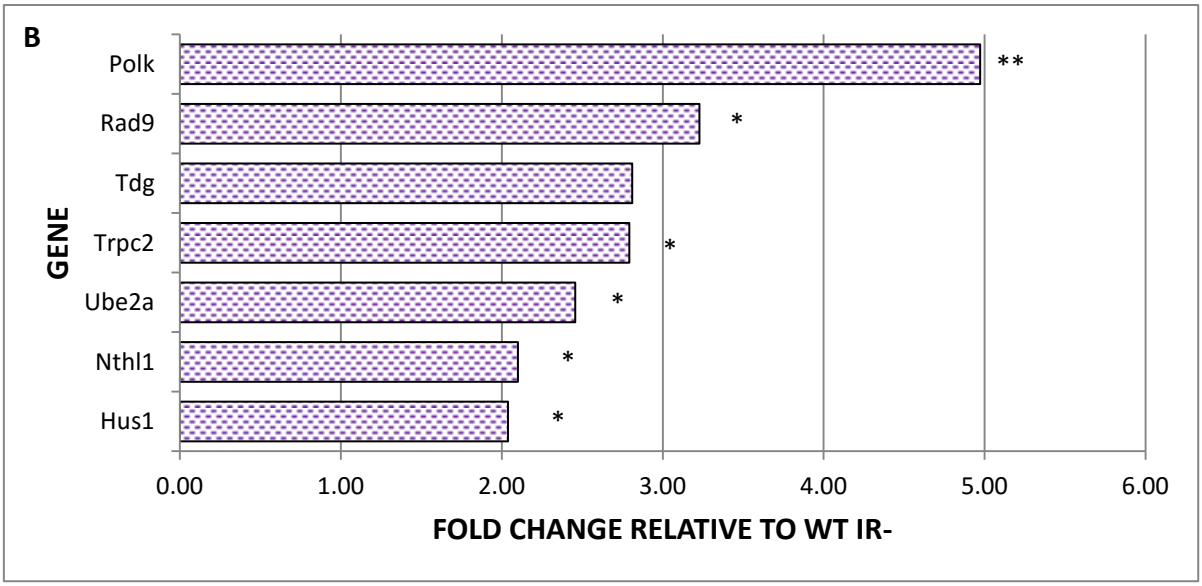

*Figure 6-3 DNA damage / DNA repair gene expression changes in PTTG+/+ IR+ PMTC less than 0.5 (A) and more than 2 (B) fold. p-values are denoted with * ($0.01 < p \leq 0.05$) and ** ($0.001 < p \leq 0.01$).*

6.3.4 **The effect of radiation on BI-Trans PMTCs**

The significant gene expression changes on the microarray for murine models overexpressing both PBF and PTTG in the thyroid gland (BI-Trans) following radiation exposure is shown in Figure 6-4. The genes of Exo1 (0.09 fold, p=0.001, n=3), Brca1 (0.14 fold, p<0.000, n=3), Pole (0.15 fold, p=0.002, n=3), Ung (0.26 fold, p=0.009, n=3), Lig1 (0.43 fold, p=0.002, n=3) and Mbd4 (0.44 fold, p=0.021, n=3) were suppressed in BI-Trans following ionising radiation (BI-Trans IR+) PMTCs. These genes were altered in all genotypes following exposure to ionising radiation and is likely the effect of radiation. The expression of genes altered in BI-Trans IR+ which were most likely to be due to the effect of PBF and radiation included Rad51l1 (0.33 fold, p=0.088, n=3) and Rad51c (0.40 fold, p=0.016, n=3). The altered genes Fen1 (0.33 fold, p=0.001, n=3), Rad18 (0.47 fold, p=0.001, n=3), Trex1 (0.50 fold, p=0.064, n=3) and Polk (2.01 fold, p=0.009, n=3) in BI-Trans IR+ PMTCs were likely the effect of PTTG because these genes were also altered in PTTG+/+ PMTCs. The genes Fancg and Pinx1, suppressed to a significant degree in BI-Trans IR-, were no longer suppressed significantly in BI-Trans IR+. Finally, genes which were significantly altered in BI-Trans IR+ and in PBF IR+, PTTG+/+ IR-, PTTG+/+IR+ and BI-Trans IR- were Chek1 (0.14 fold, p<0, n=3), Rad51 (0.15 fold, p=0.034, n=3) and Chaf1a (0.42 fold, p=0.019, n=3).

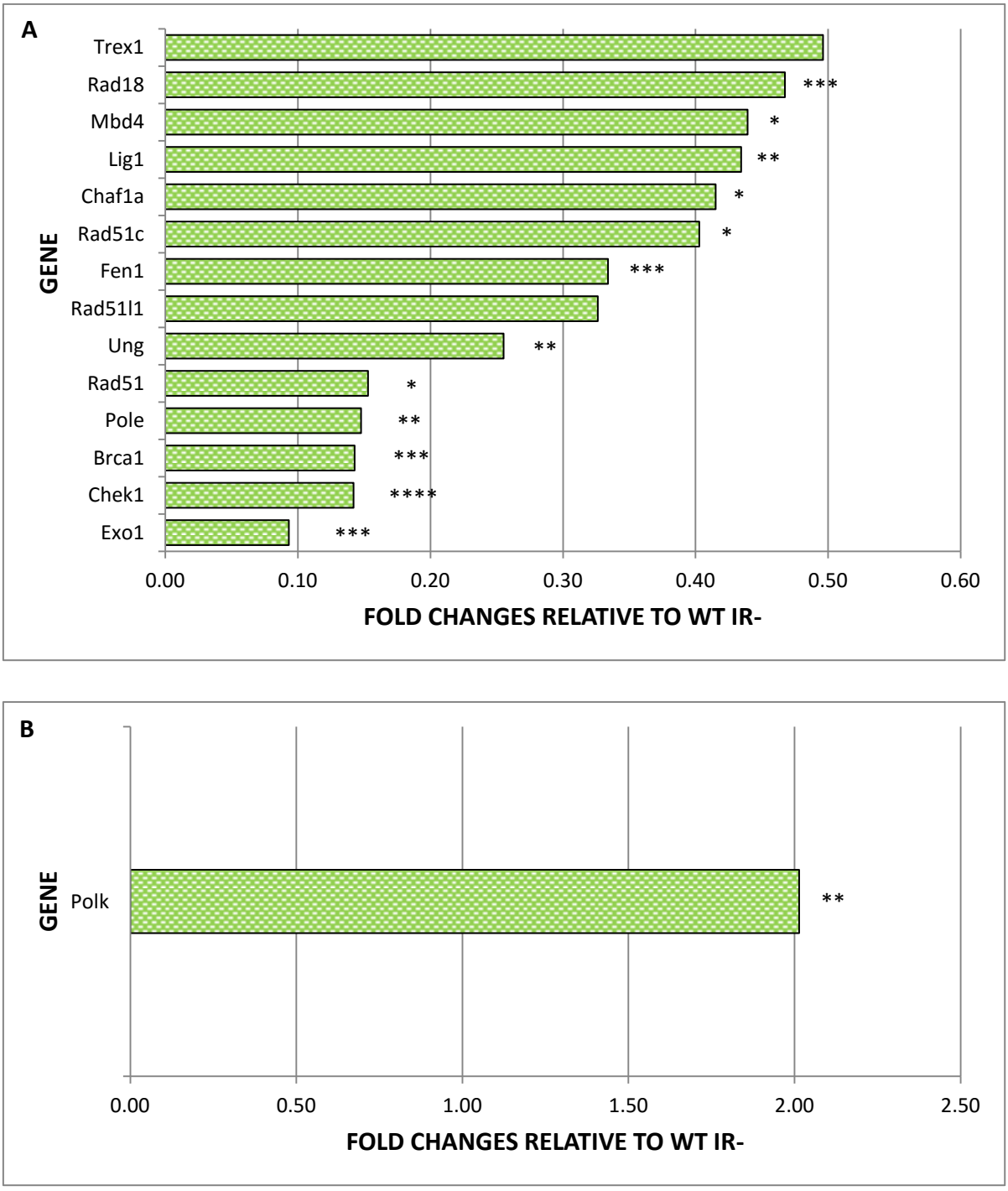

*Figure 6-4 DNA damage and DNA repair gene expression changes in BI-Trans IR+ PMTCs of less than 0.5 (A) and more than 2 (B) fold. Fold expression is relative to WT IR-. p-values are denoted with * ($0.01 < p \leq 0.05$), ** ($0.001 < p \leq 0.01$) and *** ($0.0001 < p \leq 0.001$).*

6.3.5 PBF, PTTG and radiation reduced the expression of Brca1 and Mbd4, genes involved with apoptosis.

To make sense of the enormous amount of data generated by these studies, we next examined gene expression by functional grouping to interpret the mouse DNA Damage Signalling Pathway RT^2 Profiler^{TM} PCR Array findings in a meaningful manner. Thus, in the following sections, data have been grouped according to biological pathway. For apoptosis, the expression of Brca1 (0.35 fold, p=0.004; n=3), Mbd4 (0.50 fold, p=0.072, n=3) and Mgmt (2.05 fold, p=0.003; n=3) was altered in wild type primary murine thyroid cultures (PMTCs) following treatment with ionising radiation (WT IR+) shown in Figure 6-5. Brca1 (0.23 fold, p=0.130, n=3) and Mbd4 (0.45, p=0.056, n=3) were suppressed by more than 0.5 fold in PBF IR+ compared to WT IR-. This represented a further suppression of these genes when comparing PBF IR+ with PBF IR-. In PTTG IR+ PMTCs, both Brca1 (0.16 fold, p=0.003, n=3) and Mbd4 (0.39 fold, p=0.058, n=3) were reduced relative to WT IR-. The pattern of suppression in both genes was fairly similar in PTTG IR-. As expected, Brca1 (0.14 fold p<0.000 n=3) and Mbd4 (0.44 fold p=0.021 n=3) had reduced expression in BI-Trans IR+ PMTCs. It appeared that radiation increased the suppression of Brca1 in BI-Trans IR+ PMTCs but radiation did not appear to increase the suppression of Mbd4.

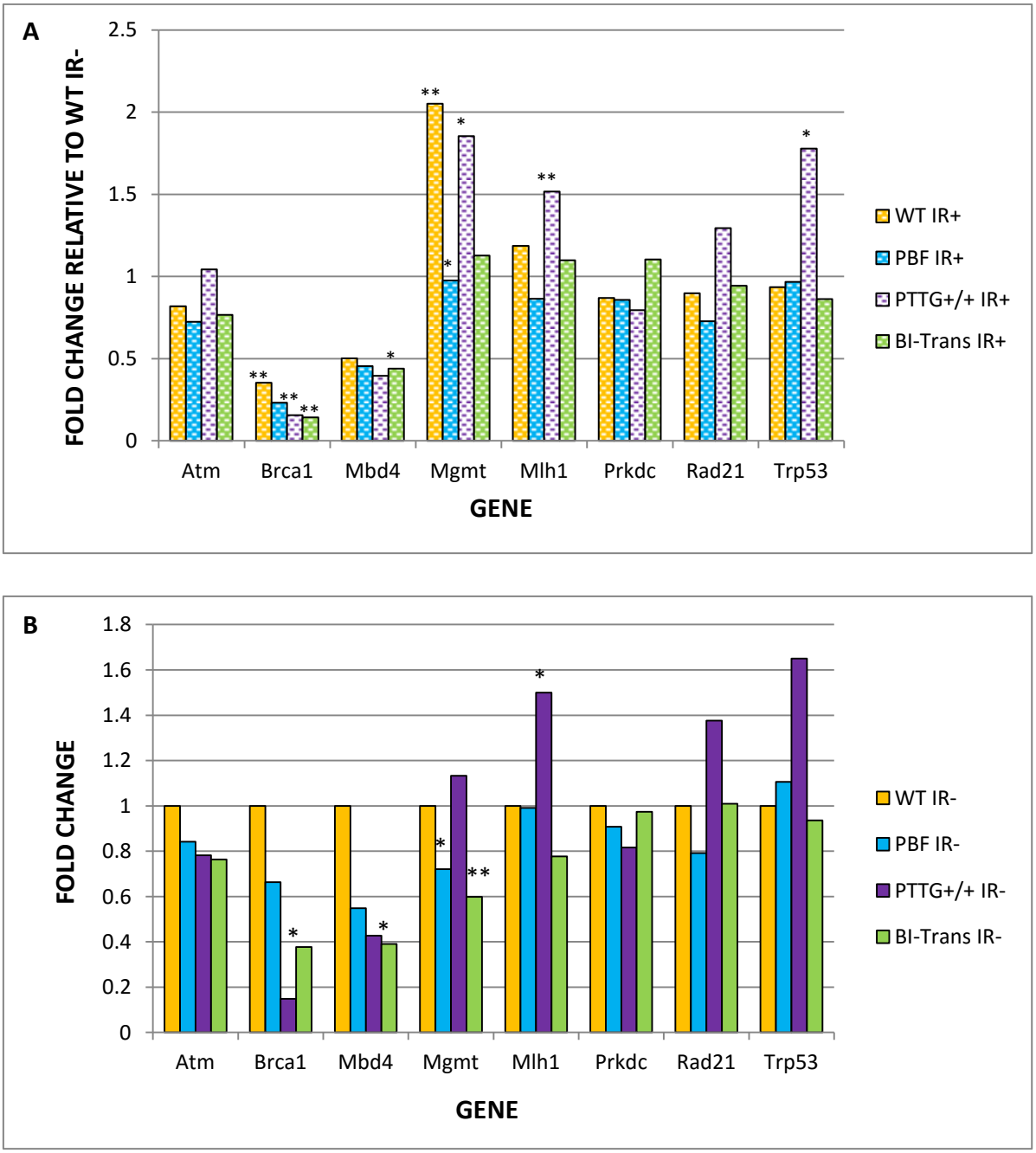

*Figure 6-5 Expression of genes involved in apoptosis by genotype. Top figure (A) denotes PMTC genotype with irradiation (IR+) and bottom figure (B) denotes PMTC genotype without irradiation (IR-). Fold expression is relative to WT PMTC without irradiation (WT IR-). p-values are denoted with * ($0.01 < p \leq 0.05$) and ** ($0.001 < p \leq 0.01$).*

6.3.6 Radiation and PTTG reduced the expression of Chek1, a gene involved in cell cycle arrest.

Radiation did not cause any significant expression changes to genes involved in cell cycle arrest in WT IR+ PMTCs as shown in Figure 6-6. The genes Chek1 (0.14 fold, p=0.013, n=3) and Hus1 (2.04 fold, p=0.011, n=3) had altered expression in PTTG IR+ compared to WT IR- PMTCs. This observed trend was also found in PTTG IR- PMTCs, suggesting the increased expression of Hus1 and reduced expression of Chek1 was likely an effect of PTTG genotype on PMTCs. The expression of Chek1 (0.14 fold, p<0.000, n=3) was significantly reduced in BI-Trans IR+ compared to WT IR- PMTCs. The expression of Chek1 was more reduced in BI-Trans IR+ compared to BI-Trans IR-.

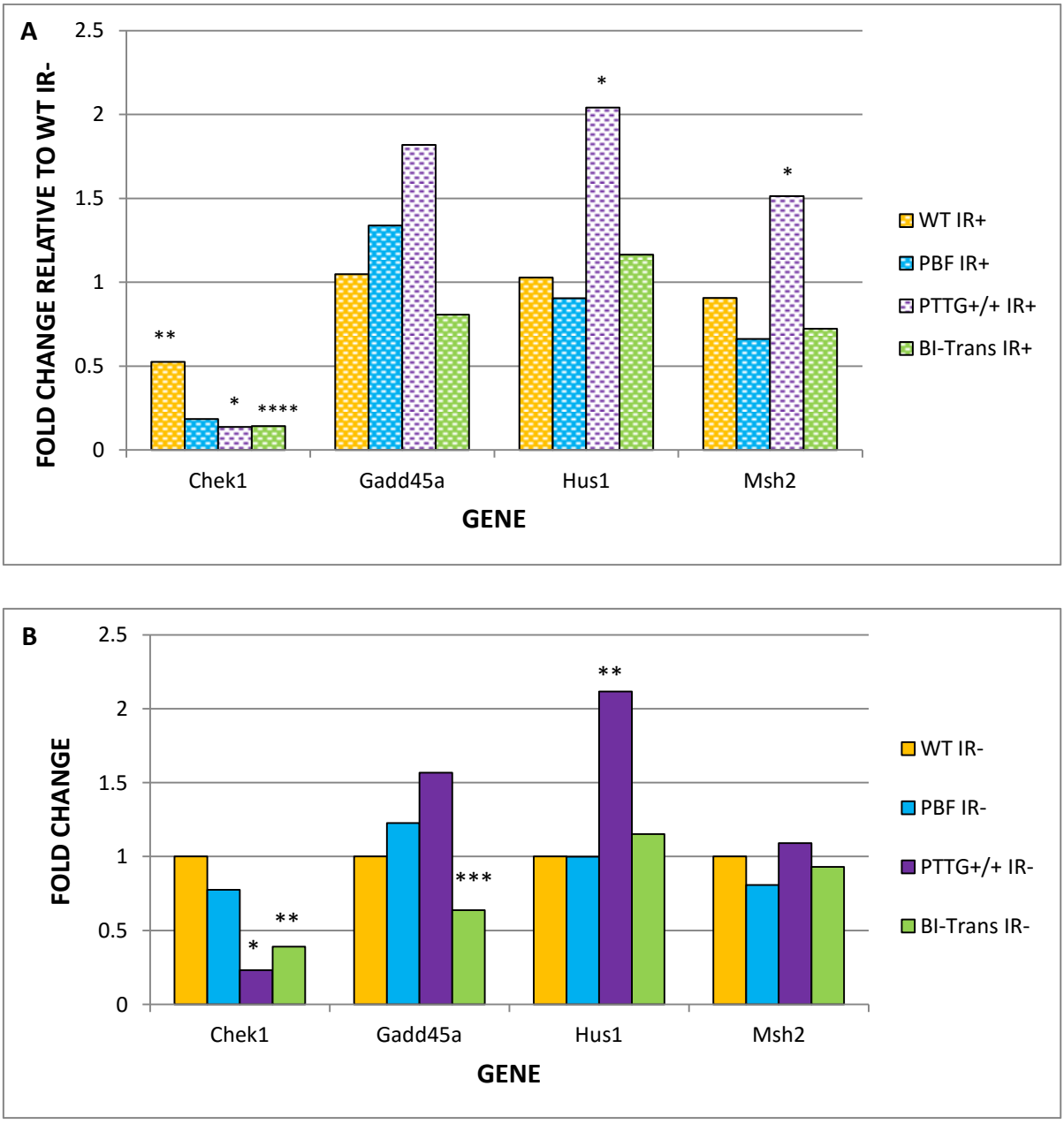

*Figure 6-6 Cell cycle arrest gene expression by genotype. Top figure (A) denotes PMTC genotype with irradiation (IR+) and bottom figure (B) denotes PMTC genotype without irradiation (IR-). Fold expression is relative to WT PMTC without irradiation (WT IR-). p-values are denoted with * ($0.01 < p \leq 0.05$), ** ($0.001 < p \leq 0.01$), *** ($0.0001 < p \leq 0.001$) and **** ($p \leq 0.0001$).*

6.3.7 Genes involved in cell cycle checkpoint remained unchanged following irradiation regardless of genotype

Radiation did not appear to impact on the expression of genes involved in cell cycle checkpoint to a significant degree, seen in Figure 6-7. The effect of genotype on the microarray genes remained essentially unaltered following irradiation. The high expression of Rad9 (3.23 fold, p=0.011, n=3) in PTTG IR+ PMTC appeared to be essentially an effect of the PTTG genotype.

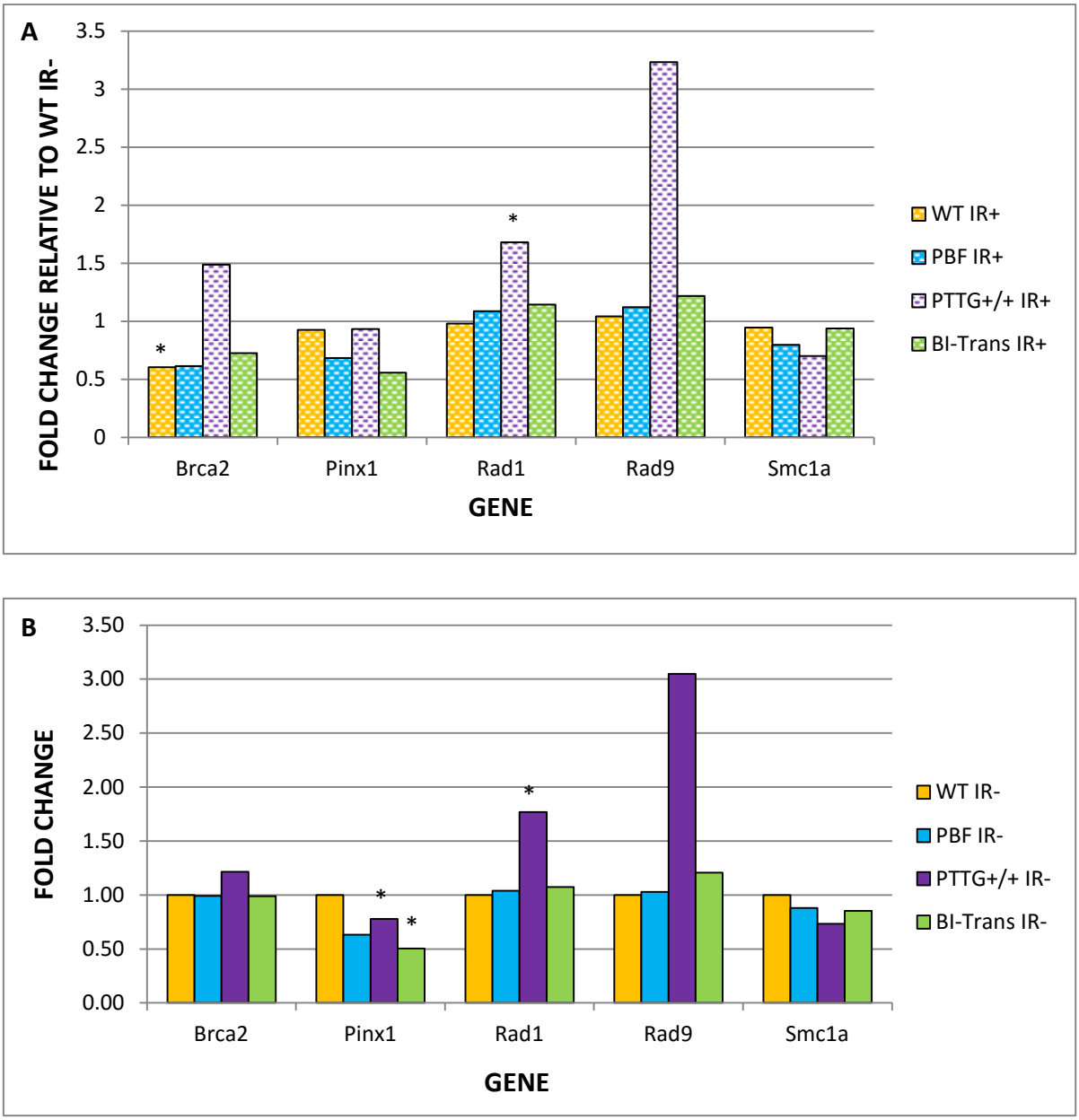

*Figure 6-7 Expression of cell cycle checkpoint genes by genotype. Chart A denotes PMTC genotype with irradiation (IR+) and chart B denotes PMTC genotype without irradiation (IR-). Fold expression is relative to WT PMTC without irradiation (WT IR-). p-values are denoted with * if $0.01 < p \leq 0.05$.*

6.3.8 Reduced Chaf1a expression in PBF and PTTG genotypes was further suppressed by radiation

In the functional grouping of other genes involved in cell cycle regulation on the microarray, gene expression was not significantly altered following radiation in WT PMTCs. Chaf1a (0.39 fold, p=0.064, n=3) and Terf1 (0.35 fold, p=0.032, n=3) was significantly reduced in PBF PMTCs following radiation. The reduced expression of these genes were exaggerated by radiation (see Figure 6-8). Chaf1a was significantly reduced in PTTG IR- PMTCs. The reduction in Chaf1a (0.30 fold, p=0.022, n=3) expression in PTTG IR+ PMTCs was increased by radiation. A similar trend was observed in Chaf1a (0.42 fold, p=0.019, n=3) expression in BI-Trans IR+ where Chaf1a expression was reduced in BI-Trans IR- but the effect of decreased expression was more profound following radiation exposure.

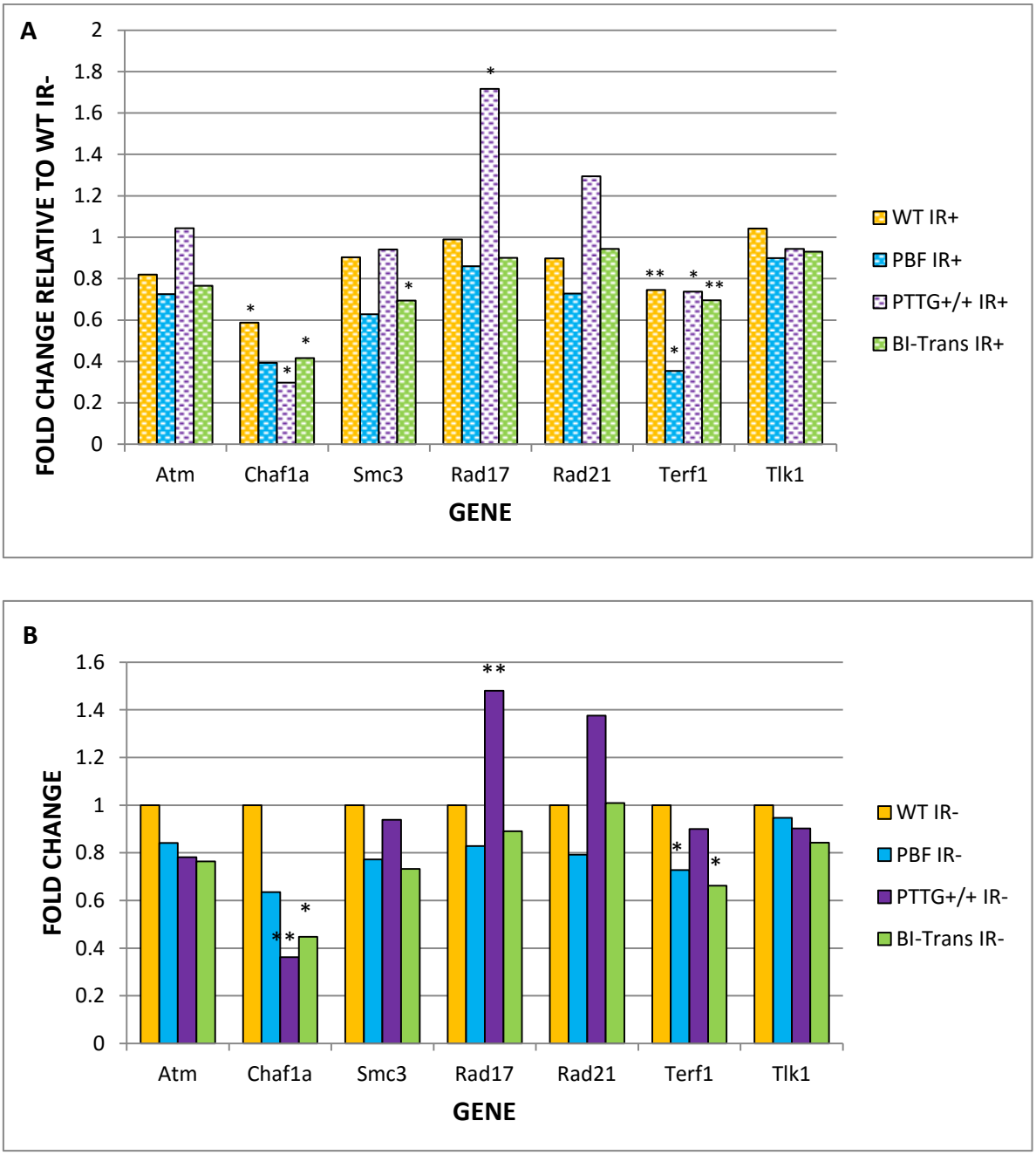

*Figure 6-8 Other genes related to cell cycle following DNA damage, gene expression by genotype. Top figure (A) denotes PMTC genotype with irradiation (IR+) and bottom figure (B) denotes PMTC genotype without irradiation (IR-). Fold expression is relative to WT PMTC without irradiation (WT IR-). p-values are denoted with * ($0.01 < p \leq 0.05$) and ** ($0.001 < p \leq 0.01$).*

6.3.9 Genes involved in damaged DNA binding

Of those genes involved in damaged DNA binding, Brca1 (0.35 fold, p=0.004, n=3) was the only gene significantly repressed following radiation, shown in Figure 6-9. PBF PMTCs showed repressed expression of Xrcc3 (0.31 fold, p=0.009, n=3), Trpc2 (0.49 fold, p=0.004), Rad51 (0.10 fold, p=0.658, n=3), Rad51c (0.35 fold, p=0.015, n=3) and Xrcc2 (0.49 fold, p=0.167, n=3) following treatment with ionising radiation. The gene repression in PBF IR+ PMTCs was enhanced following radiation induced damage seen in Figure 6-9. In PMTCs overexpressing PTTG, Brca1 (0.16 fold, p=0.003, n=3), Rad51 (0.15 fold, p=0.036, n=3), Xpa (0.48 fold, p=0.060, n=3) and Trpc2 (2.79 fold, p=0.025, n=3) had altered expression following irradiation. The gene expression changes following radiation were consistent with PTTG genotype related changes. The expression of Brca1 (0.14 fold p<0.000 n=3), Rad51 (0.15 fold p=0.034 n=3), Rad51c (0.40 fold p=0.016 n=3) and Rad51l1 (0.33 fold, p=0.088, n=3) in BI-Trans were significantly reduced following radiation. The only exception was the expression of Trpc2 (0.53 fold, p=0.171, n=3) in BI-Trans IR+ which showed reduced suppression when compared to BI-Trans IR- PMTC.

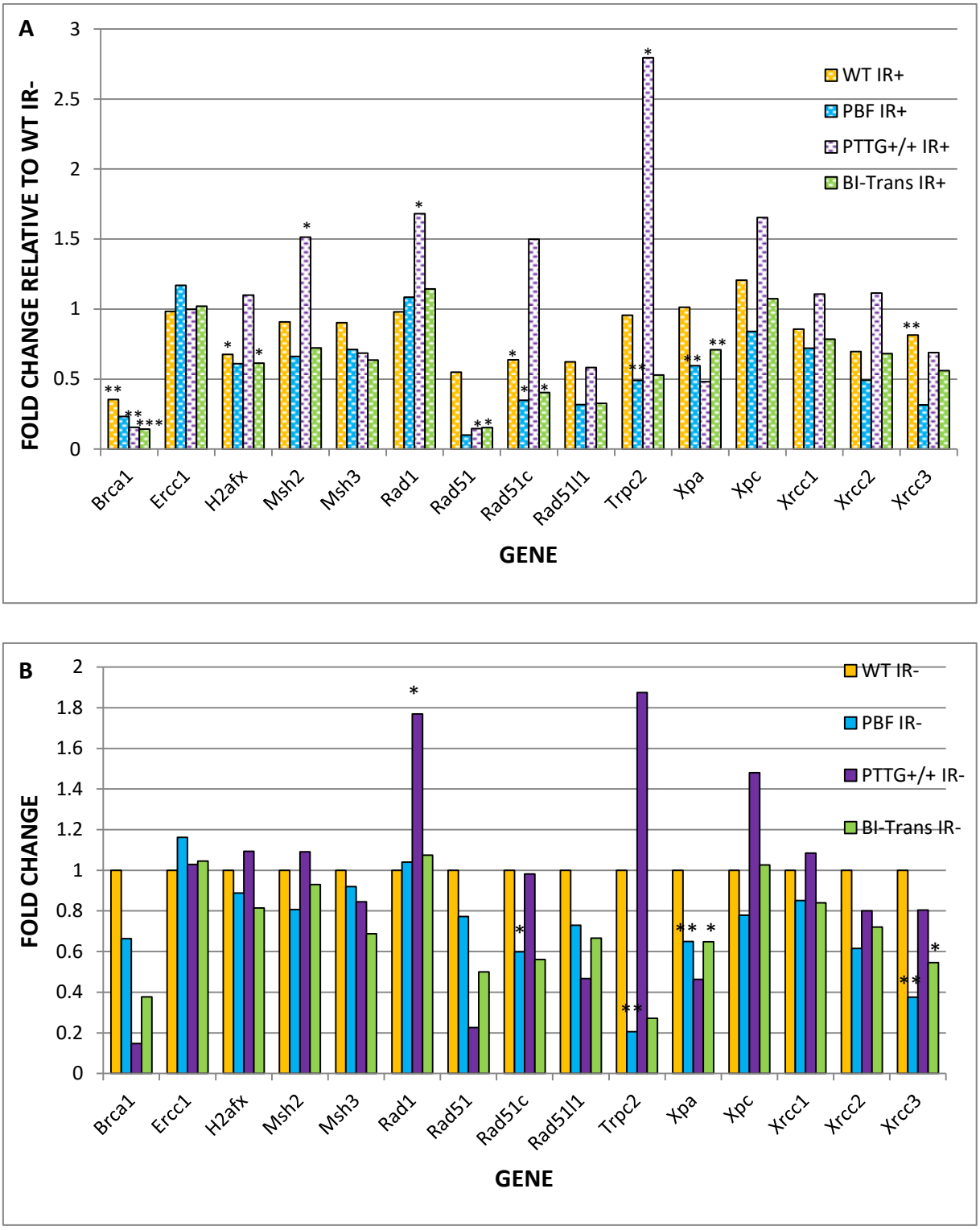

*Figure 6-9 Expression of genes involved in DNA binding by genotype. The top chart (A) denotes PMTC genotype with irradiation (IR+) and bottom chart (B) denotes PMTC genotype without irradiation (IR-). Fold expression is relative to WT PMTC without irradiation (WT IR-). p-values are denoted with * ($0.01 < p \leq 0.05$), ** ($0.001 < p \leq 0.01$) and *** ($0.0001 < p \leq 0.001$).*

6.3.10 Genes involved in base excision repair

The expression of Mbd4 (0.50 fold, p=0.072, n=3) was reduced in WT PMTC following radiation as shown in Figure 6-10. In PBF IR+ PMTCs, Mutyh (0.36 fold p=0.003 n=3), Mbd4 (0.45 fold, p=0.056, n=3) and Parp1 (0.46 fold, p=0.149, n=3) had reduced expression. The gene Mbd4 (0.44 fold p=0.021 n=3) was suppressed and Nthl1 (2.10 fold p=0.020 n=3) increased in PTTG IR+ PMTCs. This pattern of expression was comparable to PTTG IR- PMTCs. Mbd4 expression (0.44 fold, p=0.021, n=3) was reduced in BI-Trans IR+, similar to BI-Trans IR-.

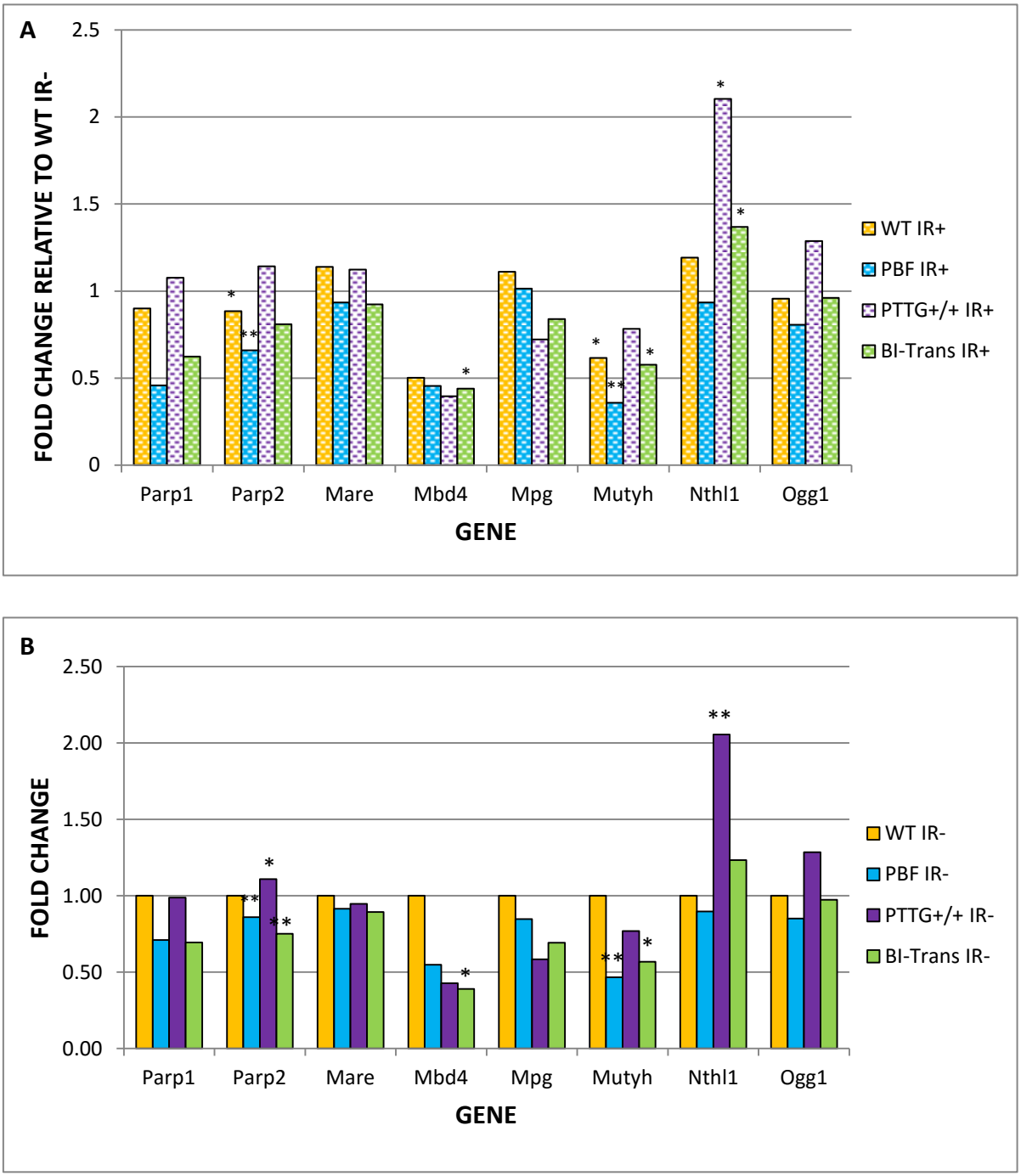

*Figure 6-10 Expression of genes involved in base excision repair by genotype. Top figure denotes PMTC genotype with irradiation (IR+) and bottom figure denotes PMTC genotype without irradiation (IR-). Fold expression is relative to WT PMTC without irradiation (WT IR-). p-values are denoted with * ($0.01 < p \leq 0.05$) and ** ($0.001 < p \leq 0.01$).*

6.3.11 Genes involved in nucleotide excision repair

Radiation did not appear to have a significant effect on nucleotide excision repair genes in WT, PBF and BI-Trans PMTCs (Figure 6-11). Fancc (0.31 fold p=0.023 n=3) and Xpa (0.48 fold, p=0.060, n=3) had reduced expression in PTTG IR+ compared to WT IR-. The expression of Fancc and Xpa were similar in PTTG IR- and PTTG IR+ PMTCs.

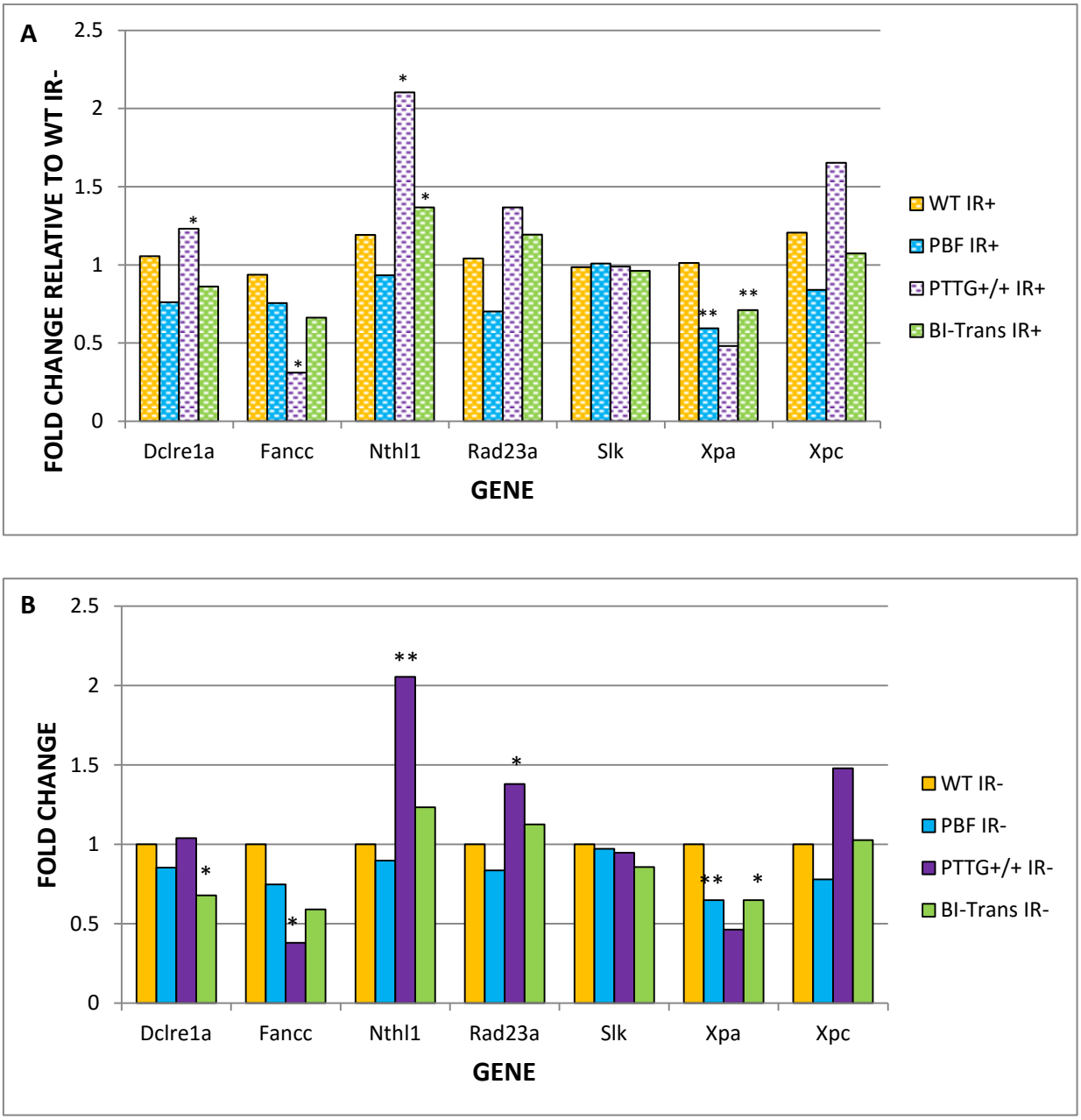

*Figure 6-11 Expression of genes involved in nucleotide excision repair by genotype. Top chart (A) denotes PMTC genotype with irradiation (IR+) and bottom chart (B) denotes PMTC genotype without irradiation (IR-). Fold expression is relative to WT PMTC without irradiation (WT IR-). p-values are denoted with * ($0.01 < p \leq 0.05$) and ** ($0.001 < p \leq 0.01$).*

6.3.12 Genes involved in double strand break repair

No genes involved in double strand break repair appeared to be expressed more than 2 or less than 0.5 fold in all genotypes 24 hours following radiation as shown in Figure 6-12. The gene expression changes in all genotypes between IR- and IR+ was similar.

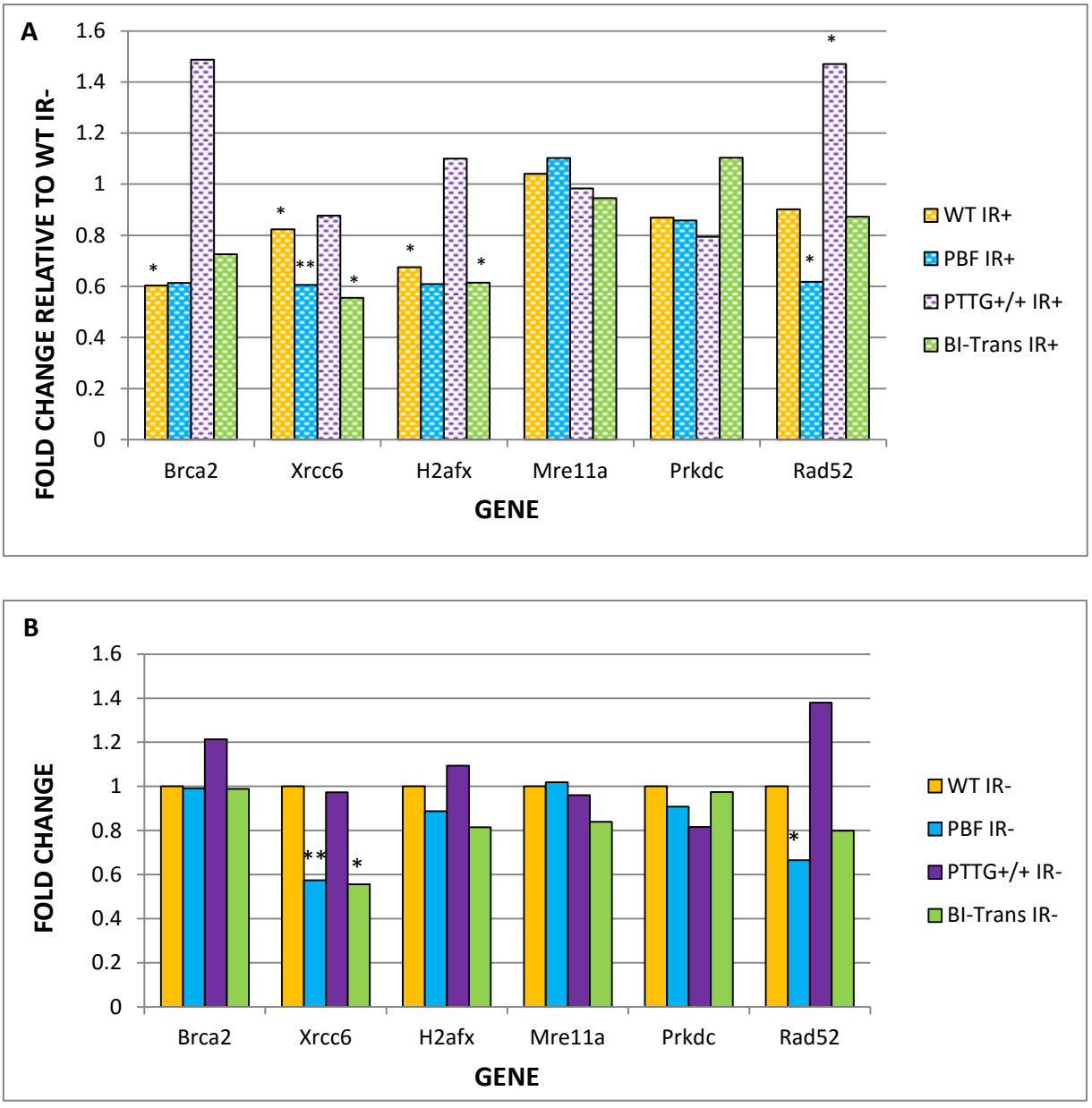

*Figure 6-12 Expression of genes involved in double break strand repair by genotype. Top figure (A) denotes PMTC genotype with irradiation (IR+) and bottom figure (B) denotes PMTC genotype without irradiation (IR-). Fold expression is relative to WT PMTC without irradiation (WT IR-). p-values are denoted with * ($0.01 < p \leq 0.05$) and ** ($0.001 < p \leq 0.01$).*

6.3.13 Genes involved in mismatch repair

Genes involved in mismatch repair did not appear to be altered significantly in WT and PBF PMTCs following radiation. The gene expression changes in WT IR- compared with WT IR+ and PBF WT IR- compared with WT IR+ were essentially similar (Figure 6-13). The altered expression of genes in PTTG IR+ PMTCs, Pms1 (1.95 fold, p=0.014, n=3), Pms2 (0.48 fold, p=0.071, n=3) and Trex1 (0.37 fold, p=0.012, n=3) compared to WT IR- had similar expression levels in PTTG IR- PMTCs. Trex1 (0.50 fold, p=0.064, n=3) had reduced expression in BI-Trans IR+ PMTCs. The level of suppression in BI-Trans IR+ PMTCs were comparable to BI-Trans IR- PMTCs.

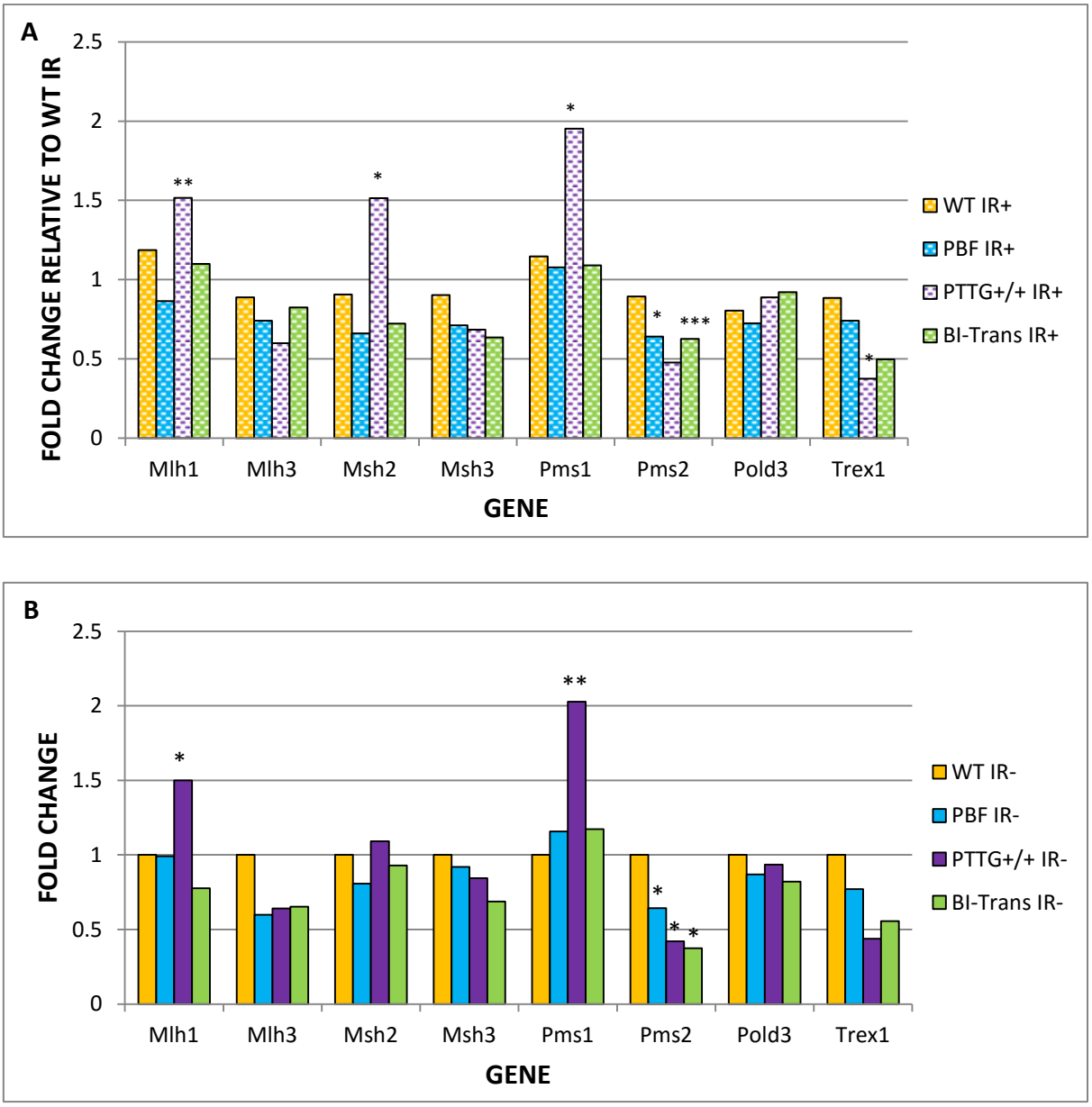

*Figure 6-13 Expression of genes involved in mismatch repair by genotype. Top chart (A) denotes PMTC genotype with irradiation (IR+) and bottom chart (B) denotes PMTC genotype without irradiation (IR-). Fold expression is relative to WT PMTC without irradiation (WT IR-). p-values are denoted with * ($0.01 < p \leq 0.05$), ** ($0.001 < p \leq 0.01$), and *** ($0.0001 < p \leq 0.001$).*

6.3.14 **Expression of other genes related to DNA repair**

We next examined genes that are involved in DNA repair but do not specifically and umabigiously belong to any of the categories described above (Figure 6-14). WT IR+ PMTCs show altered expression in Exo1 (0.3 fold p=0.006 n=3), Lig1 (0.43 fold p=0.013 n=3), Mgmt (2.05 fold, p=0.003, n=3), Pole (0.37 fold, p=0.002, n=3), Pttg1 (0.41 fold, p=0.162, n=3) and Ung (0.50 fold, p=0.085, n=3) relative to WT IR-. PBF+/+ IR+ PMTCs had reduced expression of Exo1 (0.13 fold, p=0.010, n=3), Pole (0.19 fold, p=0.003, n=3), Pttg1 (0.28 fold, p=0.386, n=3), Chaf1a (0.30 fold, p=0.022, n=3), Pold1 (0.44 fold, p=0.004, n=3), Lig1 (0.36 fold, p=0.129, n=3), Ung (0.41 fold, p=0.142, n=3) and Rad9b (0.46 fold, p=0.052, n=3). The genes suppressed to a significant extent in PBF IR+ was similarly suppressed in PBF IR- albeit not less than 0.5 fold with the exception of Rad9b. The expression of Chaf1a (0.30 fold, p=0.022, n=3), Exo1 (0.13 fold, p=0.010, n=3), Fancg (0.40 fold, p=0.032, n=3), Fen1 (0.22 fold, p=0.002, n=3), Pold1 (0.44 fold, p=0.004, n=3), Pole (0.19 fold, p=0.003, n=3), Polk (4.97 fold, p=0.004, n=3), Rad18 (0.31 fold, p=0.001, n=3), Rad9 (3.23 fold, p=0.011, n=3), Tdg (2.81 fold, p=0.090, n=3), Ube2a (2.46 fold, p=0.018, n=3) and Wrn (0.48 fold, p=0.264, n=3). The genes that were also significantly repressed in PTTG IR- PMTCs included Chaf1a, Exo1, Fancg, Fen1, Pole, Polk, Rad18, Rad9, Tdg and Ube2a. Genes that had reduced expression in BI-Trans IR+ included Chaf1a (0.42 fold, p=0.019, n=3), Exo1 (0.09 fold, p=0.001, n=3), Fen1 (0.33 fold, p=0.001, n=3), Lig1 (0.43 fold, p=0.002, n=3), Pole (0.15 fold, p=0.002, n=3), Polk (2.01 fold, p=0.009, n=3), Rad18 (0.47 fold, p=0.001, n=3) and Ung (0.26 fold, p=0.009, n=3). The expression of Chaf1a, Exo1, Fen1 and Ung was altered in BI-Trans IR-.

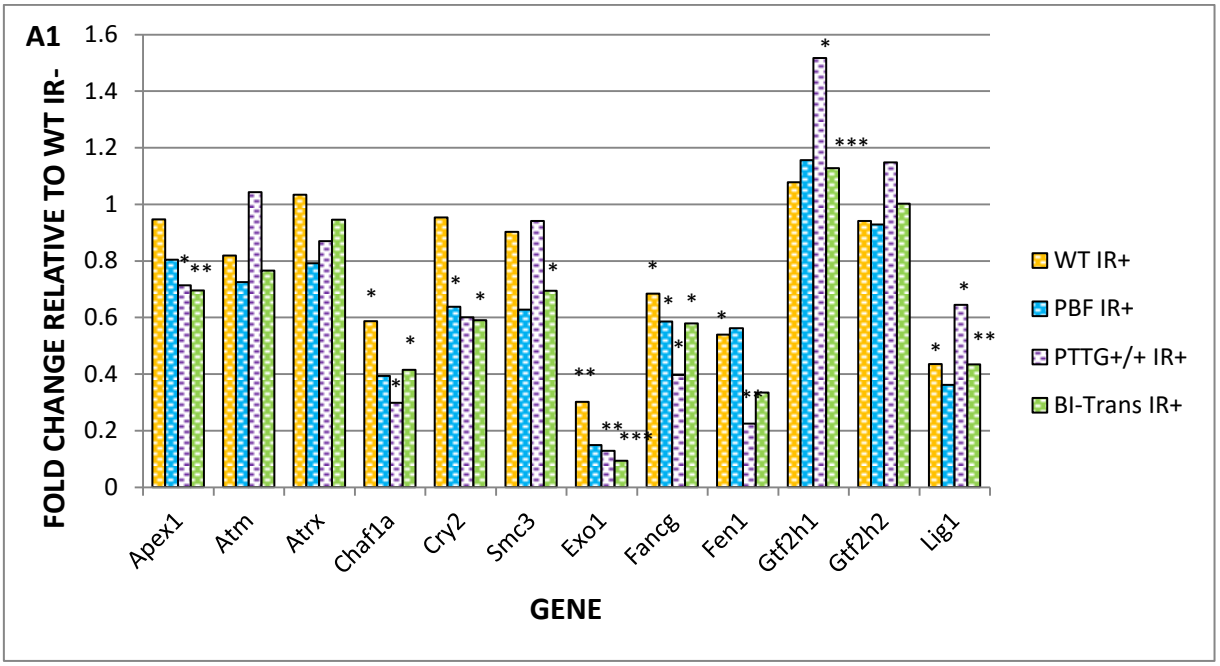
A1
FOLD CHANGE RELATIVE TO WT IR-
1.6
1.4
1.2
1
0.8
0.6
0.4
0.2
0
Apex1
Atm
Atrx
Chaf1a
Cry2
Smc3
Exo1
Fancg
Fen1
Gtf2h1
Gtf2h2
Lig1
GENE
WT IR+
PBF IR+
PTTG+/+ IR+
BI-Trans IR+

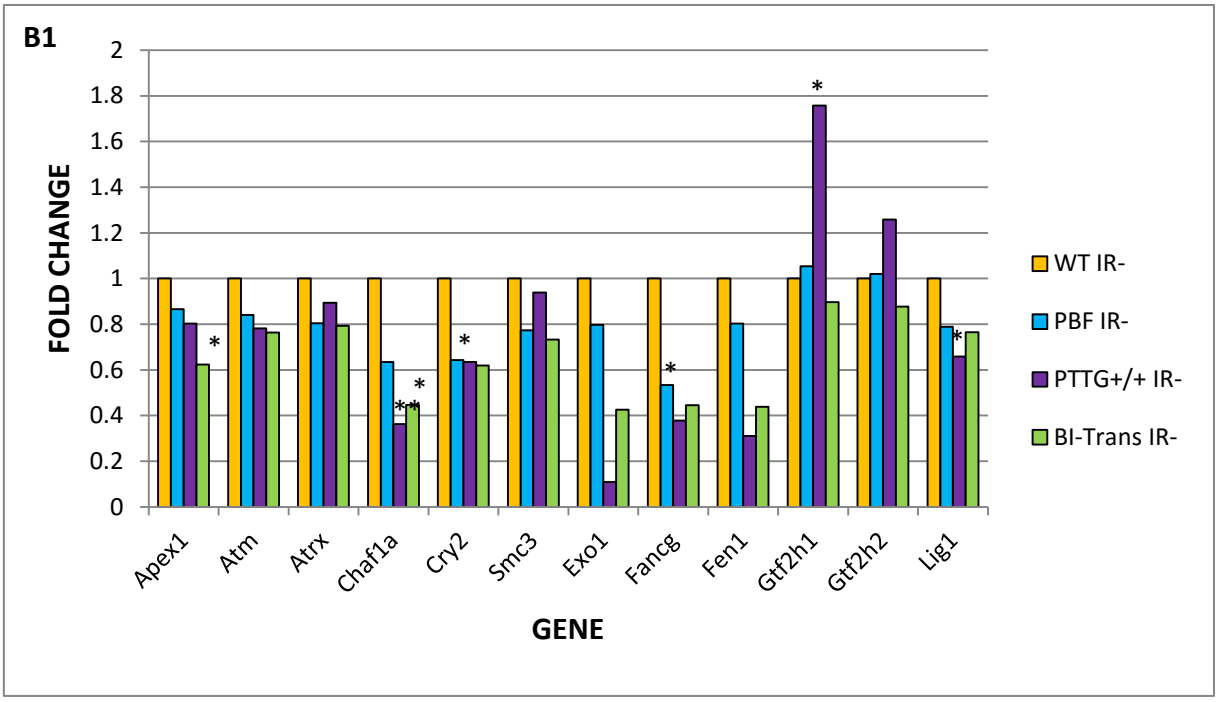
B1
FOLD CHANGE
2
1.8
1.6
1.4
1.2
1
0.8
0.6
0.4
0.2
0
Apex1
Atm
Atrx
Chaf1a
Cry2
Smc3
Exo1
Fancg
Fen1
Gtf2h1
Gtf2h2
Lig1
GENE
WT IR-
PBF IR-
PTTG+/+ IR-
BI-Trans IR-

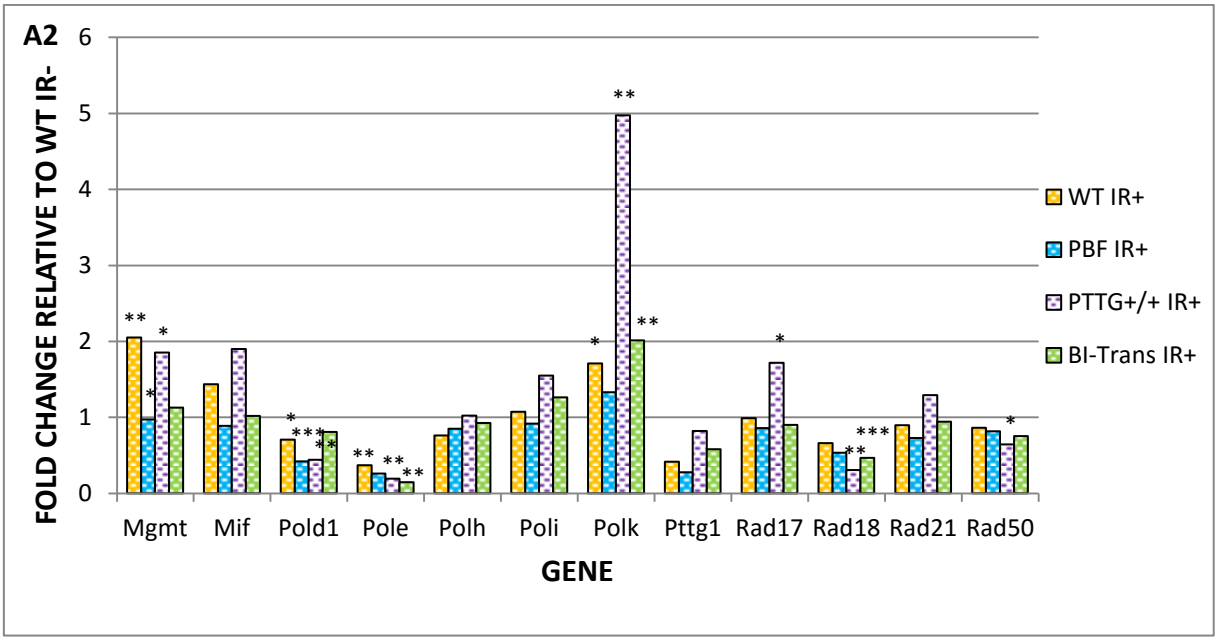
A2
FOLD CHANGE RELATIVE TO WT IR-
6
5
4
3
2
1
0
Mgmt
Mif
Pold1
Pole
Polh
Poli
Polk
Pttg1
Rad17
Rad18
Rad21
Rad50
GENE
WT IR+
PBF IR+
PTTG+/+ IR+
BI-Trans IR+

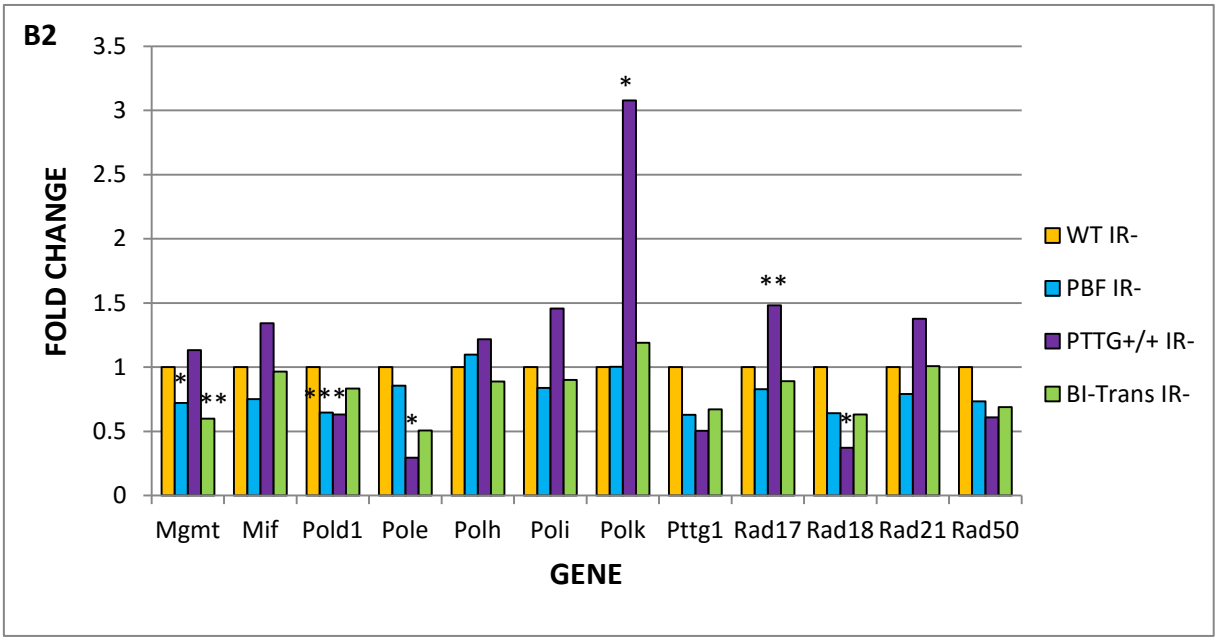
B2
FOLD CHANGE
3.5
3
2.5
2
1.5
1
0.5
0
Mgmt
Mif
Pold1
Pole
Polh
Poli
Polk
Pttg1
Rad17
Rad18
Rad21
Rad50
GENE
WT IR-
PBF IR-
PTTG+/+ IR-
BI-Trans IR-

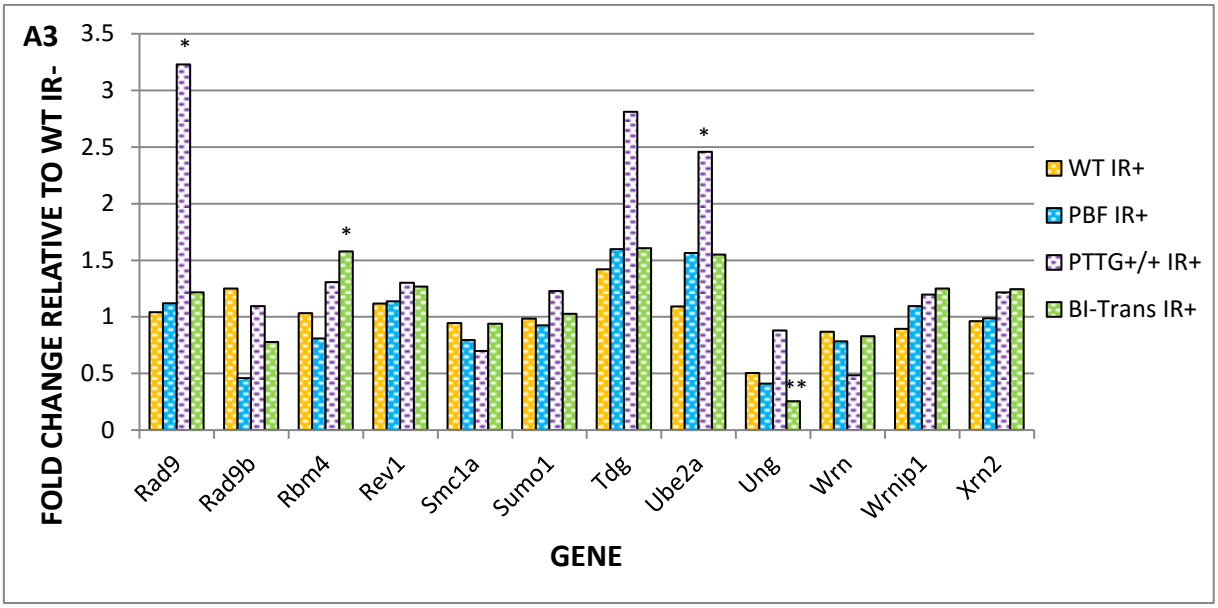

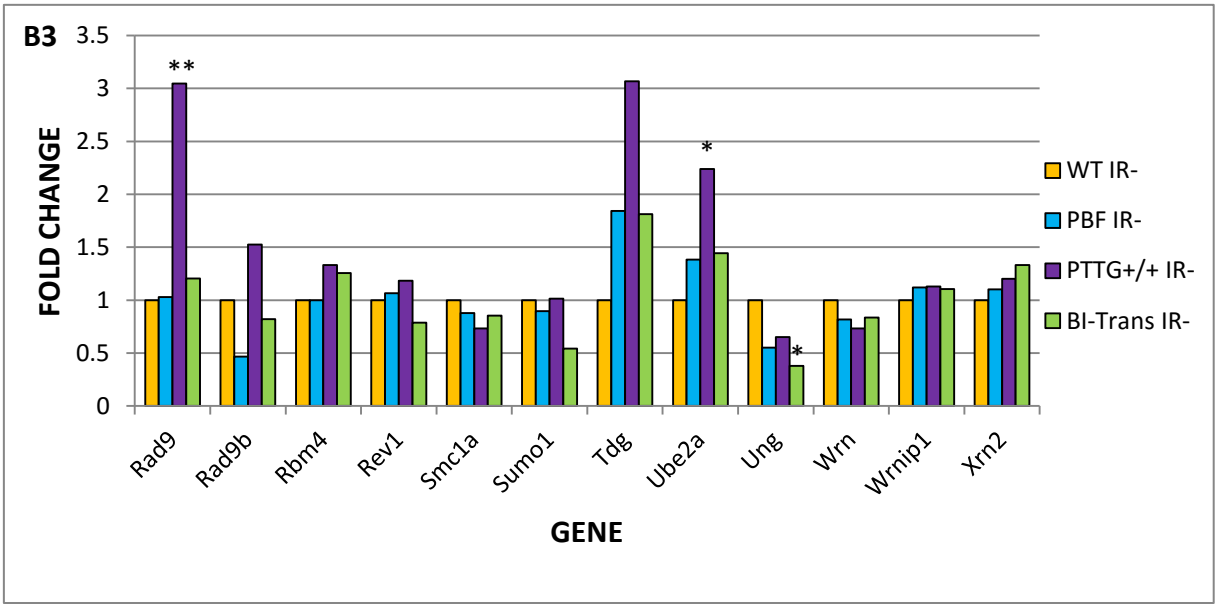

*Figure 6-14 Expression of genes related to DNA repair by genotype. Top figure (A) denotes PMTC genotype with irradiation (IR+) and bottom figure (B) denotes PMTC genotype without irradiation (IR-). Fold expression is relative to WT PMTC without irradiation (WT IR-). p-values are denoted with * ($0.01 < p \leq 0.05$), ** ($0.001 < p \leq 0.01$) and *** ($0.0001 < p \leq 0.001$).*

6.4 DISCUSSION

6.4.1 Study on gene expression changes following radiation damage in PMTCs

The purpose of this chapter has been to appraise in detail the influence of genotype and ionising radiation on a panel of 84 genes involved in DNA damage and DNA repair in order to screen for candidate genes to appraise in detail in subsequent chapters. The above study performed on PMTCs was interpreted based on the expression changes of more than 2 or less than 0.5 fold relative to WT IR- PMTCs. Although statistical significance was expressed in the above findings, the trend was more important at this stage than the actual p-values in determining the relevance of the gene identified. This assumption will be challenged when validation studies were performed to determine the reproducibility of the microarray findings.

DNA repair following DNA damage is an evolving process that activates and suppresses various genes at different stages. This experiment was performed at 24 hours following ionising radiation, considered a relatively late time point in DNA damage studies, but allowing time for all 84 genes to putatively show expression changes.

6.4.2 PBF IR+ PMTCs and DNA damage / DNA repair gene changes

In DNA damage, PBF responds to ionising radiation in a similar fashion to WT PMTCs by the suppression of downstream gene targets of Chek1 and Chaf1a. Chek1 is a cell cycle checkpoint protein and Chaf1a is involved in mediating chromatin assembly in DNA repair. The only difference the genotype PBF makes is the suppression of Terf1, a gene involved in telomerase nucleoprotein complex. The inhibition of this gene should increase telomerase activity which adds DNA sequence repeats to the 3' end of DNA strands.

The RAD51 family of proteins appeared to be suppressed to a significant degree by PBF following irradiation. The proteins encoded by this family of genes are involved in DSBs and homologous recombination (Krejci et al., 2012). The significance of this is not entirely clear but the ability to repair double stranded breaks is crucial in protecting a cell from ionising radiation.

6.4.3 PTTG IR+ PMTCs and DNA damage / DNA repair gene changes

As described previously, PTTG independently encouraged the expression of gene products necessary for the formation of the 9-1-1 complex. However, the expression of ATR, the gene required in conjuction with the 9-1-1 complex to activate the ATR pathway, remained largely unaltered.

The observed microarray changes in PBF IR+ PMTCs seems to indicate that the Rad51 system of DNA damage genes is more suppressed than in WT IR+. The changes observed in reduced Trpc2, Xrcc3, Mutyh, Lig1 and Rad9b appeared to be similar to the pattern of changes observed as a result of PBF overexpression in PMTCs. The additional suppression of genes such as Exo1, Pole, Pttg1 and Ung appeared to be exaggerated in PBF PMTCs. Although this effect was similar to WT IR+, the response was more marked when PBF was overexpressed in follicular thyroid epithelial cells.

6.4.4 The effect of both PBF and PTTG on DNA damage and DNA repair genes in PMTCs

The microarray gene expression changes indicated that the changes observed in BI-Trans IR+ PMTCs was a unique combination in PBF and PTTG overexpression and radiation. Rad51l1 and Rad51c expression was reminiscent of PBF IR+ PMTCs, whilst the altered expressions of Fen1, Rad18, Trex1 and Polk were also observed in PTTG+/+ IR.

The PBR IR+ effect is dominant mainly in the upstream genes of the Rad51 family involved in homologous recombination. Several downstream genes are suppressed apart from Polk. Polk functions

by encouraging the replication fork to continue through a DNA lesion which might stall the replication process (Haracska et al., 2002). As such, we hypothesize that an increase in Polk levels might increase genetic instability by permitting mutations within the genome.

6.5 CONCLUSION

The increased expression of Hus1, Rad1 and Rad9 involved in the formation of the 9-1-1 complex in the ATR signalling pathway is primarily PTTG related. Radiation did not appear to affect the expression of these genes. However, PBF appeared to attenuate the increased expression of the genes involved in the 9-1-1 complex. PBF PMTC response to radiation included the suppression of the Rad51 family proteins and its functionally related Xrcc proteins. In PMTCs overexpressing both PBF and PTTG, and treated with ionising radiation, the gene expression changes were a combination of PBF IR+ and PTTG IR+.

7 Evaluation of shortlisted genes within the DNA Damage / DNA Repair pathway

7.1 INTRODUCTION

7.1.1 Background

PBF and PTTG each cause genetic instability independently in the thyroid (Kim et al., 2007b, Kim et al., 2005, Read et al., 2014a). To study the effects of our genes of interest on thyroid tumourigenesis, the McCabe group created transgenic knock-in murine models of PBF, PTTG and both PBF and PTTG overexpression in the thyroid gland. The persistent level of expression of our genes of interest in thyroid cells within a physiological environment mirrors that in thyroid neoplasia and is ideal for further studies involving PBF, PTTG and their interacting genes (Kim and Zhu, 2009, Read et al., 2011).

Primary murine thyroid culture (PMTC) is a technique established in our group. PMTCs have been validated to be functional and to exhibit overexpression of our knock-in genes in culture. The presence of functional thyroid cells in culture overexpressing our genes of interest in a uniform manner makes it a flexible platform for further studies.

On the background of PBF and PTTG affecting genomic stability, we studied the interaction of our genes of interest in the context of DNA damage and DNA repair genes. Microarray studies on the effects of PBF, PTTG and both genes together have established a pattern of gene mRNA expression and suppression within the ATR/ATM signalling network.

This chapter aimed to validate the findings of genes identified and shortlisted from the microarray studies. mRNA expression of genes identified on the Mouse DNA Damage Signalling RT^2 Profiler^{TM} PCR Arrays (SABiosciences) were validated by Taqman real-time qRT-PCR and protein expression on Western blotting.

7.2 MATERIALS AND METHODS

7.2.1 Primary murine thyroid cultures

PMTC was performed on the 4 different genotypes, WT, PBF, PTTG +/+ and BI-Trans as described previously in section 2.2. PMTCs were harvested at day 10. For studies involving radiation, cells were exposed to 25 Gy ionising radiation on day 9 and harvested 24 hours later.

7.2.2 RNA extraction and reverse transcription

RNA was harvested from PMTCs on day 10 using the micro RNeasy kit (QIAGEN) and complementary DNA (cDNA) was obtained using the Promega Reverse Transcription system. Both methods were described in section 2.4 and 2.5 respectively.

7.2.3 Real-time quantitative polymerase chain reaction (qRT-PCR)

These experiments were performed using the ABI PRISM 7500 Sequence Detection System, which employs TaqMan ™ chemistry for highly accurate quantification of mRNA levels (Wang and Brown, 1999) described in section 2.6. We performed singleplexed experiments because none of our shortlisted genes could be multiplexed with β-actin, our housekeeping gene. The housekeeping gene was selected based on the microarray data that suggested β-actin was the most reliable housekeeping gene.

7.2.4 Western blotting

The resolution of protein on SDS-gel has been described previously in section 2.8. Primary antibodies used in this chapter included rabbit polyclonal antibody to Rad51 at a concentration of 1:500 (Product

code: ab63801; Abcam®), Rabbit DO-1 (courtesy of Dr. A Turnell, University of Birmingham) at a concentration of 1:100, monoclonal anti-β-actin (clone AC-15, Sigma-Aldrich, Poole, UK) at a concentration of 1:10,000 and γ-H2AX antibody at a concentration of 1:10,000 (NEWENGLAND Biolabs, MA, USA).

7.3 RESULTS

7.3.1 The presence of γ-H2AX in PMTCs confirmed the presence of DNA damage following ionising radiation

We assessed the protein expression of γ-H2AX in primary murine thyroid cultures (PMTCs) to determine whether there was DNA damage following irradiation. The expression of γ-H2AX has been used as a reliable indicator of DNA damage and its expression is linear with time following exposure to ionising radiation (Kuo and Yang, 2008, Sharma et al., 2012). On Western blot, γ-H2AX appeared as a band at approximately 15 kDa, shown in Figure 7-1.

Relative fold protein expression of γ-H2AX to WT IR- (n=6) was 2.3 ± 0.5 fold (n=7, p=0.034) in WT IR+, 1.01 ± 0.26 fold (n=7, p=0.976) in PBF IR-, 0.96 ± 0.29 fold (n=8, p=0.902) in PBF IR+, 2.14 ± 0.59 fold (n=7, p=0.099), 3.39 ± 0.86 fold (n=7, p=0.019) in PTTG IR+, 2.03 ± 0.51 (n=8, p=0.075) in BI-Trans IR- and 2.42 ± 0.34 (n=8, p=0.023) in BI-Trans IR+ on on densitometry studies, shown in Figure 7.1. This crucial experiment confirmed the presence of DNA damage in our PMTCs following exposure to ionising radiation, providing confirmation that the dose of ionising radiation and time point used in our experiments were adequate to demonstrate gene expression changes on the microarray and validation studies. Interestingly, PBF PMTCs following treatment with ionising radiation (PBF IR+) did not demonstrate a statistically significant change compared to WT IR-.

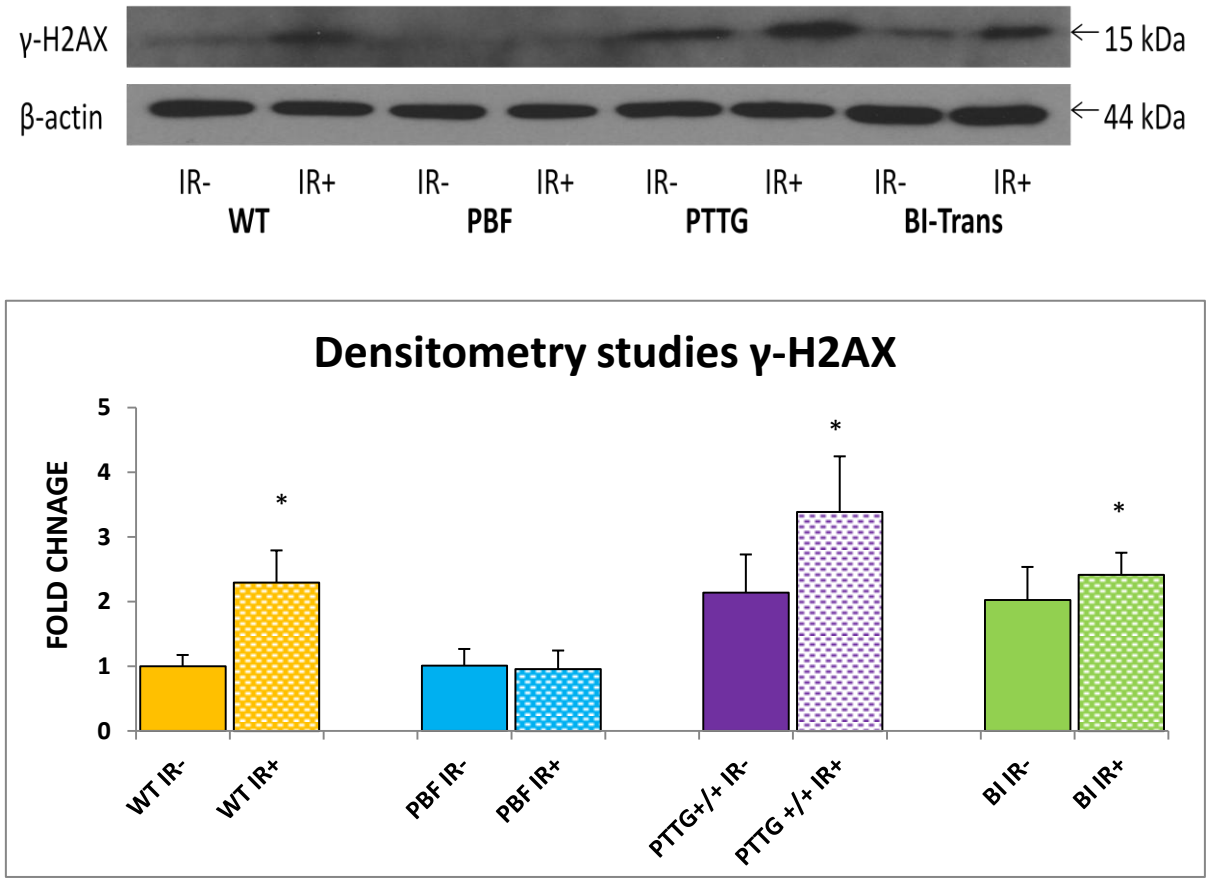

*Figure 7-1 Western blot and densitometry study of γ-H2AX in PMTCs by genotype with and without irradiation.WT IR- (n=6), WT IR+ (n=7), PBF IR- (n=7), PBF IR+ (n=8), PTTG+/+ IR-(n=7), PTTG+/+ IR+ (n=7), BI-Trans IR- (n=8) and BI-Trans IR+ (n=8). p-values are denoted with * ($0.01 < p \leq 0.05$).*

7.3.2 The mRNA expression of Brca1 was reduced by PTTG expression and ionising radiation

Brca1 maintains genomic stability via its roles in DNA repair, cell cycle checkpoint control, transcriptional regulation, apoptosis and mRNA splicing. Brca1 deficient cells have been observed to exhibit chromosomal translocations with large deletions and/or amplifications that involve multiple, non homologous chromosomes (Deng and Scott, 2000).

PTTG but not PBF appeared to inhibit the expression of Brca1 significantly on the microarray. We also observed a reduction in Brca1 in all PMTCs following radiation on our microarray (Figure 7-2A). Hence, we decided to study this gene in greater detail.

The relative fold expression of Brca1 on Taqman qRT-PCR relative to WT IR- was 0.58 ± 0.03 ($p=0.018$, $n=4$) in WT IR+, 0.92 ± 0.08 ($p=0.655$, $n=4$) in PBF IR-, 0.32 ± 0.08 ($p=0.002$, $n=4$) in PBR IR+, 0.37 ± 0.10 ($p=0.005$, $n=4$) in PTTG+/+ IR-, 0.31 ± 0.15 ($p=0.009$, $n=4$), 0.35 ± 0.14 ($p=0.004$, $n=4$) in BI-Trans IR- and 0.20 ± 0.11 ($p=0.003$, $n=4$) in BI-Trans IR+, shown in Figure 7-2B. The findings on Taqman qRT-PCR thus closely followed the pattern of changes observed on the microarray, validating our screening approach. This therefore suggests that the results obtained on the microarray closely reflects the situation in reality.

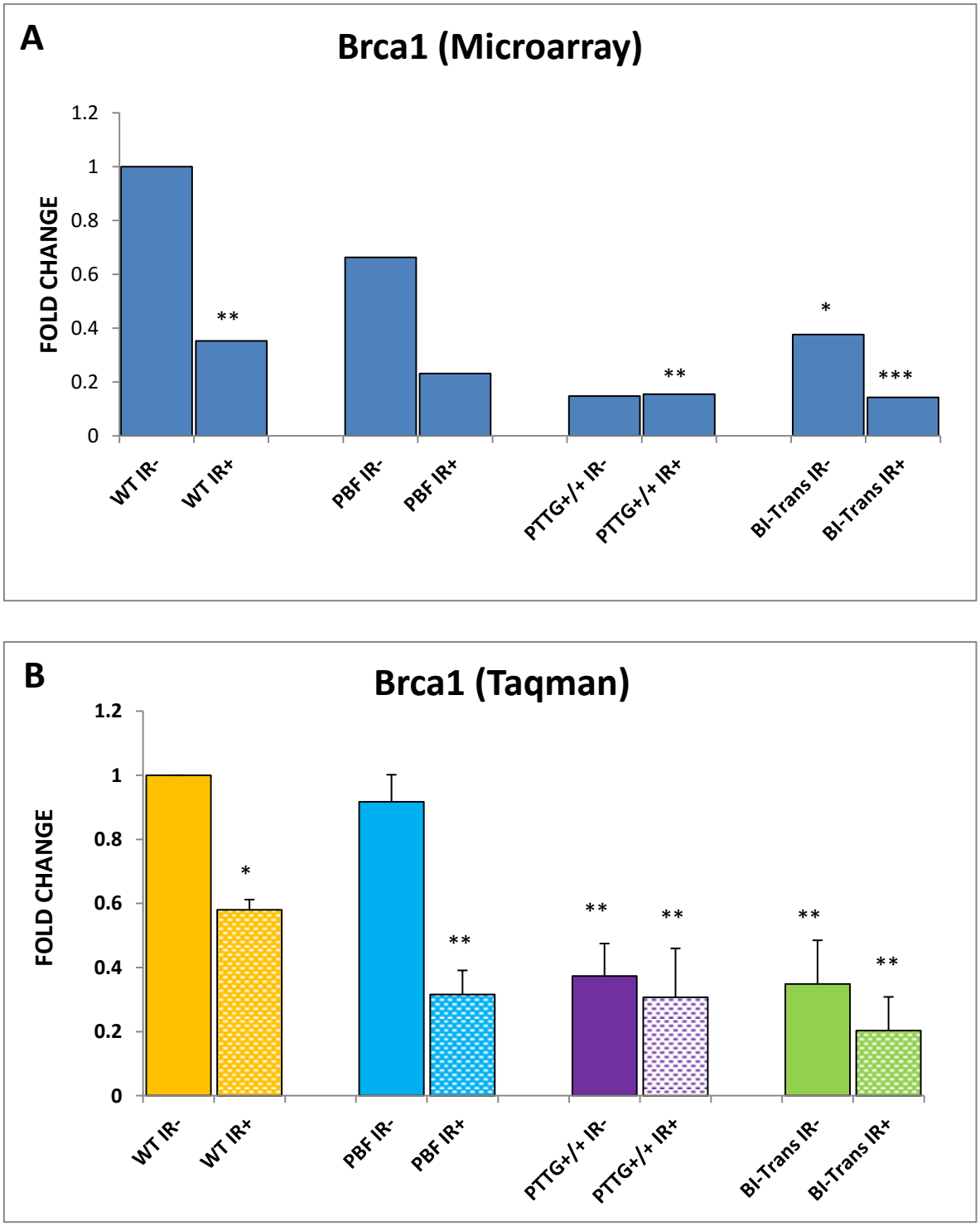

*Figure 7-2 Brca1 mRNA expression in PMTCs by genotype before and after irradiation on the microarray (A) and Taqman qRT-PCR (B). n=4 PMTCs all genotypes. p-values obtained by comparing with WT IR- are denoted with * ($0.01 < p \leq 0.05$), ** ($0.001 < p \leq 0.01$) and *** ($0.0001 < p \leq 0.001$).*

7.3.3 The mRNA expression of Chek1 was inhibited by PTTG and ionising radiation

Chek1 is a serine/threonine kinase that plays an important role in the activation of S and G2/M phase checkpoints. It regulates these checkpoints by altering the inhibitory phosphorylation of cyclin-dependent kinases which drive cell cycle progression. ATR and other intermediate proteins such as replication protein A, Claspin, Rad17, Tim/Tipin, TopBP1 involved in DNA replication are necessary for Chek1 activation. Other functions of Chek1 include stabilization of replication forks (Feijoo et al., 2001), the promotion of DNA repair and coordinating homologous recombination repair (Sorensen et al., 2005).

This upstream gene is crucial in the DNA response to damage and its mRNA expression was observed to be independently affected by PBF, PTTG and ionising radiation damage. The expression of Chek1 on our Taqman qRT-PCR shown in Figure 7-3 was 0.54 ± 0.004 ($p=0.038$, $n=4$) in WT IR+, 0.67 ± 0.09 ($p=0.059$, $n=4$) in PBF IR-, 0.18 ± 0.03 ($p<0.000$, $n=4$) in PBF IR+, 0.38 ± 0.11 ($p=0.015$, $n=4$) in PTTG+/+ IR-, 0.25 ± 0.10 ($p=0.020$, $n=4$) in PTTG+/+ IR+, 0.22 ± 0.07 ($p=0.003$, $n=4$) in BI-Trans IR- and 0.08 ± 0.02 ($p=0.001$, $n=4$) in BI-Trans IR+. Hence, it would appear that ionising radiation and overexpression of PBF and PTTG would increase genetic instability through the repression of Chek1.

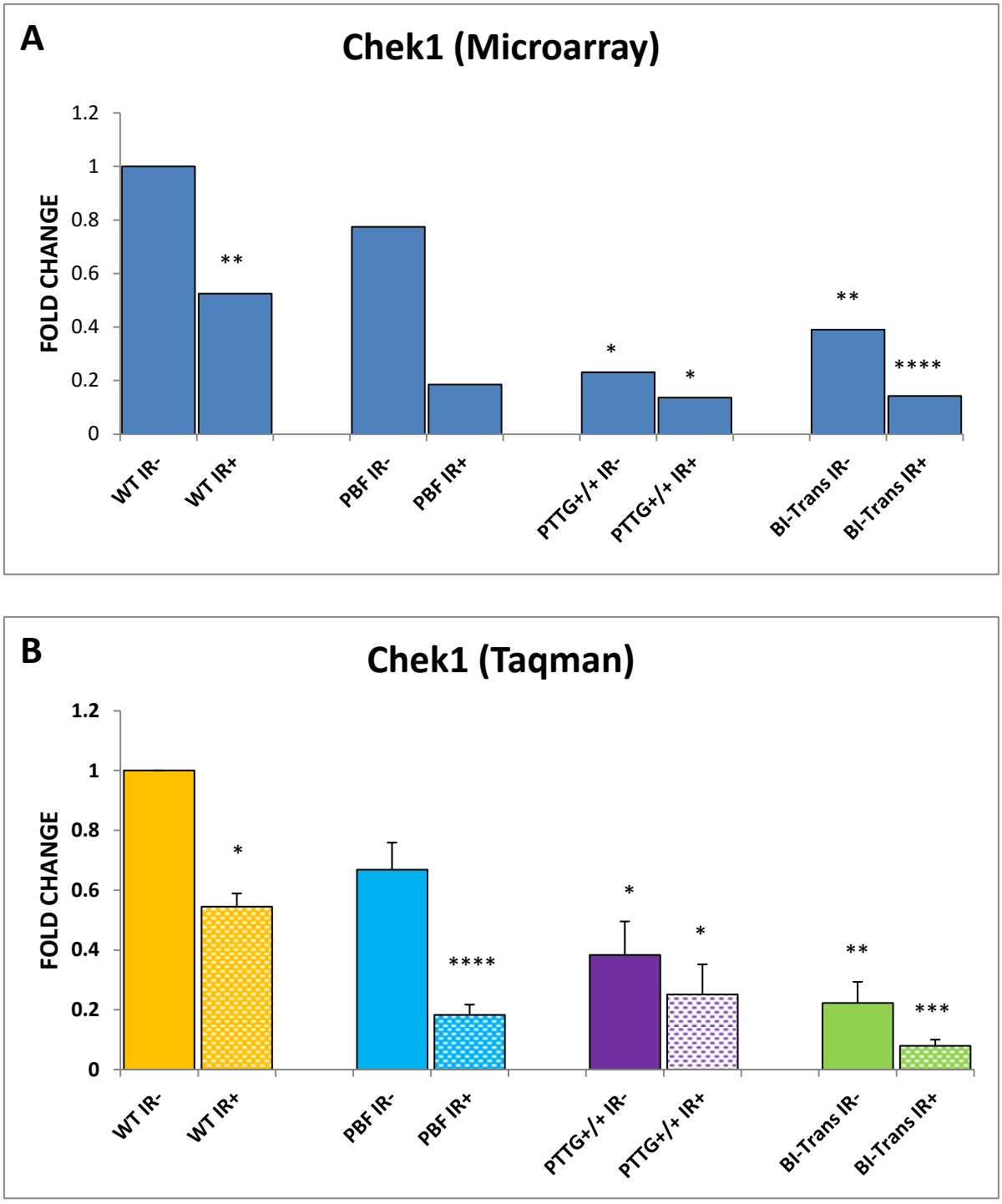

*Figure 7-3 Chek1 mRNA expression in PMTCs before and after irradiation on the microarray (A) and Taqman qRT-PCR (B). n=4 for PMTCs all genotypes. p-values shown, compared to WT IR-, are denoted with * ($0.01 < p \leq 0.05$), ** ($0.001 < p \leq 0.01$), *** ($0.0001 < p \leq 0.001$) and **** ($p \leq 0.0001$).*

7.3.4 **The mRNA expression of Exo1 was repressed by PTTG and radiation**

Exo1 interacts with Msh2 and is involved in mismatch repair and recombination. Exo1 was repressed following ionising radiation and in the presence of PTTG overexpression. The expression of Exo1 was not significantly altered in the presence of PBF. The expression of Exo1 was 0.31 ± 0.05 fold ($p=0.132$, $n=4$) in WT IR+, 0.97 ± 0.09 fold ($p=0.966$, $n=4$) in PBF IR-, 0.19 ± 0.05 fold ($p=0.061$, $n=4$) in PBF IR+, 0.22 ± 0.02 fold ($p=0.073$, $n=4$) in PTTG+/+ IR-, 0.13 ± 0.03 fold ($p=0.047$, $n=4$) in PTTG+/+ IR+, 0.24 ± 0.06 fold ($p=0.128$, $n=4$) in BI-Trans IR-, 0.08 ± 0.03 fold ($p=0.049$, $n=4$) in BI-Trans IR+ PMTCs relative to WT IR- PMTCs as shown in Figure 7-4. Hence, it appears that mismatch repair and recombination mediated by Exo1 is reduced following ionising radiation and in the presence of PTTG overexpression.

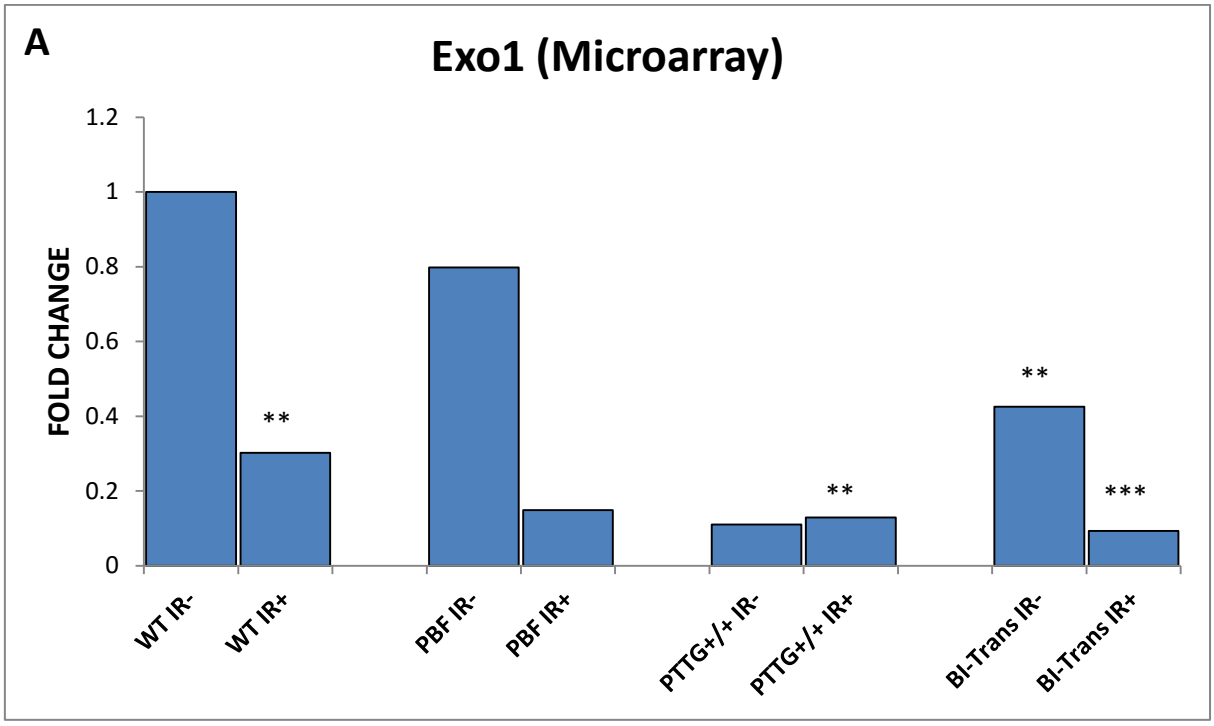

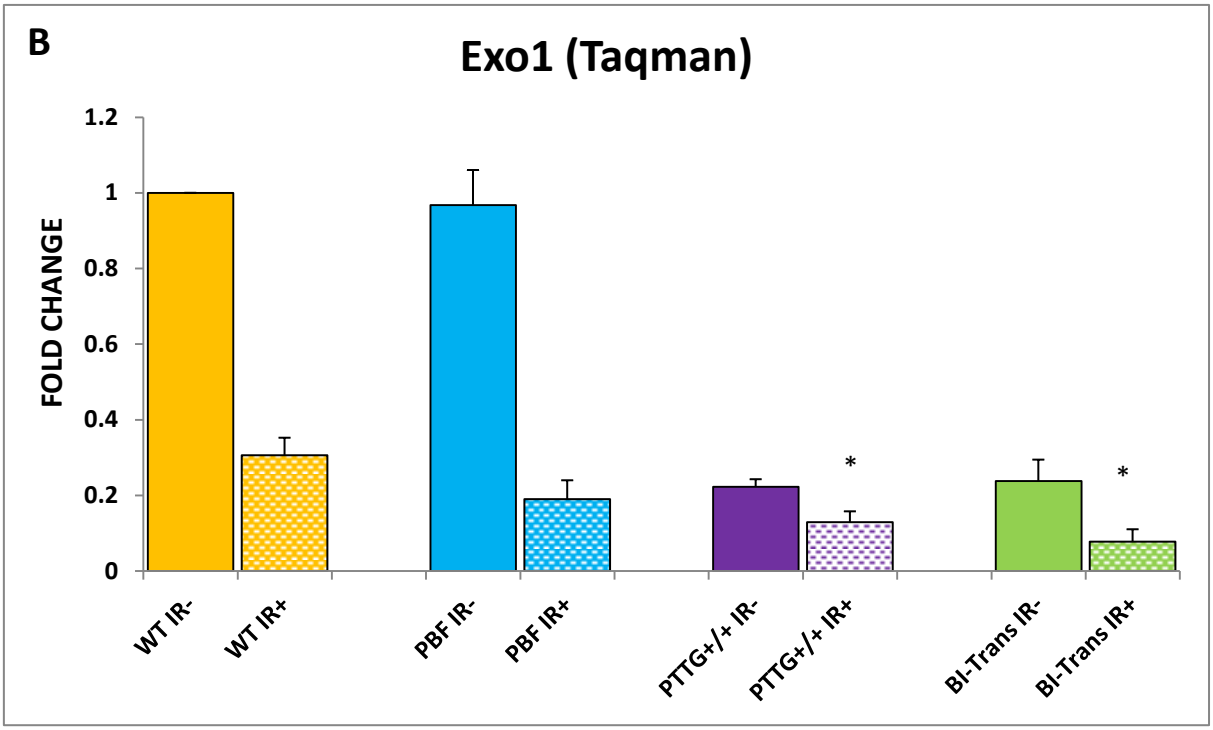

*Figure 7-4 Exo1 mRNA expression in PMTCs before and after irradiation on the microarray (A) and Taqman qRT-PCR (B). n=4 for PMTCs all genotypes. p-values obtained by comparing to WT IR- are denoted with * ($0.01 < p \leq 0.05$), ** ($0.001 < p \leq 0.01$) and *** ($0.0001 < p \leq 0.001$).*

7.3.5 **The mRNA expression of Mgmt was increased by radiation**

Naturally occurring DNA damage in the form of methylated guanine bases is repaired by Mgmt. This methylation is directly reversed by Mgmt in a suicide reaction (Sharma et al., 2009).

In the Taqman validation experiment, Mgmt had increased expression, compared to WT IR-, in WT (2.77 ± 0.07 fold, p=0.001, n=4), PBF (1.45 ± 0.15, p=0.032, n=4), PTTG (1.43 ± 0.57, p=0.373, n=4) and BI-Trans (1.89 ± 0.18, p=0.022, n=4) PMTCs following irradiation. The expression of Mgmt was reduced by the PBF (PBF IR-, 0.76 ± 0.06 fold, p=0.171, n=4) and PTTG (PTTG+/+ IR- 0.69 ± 0.38 fold, p=0.430, n=4) genotype. Interestingly, the expression of Mgmt in BI-Trans IR- (1.02 ± 0.12 fold, p=0.906, n=4) was similar to WT IR- (Figure 7-5). The upregulation of Mgmt mRNA following treatment with ionising radiation was attenuated in the presence of PBF and PTTG overexpression in the thyroid, representing a less effective response following radiation induced damage.

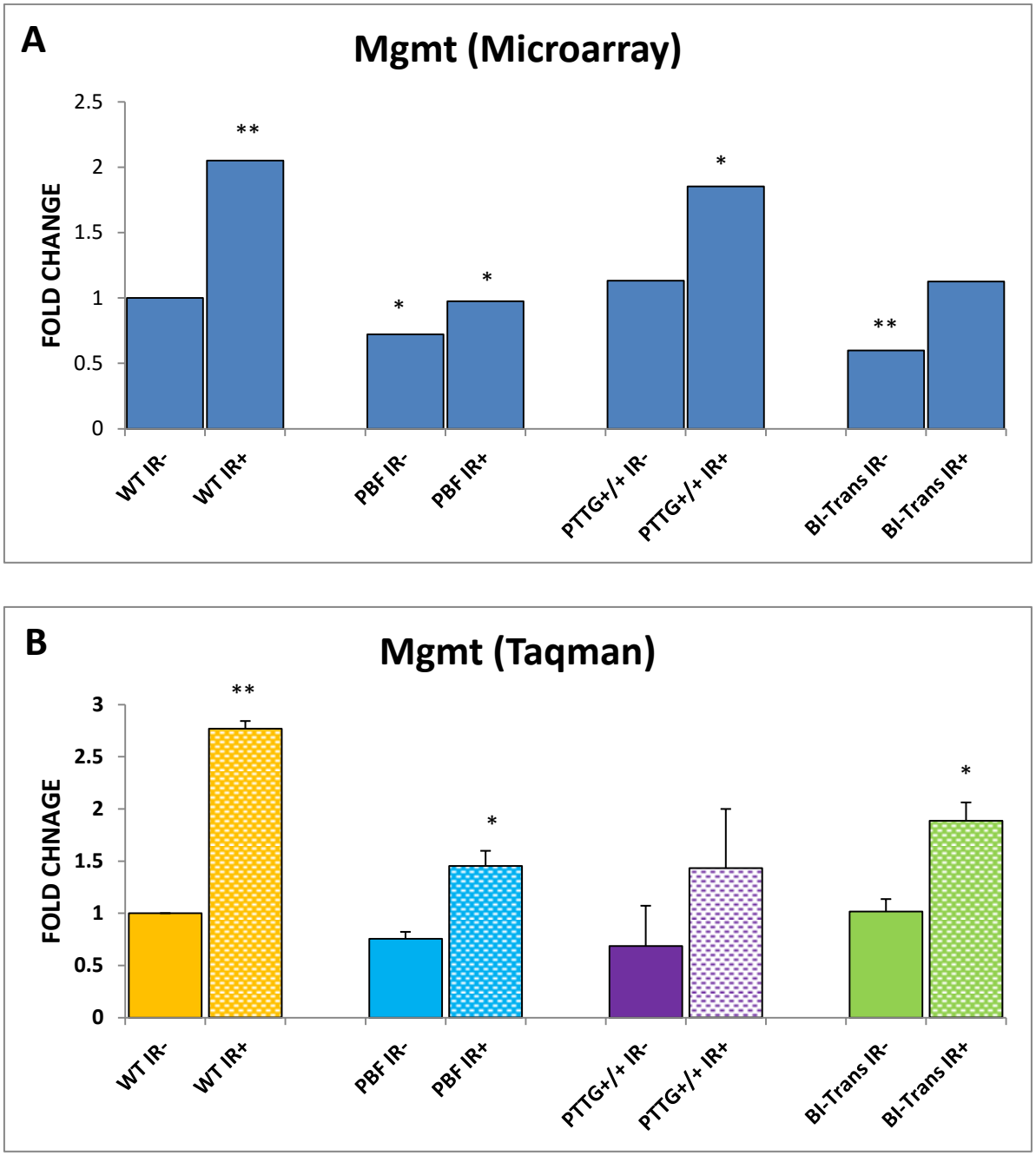

*Figure 7-5 Mgmt mRNA expression in PMTCs before and after irradiation on the microarray (A) and Taqman qRT-PCR (B). n=4 for PMTCs all genotypes. p-values obtained by comparing to WT IR- are denoted with * ($0.01 < p \leq 0.05$) and ** ($0.001 < p \leq 0.01$).*

7.3.6 **The mRNA expression of Rad51 was reduced by PTTG and radiation**

The Rad51 family of proteins participates in homologous recombination to maintain chromosomal stability and DNA repair following damage.

Ionising radiation inhibited the expression of Rad51 in the Taqman qRT-PCR to a significant degree in PBF IR+ (0.24 ± 0.03 fold, p=0.258, n=4), PTTG+/+ IR+ (0.22 ± 0.06 fold, p=0.173, n=4) and BI-Trans IR+ (0.14 ± 0.06 fold, p=0.016, n=4) PMTCs shown in Figure 7-6. The expression of Rad51 in WT IR- PMTCs (0.55 ± 0.02 fold, p=0.275, n=3) was reduced but not less than 0.50 fold and hence, not described as significant. PTTG overexpression independently repressed Rad51. The expression of Rad51 in PTTG+/+ IR- and BI-Trans IR- PMTCs was 0.32 ± 0.02 fold (p<0.000, n=4) and 0.32 ± 0.11 fold (p=0.141, n=4) respectively. PBF overexpression did not repress Rad51. The expression of Rad51 was 0.78 ± 0.07 fold (p=0.120, n=4) in PBF IR- PMTCs. Overall, the expression pattern of the various genotypes was similar in both the Taqman and the Mouse DNA Damage Signalling RT^2 Profiler™ PCR Arrays (SABiosciences). More importantly, the marked repression of Rad51 by PBF and PTTG following exposure to ionising radiation could result in increased genetic instability.

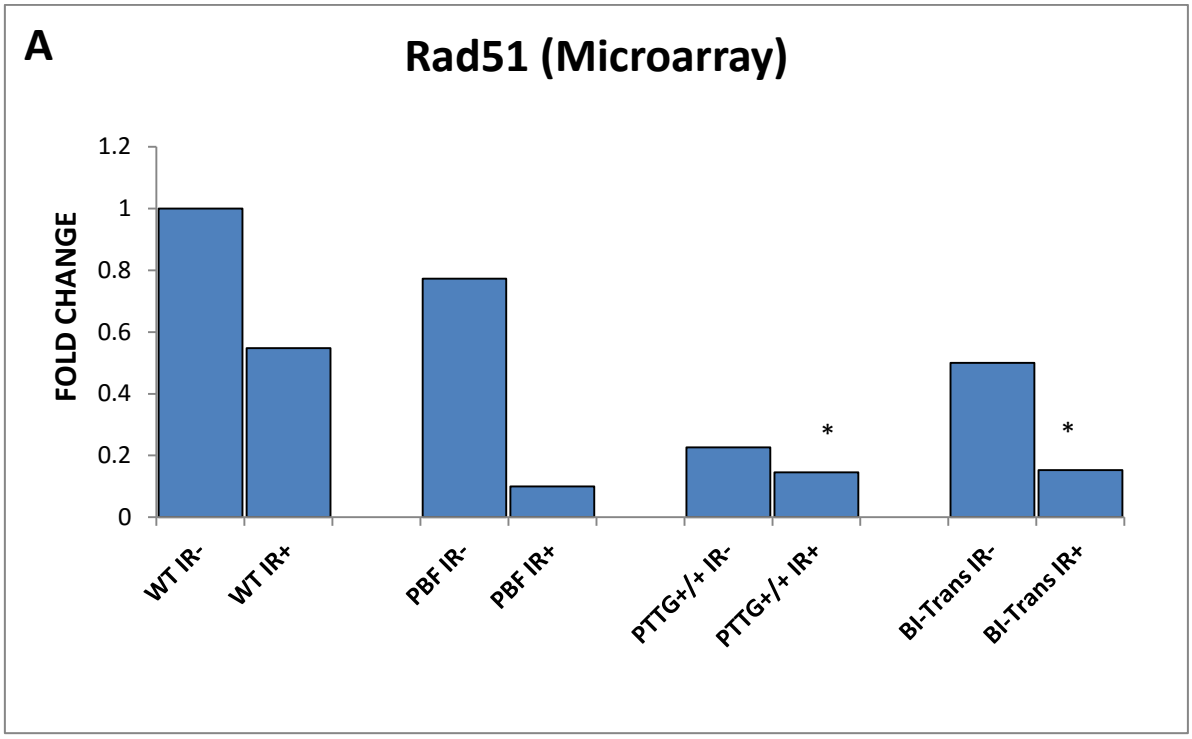

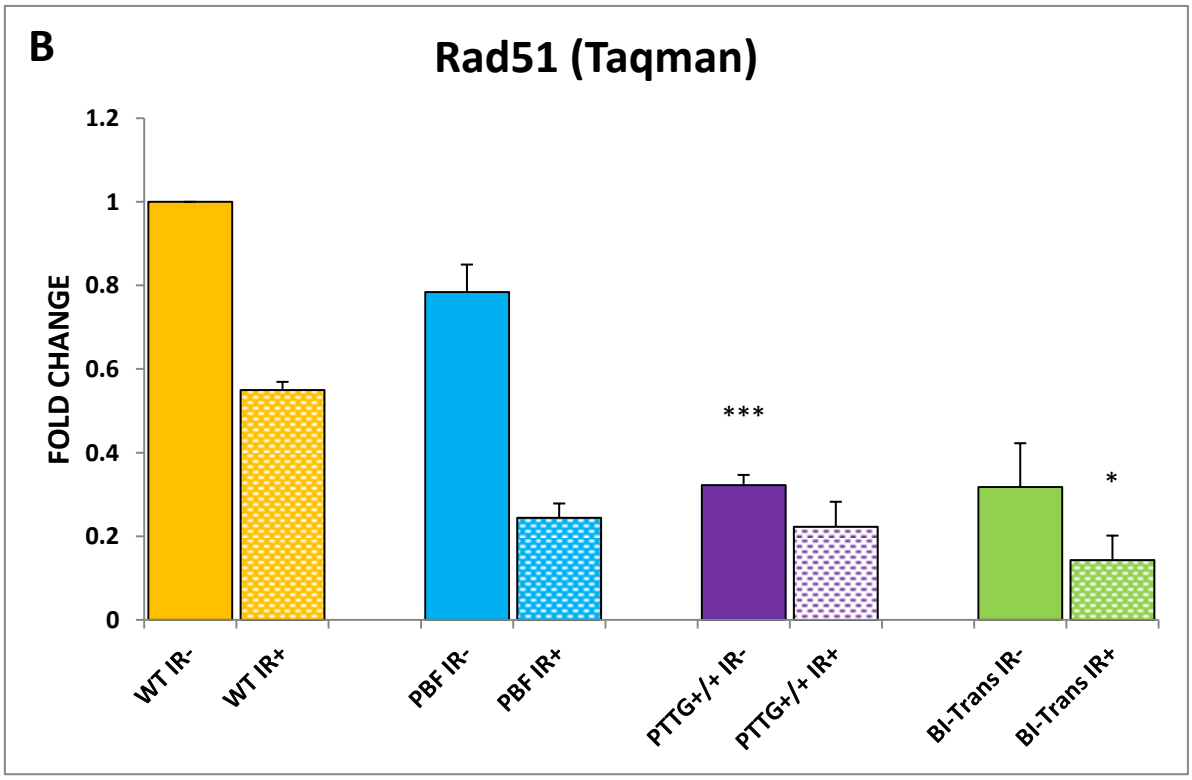

*Figure 7-6 Rad51 mRNA expression in PMTCs before and after irradiation on the microarray (A) and Taqman qRT-PCR (B). n=4 for PMTCs all genotypes. p-values obtained by comparing to WT IR- are denoted with * ($0.01 < p \leq 0.05$) and *** ($0.0001 < p \leq 0.001$).*

7.3.7 **The mRNA expression of Tdg remained unchanged**

Tdg is a downstream gene involved with DNA repair and has a major role in DNA demethylation (GeneCards®; www.genecards.org). The Mouse DNA Damage Signalling RT^2 Profiler^{TM} PCR Arrays (SABiosciences) showed an increased expression of Tdg particularly with the PTTG genotype. The expression of Tdg was unchanged in all PMTC genotypes with or without irradiation on Taqman qRT-PCR. The relative expression of Tdg to WT IR- PMTCs in the Taqman validation was 1.02 ± 0.10 fold (p=0.976, n=4) in WT IR-, 1.34 ± 0.09 fold (p=0.645, n=4) in PBF IR-, 1.36 ± 0.17 fold (p=0.619, n=4) in PBF IR+, 1.55 ± 0.67 fold (p=0.596, n=4) in PTTG+/+ IR-, 1.52 ± 0.57 fold (p=0.611, n=4) in PTTG+/+ IR+, 1.45 ± 0.25 fold (p=0.549, n=4) in BI-Trans IR- and 1.21 ± 0.16 fold (p=0.779, n=4) in BI-Trans IR+ PMTCs (Figure 7-7). Thus, the Taqman did not validate a role for Tdg in the context of genetic instability with PBF and PTTG overexpression.

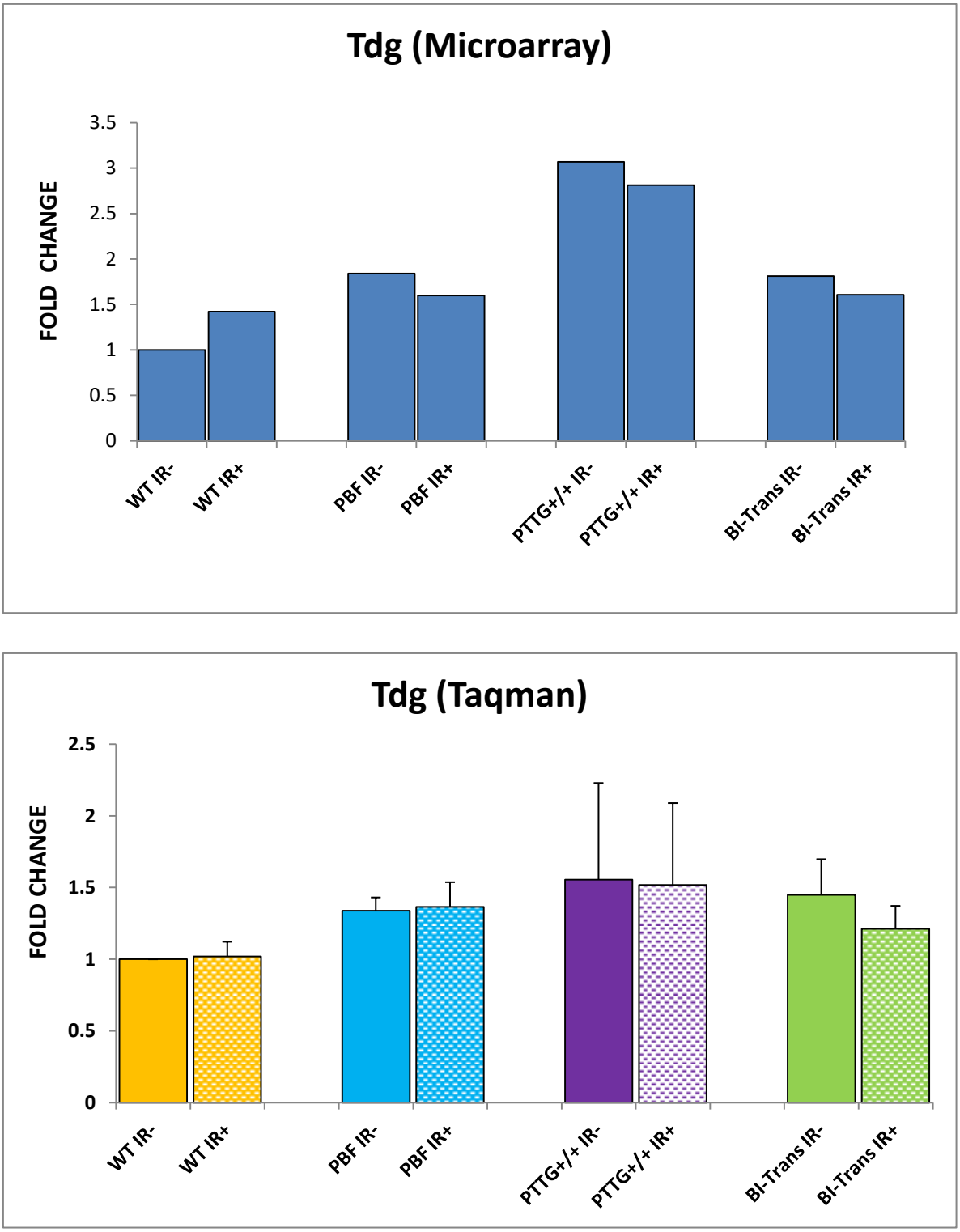

Figure 7-7 Tdg mRNA expression in PMTCs before and after irradiation on the microarray (A) and Taqman qRT-PCR (B). n=4 for PMTCs all genotypes. p-values obtained by comparing to WT IR- are not denoted because all values were statistically insignificant ie. p>0.05.

7.3.8 The mRNA expression of Trp53 was unchanged by PBF, PTTG or radiation

Both PBF and PTTG interact with Trp53 (Bernal et al., 2002, Read et al., 2014a, Read et al., 2014b). Trp53 has multiple roles follow in DNA repair following DNA damage (Efeyan and Serrano, 2007). The mRNA expression of Trp53 was relatively unchanged in the various genotypes with and without irradiation. The expression of Trp53 on Taqman qRT-PCR was 1.00 ± 0.13 fold (p=0.992, n=4) in WT IR+, 1.74 ± 0.21 fold (p=0.100, n=4) in PBF IR-, 1.62 ± 0.10 fold (p=0.112, n=4) in PBF IR+, 1.26 ± 0.32 fold (p=0.461, n=4) in PTTG+/+ IR-, 1.19 ± 0.36 fold (p=0.574, n=4) in PTTG+/+ IR+, 1.08 ± 0.55 fold (p=0.769, n=4) in BI-Trans IR-, and 0.96 ± 0.54 fold (p=0.901, n=4) in BI-Trans IR+ PMTCs shown in Figure 7-8. The results suggest that the interaction between Trp53 and our genes of interest (PBF and PTTG) overexpressed in the thyroid may occur at a protein rather than mRNA level.

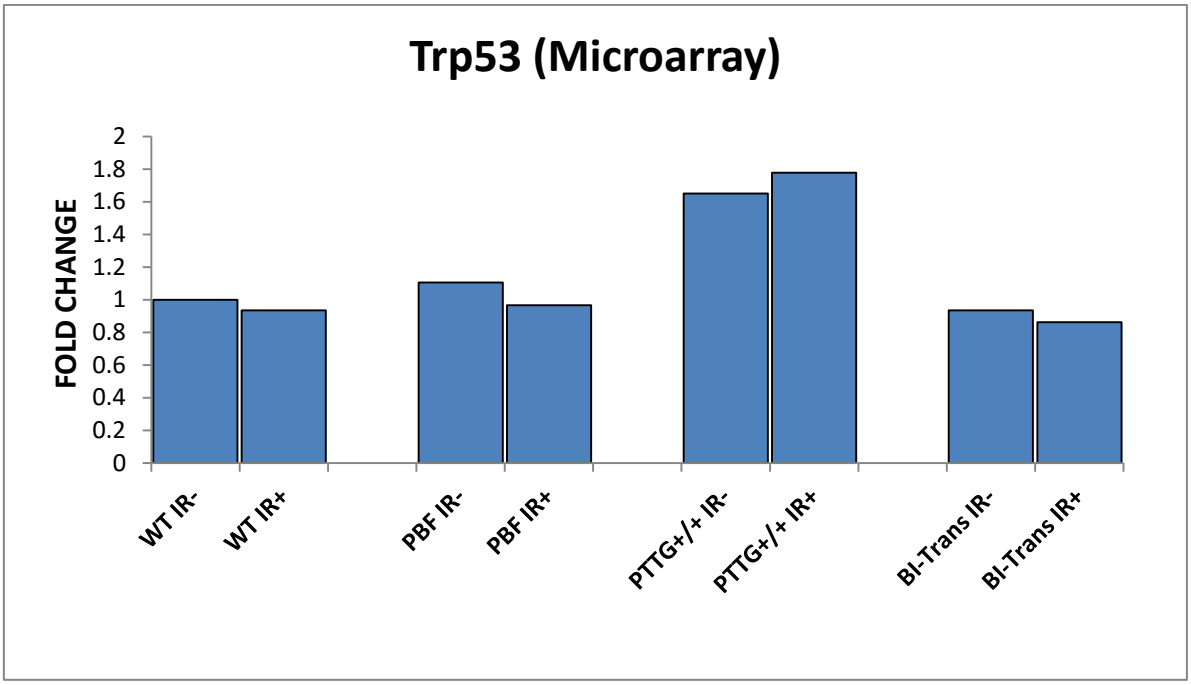

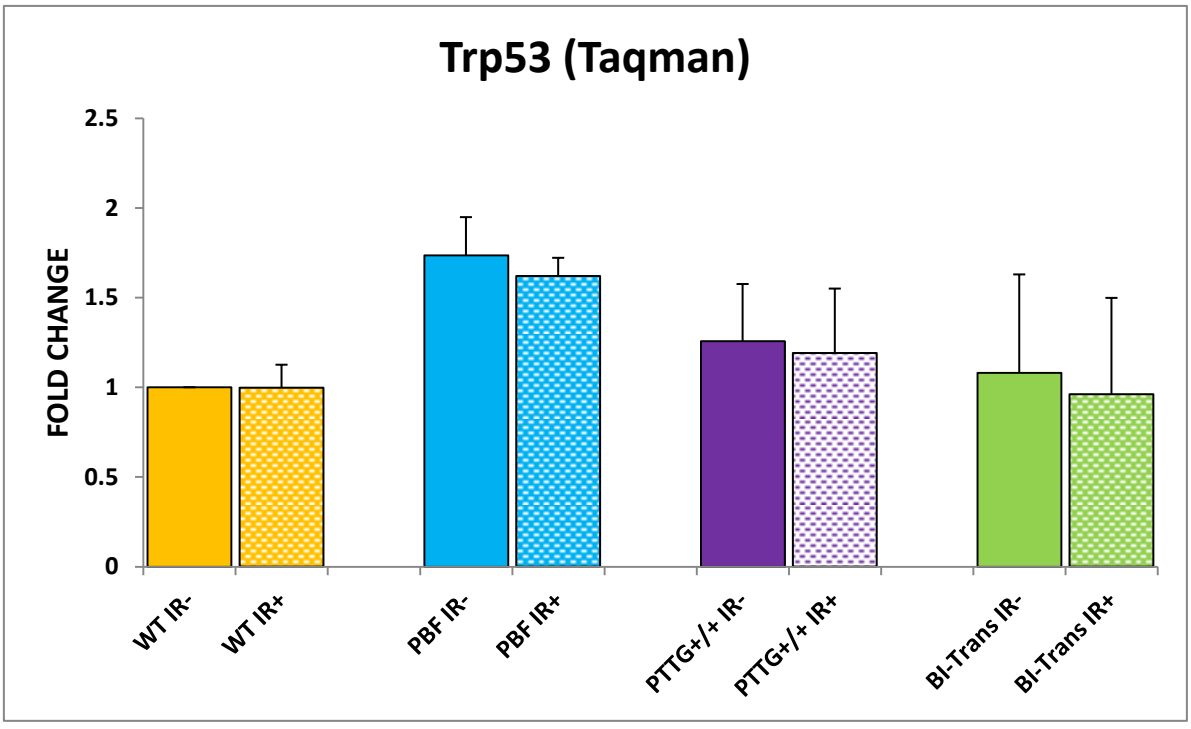

Figure 7-8 Trp53 mRNA expression in PMTCs before and after irradiation on the microarray (A) and Taqman qRT-PCR (B). n=4 for PMTCs all genotypes. p-values obtained by comparing to WT IR- are not denoted because all values were statistically insignificant ie. $p>0.05$.

7.3.9 **Rad 51 expression was not significantly altered on Western blot.**

Following the Taqman validation assays, we selected genes to be examined at a protein level. These experiments involved small quantities of protein obtained from PMTC. Rad51 mRNA levels were reduced following radiation and was significantly repressed by the presence of PTTG compared to WT IR- and may represent a potential candidate for inducing genetic instability. We studied the protein levels of Rad51 to determine whether this trend was observed further downstream, at a protein level. Unfortunately, Western blot of Rad51 on the various genotypes did not demonstrate a consistent pattern of expression (n=4), Figure 7-9.

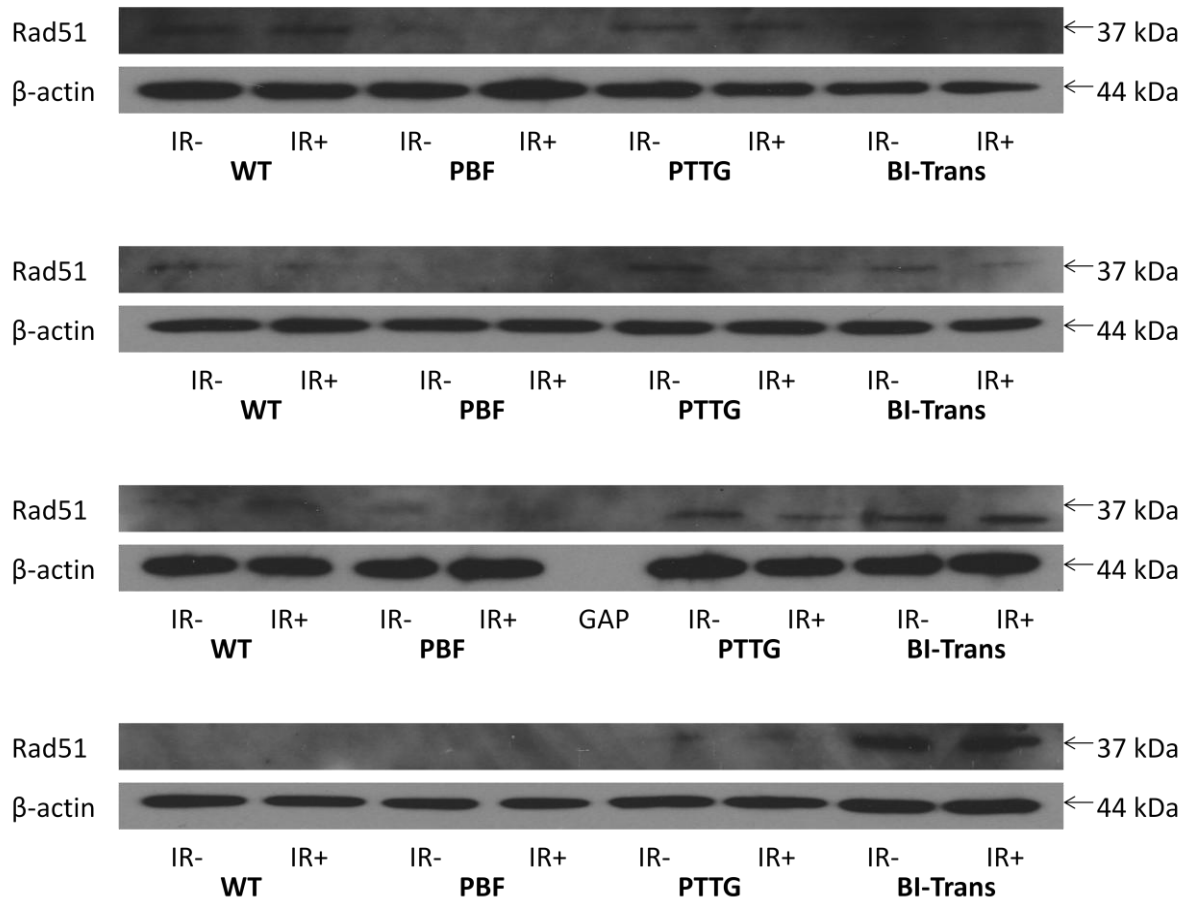

Figure 7-9 The expression of Rad51 on Western blot by genotype, with and without irradiation in 4 separate experiments.

7.3.10 **Trp53 appeared to be stabilised following radiation**

The mRNA expression of Trp53 was not significantly elevated following radiation damage in PMTCs. However, there is an established interaction between PBF (Read et al., 2014a) and and PTTG ((Hamid and Kakar, 2004) with Trp53. Since mRNA expression may not tell the entire story, we next quantified relative Trp53 protein expression on Western blot.

Trp53 protein levels were increased in the presence of PTTG and both PTTG and PBF. PBF on its own did not exert a significant effect on Trp53 levels. The relative fold expression of Trp53 in PMTCs to WT IR- was 1.50 ± 0.50 fold in PBF IR- ($p=0.422$, $n=3$), 2.63 ± 0.35 fold in PTTG+/+ IR- ($p=0.021$, $n=3$) and 2.91 ± 0.51 fold in BI-Trans IR- ($p=0.029$, $n=3$). Radiation had the effect of increasing further the protein levels of Trp53 but this was not significant in PBF IR+ PMTCs. The densitometry study of Trp53 Western blot confirmed the increased expression of Trp53 at a protein level at 3.39 ± 0.64 fold in WT IR+ ($p=0.026$, $n=3$), 1.95 ± 0.43 fold in PBF IR+ ($p=0.134$, $n=3$), 2.53 ± 0.98 fold in PTTG+/+ IR+ ($p=0.206$, $n=3$) and 5.80 ± 0.18 fold in BI-Trans ($p<0.000$, $n=3$), shown in Figure 7-10.

Added to the γ-H2AX results, Trp53 stabilisation shows that a sufficient ionising radiation dose was used in these studies. Interestingly, PBF and PTTG both attenuated Trp53 stabilisation in response to ionising radiation. However, overexpression of both proto-oncogenes was associated with increased basal Trp53 levels, and a restoration of Trp53 stabilisation in response to ionising radiation.

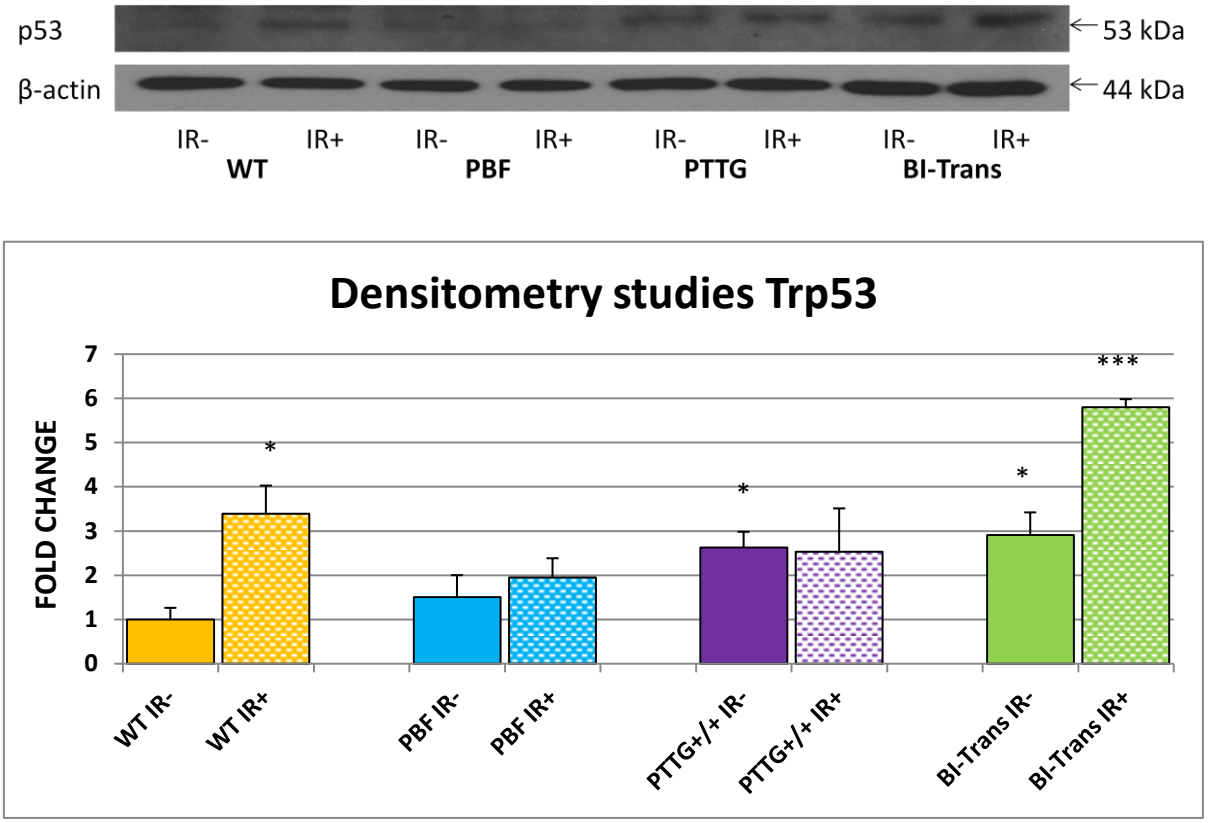

*Figure 7-10 Western blot and densitometry study of Trp53 expression by genotype, before and after irradiation (n=3). p-values obtained by comparing to WT IR- are denoted with * (0.01 < p ≤ 0.05) and *** (0.0001 < p ≤ 0.001).*

7.4 DISCUSSION

7.4.1 Validation of cDNA array gene changes

A wide array of gene changes was observed on the Mouse DNA Damage Signalling RT^2 Profiler^{TM} PCR Arrays. We carefully selected genes which were altered in the WT IR+ PMTCs because these genes represented endogenous baseline behaviour of PMTCs at 24 hours after 15 Gy radiation exposure. The genes Brca1, Chek1, Exo1 and Mgmt were hence selected. Trp53 is a gene that has known interaction with our genes of interest, PBF and PTTG, and despite not having a gross change on the microarray, we felt it was prudent that it remained on our shortlist. Tdg was selected because it was the only gene that was affected by PTTG and not by PBF on the array. The inhibition of Rad51 appeared on the microarray to be affected by PTTG and to a lesser extent PBF. However, in response to irradiation, the expression of Rad51 in PBF PMTCs was significantly repressed, to levels observed in PTTG+/+ IR+ PMTCs.

7.4.2 Taqman qRT-PCR validated the gene expression pattern on the microarray

Taqman qRT-PCR is a technique that is accurate and is widely recognised for studying the expression of mRNA. The experiments above showed an almost identical expression pattern of the gene of interest on both Taqman qRT-PCR and Mouse DNA Damage Signalling RT^2 Profiler^{TM} PCR Arrays.

The lack of statistical significance was most likely related to the low n numbers. However, the pattern of gene expression on the microarray appeared to be a good representation of gene expression and could be used for further analysis.

7.4.3 DNA damage was present in PMTCs following irradiation

The gene H2AX (H2AFX) encodes for histones which are basic nuclear proteins that are responsible for the nucleosome structure of the chromosomal fibre in eukaryotes. In response to double strand DNA breaks, ATM and PRKDC phosphorylate H2AX at serine-139, forming the protein γ-H2AX. The quantity of γ-H2AX is proportional to the amount of double strand breaks present (Kuo and Yang, 2008).

Western blotting confirmed the presence of γ-H2AX in WT IR+, PTTG+/+ IR+ and BI-Trans IR+ PMTCs following irradiation. Interestingly, PBF IR+ PMTCs did not show an increase in γ-H2AX at 24 hours as demonstrated in the other PMTCs. This raises the possibility that the phosphorylation of H2AX following DNA damage in PMTCs is ameliorated by the overexpression of PBF in PMTCs, or that PBF exerts a protective effect on the genome. Further mechanistic studies would be required to establish the likely situation.

7.4.4 The relationship between γ-H2AX and Brca1

Brca1 and γ-H2AX form a physical complex on chromatin following DNA damage. Brca1 is normally present in small quantities on chromatin (Krum et al., 2010). Following DNA damage, Brca1 and γ-H2AX interact with each other, catalysed by the phophorylation by ATM or ATR (Krum et al., 2010). It was proposed in the same study that Brca1 serves to decrease the level of γ-H2AX as a mechanism of signalling an end to early DNA damage events (Krum et al., 2010). Our observation on the microarray that Brca1 is suppressed suggests that the PMTCs were in a later stage of DNA damage/repair.

7.4.5 **Rad51**

Rad51 mRNA was suppressed to less than 0.5 fold in response to PBF and PTTG overexpression and radiation. The suppression of Rad51 in PMTCs by radiation seems to suggest that the role of Rad51 may be diminished at 24 hours. Futher work with Rad51 at various time points would be needed to clarify the situation.

Brca1 and Rad51 are recruited to areas of replication fork stalling and collapsed DNA replication forks (Cousineau et al., 2005). Our study found similar mRNA expression patterns in both Brca1 and Rad51. We used a commercial antibody for the Western blot of Rad51 which unfortunately did not show any pattern of change in multiple experiments. This may be a reflection of the sensitivity and specificity of the antibody. Alternatively, it may suggest that mRNA levels does not reflect protein concentration.

7.4.6 **The relationship between Chek1 and Rad51**

Chek1-mediated phosphorylation of the homologous recombination proteins Brca2 and Rad51 modulates their interaction (Bahassi et al., 2008). The inhibition of Chek1 following DNA damage leads to an increase in both the total burden and the persistence of double strand breaks (Sorensen et al., 2005). Interestingly, the inhibition of Chek1 mRNA was observed in murine thyroid cells overexpressing PBF and PTTG. The expression at a protein level needs to be established by Western blot to determine if the mRNA expression pattern is translated to protein. Unfortunately, time was a limiting factor in this investigation and Chek1 was not studied further.

7.4.7 The relationship between Trp53 and PBF/PTTG

The association between Trp53 with PBF (Read et al., 2014a, Read et al., 2014b) and PTTG (Hamid and Kakar, 2004) have been described previously. The expression of Trp53 on Taqman validation assays remained essentially unchanged for all genotypes before and after irradiation. Interestingly, the densitometry study of Trp53 demonstrated an increase in all genotypes following radiation and in PTTG PMTC without irradiation. This observation correlates with the stabilisation of Trp53 following radiation and in PTTG overexpression.

7.4.8 Exo1, Tdg and Mgmt

Tdg had an interesting pattern of expression on the Mouse DNA Damage Signalling RT^2 Profiler^{TM} PCR Arrays because it only appeared to be affected by the PTTG genotype. The Taqman assay did not reveal a change of less than 0.5 or more than 2 fold in all PMTCs before and after irradiation. Hence, we did not pursue the investigation of this gene.

Mgmt had increased mRNA expression in our Taqman validation experiment following exposure to ionising radiation. The overexpression of PBF and PTTG only attenuated this response slightly. We felt this observation did not differentiate the effect of PBF or PTTG on the gene and hence had a lower priority on further investigations.

Exo1 mRNA expression appeared to be influenced by PTTG and radiation. The effect was similar to Rad51, Chek1 and Brca1 on Taqman validation studies.

7.5 CONCLUSION

Given the time constraints on the above investigation, we managed to shortlist the 7 genes of Brca1, Chek1, Exo1, Mgmt, Tdg, Trp53 and Rad51 for further investigation. Western blot was performed on

the Rad51 and Trp53 because it was felt at the time that these genes could likely explain the differences between the genomic stability expressed in various genotypes with and without irradiation. However, the microarray has identified numerous genes of potential interest and numerous lines of investigation could be pursued. Overall, this study has opened up new areas which could define the mechanistic role of PTTG and PBF in genetic instability.

8 Final Conclusions and Future Studies

The work in this thesis investigated some of the roles of PTTG and its binding factor, PBF in maintaining genomic stability in thyroid cells. Our hypothesis was that PTTG and PBF both affected genomic stability in the thyroid. In-vivo investigations were facilitated by the generation of a transgenic murine model of PBF and PTTG overexpression in the thyroid gland. The tool used for measuring genetic instability (GI), fluoresecent inter-simple sequence repeat-PCR (FISSR-PCR), was modified for work with murine thyroids. Further investigation to establish the molecular mechanism by which PBF and PTTG affected genomic stability was studied using microarrays.

8.1 The interaction between PBF and PTTG overexpression in transgenic murine thyroid gland

PTTG is known to bind to PBF for its transport to the nucleus and hence, its transcription function (Chien and Pei, 2000). Murine models of PTTG overexpression in the thyroid gland do not develop neoplasms but have small thyroids instead (Lewy et al., 2013). Transgenic murine models of PBF overexpression develop goitres and hyperplastic nodules (Read et al., 2011). Our transgenic murine model of PBF and PTTG overexpression in the thyroid gland (BI-Trans) all developed goitres and have partial penetrance for the development of thyroid adenomas (50 % at 18 months with a female gender preponderance), which was not driven by thyroid stimulating hormone. The finding in our BI-Trans model is similar to the observed thyroid phenotype of PBF transgenic mice. This suggests that although PTTG and PBF should hypothetically be synergistic with each other, in vivo work in the thyroid gland has demonstrated otherwise. The molecular mechanism behind this phenotype was investigated further by looking at the expression of genes intimately involved in DNA damage and DNA repair pathways. The establishment of this exciting murine model of thyroid cancer could provide a base for further experimentation involving known pathways such as MAPK and the

PI3K/Akt pathways involved in thyroid cancer. Additionally, little is known about goitrogenesis and this murine model could be used for investigations into goitre formation. See Figure 8-1.

Finally, the BI-Trans murine model had reduced fertility and survival. Hence, future use of this model will have to adapt breeding strategies to maintain perpetuity of this line and to be aware of the survival of this model for long term observations.

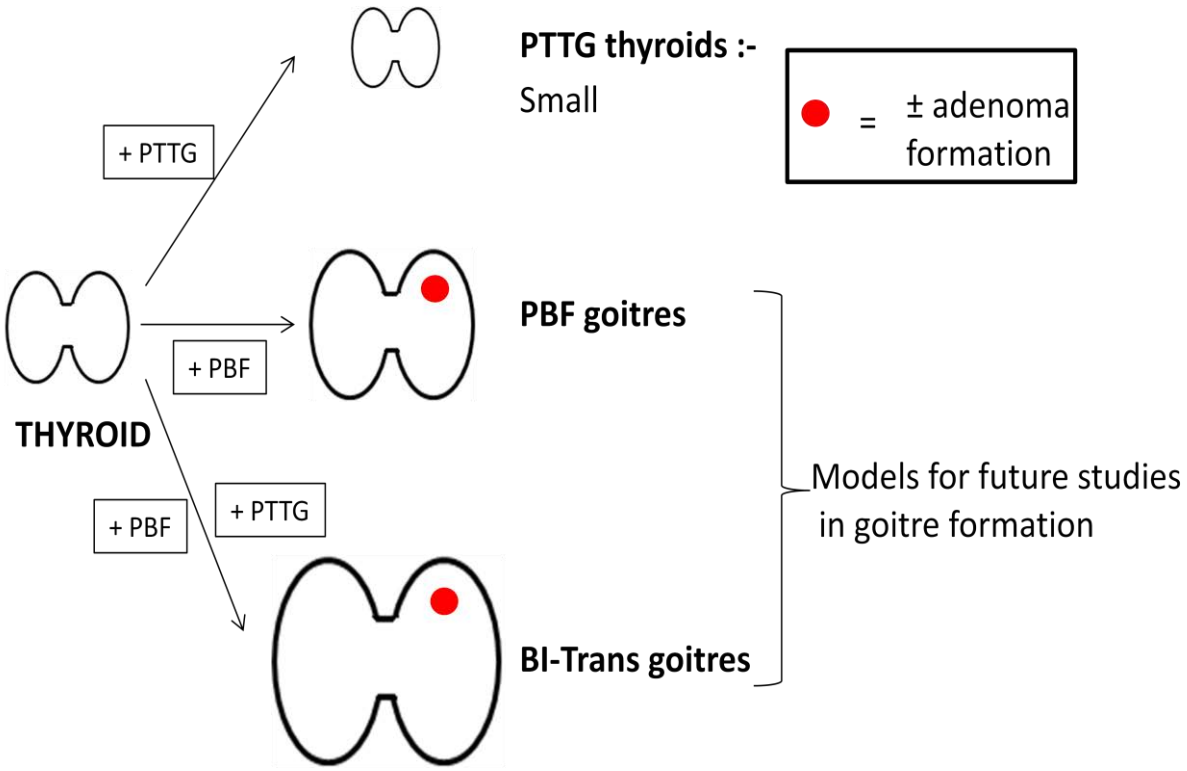

Figure 8-1 Thyroid changes in the various murine models and potential for future studies.

8.2 Use of FISSR-PCR for measuring genetic instability

Genetic instability is a hallmark feature of human cancers but the relationship between genetic instability in tumourigenesis is not fully understood. A validated technique used by others in measuring genetic instability and established in our group is fluorescent inter-simple sequence repeat PCR (FISSR-PCR) (Kim et al., 2005). FISSR-PCR provides a unique fingerprint of the genome from which the index of genetic instability (GI) can be derived. We found that murine thyroids overexpressing PBF or PTTG on its own did not exhibit significant GI. BI-trans thyroids which overexpressed both PBF and PTTG did have increased genetic instability, in keeping with the synergistic effect of both PBF and PTTG.

Primary murine thyroid cultures (PMTCs) were used to study the effects of ionising radiation in a background of PBF and PTTG overexpression. The relationship between thyroid cancer and ionising radiation has been extensively published (Bounacer et al., 1997, Holm, 1985, Kaplan et al., 2009, Nikiforov et al., 1997, Ricarte-Filho et al., 2013). Ionising radiation induces DNA damage and the most severe variety of damage caused is double-strand breaks (DSB). This type of damage is difficult to repair with high fidelity. PTTG has been shown to inhibit Ku70 which is involved in non-homologous end-joining in DSBs (Kim et al., 2007b). Not surprisingly, PTTG PMTCs showed most genetic instability following exposure to ionising radiation. Unexpected was the finding of reduced genetic instability in PBF and BI-Trans PMTCs which suggests PBF had a thyroid protective role following radiation-induced damage. If this observation holds true, this will be an intriguing area for further investigation.

8.3 The expression of genes associated with PBF, PTTG and ionising radiation in the thyroid gland

The use of microarrays to screen for the regulation of genes involved in the DNA damage and DNA repair response pathways in the context of PBF, PTTG and ionising radiation was carried out to investigate the molecular mechanisms for the above findings. We found that PTTG appeared to upregulate the mRNA expression genes constituting the 9-1-1 complex, involved in the activation of the critical gene ATR. The ATR gene is involved in a variety of cellular functions including DNA replication, repair, recombination and cell cycle checkpoint. This investigation was limited to studying gene expression at an mRNA level and further studies at a protein level could prove to be insightful in establishing an alternative means by which PTTG affects genomic stability. See Figure 8-2.

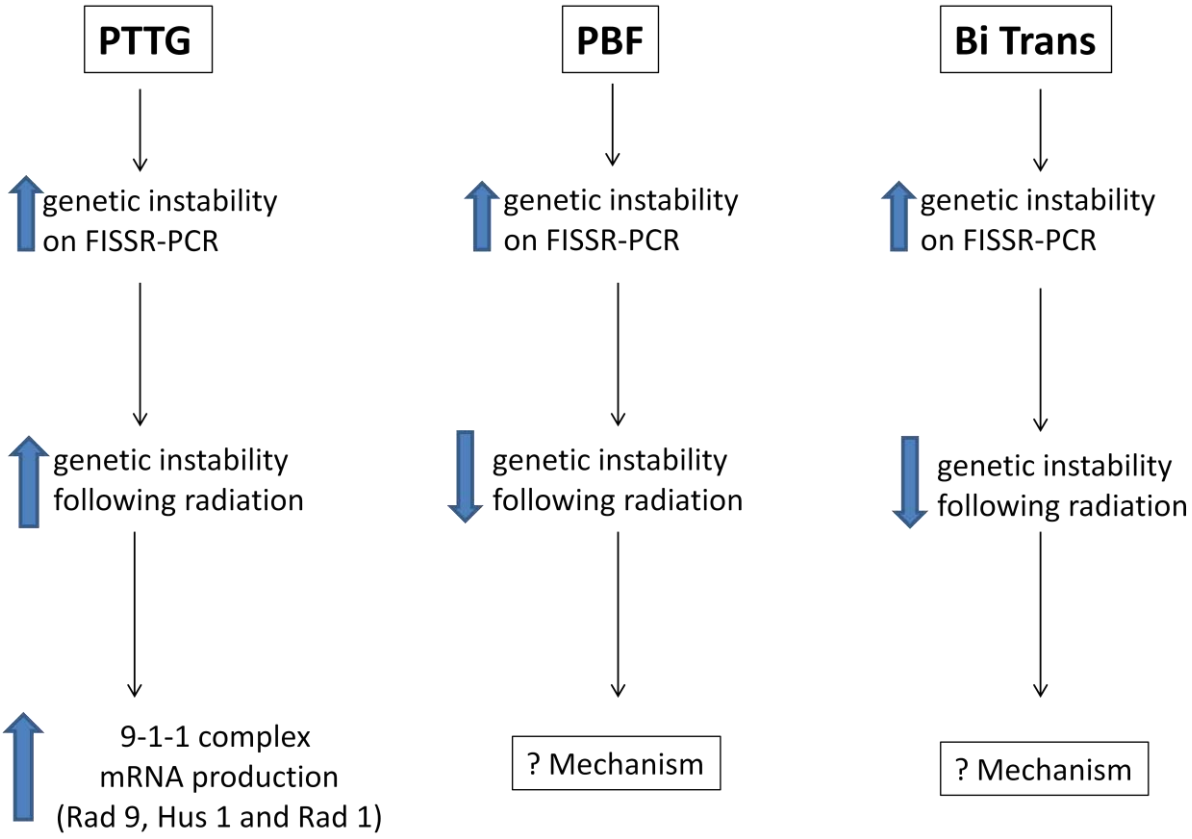

Figure 8-2 Diagram of key findings.

REFERENCES

ABBUD, R. A., TAKUMI, I., BARKER, E. M., REN, S. G., CHEN, D. Y., WAWROWSKY, K. & MELMED, S. 2005. Early multipotential pituitary focal hyperplasia in the alpha-subunit of glycoprotein hormone-driven pituitary tumor-transforming gene transgenic mice. *Mol Endocrinol,* 19**,** 1383-91.

ALBERTS, B., BRAY, D., HOPKIN, K., JOHNSON, A., LEWIS, J., RAFF, M., ROBERTS, K. & WALTER, P. 2014. *Essential cell biology*, Garland Science.

AMBESI-IMPIOMBATO, F. S., PARKS, L. A. & COON, H. G. 1980. Culture of hormone-dependent functional epithelial cells from rat thyroids. *Proc Natl Acad Sci U S A,* 77**,** 3455-9.

AMERICAN THYROID ASSOCIATION GUIDELINES TASKFORCE ON THYROID, N., DIFFERENTIATED THYROID, C., COOPER, D. S., DOHERTY, G. M., HAUGEN, B. R., KLOOS, R. T., LEE, S. L., MANDEL, S. J., MAZZAFERRI, E. L., MCIVER, B., PACINI, F., SCHLUMBERGER, M., SHERMAN, S. I., STEWARD, D. L. & TUTTLE, R. M. 2009. Revised American Thyroid Association management guidelines for patients with thyroid nodules and differentiated thyroid cancer. *Thyroid,* 19**,** 1167-214.

AQUILINA, G., BIONDO, R., DOGLIOTTI, E., MEUTH, M. & BIGNAMI, M. 1992. Expression of the endogenous O6-methylguanine-DNA-methyltransferase protects Chinese hamster ovary cells from spontaneous G:C to A:T transitions. *Cancer Res,* 52**,** 6471-5.

ARIGHI, E., BORRELLO, M. G. & SARIOLA, H. 2005. RET tyrosine kinase signaling in development and cancer. *Cytokine Growth Factor Rev,* 16**,** 441-67.

ASHLEY, D. J. 1969. The two "hit" and multiple "hit" theories of carcinogenesis. *Br J Cancer,* 23**,** 313-28.

BAHASSI, E. M., OVESEN, J. L., RIESENBERG, A. L., BERNSTEIN, W. Z., HASTY, P. E. & STAMBROOK, P. J. 2008. The checkpoint kinases Chk1 and Chk2 regulate the functional associations between hBRCA2 and Rad51 in response to DNA damage. *Oncogene,* 27**,** 3977-85.

BANIN, S., MOYAL, L., SHIEH, S., TAYA, Y., ANDERSON, C. W., CHESSA, L., SMORODINSKY, N. I., PRIVES, C., REISS, Y., SHILOH, Y. & ZIV, Y. 1998. Enhanced phosphorylation of p53 by ATM in response to DNA damage. *Science,* 281**,** 1674-7.

BARTEK, J., LUKAS, C. & LUKAS, J. 2004. Checking on DNA damage in S phase. *Nat Rev Mol Cell Biol,* 5**,** 792-804.

BASIK, M., STOLER, D. L., KONTZOGLOU, K. C., RODRIGUEZ-BIGAS, M. A., PETRELLI, N. J. & ANDERSON, G. R. 1997. Genomic instability in sporadic colorectal cancer quantitated by inter-simple sequence repeat PCR analysis. *Genes Chromosomes Cancer,* 18**,** 19-29.

BAUER, A. J., CAVALLI, L. R., RONE, J. D., FRANCIS, G. L., BURCH, H. B., TUTTLE, R. M., RINGEL, M. D., STRATAKIS, C. A. & HADDAD, B. R. 2002. Evaluation of adult papillary thyroid carcinomas by comparative genomic hybridization and microsatellite instability analysis. *Cancer Genet Cytogenet,* 135**,** 182-6.

BENSIMON, A., SCHMIDT, A., ZIV, Y., ELKON, R., WANG, S. Y., CHEN, D. J., AEBERSOLD, R. & SHILOH, Y. 2010. ATM-dependent and -independent dynamics of the nuclear phosphoproteome after DNA damage. *Sci Signal,* 3**,** rs3.

BENTZ, M., PLESCH, A., STILGENBAUER, S., DOHNER, H. & LICHTER, P. 1998. Minimal sizes of deletions detected by comparative genomic hybridization. *Genes Chromosomes Cancer,* 21**,** 172-5.

BERNAL, J. A., LUNA, R., ESPINA, A., LAZARO, I., RAMOS-MORALES, F., ROMERO, F., ARIAS, C., SILVA, A., TORTOLERO, M. & PINTOR-TORO, J. A. 2002. Human securin interacts with p53 and modulates p53-mediated transcriptional activity and apoptosis. *Nat Genet,* 32**,** 306-11.

BHAIJEE, F. & NIKIFOROV, Y. E. 2011. Molecular analysis of thyroid tumors. *Endocr Pathol,* 22**,** 126-33.

BHATTI, S., KOZLOV, S., FAROOQI, A. A., NAQI, A., LAVIN, M. & KHANNA, K. K. 2011. ATM protein kinase: the linchpin of cellular defenses to stress. *Cell Mol Life Sci,* 68**,** 2977-3006.

BIKFALVI, A., KLEIN, S., PINTUCCI, G. & RIFKIN, D. B. 1997. Biological roles of fibroblast growth factor-2. *Endocr Rev,* 18**,** 26-45.

BLOMBERG, M., FELDT-RASMUSSEN, U., ANDERSEN, K. K. & KJAER, S. K. 2012. Thyroid cancer in Denmark 1943-2008, before and after iodine supplementation. *Int J Cancer,* 131**,** 2360-6.

BOELAERT, K. 2009. The association between serum TSH concentration and thyroid cancer. *Endocr Relat Cancer,* 16**,** 1065-72.

BOELAERT, K., HORACEK, J., HOLDER, R. L., WATKINSON, J. C., SHEPPARD, M. C. & FRANKLYN, J. A. 2006. Serum thyrotropin concentration as a novel predictor of malignancy in thyroid nodules investigated by fine-needle aspiration. *J Clin Endocrinol Metab,* 91**,** 4295-301.

BOELAERT, K., MCCABE, C. J., TANNAHILL, L. A., GITTOES, N. J., HOLDER, R. L., WATKINSON, J. C., BRADWELL, A. R., SHEPPARD, M. C. & FRANKLYN, J. A. 2003. Pituitary tumor transforming gene and fibroblast growth factor-2 expression: potential prognostic indicators in differentiated thyroid cancer. *J Clin Endocrinol Metab,* 88**,** 2341-7.

BOELAERT, K., SMITH, V. E., STRATFORD, A. L., KOGAI, T., TANNAHILL, L. A., WATKINSON, J. C., EGGO, M. C., FRANKLYN, J. A. & MCCABE, C. J. 2007. PTTG and PBF repress the human sodium iodide symporter. *Oncogene,* 26**,** 4344-56.

BOELAERT, K., YU, R., TANNAHILL, L. A., STRATFORD, A. L., KHANIM, F. L., EGGO, M. C., MOORE, J. S., YOUNG, L. S., GITTOES, N. J., FRANKLYN, J. A., MELMED, S. & MCCABE, C. J. 2004. PTTG's C-terminal PXXP motifs modulate critical cellular processes in vitro. *J Mol Endocrinol,* 33**,** 663-77.

BONGARZONE, I., VIGNERI, P., MARIANI, L., COLLINI, P., PILOTTI, S. & PIEROTTI, M. A. 1998. RET/NTRK1 rearrangements in thyroid gland tumors of the papillary carcinoma family: correlation with clinicopathological features. *Clin Cancer Res,* 4**,** 223-8.

BOUNACER, A., WICKER, R., CAILLOU, B., CAILLEUX, A. F., SARASIN, A., SCHLUMBERGER, M. & SUAREZ, H. G. 1997. High prevalence of activating ret proto-oncogene rearrangements, in thyroid tumors from patients who had received external radiation. *Oncogene,* 15**,** 1263-73.

BRZEZIANSKA, E., KARBOWNIK, M., MIGDALSKA-SEK, M., PASTUSZAK-LEWANDOSKA, D., WLOCH, J. & LEWINSKI, A. 2006. Molecular analysis of the RET and NTRK1 gene rearrangements in papillary thyroid carcinoma in the Polish population. *Mutat Res,* 599**,** 26-35.

BUBIEN, V., BONNET, F., BROUSTE, V., HOPPE, S., BAROUK-SIMONET, E., DAVID, A., EDERY, P., BOTTANI, A., LAYET, V., CARON, O., GILBERT-DUSSARDIER, B., DELNATTE, C., DUGAST, C., FRICKER, J. P., BONNEAU, D., SEVENET, N., LONGY, M., CAUX, F. & FRENCH COWDEN DISEASE, N. 2013. High cumulative risks of cancer in patients with PTEN hamartoma tumour syndrome. *J Med Genet,* 50**,** 255-63.

CANCER GENOME ATLAS RESEARCH, N. 2014. Integrated genomic characterization of papillary thyroid carcinoma. *Cell,* 159**,** 676-90.

CHAMAON, K., KANAKIS, D., MAWRIN, C., DIETZMANN, K. & KIRCHES, E. 2010. Transcripts of PTTG and growth factors bFGF and IGF-1 are correlated in pituitary adenomas. *Exp Clin Endocrinol Diabetes,* 118**,** 121-6.

CHAMAON, K., KIRCHES, E., KANAKIS, D., BRAEUNINGER, S., DIETZMANN, K. & MAWRIN, C. 2005. Regulation of the pituitary tumor transforming gene by insulin-like-growth factor-I and insulin differs between malignant and non-neoplastic astrocytes. *Biochem Biophys Res Commun,* 331**,** 86-92.

CHEN, A. Y., JEMAL, A. & WARD, E. M. 2009. Increasing incidence of differentiated thyroid cancer in the United States, 1988-2005. *Cancer,* 115**,** 3801-7.

CHEN, L., PURI, R., LEFKOWITZ, E. J. & KAKAR, S. S. 2000. Identification of the human pituitary tumor transforming gene (hPTTG) family: molecular structure, expression, and chromosomal localization. *Gene,* 248**,** 41-50.

CHENG, S. Y. 2000. Multiple mechanisms for regulation of the transcriptional activity of thyroid hormone receptors. *Rev Endocr Metab Disord,* 1**,** 9-18.

CHESNOKOVA, V., WONG, C., ZONIS, S., GRUSZKA, A., WAWROWSKY, K., REN, S. G., BENSHLOMO, A. & YU, R. 2009. Diminished pancreatic beta-cell mass in securin-null mice is caused by beta-cell apoptosis and senescence. *Endocrinology,* 150**,** 2603-10.

CHIEN, W. & PEI, L. 2000. A novel binding factor facilitates nuclear translocation and transcriptional activation function of the pituitary tumor-transforming gene product. *J Biol Chem,* 275**,** 19422-7.

CHO-ROK, J., YOO, J., JANG, Y. J., KIM, S., CHU, I. S., YEOM, Y. I., CHOI, J. Y. & IM, D. S. 2006. Adenovirus-mediated transfer of siRNA against PTTG1 inhibits liver cancer cell growth in vitro and in vivo. *Hepatology,* 43**,** 1042-52.

CIMPRICH, K. A. & CORTEZ, D. 2008. ATR: an essential regulator of genome integrity. *Nat Rev Mol Cell Biol,* 9**,** 616-627.

CLEM, A. L., HAMID, T. & KAKAR, S. S. 2003. Characterization of the role of Sp1 and NF-Y in differential regulation of PTTG/securin expression in tumor cells. *Gene,* 322**,** 113-21.

COUSINEAU, I., ABAJI, C. & BELMAAZA, A. 2005. BRCA1 regulates RAD51 function in response to DNA damage and suppresses spontaneous sister chromatid replication slippage: implications for sister chromatid cohesion, genome stability, and carcinogenesis. *Cancer Res,* 65**,** 11384-91.

DAVIES, H., BIGNELL, G. R., COX, C., STEPHENS, P., EDKINS, S., CLEGG, S., TEAGUE, J., WOFFENDIN, H., GARNETT, M. J., BOTTOMLEY, W., DAVIS, N., DICKS, E., EWING, R., FLOYD, Y., GRAY, K., HALL, S., HAWES, R., HUGHES, J., KOSMIDOU, V., MENZIES, A., MOULD, C., PARKER, A., STEVENS, C., WATT, S., HOOPER, S., WILSON, R., JAYATILAKE, H., GUSTERSON, B. A., COOPER, C., SHIPLEY, J., HARGRAVE, D., PRITCHARD-JONES, K., MAITLAND, N., CHENEVIX-TRENCH, G., RIGGINS, G. J., BIGNER, D. D., PALMIERI, G., COSSU, A., FLANAGAN, A., NICHOLSON, A., HO, J. W., LEUNG, S. Y., YUEN, S. T., WEBER, B. L., SEIGLER, H. F., DARROW, T. L., PATERSON, H., MARAIS, R., MARSHALL, C. J., WOOSTER, R., STRATTON, M. R. & FUTREAL, P. A. 2002. Mutations of the BRAF gene in human cancer. *Nature,* 417**,** 949-54.

DENG, C. X. & SCOTT, F. 2000. Role of the tumor suppressor gene Brca1 in genetic stability and mammary gland tumor formation. *Oncogene,* 19**,** 1059-64.

DHILLON, A. S., HAGAN, S., RATH, O. & KOLCH, W. 2007. MAP kinase signalling pathways in cancer. *Oncogene,* 26**,** 3279-90.

DOBASHI, Y., SAKAMOTO, A., SUGIMURA, H., MERNYEI, M., MORI, M., OYAMA, T. & MACHINAMI, R. 1993. Overexpression of p53 as a possible prognostic factor in human thyroid carcinoma. *Am J Surg Pathol,* 17**,** 375-81.

DOBASHI, Y., SUGIMURA, H., SAKAMOTO, A., MERNYEI, M., MORI, M., OYAMA, T. & MACHINAMI, R. 1994. Stepwise participation of p53 gene mutation during dedifferentiation of human thyroid carcinomas. *Diagn Mol Pathol,* 3**,** 9-14.

DODSON, G. E. & TIBBETTS, R. S. 2006. DNA replication stress-induced phosphorylation of cyclic AMP response element-binding protein mediated by ATM. *J Biol Chem,* 281**,** 1692-7.

DOHAN, O., DE LA VIEJA, A., PARODER, V., RIEDEL, C., ARTANI, M., REED, M., GINTER, C. S. & CARRASCO, N. 2003. The sodium/iodide Symporter (NIS): characterization, regulation, and medical significance. *Endocr Rev,* 24**,** 48-77.

DOMINGUEZ, A., RAMOS-MORALES, F., ROMERO, F., RIOS, R. M., DREYFUS, F., TORTOLERO, M. & PINTOR-TORO, J. A. 1998. hpttg, a human homologue of rat pttg, is overexpressed in hematopoietic neoplasms. Evidence for a transcriptional activation function of hPTTG. *Oncogene,* 17**,** 2187-93.

DONGHI, R., LONGONI, A., PILOTTI, S., MICHIELI, P., DELLA PORTA, G. & PIEROTTI, M. A. 1993. Gene p53 mutations are restricted to poorly differentiated and undifferentiated carcinomas of the thyroid gland. *J Clin Invest,* 91**,** 1753-60.

DORION, D. & LEMAIRE, D. 2008. Thyroid Anatomy. *eMedicine,* eMedicine Specialties>Clinical Procedures>Anatomy.

DUFFY, B. J., JR. & FITZGERALD, P. J. 1950. Thyroid cancer in childhood and adolescence; a report on 28 cases. *Cancer,* 3**,** 1018-32.

DWIGHT, T., THOPPE, S. R., FOUKAKIS, T., LUI, W. O., WALLIN, G., HOOG, A., FRISK, T., LARSSON, C. & ZEDENIUS, J. 2003. Involvement of the PAX8/peroxisome proliferator-activated receptor gamma rearrangement in follicular thyroid tumors. *J Clin Endocrinol Metab,* 88**,** 4440-5.

EFEYAN, A. & SERRANO, M. 2007. p53: guardian of the genome and policeman of the oncogenes. *Cell Cycle,* 6**,** 1006-10.

EGGO, M. C., KING, W. J., BLACK, E. G. & SHEPPARD, M. C. 1996. Functional human thyroid cells and their insulin-like growth factor-binding proteins: regulation by thyrotropin, cyclic 3',5' adenosine monophosphate, and growth factors. *J Clin Endocrinol Metab,* 81**,** 3056-62.

EJIMA, Y., YANG, L. & SASAKI, M. S. 2000. Aberrant splicing of the ATM gene associated with shortening of the intronic mononucleotide tract in human colon tumor cell lines: a novel mutation target of microsatellite instability. *Int J Cancer,* 86**,** 262-8.

EL-NAGGAR, S. M., MALIK, M. T., MARTIN, A., MOORE, J. P., PROCTOR, M., HAMID, T. & KAKAR, S. S. 2007. Development of cystic glandular hyperplasia of the endometrium in Mullerian inhibitory substance type II receptor-pituitary tumor transforming gene transgenic mice. *J Endocrinol,* 194**,** 179-91.

ESASHI, F., CHRIST, N., GANNON, J., LIU, Y., HUNT, T., JASIN, M. & WEST, S. C. 2005. CDK-dependent phosphorylation of BRCA2 as a regulatory mechanism for recombinational repair. *Nature,* 434**,** 598-604.

FAGIN, J. A., MATSUO, K., KARMAKAR, A., CHEN, D. L., TANG, S. H. & KOEFFLER, H. P. 1993. High prevalence of mutations of the p53 gene in poorly differentiated human thyroid carcinomas. *J Clin Invest,* 91**,** 179-84.

FALLAH, M., PUKKALA, E., TRYGGVADOTTIR, L., OLSEN, J. H., TRETLI, S., SUNDQUIST, K. & HEMMINKI, K. 2013. Risk of thyroid cancer in first-degree relatives of patients with non-medullary thyroid cancer by histology type and age at diagnosis: a joint study from five Nordic countries. *J Med Genet,* 50**,** 373-82.

FEIJOO, C., HALL-JACKSON, C., WU, R., JENKINS, D., LEITCH, J., GILBERT, D. M. & SMYTHE, C. 2001. Activation of mammalian Chk1 during DNA replication arrest: a role for Chk1 in the intra-S phase checkpoint monitoring replication origin firing. *J Cell Biol,* 154**,** 913-23.

FELDT-RASMUSSEN, U. 2001. Iodine and cancer. *Thyroid,* 11**,** 483-6.

FENG, Z. & ZHANG, J. 2012. A dual role of BRCA1 in two distinct homologous recombination mediated repair in response to replication arrest. *Nucleic Acids Res,* 40**,** 726-38.

FERRARA, N. & DAVIS-SMYTH, T. 1997. The biology of vascular endothelial growth factor. *Endocr Rev,* 18**,** 4-25.

FERRARI, S. M., FALLAHI, P., POLITTI, U., MATERAZZI, G., BALDINI, E., ULISSE, S., MICCOLI, P. & ANTONELLI, A. 2015. Molecular Targeted Therapies of Aggressive Thyroid Cancer. *Front Endocrinol (Lausanne),* 6**,** 176.

FERRAZ, C., REHFELD, C., KROGDAHL, A., PRECHT JENSEN, E. M., BOSENBERG, E., NARZ, F., HEGEDUS, L., PASCHKE, R. & ESZLINGER, M. 2012. Detection of PAX8/PPARG and RET/PTC rearrangements is feasible in routine air-dried fine needle aspiration smears. *Thyroid,* 22**,** 1025-30.

FISHEL, R., LESCOE, M. K., RAO, M. R., COPELAND, N. G., JENKINS, N. A., GARBER, J., KANE, M. & KOLODNER, R. 1993. The human mutator gene homolog MSH2 and its association with hereditary nonpolyposis colon cancer. *Cell,* 75**,** 1027-38.

FOLKMAN, J. 1972. Anti-angiogenesis: new concept for therapy of solid tumors. *Ann Surg,* 175**,** 409-16.

FOLKMAN, J. 1990. What is the evidence that tumors are angiogenesis dependent? *J Natl Cancer Inst,* 82**,** 4-6.

FOLKMAN, J. 1992. The role of angiogenesis in tumor growth. *Semin Cancer Biol,* 3**,** 65-71.

FOLKMAN, J. & SHING, Y. 1992. Control of angiogenesis by heparin and other sulfated polysaccharides. *Adv Exp Med Biol,* 313**,** 355-64.

FOULDS, L. 1958. The natural history of cancer. *J Chronic Dis,* 8**,** 2-37.

FRANCO, A. T., MALAGUARNERA, R., REFETOFF, S., LIAO, X. H., LUNDSMITH, E., KIMURA, S., PRITCHARD, C., MARAIS, R., DAVIES, T. F., WEINSTEIN, L. S., CHEN, M., ROSEN, N., GHOSSEIN, R., KNAUF, J. A. & FAGIN, J. A. 2011. Thyrotrophin receptor signaling dependence of Braf-induced thyroid tumor initiation in mice. *Proc Natl Acad Sci U S A,* 108**,** 1615-20.

FRENCH, C. A., ALEXANDER, E. K., CIBAS, E. S., NOSE, V., LAGUETTE, J., FAQUIN, W., GARBER, J., MOORE, F., JR., FLETCHER, J. A., LARSEN, P. R. & KROLL, T. G. 2003. Genetic and biological subgroups of low-stage follicular thyroid cancer. *Am J Pathol,* 162**,** 1053-60.

FUGAZZOLA, L., PILOTTI, S., PINCHERA, A., VORONTSOVA, T. V., MONDELLINI, P., BONGARZONE, I., GRECO, A., ASTAKHOVA, L., BUTTI, M. G., DEMIDCHIK, E. P. & ET AL. 1995. Oncogenic rearrangements of the RET proto-oncogene in papillary thyroid carcinomas from children exposed to the Chernobyl nuclear accident. *Cancer Res,* 55**,** 5617-20.

FUJII, T., NOMOTO, S., KOSHIKAWA, K., YATABE, Y., TESHIGAWARA, O., MORI, T., INOUE, S., TAKEDA, S. & NAKAO, A. 2006. Overexpression of pituitary tumor transforming gene 1 in HCC is associated with angiogenesis and poor prognosis. *Hepatology,* 43**,** 1267-75.

FURUKAWA, K., PRESTON, D., FUNAMOTO, S., YONEHARA, S., ITO, M., TOKUOKA, S., SUGIYAMA, H., SODA, M., OZASA, K. & MABUCHI, K. 2013. Long-term trend of thyroid cancer risk among Japanese atomic-bomb survivors: 60 years after exposure. *Int J Cancer,* 132**,** 1222-6.

GOMEZ SAEZ, J. M., JIMENEZ-FONSECA, P., SANTAMARIA SANDI, J., CAPDEVILA CASTILLON, J., NAVARRO GONZALEZ, E., ZAFON LLOPIS, C., RAMON, Y. C. A. T., RIESCO EIZAGUIRRE, G., GRANDE PULIDO, E. & GALOFRE FERRATER, J. C. 2015. Spanish consensus for the management of patients with anaplastic cell thyroid carcinoma. *Endocrinol Nutr,* 62**,** e15-22.

GOSPODAROWICZ, D., FERRARA, N., SCHWEIGERER, L. & NEUFELD, G. 1987. Structural characterization and biological functions of fibroblast growth factor. *Endocr Rev,* 8**,** 95-114.

GRECO, A., MARIANI, C., MIRANDA, C., LUPAS, A., PAGLIARDINI, S., POMATI, M. & PIEROTTI, M. A. 1995. The DNA rearrangement that generates the TRK-T3 oncogene involves a novel gene on chromosome 3 whose product has a potential coiled-coil domain. *Mol Cell Biol,* 15**,** 6118-27.

GRECO, A., MIRANDA, C., PAGLIARDINI, S., FUSETTI, L., BONGARZONE, I. & PIEROTTI, M. A. 1997. Chromosome 1 rearrangements involving the genes TPR and

NTRK1 produce structurally different thyroid-specific TRK oncogenes. *Genes Chromosomes Cancer,* 19**,** 112-23.

GRECO, A., PIEROTTI, M. A., BONGARZONE, I., PAGLIARDINI, S., LANZI, C. & DELLA PORTA, G. 1992. TRK-T1 is a novel oncogene formed by the fusion of TPR and TRK genes in human papillary thyroid carcinomas. *Oncogene,* 7**,** 237-42.

GREGORY POWELL, J., WANG, X., ALLARD, B. L., SAHIN, M., WANG, X. L., HAY, I. D., HIDDINGA, H. J., DESHPANDE, S. S., KROLL, T. G., GREBE, S. K., EBERHARDT, N. L. & MCIVER, B. 2004. The PAX8/PPARgamma fusion oncoprotein transforms immortalized human thyrocytes through a mechanism probably involving wild-type PPARgamma inhibition. *Oncogene,* 23**,** 3634-41.

GUO, H. H. & LOEB, L. A. 2003. Tumbling down a different pathway to genetic instability. *J Clin Invest,* 112**,** 1793-5.

HAKEM, R. 2008. DNA-damage repair; the good, the bad, and the ugly. *EMBO J,* 27**,** 589-605.

HALAZONETIS, T. D., GORGOULIS, V. G. & BARTEK, J. 2008. An oncogene-induced DNA damage model for cancer development. *Science,* 319**,** 1352-5.

HAMID, T. & KAKAR, S. S. 2004. PTTG/securin activates expression of p53 and modulates its function. *Mol Cancer,* 3**,** 18.

HANAHAN, D. & FOLKMAN, J. 1996. Patterns and emerging mechanisms of the angiogenic switch during tumorigenesis. *Cell,* 86**,** 353-64.

HARACSKA, L., PRAKASH, L. & PRAKASH, S. 2002. Role of human DNA polymerase kappa as an extender in translesion synthesis. *Proc Natl Acad Sci U S A,* 99**,** 16000-5.

HAYMART, M. R., GLINBERG, S. L., LIU, J., SIPPEL, R. S., JAUME, J. C. & CHEN, H. 2009. Higher serum TSH in thyroid cancer patients occurs independent of age and correlates with extrathyroidal extension. *Clin Endocrinol (Oxf),* 71**,** 434-9.

HAYMART, M. R., REPPLINGER, D. J., LEVERSON, G. E., ELSON, D. F., SIPPEL, R. S., JAUME, J. C. & CHEN, H. 2008. Higher serum thyroid stimulating hormone level in thyroid nodule patients is associated with greater risks of differentiated thyroid cancer and advanced tumor stage. *J Clin Endocrinol Metab,* 93**,** 809-14.

HEANEY, A. P., HORWITZ, G. A., WANG, Z., SINGSON, R. & MELMED, S. 1999. Early involvement of estrogen-induced pituitary tumor transforming gene and fibroblast growth factor expression in prolactinoma pathogenesis. *Nat Med,* 5**,** 1317-21.

HEANEY, A. P., NELSON, V., FERNANDO, M. & HORWITZ, G. 2001. Transforming events in thyroid tumorigenesis and their association with follicular lesions. *J Clin Endocrinol Metab,* 86**,** 5025-32.

HEANEY, A. P., SINGSON, R., MCCABE, C. J., NELSON, V., NAKASHIMA, M. & MELMED, S. 2000. Expression of pituitary-tumour transforming gene in colorectal tumours. *Lancet,* 355**,** 716-9.

HEGI, M. E., DISERENS, A. C., GORLIA, T., HAMOU, M. F., DE TRIBOLET, N., WELLER, M., KROS, J. M., HAINFELLNER, J. A., MASON, W., MARIANI, L., BROMBERG, J. E., HAU, P., MIRIMANOFF, R. O., CAIRNCROSS, J. G., JANZER, R. C. & STUPP, R. 2005. MGMT gene silencing and benefit from temozolomide in glioblastoma. *N Engl J Med,* 352**,** 997-1003.

HIDALGO, M., GALAN, J. J., SAEZ, C., FERRERO, E., CASTILLA, C., RAMIREZ-LORCA, R., PELAEZ, P., RUIZ, A., JAPON, M. A. & ROYO, J. L. 2008. Methylation alterations are not a major cause of PTTG1 misregulation. *BMC Cancer,* 8**,** 110.

HILGER, R. A., SCHEULEN, M. E. & STRUMBERG, D. 2002. The Ras-Raf-MEK-ERK pathway in the treatment of cancer. *Onkologie,* 25**,** 511-8.

HLUBEK, F., PFEIFFER, S., BUDCZIES, J., SPADERNA, S., JUNG, A., KIRCHNER, T. & BRABLETZ, T. 2006. Securin (hPTTG1) expression is regulated by beta-catenin/TCF in human colorectal carcinoma. *Br J Cancer,* 94**,** 1672-7.

HO, A. L., GREWAL, R. K., LEBOEUF, R., SHERMAN, E. J., PFISTER, D. G., DEANDREIS, D., PENTLOW, K. S., ZANZONICO, P. B., HAQUE, S., GAVANE, S., GHOSSEIN, R. A., RICARTE-FILHO, J. C., DOMINGUEZ, J. M., SHEN, R., TUTTLE, R. M., LARSON, S. M. & FAGIN, J. A. 2013. Selumetinib-enhanced radioiodine uptake in advanced thyroid cancer. *N Engl J Med,* 368**,** 623-32.

HOLLSTEIN, M., RICE, K., GREENBLATT, M. S., SOUSSI, T., FUCHS, R., SORLIE, T., HOVIG, E., SMITH-SORENSEN, B., MONTESANO, R. & HARRIS, C. C. 1994. Database of p53 gene somatic mutations in human tumors and cell lines. *Nucleic Acids Res,* 22**,** 3551-5.

HOLM, L. E. 1985. Thyroid cancer after exposure to radioiodine. *Strahlenschutz Forsch Prax,* 25**,** 36-56.

HOLT, L. J., KRUTCHINSKY, A. N. & MORGAN, D. O. 2008. Positive feedback sharpens the anaphase switch. *Nature,* 454**,** 353-7.

HOWELL, G. M., HODAK, S. P. & YIP, L. 2013. RAS mutations in thyroid cancer. *Oncologist,* 18**,** 926-32.

HSUEH, C., LIN, J. D., CHANG, Y. S., HSUEH, S., CHAO, T. C., YU, J. S., JUNG, S. M., TSENG, N. M., SUN, J. H., KUO, S. Y. & UENG, S. H. 2013. Prognostic significance of pituitary tumour-transforming gene-binding factor (PBF) expression in papillary thyroid carcinoma. *Clin Endocrinol (Oxf),* 78**,** 303-9.

IONOV, Y., PEINADO, M. A., MALKHOSYAN, S., SHIBATA, D. & PERUCHO, M. 1993. Ubiquitous somatic mutations in simple repeated sequences reveal a new mechanism for colonic carcinogenesis. *Nature,* 363**,** 558-61.

ISHIZAKA, Y., ITOH, F., TAHIRA, T., IKEDA, I., SUGIMURA, T., TUCKER, J., FERTITTA, A., CARRANO, A. V. & NAGAO, M. 1989. Human ret proto-oncogene mapped to chromosome 10q11.2. *Oncogene,* 4**,** 1519-21.

ISHIZAKA, Y., KOBAYASHI, S., USHIJIMA, T., HIROHASHI, S., SUGIMURA, T. & NAGAO, M. 1991. Detection of retTPC/PTC transcripts in thyroid adenomas and adenomatous goiter by an RT-PCR method. *Oncogene,* 6**,** 1667-72.

ITO, T., SEYAMA, T., MIZUNO, T., TSUYAMA, N., HAYASHI, T., HAYASHI, Y., DOHI, K., NAKAMURA, N. & AKIYAMA, M. 1992. Unique association of p53 mutations with undifferentiated but not with differentiated carcinomas of the thyroid gland. *Cancer Res,* 52**,** 1369-71.

JHIANG, S. M., SAGARTZ, J. E., TONG, Q., PARKER-THORNBURG, J., CAPEN, C. C., CHO, J. Y., XING, S. & LEDENT, C. 1996. Targeted expression of the ret/PTC1 oncogene induces papillary thyroid carcinomas. *Endocrinology,* 137**,** 375-8.

JONKLAAS, J., NSOULI-MAKTABI, H. & SOLDIN, S. J. 2008. Endogenous thyrotropin and triiodothyronine concentrations in individuals with thyroid cancer. *Thyroid,* 18**,** 943-52.

KAKAR, S. S. & JENNES, L. 1999. Molecular cloning and characterization of the tumor transforming gene (TUTR1): a novel gene in human tumorigenesis. *Cytogenet Cell Genet,* 84**,** 211-6.

KAKAR, S. S. & MALIK, M. T. 2006. Suppression of lung cancer with siRNA targeting PTTG. *Int J Oncol,* 29**,** 387-95.

KAMIYA, Y., ZHANG, X. Y., YING, H., KATO, Y., WILLINGHAM, M. C., XU, J., O'MALLEY, B. W. & CHENG, S. Y. 2003. Modulation by steroid receptor coactivator-1 of target-tissue responsiveness in resistance to thyroid hormone. *Endocrinology,* 144**,** 4144-53.

KANAKIS, D., KIRCHES, E., MAWRIN, C. & DIETZMANN, K. 2003. Promoter mutations are no major cause of PTTG overexpression in pituitary adenomas. *Clin Endocrinol (Oxf),* 58**,** 151-5.

KANESHIGE, M., KANESHIGE, K., ZHU, X., DACE, A., GARRETT, L., CARTER, T. A., KAZLAUSKAITE, R., PANKRATZ, D. G., WYNSHAW-BORIS, A., REFETOFF, S., WEINTRAUB, B., WILLINGHAM, M. C., BARLOW, C. & CHENG, S. 2000. Mice with a targeted mutation in the thyroid hormone beta receptor gene exhibit impaired growth and resistance to thyroid hormone. *Proc Natl Acad Sci U S A,* 97**,** 13209-14.

KAPLAN, E. L., MHOON, D., KAPLAN, S. P. & ANGELOS, P. 2009. Radiation-induced thyroid cancer: the Chicago experience. *Surgery,* 146**,** 979-85.

KASTAN, M. B. & BARTEK, J. 2004. Cell-cycle checkpoints and cancer. *Nature,* 432**,** 316-23.

KATO, I., TAJIMA, K., SUCHI, T., AOZASA, K., MATSUZUKA, F., KUMA, K. & TOMINAGA, S. 1985. Chronic thyroiditis as a risk factor of B-cell lymphoma in the thyroid gland. *Jpn J Cancer Res,* 76**,** 1085-90.

KHARBANDA, S., YUAN, Z. M., WEICHSELBAUM, R. & KUFE, D. 1998. Determination of cell fate by c-Abl activation in the response to DNA damage. *Oncogene,* 17**,** 3309-18.

KHO, P. S., WANG, Z., ZHUANG, L., LI, Y., CHEW, J. L., NG, H. H., LIU, E. T. & YU, Q. 2004. p53-regulated transcriptional program associated with genotoxic stress-induced apoptosis. *J Biol Chem,* 279**,** 21183-92.

KIM, C. S., YING, H., WILLINGHAM, M. C. & CHENG, S. Y. 2007a. The pituitary tumor-transforming gene promotes angiogenesis in a mouse model of follicular thyroid cancer. *Carcinogenesis,* 28**,** 932-9.

KIM, C. S. & ZHU, X. 2009. Lessons from Mouse Models of Thyroid Cancer. *Thyroid,* 19**,** 1317-1331.

KIM, D., PEMBERTON, H., STRATFORD, A. L., BUELAERT, K., WATKINSON, J. C., LOPES, V., FRANKLYN, J. A. & MCCABE, C. J. 2005. Pituitary tumour transforming gene (PTTG) induces genetic instability in thyroid cells. *Oncogene,* 24**,** 4861-6.

KIM, D. S., FRANKLYN, J. A., SMITH, V. E., STRATFORD, A. L., PEMBERTON, H. N., WARFIELD, A., WATKINSON, J. C., ISHMAIL, T., WAKELAM, M. J. & MCCABE, C. J. 2007b. Securin induces genetic instability in colorectal cancer by inhibiting double-stranded DNA repair activity. *Carcinogenesis,* 28**,** 749-59.

KNAUF, J. A., MA, X., SMITH, E. P., ZHANG, L., MITSUTAKE, N., LIAO, X. H., REFETOFF, S., NIKIFOROV, Y. E. & FAGIN, J. A. 2005. Targeted expression of BRAFV600E in thyroid cells of transgenic mice results in papillary thyroid cancers that undergo dedifferentiation. *Cancer Res,* 65**,** 4238-45.

KNUDSON, A. G., JR. 1971. Mutation and cancer: statistical study of retinoblastoma. *Proc Natl Acad Sci U S A,* 68**,** 820-3.

KRAUSE, W. J. 2005. Krause's Essential Human Histology for Medical Students. 3rd Edition**,** 260 - 262.

KREJCI, L., ALTMANNOVA, V., SPIREK, M. & ZHAO, X. 2012. Homologous recombination and its regulation. *Nucleic Acids Research*.

KROLL, T. G., SARRAF, P., PECCIARINI, L., CHEN, C. J., MUELLER, E., SPIEGELMAN, B. M. & FLETCHER, J. A. 2000. PAX8-PPARgamma1 fusion oncogene in human thyroid carcinoma [corrected]. *Science,* 289**,** 1357-60.

KRUM, S. A., LA ROSA DALUGDUGAN, E., MIRANDA-CARBONI, G. A. & LANE, T. F. 2010. BRCA1 Forms a Functional Complex with gamma-H2AX as a Late Response to Genotoxic Stress. *J Nucleic Acids,* 2010.

KUO, L. J. & YANG, L. X. 2008. Gamma-H2AX - a novel biomarker for DNA double-strand breaks. *In Vivo,* 22**,** 305-9.

LA PERLE, K. M., JHIANG, S. M. & CAPEN, C. C. 2000. Loss of p53 promotes anaplasia and local invasion in ret/PTC1-induced thyroid carcinomas. *Am J Pathol,* 157**,** 671-7.

LAI, Y., XIN, D., BAI, J., MAO, Z. & NA, Y. 2007. The important anti-apoptotic role and its regulation mechanism of PTTG1 in UV-induced apoptosis. *J Biochem Mol Biol,* 40**,** 966-72.

LAVIN, M. F. 2008. Ataxia-telangiectasia: from a rare disorder to a paradigm for cell signalling and cancer. *Nat Rev Mol Cell Biol,* 9**,** 759-69.

LEE, J. H., LEE, E. S. & KIM, Y. S. 2007. Clinicopathologic significance of BRAF V600E mutation in papillary carcinomas of the thyroid: a meta-analysis. *Cancer,* 110**,** 38-46.

LEENHARDT, L., BERNIER, M. O., BOIN-PINEAU, M. H., CONTE DEVOLX, B., MARECHAUD, R., NICCOLI-SIRE, P., NOCAUDIE, M., ORGIAZZI, J., SCHLUMBERGER, M., WEMEAU, J. L., CHERIE-CHALLINE, L. & DE VATHAIRE, F. 2004. Advances in diagnostic practices affect thyroid cancer incidence in France. *Eur J Endocrinol,* 150**,** 133-9.

LENGAUER, C., KINZLER, K. W. & VOGELSTEIN, B. 1997. Genetic instability in colorectal cancers. *Nature,* 386**,** 623-7.

LENGAUER, C., KINZLER, K. W. & VOGELSTEIN, B. 1998. Genetic instabilities in human cancers. *Nature,* 396**,** 643-9.

LEVINE, A. J. 1997. p53, the cellular gatekeeper for growth and division. *Cell,* 88**,** 323-31.

LEWY, G. D., RYAN, G. A., READ, M. L., FONG, J. C., POOLE, V., SEED, R. I., SHARMA, N., SMITH, V. E., KWAN, P. P., STEWART, S. L., BACON, A., WARFIELD, A., FRANKLYN, J. A., MCCABE, C. J. & BOELAERT, K. 2013. Regulation of pituitary tumor transforming gene (PTTG) expression and phosphorylation in thyroid cells. *Endocrinology,* 154**,** 4408-22.

LI, F. P., FRAUMENI, J. F., JR., MULVIHILL, J. J., BLATTNER, W. A., DREYFUS, M. G., TUCKER, M. A. & MILLER, R. W. 1988. A cancer family syndrome in twenty-four kindreds. *Cancer Res,* 48**,** 5358-62.

LI, T., HUANG, H., HUANG, B., HUANG, B. & LU, J. 2009. Histone acetyltransferase p300 regulates the expression of human pituitary tumor transforming gene (hPTTG). *J Genet Genomics,* 36**,** 335-42.

LIANG, H., ZHONG, Y., LUO, Z., HUANG, Y., LIN, H., ZHAN, S., XIE, K. & LI, Q. Q. 2011. Diagnostic value of 16 cellular tumor markers for metastatic thyroid cancer: an immunohistochemical study. *Anticancer Res,* 31**,** 3433-40.

LIND, P., LANGSTEGER, W., MOLNAR, M., GALLOWITSCH, H. J., MIKOSCH, P. & GOMEZ, I. 1998. Epidemiology of thyroid diseases in iodine sufficiency. *Thyroid,* 8**,** 1179-83.

LIU, R. T., HOU, C. Y., YOU, H. L., HUANG, C. C., HOCK, L., CHOU, F. F., WANG, P. W. & CHENG, J. T. 2004. Selective occurrence of ras mutations in benign and malignant thyroid follicular neoplasms in Taiwan. *Thyroid,* 14**,** 616-21.

LOEB, K. R. & LOEB, L. A. 1999. Genetic instability and the mutator phenotype. Studies in ulcerative colitis. *Am J Pathol,* 154**,** 1621-6.

LOEB, L. A. 2001. A mutator phenotype in cancer. *Cancer Res,* 61**,** 3230-9.

LOEB, L. A. & MONNAT, R. J., JR. 2008. DNA polymerases and human disease. *Nat Rev Genet,* 9**,** 594-604.

LOHRER, H. D., BRASELMANN, H., RICHTER, H. E., JACKL, G., HERBECK, J., HIEBER, L., KELLERER, A. M. & BAUCHINGER, M. 2001. Instability of microsatellites in radiation-associated thyroid tumours with short latency periods. *Int J Radiat Biol,* 77**,** 891-9.

MALKIN, D., LI, F. P., STRONG, L. C., FRAUMENI, J. F., JR., NELSON, C. E., KIM, D. H., KASSEL, J., GRYKA, M. A., BISCHOFF, F. Z., TAINSKY, M. A. & ET AL. 1990. Germ line p53 mutations in a familial syndrome of breast cancer, sarcomas, and other neoplasms. *Science,* 250**,** 1233-8.

MALUMBRES, M. & BARBACID, M. 2005. Mammalian cyclin-dependent kinases. *Trends Biochem Sci,* 30**,** 630-41.

MALUMBRES, M. & BARBACID, M. 2009. Cell cycle, CDKs and cancer: a changing paradigm. *Nat Rev Cancer,* 9**,** 153-166.

MARQUES, A. R., ESPADINHA, C., CATARINO, A. L., MONIZ, S., PEREIRA, T., SOBRINHO, L. G. & LEITE, V. 2002. Expression of PAX8-PPAR gamma 1 rearrangements in both follicular thyroid carcinomas and adenomas. *J Clin Endocrinol Metab,* 87**,** 3947-52.

MCCABE, C. J., BOELAERT, K., TANNAHILL, L. A., HEANEY, A. P., STRATFORD, A. L., KHAIRA, J. S., HUSSAIN, S., SHEPPARD, M. C., FRANKLYN, J. A. & GITTOES, N. J. 2002. Vascular endothelial growth factor, its receptor KDR/Flk-1, and pituitary tumor transforming gene in pituitary tumors. *J Clin Endocrinol Metab,* 87**,** 4238-44.

MEI, J., HUANG, X. & ZHANG, P. 2001. Securin is not required for cellular viability, but is required for normal growth of mouse embryonic fibroblasts. *Curr Biol,* 11**,** 1197-201.

MILLER, K. A., YEAGER, N., BAKER, K., LIAO, X. H., REFETOFF, S. & DI CRISTOFANO, A. 2009. Oncogenic Kras requires simultaneous PI3K signaling to induce ERK activation and transform thyroid epithelial cells in vivo. *Cancer Res,* 69**,** 3689-94.

MINEMATSU, T., EGASHIRA, N., KAJIYA, H., TAKEI, M., TAKEKOSHI, S., ITOH, Y., TSUKAMOTO, H., ITOH, J., SANNO, N., TERAMOTO, A. & OSAMURA, R. Y. 2007. PTTG is a secretory protein in human pituitary adenomas and in mouse pituitary tumor cell lines. *Endocr Pathol,* 18**,** 8-15.

MIRANDA, C., MINOLETTI, F., GRECO, A., SOZZI, G. & PIEROTTI, M. A. 1994. Refined localization of the human TPR gene to chromosome 1q25 by in situ hybridization. *Genomics,* 23**,** 714-5.

MITCHELL, I., LIVINGSTON, E. H., CHANG, A. Y., HOLT, S., SNYDER, W. H., 3RD, LINGVAY, I. & NWARIAKU, F. E. 2007. Trends in thyroid cancer demographics and surgical therapy in the United States. *Surgery,* 142**,** 823-8; discussion 828 e1.

MITMAKER, E., ALVARADO, C., BEGIN, L. R. & TRIFIRO, M. 2008. Microsatellite instability in benign and malignant thyroid neoplasms. *J Surg Res,* 150**,** 40-8.

MITSUTAKE, N., KNAUF, J. A., MITSUTAKE, S., MESA, C., ZHANG, L. & FAGIN, J. A. 2005. Conditional BRAFV600E Expression Induces DNA Synthesis, Apoptosis, Dedifferentiation, and Chromosomal Instability in Thyroid PCCL3 Cells. *Cancer Research,* 65**,** 2465-2473.

MIZUNO, T., IWAMOTO, K. S., KYOIZUMI, S., NAGAMURA, H., SHINOHARA, T., KOYAMA, K., SEYAMA, T. & HAMATANI, K. 2000. Preferential induction of RET/PTC1 rearrangement by X-ray irradiation. *Oncogene,* 19**,** 438-43.

MONSALVES, E., JURASCHKA, K., TATENO, T., AGNIHOTRI, S., ASA, S. L., EZZAT, S. & ZADEH, G. 2014. The PI3K/AKT/mTOR pathway in the pathophysiology and treatment of pituitary adenomas. *Endocr Relat Cancer,* 21**,** R331-44.

MU, Y. M., OBA, K., YANASE, T., ITO, T., ASHIDA, K., GOTO, K., MORINAGA, H., IKUYAMA, S., TAKAYANAGI, R. & NAWATA, H. 2003. Human pituitary tumor transforming gene (hPTTG) inhibits human lung cancer A549 cell growth through activation of p21(WAF1/CIP1). *Endocr J,* 50**,** 771-81.

MUSACCHIO, A. & SALMON, E. D. 2007. The spindle-assembly checkpoint in space and time. *Nat Rev Mol Cell Biol,* 8**,** 379-393.

MUSHOLT, T. J., MUSHOLT, P. B., KHALADJ, N., SCHULZ, D., SCHEUMANN, G. F. & KLEMPNAUER, J. 2000. Prognostic significance of RET and NTRK1 rearrangements in sporadic papillary thyroid carcinoma. *Surgery,* 128**,** 984-93.

NAGAIAH, G., HOSSAIN, A., MOONEY, C. J., PARMENTIER, J. & REMICK, S. C. 2011. Anaplastic thyroid cancer: a review of epidemiology, pathogenesis, and treatment. *J Oncol,* 2011**,** 542358.

NAKAGAWA, K., TAYA, Y., TAMAI, K. & YAMAIZUMI, M. 1999. Requirement of ATM in phosphorylation of the human p53 protein at serine 15 following DNA double-strand breaks. *Mol Cell Biol,* 19**,** 2828-34.

NAM, E. A. & CORTEZ, D. 2011. ATR signalling: more than meeting at the fork. *Biochem J,* 436**,** 527-36.

NASMYTH, K. 2002. Segregating sister genomes: the molecular biology of chromosome separation. *Science,* 297**,** 559-65.

NEGRINI, S., GORGOULIS, V. G. & HALAZONETIS, T. D. 2010. Genomic instability--an evolving hallmark of cancer. *Nat Rev Mol Cell Biol,* 11**,** 220-8.

NIKIFOROV, Y. E. 2006. Radiation-induced thyroid cancer: what we have learned from chernobyl. *Endocr Pathol,* 17**,** 307-17.

NIKIFOROV, Y. E., NIKIFOROVA, M. N., GNEPP, D. R. & FAGIN, J. A. 1996. Prevalence of mutations of ras and p53 in benign and malignant thyroid tumors from children exposed to radiation after the Chernobyl nuclear accident. *Oncogene,* 13**,** 687-93.

NIKIFOROV, Y. E., ROWLAND, J. M., BOVE, K. E., MONFORTE-MUNOZ, H. & FAGIN, J. A. 1997. Distinct pattern of ret oncogene rearrangements in morphological variants of radiation-induced and sporadic thyroid papillary carcinomas in children. *Cancer Res,* 57**,** 1690-4.

NIKIFOROVA, M. N., BIDDINGER, P. W., CAUDILL, C. M., KROLL, T. G. & NIKIFOROV, Y. E. 2002. PAX8-PPARgamma rearrangement in thyroid tumors: RT-PCR and immunohistochemical analyses. *Am J Surg Pathol,* 26**,** 1016-23.

NIKIFOROVA, M. N., LYNCH, R. A., BIDDINGER, P. W., ALEXANDER, E. K., DORN, G. W., 2ND, TALLINI, G., KROLL, T. G. & NIKIFOROV, Y. E. 2003. RAS point mutations and PAX8-PPAR gamma rearrangement in thyroid tumors: evidence for distinct molecular pathways in thyroid follicular carcinoma. *J Clin Endocrinol Metab,* 88**,** 2318-26.

NIKIFOROVA, M. N., STRINGER, J. R., BLOUGH, R., MEDVEDOVIC, M., FAGIN, J. A. & NIKIFOROV, Y. E. 2000. Proximity of chromosomal loci that participate in radiation-induced rearrangements in human cells. *Science,* 290**,** 138-41.

NOWELL, P. C. 1976. The clonal evolution of tumor cell populations. *Science,* 194**,** 23-8.

O'DRISCOLL, M., DOBYNS, W. B., VAN HAGEN, J. M. & JEGGO, P. A. 2007. Cellular and clinical impact of haploinsufficiency for genes involved in ATR signaling. *Am J Hum Genet,* 81**,** 77-86.

OGBAGABRIEL, S., FERNANDO, M., WALDMAN, F. M., BOSE, S. & HEANEY, A. P. 2005. Securin is overexpressed in breast cancer. *Mod Pathol,* 18**,** 985-90.

PACHNIS, V., MANKOO, B. & COSTANTINI, F. 1993. Expression of the c-ret proto-oncogene during mouse embryogenesis. *Development,* 119**,** 1005-17.

PAN, H., GAO, F., PAPAGEORGIS, P., ABDOLMALEKY, H. M., FALLER, D. V. & THIAGALINGAM, S. 2007. Aberrant activation of gamma-catenin promotes genomic instability and oncogenic effects during tumor progression. *Cancer Biol Ther,* 6**,** 1638-43.

PAUZAR, B., KARNER, I., GLAVAS-OBROVAC, L., STEFANIC, M. & DMITROVIC, B. 2012. PAX8-PPARgamma oncogene in follicular thyroid tumors: RT-PCR and immunohistochemical analyses. *Coll Antropol,* 36 Suppl 2**,** 79-82.

PEARSON, G., ROBINSON, F., BEERS GIBSON, T., XU, B. E., KARANDIKAR, M., BERMAN, K. & COBB, M. H. 2001. Mitogen-activated protein (MAP) kinase pathways: regulation and physiological functions. *Endocr Rev,* 22**,** 153-83.

PEI, L. 1999. Pituitary tumor-transforming gene protein associates with ribosomal protein S10 and a novel human homologue of DnaJ in testicular cells. *J Biol Chem,* 274**,** 3151-8.

PEI, L. 2000. Activation of mitogen-activated protein kinase cascade regulates pituitary tumor-transforming gene transactivation function. *J Biol Chem,* 275**,** 31191-8.

PEI, L. 2001. Identification of c-myc as a down-stream target for pituitary tumor-transforming gene. *J Biol Chem,* 276**,** 8484-91.

PEI, L. & MELMED, S. 1997. Isolation and characterization of a pituitary tumor-transforming gene (PTTG). *Mol Endocrinol,* 11**,** 433-41.

PEINADO, M. A., MALKHOSYAN, S., VELAZQUEZ, A. & PERUCHO, M. 1992. Isolation and characterization of allelic losses and gains in colorectal tumors by arbitrarily primed polymerase chain reaction. *Proc Natl Acad Sci U S A,* 89**,** 10065-9.

PERLMAN, S. L., BODER DECEASED, E., SEDGEWICK, R. P. & GATTI, R. A. 2012. Ataxia-telangiectasia. *Handb Clin Neurol,* 103**,** 307-32.

PERROS, P., BOELAERT, K., COLLEY, S., EVANS, C., EVANS, R. M., GERRARD BA, G., GILBERT, J., HARRISON, B., JOHNSON, S. J., GILES, T. E., MOSS, L., LEWINGTON, V., NEWBOLD, K., TAYLOR, J., THAKKER, R. V., WATKINSON, J. & WILLIAMS, G. R. 2014. Guidelines for the management of thyroid cancer. *Clin Endocrinol (Oxf),* 81 Suppl 1**,** 1-122.

PETERSON, E., DE, P. & NUTTALL, R. 2012. BMI, diet and female reproductive factors as risks for thyroid cancer: a systematic review. *PLoS One,* 7**,** e29177.

PETITJEAN, A., MATHE, E., KATO, S., ISHIOKA, C., TAVTIGIAN, S. V., HAINAUT, P. & OLIVIER, M. 2007. Impact of mutant p53 functional properties on TP53 mutation

patterns and tumor phenotype: lessons from recent developments in the IARC TP53 database. *Hum Mutat,* 28**,** 622-9.

PEYSSONNAUX, C. & EYCHENE, A. 2001. The Raf/MEK/ERK pathway: new concepts of activation. *Biol Cell,* 93**,** 53-62.

PIGOZZI, D., TOMBAL, B., DUCRET, T., VACHER, P. & GAILLY, P. 2004. Role of store-dependent influx of Ca2+ and efflux of K+ in apoptosis of CHO cells. *Cell Calcium,* 36**,** 421-430.

POHLENZ, J., MAQUEEM, A., CUA, K., WEISS, R. E., VAN SANDE, J. & REFETOFF, S. 1999. Improved radioimmunoassay for measurement of mouse thyrotropin in serum: strain differences in thyrotropin concentration and thyrotroph sensitivity to thyroid hormone. *Thyroid,* 9**,** 1265-71.

POLYZOS, S. A., KITA, M., EFSTATHIADOU, Z., POULAKOS, P., SLAVAKIS, A., SOFIANOU, D., FLARIS, N., LEONTSINI, M., KOURTIS, A. & AVRAMIDIS, A. 2008. Serum thyrotropin concentration as a biochemical predictor of thyroid malignancy in patients presenting with thyroid nodules. *J Cancer Res Clin Oncol,* 134**,** 953-60.

POWELL, D. J., JR., RUSSELL, J., NIBU, K., LI, G., RHEE, E., LIAO, M., GOLDSTEIN, M., KEANE, W. M., SANTORO, M., FUSCO, A. & ROTHSTEIN, J. L. 1998. The RET/PTC3 oncogene: metastatic solid-type papillary carcinomas in murine thyroids. *Cancer Res,* 58**,** 5523-8.

PRESCOTT, J. D. & ZEIGER, M. A. 2015. The RET oncogene in papillary thyroid carcinoma. *Cancer*.

PREZANT, T. R., KADIOGLU, P. & MELMED, S. 1999. An intronless homolog of human proto-oncogene hPTTG is expressed in pituitary tumors: evidence for hPTTG family. *J Clin Endocrinol Metab,* 84**,** 1149-52.

PURI, R., TOUSSON, A., CHEN, L. & KAKAR, S. S. 2001. Molecular cloning of pituitary tumor transforming gene 1 from ovarian tumors and its expression in tumors. *Cancer Lett,* 163**,** 131-9.

QUERALT, E., LEHANE, C., NOVAK, B. & UHLMANN, F. 2006. Downregulation of PP2A(Cdc55) phosphatase by separase initiates mitotic exit in budding yeast. *Cell,* 125**,** 719-32.

RABES, H. M., DEMIDCHIK, E. P., SIDOROW, J. D., LENGFELDER, E., BEIMFOHR, C., HOELZEL, D. & KLUGBAUER, S. 2000. Pattern of radiation-induced RET and NTRK1 rearrangements in 191 post-chernobyl papillary thyroid carcinomas: biological, phenotypic, and clinical implications. *Clin Cancer Res,* 6**,** 1093-103.

RAJAGOPALAN, H., BARDELLI, A., LENGAUER, C., KINZLER, K. W., VOGELSTEIN, B. & VELCULESCU, V. E. 2002. Tumorigenesis: RAF/RAS oncogenes and mismatch-repair status. *Nature,* 418**,** 934.

RAJAGOPALAN, H., NOWAK, M. A., VOGELSTEIN, B. & LENGAUER, C. 2003. The significance of unstable chromosomes in colorectal cancer. *Nat Rev Cancer,* 3**,** 695-701.

RAMOS-MORALES, F., DOMINGUEZ, A., ROMERO, F., LUNA, R., MULTON, M. C., PINTOR-TORO, J. A. & TORTOLERO, M. 2000. Cell cycle regulated expression and phosphorylation of hpttg proto-oncogene product. *Oncogene,* 19**,** 403-9.

READ, M. L., LEWY, G. D., FONG, J. C., SHARMA, N., SEED, R. I., SMITH, V. E., GENTILIN, E., WARFIELD, A., EGGO, M. C., KNAUF, J. A., LEADBEATER, W. E., WATKINSON, J. C., FRANKLYN, J. A., BOELAERT, K. & MCCABE, C. J. 2011. Proto-oncogene PBF/PTTG1IP regulates thyroid cell growth and represses radioiodide treatment. *Cancer Res,* 71**,** 6153-64.

READ, M. L., SEED, R. I., FONG, J. C., MODASIA, B., RYAN, G. A., WATKINS, R. J., GAGLIANO, T., SMITH, V. E., STRATFORD, A. L., KWAN, P. K., SHARMA, N., DIXON, O. M., WATKINSON, J. C., BOELAERT, K., FRANKLYN, J. A., TURNELL, A. S. & MCCABE, C. J. 2014a. The PTTG1-binding factor (PBF/PTTG1IP) regulates p53 activity in thyroid cells. *Endocrinology,* 155**,** 1222-34.

READ, M. L., SEED, R. I., MODASIA, B., KWAN, P. P., SHARMA, N., SMITH, V. E., WATKINS, R. J., BANSAL, S., GAGLIANO, T., STRATFORD, A. L., ISMAIL, T., WAKELAM, M. J., KIM, D. S., WARD, S. T., BOELAERT, K., FRANKLYN, J. A., TURNELL, A. S. & MCCABE, C. J. 2014b. The proto-oncogene PBF binds p53 and is associated with prognostic features in colorectal cancer. *Mol Carcinog*.

REMONTI, L. R., KRAMER, C. K., LEITAO, C. B., PINTO, L. C. & GROSS, J. L. 2015. Thyroid ultrasound features and risk of carcinoma: a systematic review and meta-analysis of observational studies. *Thyroid*.

REYNOLDS, L. E., WATSON, A. R., BAKER, M., JONES, T. A., D'AMICO, G., ROBINSON, S. D., JOFFRE, C., GARRIDO-URBANI, S., RODRIGUEZ-MANZANEQUE, J. C., MARTINO-ECHARRI, E., AURRAND-LIONS, M., SHEER, D., DAGNA-BRICARELLI, F., NIZETIC, D., MCCABE, C. J., TURNELL, A. S., KERMORGANT, S., IMHOF, B. A., ADAMS, R., FISHER, E. M., TYBULEWICZ, V. L., HART, I. R. & HODIVALA-DILKE, K. M. 2010. Tumour angiogenesis is reduced in the Tc1 mouse model of Down's syndrome. *Nature,* 465**,** 813-7.

REYNOLDS, R. M., WEIR, J., STOCKTON, D. L., BREWSTER, D. H., SANDEEP, T. C. & STRACHAN, M. W. 2005. Changing trends in incidence and mortality of thyroid cancer in Scotland. *Clin Endocrinol (Oxf),* 62**,** 156-62.

RHODEN, K. J., UNGER, K., SALVATORE, G., YILMAZ, Y., VOVK, V., CHIAPPETTA, G., QUMSIYEH, M. B., ROTHSTEIN, J. L., FUSCO, A., SANTORO, M., ZITZELSBERGER, H. & TALLINI, G. 2006. RET/papillary thyroid cancer rearrangement in nonneoplastic thyrocytes: follicular cells of Hashimoto's thyroiditis share low-level recombination events with a subset of papillary carcinoma. *J Clin Endocrinol Metab,* 91**,** 2414-23.

RICARTE-FILHO, J. C., LI, S., GARCIA-RENDUELES, M. E., MONTERO-CONDE, C., VOZA, F., KNAUF, J. A., HEGUY, A., VIALE, A., BOGDANOVA, T., THOMAS, G. A., MASON, C. E. & FAGIN, J. A. 2013. Identification of kinase fusion oncogenes in post-Chernobyl radiation-induced thyroid cancers. *J Clin Invest,* 123**,** 4935-44.

RICHARDSON, D. B. 2009. Exposure to ionizing radiation in adulthood and thyroid cancer incidence. *Epidemiology,* 20**,** 181-7.

ROCCATO, E., BRESSAN, P., SABATELLA, G., RUMIO, C., VIZZOTTO, L., PIEROTTI, M. A. & GRECO, A. 2005. Proximity of TPR and NTRK1 rearranging loci in human thyrocytes. *Cancer Res,* 65**,** 2572-6.

ROMERO, F., GIL-BERNABE, A. M., SAEZ, C., JAPON, M. A., PINTOR-TORO, J. A. & TORTOLERO, M. 2004. Securin is a target of the UV response pathway in mammalian cells. *Mol Cell Biol,* 24**,** 2720-33.

ROMERO, F., MULTON, M. C., RAMOS-MORALES, F., DOMINGUEZ, A., BERNAL, J. A., PINTOR-TORO, J. A. & TORTOLERO, M. 2001. Human securin, hPTTG, is associated with Ku heterodimer, the regulatory subunit of the DNA-dependent protein kinase. *Nucleic Acids Res,* 29**,** 1300-7.

ROSCHKE, A. V., GLEBOV, O. K., LABABIDI, S., GEHLHAUS, K. S., WEINSTEIN, J. N. & KIRSCH, I. R. 2008. Chromosomal instability is associated with higher expression of genes implicated in epithelial-mesenchymal transition, cancer invasiveness, and metastasis and with lower expression of genes involved in cell cycle checkpoints, DNA repair, and chromatin maintenance. *Neoplasia,* 10**,** 1222-30.

RUSSELL, J. P., POWELL, D. J., CUNNANE, M., GRECO, A., PORTELLA, G., SANTORO, M., FUSCO, A. & ROTHSTEIN, J. L. 2000. The TRK-T1 fusion protein induces neoplastic transformation of thyroid epithelium. *Oncogene,* 19**,** 5729-35.

RUZANKINA, Y., PINZON-GUZMAN, C., ASARE, A., ONG, T., PONTANO, L., COTSARELIS, G., ZEDIAK, V. P., VELEZ, M., BHANDOOLA, A. & BROWN, E. J. 2007. Deletion of the developmentally essential gene ATR in adult mice leads to age-related phenotypes and stem cell loss. *Cell Stem Cell,* 1**,** 113-26.

SAAVEDRA, H. I., KNAUF, J. A., SHIROKAWA, J. M., WANG, J., OUYANG, B., ELISEI, R., STAMBROOK, P. J. & FAGIN, J. A. 2000. The RAS oncogene induces genomic instability in thyroid PCCL3 cells via the MAPK pathway. *Oncogene,* 19**,** 3948-54.

SAEZ, C., JAPON, M. A., RAMOS-MORALES, F., ROMERO, F., SEGURA, D. I., TORTOLERO, M. & PINTOR-TORO, J. A. 1999. hpttg is over-expressed in pituitary adenomas and other primary epithelial neoplasias. *Oncogene,* 18**,** 5473-6.

SAEZ, C., MARTINEZ-BROCCA, M. A., CASTILLA, C., SOTO, A., NAVARRO, E., TORTOLERO, M., PINTOR-TORO, J. A. & JAPON, M. A. 2006. Prognostic significance of human pituitary tumor-transforming gene immunohistochemical expression in differentiated thyroid cancer. *J Clin Endocrinol Metab,* 91**,** 1404-9.

SANCAR, A., LINDSEY-BOLTZ, L. A., UNSAL-KACMAZ, K. & LINN, S. 2004. Molecular mechanisms of mammalian DNA repair and the DNA damage checkpoints. *Annu Rev Biochem,* 73**,** 39-85.

SANTIN, A. P. & FURLANETTO, T. W. 2011. Role of Estrogen in Thyroid Function and Growth Regulation. *Journal of Thyroid Research,* 2011.

SCHUCHARDT, A., D'AGATI, V., LARSSON-BLOMBERG, L., COSTANTINI, F. & PACHNIS, V. 1994. Defects in the kidney and enteric nervous system of mice lacking the tyrosine kinase receptor Ret. *Nature,* 367**,** 380-3.

SHARMA, A., SINGH, K. & ALMASAN, A. 2012. Histone H2AX phosphorylation: a marker for DNA damage. *Methods Mol Biol,* 920**,** 613-26.

SHARMA, S., SALEHI, F., SCHEITHAUER, B. W., ROTONDO, F., SYRO, L. V. & KOVACS, K. 2009. Role of MGMT in Tumor Development, Progression, Diagnosis, Treatment and Prognosis. *Anticancer Research,* 29**,** 3759-3768.

SHIBATA, Y., HARUKI, N., KUWABARA, Y., NISHIWAKI, T., KATO, J., SHINODA, N., SATO, A., KIMURA, M., KOYAMA, H., TOYAMA, T., ISHIGURO, H., KUDO, J., TERASHITA, Y., KONISHI, S. & FUJII, Y. 2002. Expression of PTTG (pituitary tumor transforming gene) in esophageal cancer. *Jpn J Clin Oncol,* 32**,** 233-7.

SHIOTANI, B. & ZOU, L. 2009. ATR signaling at a glance. *J Cell Sci,* 122**,** 301-4.

SIPOS, J. A. & MAZZAFERRI, E. L. 2010. Thyroid cancer epidemiology and prognostic variables. *Clin Oncol (R Coll Radiol),* 22**,** 395-404.

SIRBU, B. M., COUCH, F. B., FEIGERLE, J. T., BHASKARA, S., HIEBERT, S. W. & CORTEZ, D. 2011. Analysis of protein dynamics at active, stalled, and collapsed replication forks. *Genes Dev,* 25**,** 1320-7.

SMAILYTE, G., MISEIKYTE-KAUBRIENE, E. & KURTINAITIS, J. 2006. Increasing thyroid cancer incidence in Lithuania in 1978-2003. *BMC Cancer,* 6**,** 284.

SMALLRIDGE, R. C., MARLOW, L. A. & COPLAND, J. A. 2009. Anaplastic thyroid cancer: molecular pathogenesis and emerging therapies. *Endocr Relat Cancer,* 16**,** 17-44.

SMITH, G. C. & JACKSON, S. P. 1999. The DNA-dependent protein kinase. *Genes Dev,* 13**,** 916-34.

SMITH, V. E., FRANKLYN, J. A. & MCCABE, C. J. 2010. Pituitary tumor-transforming gene and its binding factor in endocrine cancer. *Expert Rev Mol Med,* 12**,** e38.

SMITH, V. E., READ, M. L., TURNELL, A. S., SHARMA, N., LEWY, G. D., FONG, J. C., SEED, R. I., KWAN, P., RYAN, G., MEHANNA, H., CHAN, S. Y., DARRAS, V. M., BOELAERT, K., FRANKLYN, J. A. & MCCABE, C. J. 2012. PTTG-binding factor (PBF) is a novel regulator of the thyroid hormone transporter MCT8. *Endocrinology,* 153**,** 3526-36.

SMITH, V. E., READ, M. L., TURNELL, A. S., WATKINS, R. J., WATKINSON, J. C., LEWY, G. D., FONG, J. C., JAMES, S. R., EGGO, M. C., BOELAERT, K., FRANKLYN, J. A. & MCCABE, C. J. 2009. A novel mechanism of sodium iodide symporter repression in differentiated thyroid cancer. *J Cell Sci,* 122**,** 3393-402.

SMITH, V. E., SHARMA, N., WATKINS, R. J., READ, M. L., RYAN, G. A., KWAN, P. P., MARTIN, A., WATKINSON, J. C., BOELAERT, K., FRANKLYN, J. A. & MCCABE, C. J. 2013. Manipulation of PBF/PTTG1IP phosphorylation status; a potential new therapeutic strategy for improving radioiodine uptake in thyroid and other tumors. *J Clin Endocrinol Metab,* 98**,** 2876-86.

SORENSEN, C. S., HANSEN, L. T., DZIEGIELEWSKI, J., SYLJUASEN, R. G., LUNDIN, C., BARTEK, J. & HELLEDAY, T. 2005. The cell-cycle checkpoint kinase Chk1 is required for mammalian homologous recombination repair. *Nat Cell Biol,* 7**,** 195-201.

STEGMEIER, F., VISINTIN, R. & AMON, A. 2002. Separase, polo kinase, the kinetochore protein Slk19, and Spo12 function in a network that controls Cdc14 localization during early anaphase. *Cell,* 108**,** 207-20.

STIFF, T., WALKER, S. A., CEROSALETTI, K., GOODARZI, A. A., PETERMANN, E., CONCANNON, P., O'DRISCOLL, M. & JEGGO, P. A. 2006. ATR-dependent phosphorylation and activation of ATM in response to UV treatment or replication fork stalling. *EMBO J,* 25**,** 5775-82.

STOLER, D. L., CHEN, N., BASIK, M., KAHLENBERG, M. S., RODRIGUEZ-BIGAS, M. A., PETRELLI, N. J. & ANDERSON, G. R. 1999. The onset and extent of genomic instability in sporadic colorectal tumor progression. *Proc Natl Acad Sci U S A,* 96**,** 15121-6.

STORCHOVA, Z. & PELLMAN, D. 2004. From polyploidy to aneuploidy, genome instability and cancer. *Nat Rev Mol Cell Biol,* 5**,** 45-54.

STRATFORD, A. L., BOELAERT, K., TANNAHILL, L. A., KIM, D. S., WARFIELD, A., EGGO, M. C., GITTOES, N. J., YOUNG, L. S., FRANKLYN, J. A. & MCCABE, C. J. 2005. Pituitary tumor transforming gene binding factor: a novel transforming gene in thyroid tumorigenesis. *J Clin Endocrinol Metab,* 90**,** 4341-9.

STSJAZHKO, V. A., TSYB, A. F., TRONKO, N. D., SOUCHKEVITCH, G. & BAVERSTOCK, K. F. 1995. Childhood thyroid cancer since accident at Chernobyl. *BMJ,* 310**,** 801.

SUZUKI, H., WILLINGHAM, M. C. & CHENG, S. Y. 2002. Mice with a mutation in the thyroid hormone receptor β gene spontaneously develop thyroid carcinoma: A mouse model of thyroid carcinogenesis. *Thyroid,* 12**,** 963-969.

SUZUKI, H., ZHANG, X. Y., FORREST, D., WILLINGHAM, M. C. & CHENG, S. Y. 2003. Marked potentiation of the dominant negative action of a mutant thyroid hormone receptor beta in mice by the ablation of one wild-type beta allele. *Mol Endocrinol,* 17**,** 895-907.

TAKAHASHI, M., ASAI, N., IWASHITA, T., ISOMURA, T., MIYAZAKI, K. & MATSUYAMA, M. 1993. Characterization of the ret proto-oncogene products expressed in mouse L cells. *Oncogene,* 8**,** 2925-9.

TAKAYA, K., YOSHIMASA, T., ARAI, H., TAMURA, N., MIYAMOTO, Y., ITOH, H. & NAKAO, K. 1996. Expression of the RET proto-oncogene in normal human tissues, pheochromocytomas, and other tumors of neural crest origin. *J Mol Med (Berl),* 74**,** 617-21.

TAKETO, M., SCHROEDER, A. C., MOBRAATEN, L. E., GUNNING, K. B., HANTEN, G., FOX, R. R., RODERICK, T. H., STEWART, C. L., LILLY, F., HANSEN, C. T. & ET AL. 1991. FVB/N: an inbred mouse strain preferable for transgenic analyses. *Proc Natl Acad Sci U S A,* 88**,** 2065-9.

TALLINI, G. 2002. Molecular pathobiology of thyroid neoplasms. *Endocr Pathol,* 13**,** 271-88.

TALOS, F., NEMAJEROVA, A., FLORES, E. R., PETRENKO, O. & MOLL, U. M. 2007. p73 suppresses polyploidy and aneuploidy in the absence of functional p53. *Mol Cell,* 27**,** 647-59.

TFELT-HANSEN, J., YANO, S., BANDYOPADHYAY, S., CARROLL, R., BROWN, E. M. & CHATTOPADHYAY, N. 2004. Expression of pituitary tumor transforming gene (PTTG) and its binding protein in human astrocytes and astrocytoma cells: function and regulation of PTTG in U87 astrocytoma cells. *Endocrinology,* 145**,** 4222-31.

THOMPSON, A. D., 3RD & KAKAR, S. S. 2005. Insulin and IGF-1 regulate the expression of the pituitary tumor transforming gene (PTTG) in breast tumor cells. *FEBS Lett,* 579**,** 3195-200.

TOMASINI, R., MAK, T. W. & MELINO, G. 2008. The impact of p53 and p73 on aneuploidy and cancer. *Trends Cell Biol,* 18**,** 244-52.

TOMLINSON, I. & BODMER, W. 1999. Selection, the mutation rate and cancer: ensuring that the tail does not wag the dog. *Nat Med,* 5**,** 11-2.

TONG, Y., BEN-SHLOMO, A., ZHOU, C., WAWROWSKY, K. & MELMED, S. 2008. Pituitary tumor transforming gene 1 regulates Aurora kinase A activity. *Oncogene,* 27**,** 6385-95.

TONG, Y., TAN, Y., ZHOU, C. & MELMED, S. 2007. Pituitary tumor transforming gene interacts with Sp1 to modulate G1/S cell phase transition. *Oncogene,* 26**,** 5596-605.

TSAI, S. J., LIN, S. J., CHENG, Y. M., CHEN, H. M. & WING, L. Y. 2005. Expression and functional analysis of pituitary tumor transforming gene-1 [corrected] in uterine leiomyomas. *J Clin Endocrinol Metab,* 90**,** 3715-23.

TUNG, W. S., SHEVLIN, D. W., KALEEM, Z., TRIBUNE, D. J., WELLS, S. A., JR. & GOODFELLOW, P. J. 1997. Allelotype of follicular thyroid carcinomas reveals

genetic instability consistent with frequent nondisjunctional chromosomal loss. *Genes Chromosomes Cancer,* 19**,** 43-51.

UNGER, K., ZITZELSBERGER, H., SALVATORE, G., SANTORO, M., BOGDANOVA, T., BRASELMANN, H., KASTNER, P., ZURNADZHY, L., TRONKO, N., HUTZLER, P. & THOMAS, G. 2004. Heterogeneity in the distribution of RET/PTC rearrangements within individual post-Chernobyl papillary thyroid carcinomas. *J Clin Endocrinol Metab,* 89**,** 4272-9.

VAISH, M., MISHRA, A., KAUSHAL, M., MISHRA, S. K. & MITTAL, B. 2004. Microsatellite instability and its correlation with clinicopathological features in a series of thyroid tumors prevalent in iodine deficient areas. *Exp Mol Med,* 36**,** 122-9.

VASKO, V., FERRAND, M., DI CRISTOFARO, J., CARAYON, P., HENRY, J. F. & DE MICCO, C. 2003. Specific pattern of RAS oncogene mutations in follicular thyroid tumors. *J Clin Endocrinol Metab,* 88**,** 2745-52.

VISSER, W. E., VAN MULLEM, A. A., JANSEN, J. & VISSER, T. J. 2011. The thyroid hormone transporters MCT8 and MCT10 transport the affinity-label N-bromoacetyl-[(125)I]T3 but are not modified by it. *Mol Cell Endocrinol,* 337**,** 96-100.

VIVANCO, I. & SAWYERS, C. L. 2002. The phosphatidylinositol 3-Kinase AKT pathway in human cancer. *Nat Rev Cancer,* 2**,** 489-501.

VOUSDEN, K. H. 2000. p53: death star. *Cell,* 103**,** 691-4.

VOUSDEN, K. H. 2006. Outcomes of p53 activation--spoilt for choice. *J Cell Sci,* 119**,** 5015-20.

WANG, Y., HOU, P., YU, H., WANG, W., JI, M., ZHAO, S., YAN, S., SUN, X., LIU, D., SHI, B., ZHU, G., CONDOURIS, S. & XING, M. 2007. High prevalence and mutual exclusivity of genetic alterations in the phosphatidylinositol-3-kinase/akt pathway in thyroid tumors. *J Clin Endocrinol Metab,* 92**,** 2387-90.

WANG, Y. K., CUI, N., LI, J. & LUO, B. 2004. [Expression of pituitary tumor-transforming gene in endometrial carcinoma]. *Zhonghua Fu Chan Ke Za Zhi,* 39**,** 538-42.

WANG, Z. & MELMED, S. 2000. Pituitary tumor transforming gene (PTTG) transforming and transactivation activity. *J Biol Chem,* 275**,** 7459-61.

WANG, Z., MORO, E., KOVACS, K., YU, R. & MELMED, S. 2003. Pituitary tumor transforming gene-null male mice exhibit impaired pancreatic beta cell proliferation and diabetes. *Proc Natl Acad Sci U S A,* 100**,** 3428-32.

WANG, Z., YU, R. & MELMED, S. 2001. Mice lacking pituitary tumor transforming gene show testicular and splenic hypoplasia, thymic hyperplasia, thrombocytopenia, aberrant cell cycle progression, and premature centromere division. *Mol Endocrinol,* 15**,** 1870-9.

WARD, L. S., BRENTA, G., MEDVEDOVIC, M. & FAGIN, J. A. 1998. Studies of Allelic Loss in Thyroid Tumors Reveal Major Differences in Chromosomal Instability between Papillary and Follicular Carcinomas. *The Journal of Clinical Endocrinology & Metabolism,* 83**,** 525-530.

WATKINS, R. J., READ, M. L., SMITH, V. E., SHARMA, N., REYNOLDS, G. M., BUCKLEY, L., DOIG, C., CAMPBELL, M. J., LEWY, G., EGGO, M. C., LOUBIERE, L. S., FRANKLYN, J. A., BOELAERT, K. & MCCABE, C. J. 2010. Pituitary tumor transforming gene binding factor: a new gene in breast cancer. *Cancer Res,* 70**,** 3739-49.

WEN, C. Y., NAKAYAMA, T., WANG, A. P., NAKASHIMA, M., DING, Y. T., ITO, M., ISHIBASHI, H., MATSUU, M., SHICHIJO, K. & SEKINE, I. 2004. Expression of pituitary tumor transforming gene in human gastric carcinoma. *World J Gastroenterol,* 10**,** 481-3.

WILLENBUCHER, R. F., AUST, D. E., CHANG, C. G., ZELMAN, S. J., FERRELL, L. D., MOORE, D. H., 2ND & WALDMAN, F. M. 1999. Genomic instability is an early event during the progression pathway of ulcerative-colitis-related neoplasia. *Am J Pathol,* 154**,** 1825-30.

WILTON, S. D., EYRE, H., AKKARI, P. A., WATKINS, H. C., MACRAE, C., LAING, N. G. & CALLEN, D. C. 1995. Assignment of the human a-tropomyosin gene TPM3 to 1q22-->q23 by fluorescence in situ hybridisation. *Cytogenet Cell Genet,* 68**,** 122-4.

WINNEPENNINCKX, V., DEBIEC-RYCHTER, M., BELIEN, J. A., FITEN, P., MICHIELS, S., LAZAR, V., OPDENAKKER, G., MEIJER, G. A., SPATZ, A. & VAN DEN OORD, J. J. 2006. Expression and possible role of hPTTG1/securin in cutaneous malignant melanoma. *Mod Pathol,* 19**,** 1170-80.

WREESMANN, V. B., GHOSSEIN, R. A., PATEL, S. G., HARRIS, C. P., SCHNASER, E. A., SHAHA, A. R., TUTTLE, R. M., SHAH, J. P., RAO, P. H. & SINGH, B. Genome-Wide Appraisal of Thyroid Cancer Progression. *The American Journal of Pathology,* 161**,** 1549-1556.

XIAO, W. & SAMSON, L. 1993. In vivo evidence for endogenous DNA alkylation damage as a source of spontaneous mutation in eukaryotic cells. *Proc Natl Acad Sci U S A,* 90**,** 2117-21.

XING, M. 2010. Genetic alterations in the phosphatidylinositol-3 kinase/Akt pathway in thyroid cancer. *Thyroid,* 20**,** 697-706.

XING, M., ALZAHRANI, A. S., CARSON, K. A., SHONG, Y. K., KIM, T. Y., VIOLA, D., ELISEI, R., BENDLOVA, B., YIP, L., MIAN, C., VIANELLO, F., TUTTLE, R. M., ROBENSHTOK, E., FAGIN, J. A., PUXEDDU, E., FUGAZZOLA, L., CZARNIECKA, A., JARZAB, B., O'NEILL, C. J., SYWAK, M. S., LAM, A. K., RIESCO-EIZAGUIRRE, G., SANTISTEBAN, P., NAKAYAMA, H., CLIFTON-BLIGH, R., TALLINI, G., HOLT, E. H. & SYKOROVA, V. 2015. Association

between BRAF V600E mutation and recurrence of papillary thyroid cancer. *J Clin Oncol,* 33**,** 42-50.

XING, M., WESTRA, W. H., TUFANO, R. P., COHEN, Y., ROSENBAUM, E., RHODEN, K. J., CARSON, K. A., VASKO, V., LARIN, A., TALLINI, G., TOLANEY, S., HOLT, E. H., HUI, P., UMBRICHT, C. B., BASARIA, S., EWERTZ, M., TUFARO, A. P., CALIFANO, J. A., RINGEL, M. D., ZEIGER, M. A., SIDRANSKY, D. & LADENSON, P. W. 2005. BRAF mutation predicts a poorer clinical prognosis for papillary thyroid cancer. *J Clin Endocrinol Metab,* 90**,** 6373-9.

YAJIMA, H., LEE, K. J., ZHANG, S., KOBAYASHI, J. & CHEN, B. P. 2009. DNA double-strand break formation upon UV-induced replication stress activates ATM and DNA-PKcs kinases. *J Mol Biol,* 385**,** 800-10.

YASPO, M. L., AALTONEN, J., HORELLI-KUITUNEN, N., PELTONEN, L. & LEHRACH, H. 1998. Cloning of a novel human putative type Ia integral membrane protein mapping to 21q22.3. *Genomics,* 49**,** 133-6.

YATA, K. & ESASHI, F. 2009. Dual role of CDKs in DNA repair: to be, or not to be. *DNA Repair (Amst),* 8**,** 6-18.

YEAGER, N., KLEIN-SZANTO, A., KIMURA, S. & DI CRISTOFANO, A. 2007. Pten loss in the mouse thyroid causes goiter and follicular adenomas: insights into thyroid function and Cowden disease pathogenesis. *Cancer Res,* 67**,** 959-66.

YEN, P. M. 2001. Physiological and molecular basis of thyroid hormone action. *Physiol Rev,* 81**,** 1097-142.

YU, R., HEANEY, A. P., LU, W., CHEN, J. & MELMED, S. 2000a. Pituitary tumor transforming gene causes aneuploidy and p53-dependent and p53-independent apoptosis. *J Biol Chem,* 275**,** 36502-5.

YU, R., LU, W., CHEN, J., MCCABE, C. J. & MELMED, S. 2003. Overexpressed pituitary tumor-transforming gene causes aneuploidy in live human cells. *Endocrinology,* 144**,** 4991-8.

YU, R., REN, S. G., HORWITZ, G. A., WANG, Z. & MELMED, S. 2000b. Pituitary tumor transforming gene (PTTG) regulates placental JEG-3 cell division and survival: evidence from live cell imaging. *Mol Endocrinol,* 14**,** 1137-46.

ZABLOTSKA, L. B., NADYROV, E. A., ROZHKO, A. V., GONG, Z., POLYANSKAYA, O. N., MCCONNELL, R. J., O'KANE, P., BRENNER, A. V., LITTLE, M. P., OSTROUMOVA, E., BOUVILLE, A., DROZDOVITCH, V., MINENKO, V., DEMIDCHIK, Y., NEROVNYA, A., YAUSEYENKA, V., SAVASTEEVA, I., NIKONOVICH, S., MABUCHI, K. & HATCH, M. 2015. Analysis of thyroid malignant pathologic findings identified during 3 rounds of screening (1997-2008) of a cohort of children and adolescents from belarus exposed to radioiodines after the Chernobyl accident. *Cancer,* 121**,** 457-466.

ZATELLI, M. C., TAGLIATI, F., AMODIO, V., BURATTO, M., PELIZZO, M., PANSINI, G., BONDANELLI, M., AMBROSIO, M. R. & DEGLI UBERTI, E. C. 2010. Role of pituitary tumour transforming gene 1 in medullary thyroid carcinoma. *Anal Cell Pathol (Amst),* 33**,** 207-16.

ZHANG, X., HORWITZ, G. A., PREZANT, T. R., VALENTINI, A., NAKASHIMA, M., BRONSTEIN, M. D. & MELMED, S. 1999. Structure, expression, and function of human pituitary tumor-transforming gene (PTTG). *Mol Endocrinol,* 13**,** 156-66.

ZHAO, Z. G., GUO, X. G., BA, C. X., WANG, W., YANG, Y. Y., WANG, J. & CAO, H. Y. 2012. Overweight, obesity and thyroid cancer risk: a meta-analysis of cohort studies. *J Int Med Res,* 40**,** 2041-50.

ZHOU, C., LIU, S., ZHOU, X., XUE, L., QUAN, L., LU, N., ZHANG, G., BAI, J., WANG, Y., LIU, Z., ZHAN, Q., ZHU, H. & XU, N. 2005. Overexpression of human pituitary tumor transforming gene (hPTTG), is regulated by beta-catenin /TCF pathway in human esophageal squamous cell carcinoma. *Int J Cancer,* 113**,** 891-8.

ZHOU, C., TONG, Y., WAWROWSKY, K., BANNYKH, S., DONANGELO, I. & MELMED, S. 2008. Oct-1 induces pituitary tumor transforming gene expression in endocrine tumors. *Endocr Relat Cancer,* 15**,** 817-31.

ZHOU, Y., MEHTA, K. R., CHOI, A. P., SCOLAVINO, S. & ZHANG, X. 2003. DNA damage-induced inhibition of securin expression is mediated by p53. *J Biol Chem,* 278**,** 462-70.

ZOU, H., MCGARRY, T. J., BERNAL, T. & KIRSCHNER, M. W. 1999. Identification of a vertebrate sister-chromatid separation inhibitor involved in transformation and tumorigenesis. *Science,* 285**,** 418-22.

ZUR, A. & BRANDEIS, M. 2001. Securin degradation is mediated by fzy and fzr, and is required for complete chromatid separation but not for cytokinesis. *EMBO J,* 20**,** 792-801.

A novel mechanism of sodium iodide symporter repression in differentiated thyroid cancer

Vicki E. Smith[1], Martin L. Read[1], Andrew S. Turnell[2], Rachel J. Watkins[1], John C. Watkinson[1], Greg D. Lewy[1], Jim C. W. Fong[1], Sally R. James[1], Margaret C. Eggo[1], Kristien Boelaert[1], Jayne A. Franklyn[1] and Christopher J. McCabe[1,*]

[1]School of Clinical and Experimental Medicine, Institute of Biomedical Research and [2]School of Cancer Sciences, University of Birmingham, B15 2TH, UK

*Author for correspondence (mccabcjz@bham.ac.uk)

Accepted 13 June 2009
Journal of Cell Science 122, 3393-3402 Published by The Company of Biologists 2009
doi:10.1242/jcs.045427

Summary

Differentiated thyroid cancers and their metastases frequently exhibit reduced iodide uptake, impacting on the efficacy of radioiodine ablation therapy. PTTG binding factor (PBF) is a proto-oncogene implicated in the pathogenesis of thyroid cancer. We recently reported that PBF inhibits iodide uptake, and have now elucidated a mechanism by which PBF directly modulates sodium iodide symporter (NIS) activity in vitro. In subcellular localisation studies, PBF overexpression resulted in the redistribution of NIS from the plasma membrane into intracellular vesicles, where it colocalised with the tetraspanin CD63. Cell-surface biotinylation assays confirmed a reduction in plasma membrane NIS expression following PBF transfection compared with vector-only treatment. Coimmunoprecipitation and GST-pull-down experiments demonstrated a direct interaction between NIS and PBF, the functional consequence of which was assessed using iodide-uptake studies in rat thyroid FRTL-5 cells. PBF repressed iodide uptake, whereas three deletion mutants, which did not localise within intracellular vesicles, lost the ability to inhibit NIS activity. In summary, we present an entirely novel mechanism by which the proto-oncogene PBF binds NIS and alters its subcellular localisation, thereby regulating its ability to uptake iodide. Given that PBF is overexpressed in thyroid cancer, these findings have profound implications for thyroid cancer ablation using radioiodine.

Supplementary material available online at
http://jcs.biologists.org/cgi/content/full/122/18/3393/DC1

Key words: PBF, NIS, Iodide uptake, Thyroid cancer

Introduction

The sodium iodide symporter (NIS) is an integral membrane glycoprotein located in the basolateral plasma membrane of thyroid follicular epithelial cells. NIS is responsible for mediating iodide uptake and is consequently essential for thyroid hormone synthesis in thyroid cells. The ability of the thyroid to accumulate radioiodine has long been used to image and treat tumours of the thyroid and their metastases, distinguishing NIS as both a diagnostic and a therapeutic tool (Boelaert and Franklyn, 2003).

Thyroid carcinomas are the most common endocrine neoplasm and their annual incidence is rising (Ries et al., 2008). Although most differentiated thyroid carcinomas have a good prognosis, up to 35% recur (Mazzaferri and Kloos, 2001). Crucially, many thyroid cancers and their metastases demonstrate reduced iodide uptake in comparison to normal thyroid tissue and, even after thyrotrophin (thyroid-stimulating hormone, TSH) stimulation, 10-20% of these tumours are unable to concentrate enough radioiodine for effective therapy (Kogai et al., 2006). Tumours with reduced NIS activity are therefore generally associated with a poor prognosis. An understanding of the factors repressing NIS activity is thus important for improvement of radioiodine delivery to tumours that fail to uptake radioiodine effectively. Furthermore, such advances might have profound implications for the treatment of breast cancer and other nonthyroidal cancers currently being assessed for potential NIS-mediated radioiodine therapy (Boelaert and Franklyn, 2003).

Pituitary tumor transforming gene (*PTTG*) produces a multifunctional protein, that can transactivate basic fibroblast growth factor (FGF-2), an action that is dependent on PTTG-binding factor (PBF) (Chien and Pei, 2000). PBF, also known as PTTG1IP or c21orf3 (Yaspo et al., 1998), promotes transformation in vitro and is tumourigenic in vivo (Stratford et al., 2005). However, its exact function is not known. Heaney and colleagues initially implicated PTTG and FGF-2 in the downregulation of NIS activity (Heaney et al., 2001). Subsequently, an association between PTTG overexpression in differentiated thyroid cancers and decreased radioiodine uptake during follow-up was reported (Saez et al., 2006). PTTG and PBF are both overexpressed in thyroid and other tumours, and we have shown that high expression of each gene in thyroid cancer is independently associated with aggressive tumour behaviour (Boelaert et al., 2003; Stratford et al., 2005). We recently examined the influence of PTTG and PBF on human NIS activity and found that both inhibited iodide uptake and NIS expression in vitro. Furthermore, we used promoter studies to map the elements responsible for this transcriptional repression (Boelaert et al., 2007).

Although PTTG and PBF repressed iodide uptake in primary thyroid cells by ~70%, inhibition of NIS promoter activity approximated 40-50% (Boelaert et al., 2007). This led us to speculate that other mechanisms might exist by which PTTG and PBF regulate NIS in thyroid cells. Our data implied that PTTG repression of NIS activity is at least partially dependent on FGF-2, but that an alternative pathway exists for PBF, given that PBF also independently inhibited NIS activity, despite being unable to stimulate FGF-2 (our unpublished data). For active iodide uptake

Journal of Cell Science

to occur, NIS must be expressed, targeted and retained at the basolateral plasma membrane of polarised thyroid follicular epithelial cells (Dohan et al., 2001). A number of studies have noted that some thyroid cancers show increased intracellular expression of NIS (Castro et al., 1999b; Dohan et al., 2001; Wapnir et al., 2003). Clearly, altered post-translational regulation of NIS could contribute to a reduction in iodide uptake in thyroid cancers by influencing its subcellular localisation.

In the current investigation, we examined the subcellular localisation of NIS in relation to that of the relatively uncharacterised protein PBF. Our data suggest an entirely novel mechanism by which PBF binds to NIS and alters its subcellular localisation, thereby regulating its ability to uptake iodide.

Results

NIS colocalises with PBF

In fluorescent immunocytochemistry experiments, we determined the localisation of transiently transfected HA-tagged NIS (NIS-HA) and Myc-tagged NIS (NIS-MYC) in monkey kidney COS-7 cells. Both NIS-HA (Fig. 1Ai) and NIS-MYC (Fig. 1Aii) were expressed predominantly at the plasma membrane, but were also apparent in the cytoplasm, where they appeared to reside within intracellular vesicles. To confirm NIS plasma membrane expression, CD8 (cluster of differentiation 8) cDNA was cotransfected with NIS-HA. This encodes a co-receptor involved in antigen recognition, used as a marker for localisation to the plasma membrane (James et al., 2008). A good degree of colocalisation between NIS-HA and CD8 verified the presence of NIS at the cell membrane (Fig. 1B). To determine whether transfected NIS was functional in COS-7 cells, we assessed iodide uptake. NIS-HA transfection resulted in a significant induction of uptake compared with untransfected cells (3425±501 c.p.m. vs 391±95 c.p.m.; $P<0.001$; $n=5$). This confirmed the functionality of exogenous NIS in COS-7 cells, as has been demonstrated previously in a number of publications (Castro et al., 1999a; De la Vieja et al., 2004; De la Vieja et al., 2005; Smanik et al., 1996; Smanik et al., 1997; Van Sande et al., 2003; Zhang et al., 2005). Furthermore, the level of uptake was very similar to that demonstrated by Zhang and colleagues (Zhang et al., 2005).

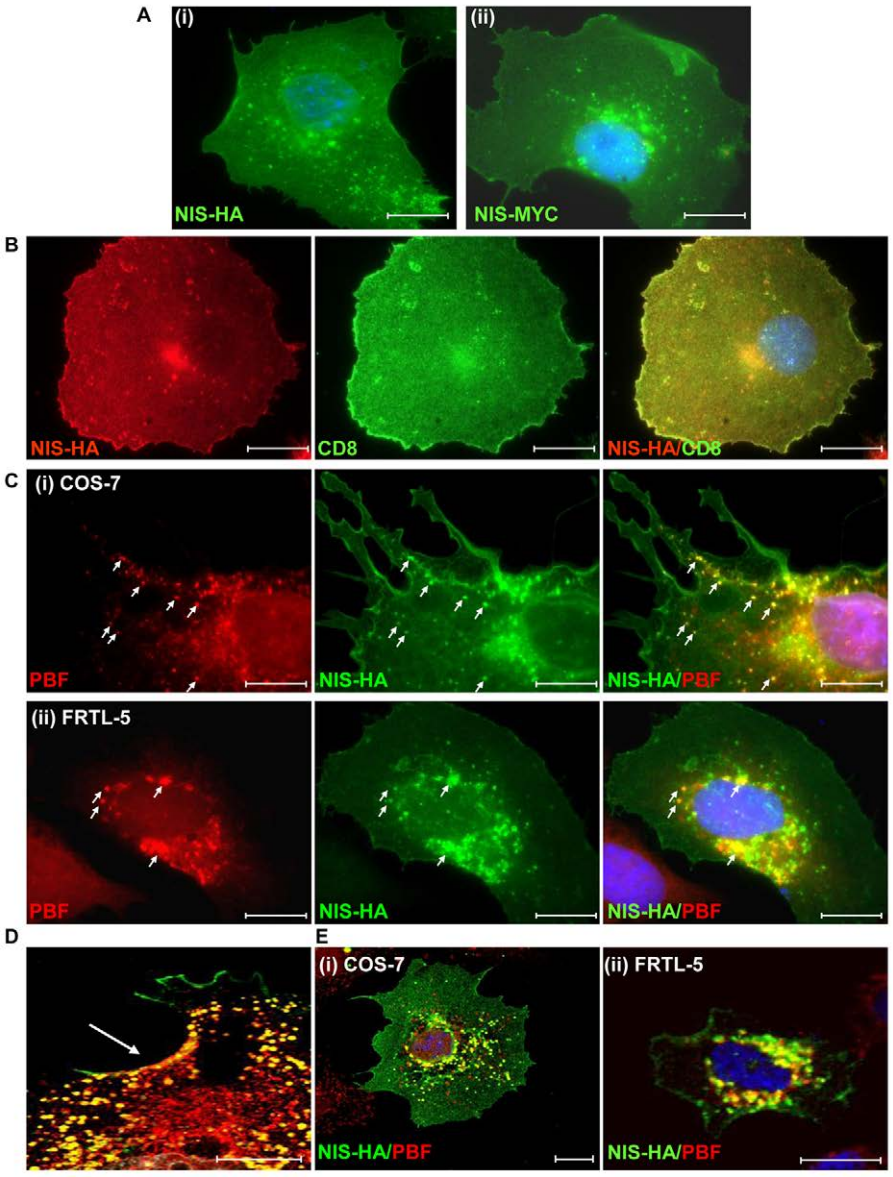

Fig. 1. NIS and PBF localisation in COS-7 and FRTL-5 cells. (A) Following transfection into COS-7 cells and detection by immunofluorescence analysis, NIS-HA (i) and NIS-MYC (ii) demonstrated a similar pattern of expression. Both proteins were located predominantly within the plasma membrane, with partial staining within intracellular vesicles. (B) Coexpression of NIS-HA (red) with the plasma membrane marker CD8 (green) resulted in a high degree of colocalisation as seen in the merged image (yellow). (C) Representative fluorescence immunocytochemistry experiments examining staining of PBF (red) and NIS-HA (green) following transient transfection in COS-7 (i) and FRTL-5 (ii) cells. PBF is predominantly expressed within cytoplasmic vesicles. Merged images demonstrate strong colocalisation between PBF and NIS (yellow) (arrows). (D) Enlarged merged confocal image of PBF (red) and NIS-HA (green) colocalisation (yellow) at the cell surface (arrowed) of a COS-7 cell. (E) Confocal microscopy of NIS and PBF localisation in representative COS-7 and FRTL-5 cells. Colocalisation of PBF and NIS was confirmed by yellow staining in the merged images. Nuclei are visualised in blue with Hoechst 33342 stain in the merged images. Scale bars: 20 μM.

We then assessed the localisation of transiently transfected PBF and NIS-HA in COS-7 cells and rat-thyroid-derived FRTL-5 cells. In COS-7 cells, PBF was expressed at relatively low levels in the nucleus, whereas the majority of PBF protein was concentrated within intracellular vesicles in the cytoplasm (Fig. 1Ci, arrows). Merged images demonstrated strong colocalisation between PBF and NIS, particularly within vesicles. Colocalisation of NIS and PBF was also apparent in the thyroid cell model of FRTL-5 cells (Fig. 1Cii), which demonstrate endogenous NIS expression and iodide uptake (Kogai et al., 1997; Riedel et al., 2001; Schmutzler et al., 1997; Spitzweg et al., 1999). Sites of coincident PBF and NIS staining at the cell membrane were also observed in COS-7 cells (Fig. 1D). Confocal microscopy further delineated the marked overlap between NIS and PBF localisation within COS-7 and FRTL-5 cells (Fig. 1E).

PBF binds NIS in vitro

Having observed strong evidence of PBF and NIS colocalisation in both thyroid and non-thyroidal cell lines, we next investigated whether the two proteins were able to bind in vitro. We performed pull-down assays with in vitro translated L-α-[^{35}S]methionine-labelled NIS and glutathione-S-transferase (GST)-tagged PBF. Binding reactions consistently demonstrated the interaction of labelled NIS with GST-PBF but not with the GST control (Fig. 2A).

Subsequently, coimmunoprecipitation assays were used to assess this interaction in a cellular environment. Following the transient transfection of HA-tagged PBF (PBF-HA) and NIS-MYC into COS-7 cells, NIS was precipitated with an anti-Myc antibody. Coprecipitation of PBF-HA with NIS-MYC was observed by probing with an anti-HA antibody following western blotting (Fig. 2B). By contrast, PBF was not detected in controls in which NIS-MYC and vector-only (VO) or PBF-HA and VO were transfected (Fig. 2B). The reciprocal coimmunoprecipitation was performed using the anti-HA antibody for precipitation of PBF-HA and immunoblotting for NIS-MYC, which similarly resulted in successful coimmunoprecipitation (Fig. 2C, arrows). These results confirm that NIS and PBF not only colocalise, but also interact within these cells.

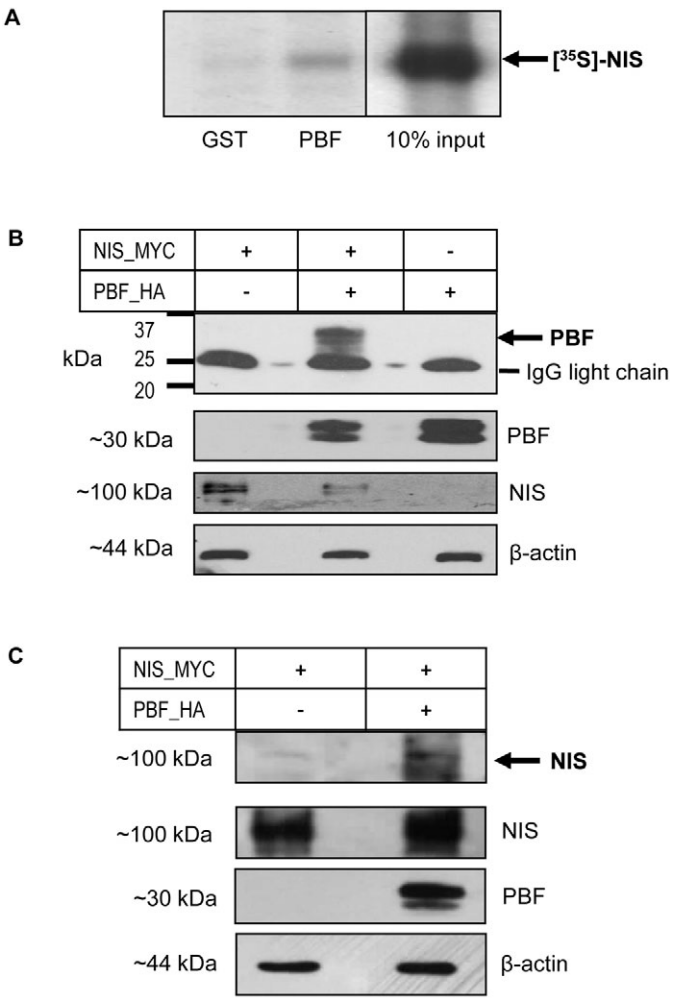

Fig. 2. PBF binds NIS in vitro. (A) Pull-down assay showing in vitro translated L-α- [^{35}S]methionine-labelled NIS binding GST-tagged PBF versus a GST-only control. (B) Coimmunoprecipitation assays in COS-7 cells transfected with NIS-MYC and VO, PBF-HA and VO, or NIS-MYC and PBF-HA. A band corresponding to PBF (arrowed) was observed at approximately 30 kDa when NIS-MYC and PBF-HA were cotransfected but was not present when either NIS-MYC or PBF-HA were transfected with VO. Analysis of total protein cell lysate shown below demonstrates the presence of NIS-MYC or PBF-HA in each sample along with a β-actin loading control. (C) Reciprocal assay following transfection of NIS-MYC and VO or NIS-MYC and PBF-HA. NIS-MYC was coprecipitated along with PBF-HA and detected as a band at approximately 100 kDa (arrow).

PBF alters the subcellular localisation of NIS

In COS-7 cells transfected with NIS-HA (Fig. 3Ai), NIS-HA was localised predominantly within the plasma membrane, with partial staining within intracellular vesicles. Endogenous PBF was mainly localised within cytoplasmic vesicles, with some apparent nuclear staining. However, when PBF was cotransfected with NIS-HA, there was an increase of NIS staining within intracellular vesicles and a concomitant reduction in membrane staining (Fig. 3Aii). Given that PBF and NIS bound each other in pull-down and coimmunoprecipitation assays, we therefore investigated by quantitative means whether PBF overexpression was associated with diminished NIS localisation at the cell membrane, where NIS is functional. We transfected COS-7 cells with NIS-HA, and either VO control or human PBF. Cell surface biotinylation assays confirmed a reduction in plasma membrane expression of NIS following PBF transfection compared with VO treatment (32±9% reduction; P=0.018; n=3) (Fig. 3Bi). By contrast, total NIS-HA expression was not significantly altered by PBF overexpression compared with VO (2±3% reduction; P=0.529; n=3) (Fig. 3Bii). Hence, when PBF expression is increased in COS-7 cells, plasma membrane expression of NIS decreases.

Colocalisation of PBF, NIS and CD63

Detailed examination of our patterns of intracellular staining for PBF and NIS (as shown in Figs 1 and 3) raised the possibility that these proteins were localised to late endosomes. To assess this hypothesis, we examined expression of the late endosome marker CD63, a member of the tetraspanin family commonly associated with clathrin-dependent trafficking. We transfected COS-7 cells with NIS-HA, and examined its relationship to endogenous CD63. Merged images revealed a high degree of colocalisation (Fig. 4Ai). We performed analogous studies with PBF and CD63, which revealed similar patterns of colocalisation within late endosomes (Fig. 4Aii). Finally, we assessed staining of caveolin-1, the main constituent of caveolae which acts as a regulator of caveolae-

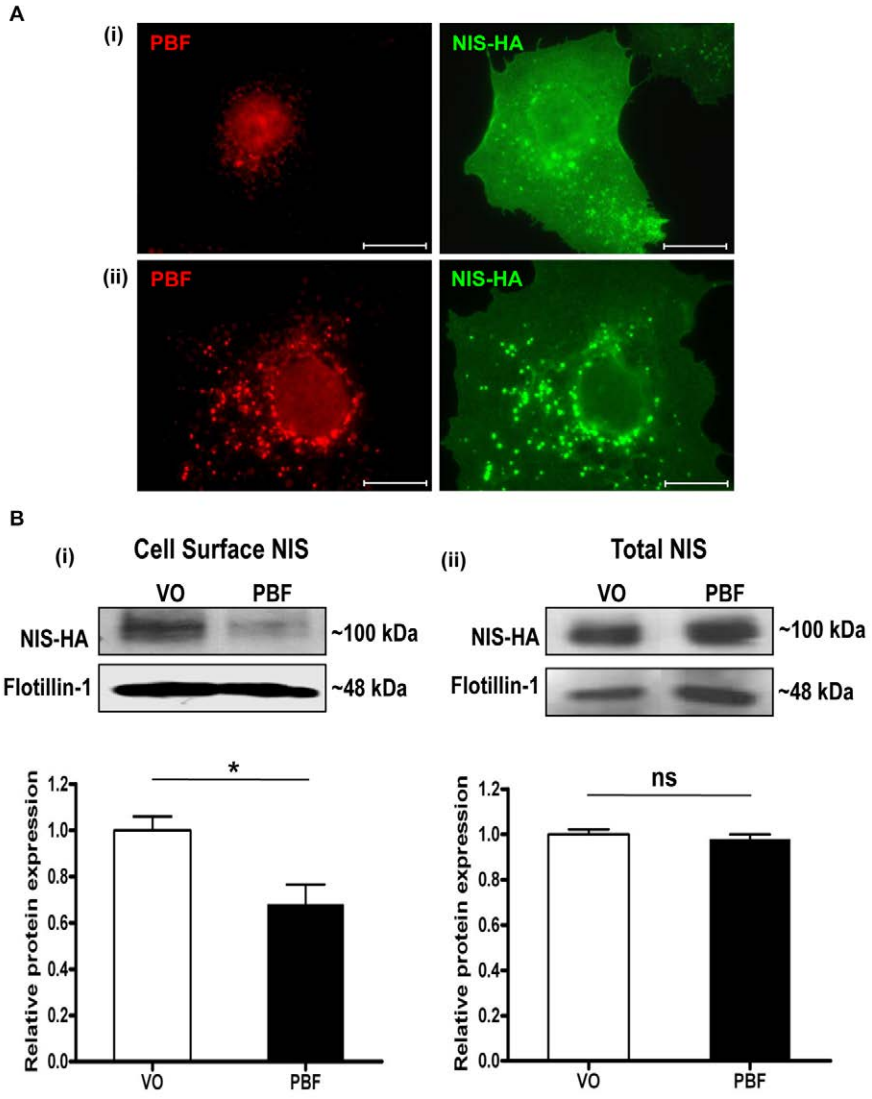

Fig. 3. PBF alters the subcellular localisation of NIS. (A) (i) Immunofluorescent detection of NIS-HA and endogenous PBF in cells transfected with NIS-HA and VO control. (ii) PBF overexpression is associated with an increase in NIS staining within intracellular vesicles. Scale bars: 20 μM. (B) Cell-surface biotinylation assay in COS-7 cells transfected with a VO control or with human PBF. (i) Representative immunoblot analysis of surface-biotinylated polypeptides precipitated with streptavidin-agarose beads and probed with anti-HA antibody, which revealed HA-tagged human NIS detection at around 100 kDa. Flotillin-1 was used as a marker of membrane protein expression to determine loading between samples. (ii) Total NIS-HA protein expression. Graphs indicate mean differences in cell-surface and total expression of NIS (n=3 separate scanning densitometry experiments were performed). *P<0.05; ns, not significant.

dependent lipid trafficking and endocytosis. When we examined caveolin-1 localisation in COS-7 cells, we found no overlap with either PBF or NIS expression (Fig. 4Aiii). Confocal microscopy confirmed the strong colocalisation apparent between NIS, PBF and CD63 (Fig. 4Bi), and the lack of association between NIS, PBF and caveolin-1 (Fig. 4Bii). Thus, NIS and PBF colocalise with CD63 but not with caveolin-1, suggesting that clathrin-dependent rather than caveolin-dependent endocytosis is responsible for the internalisation of these proteins.

Localisation of PBF deletion mutants

To investigate the relationship between PBF and NIS further, we constructed three deletion mutants of PBF. The PBF protein is extremely poorly characterised, and has no significant homology to other human proteins. A putative signal peptide lies at the N-terminus, followed by a putative PSI domain (a cysteine-rich region common to plexins, semaphorins and integrins) between amino acids 39 and 92, and a potential transmembrane region between residues 95 and 122 (Fig. 5A). At the C-terminus, predicted nuclear localisation and tyrosine-based sorting signals lie between amino acids 149 and 174. Given the lack of functional data on PBF, we therefore created three HA-tagged deletion mutants. Mutant 1 (M1) lacked the C-terminal 30 amino acids (149-180), which have previously been shown to mediate its binding to PTTG (Chien and Pei, 2000). Mutant 2 (M2) had a deletion of residues 29-93, which encompassed part of the signal peptide and the putative PSI domain, and Mutant 3 (M3) lacked amino acids 94-149, containing the potential transmembrane domain (Fig. 5A).

The localisation of each of the mutants in comparison to HA-tagged wild-type (WT) PBF was initially assessed following transient transfection into COS-7 cells. Confocal images once more identified WT PBF predominantly within intracellular vesicles (Fig. 5Bi). By contrast, M1 was located almost exclusively in the plasma membrane. M2 and M3 appeared to be expressed predominantly in the endoplasmic reticulum (Fig. 5Bi). Strong colocalisation of M1 was observed with the CD8 plasma membrane marker whereas no significant colocalisation was seen with WT PBF, M2 or M3 (Fig. 5Bii). Similarly, M2 and M3 demonstrated a high degree of colocalisation with endogenous protein disulphide isomerase (PDI), a marker for the endoplasmic reticulum, whereas WT PBF and M1 showed minimal costaining

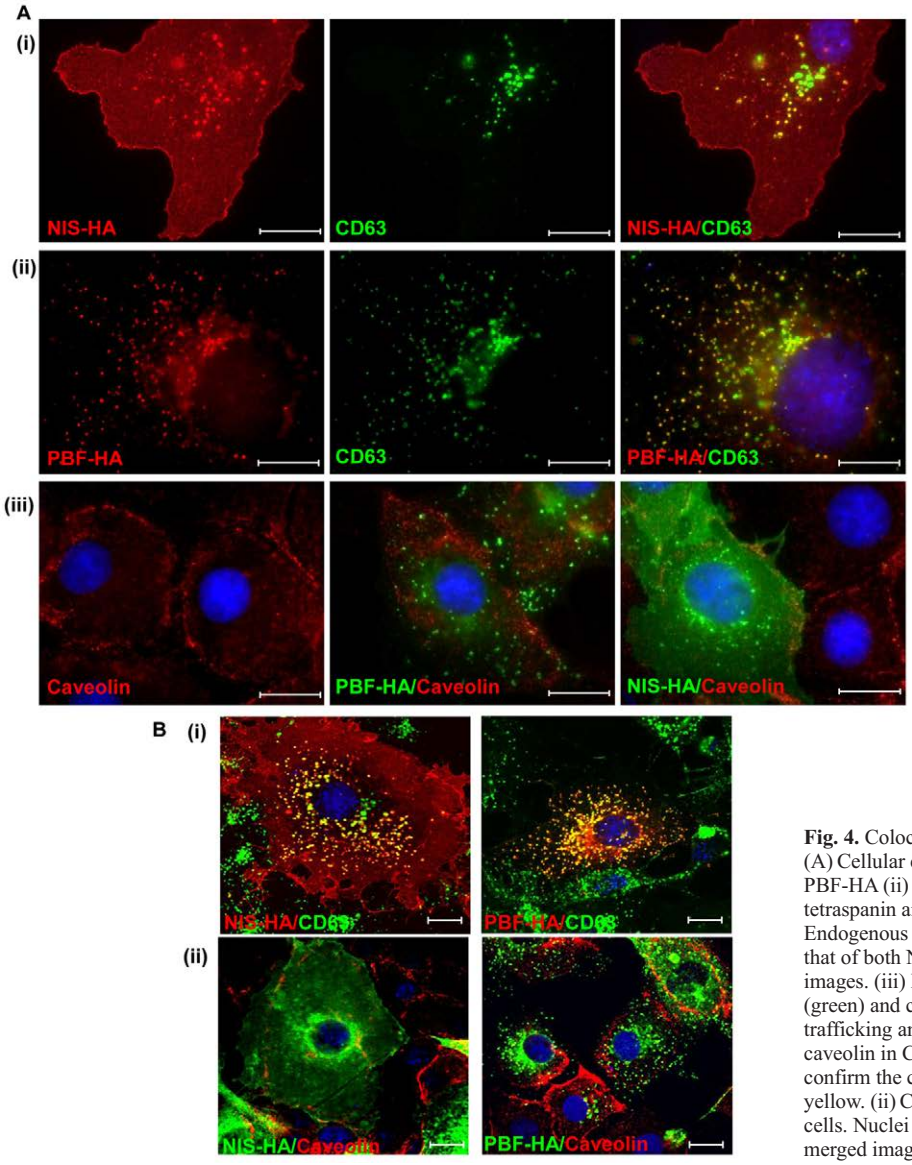

Fig. 4. Colocalisation studies of NIS, CD63, PBF and caveolin. (A) Cellular expression of transiently transfected NIS-HA (i) and PBF-HA (ii) (both red) with endogenous CD63 (green), a tetraspanin and a marker of late endosomes, in COS-7 cells. Endogenous CD63 staining in late endosomes is coincident with that of both NIS and PBF, as indicated by yellow staining in merged images. (iii) Relationship between PBF-HA (green), NIS-HA (green) and caveolin-1 (red), a marker of caveolae-dependent lipid trafficking and endocytosis. Neither PBF nor NIS colocalises with caveolin in COS-7 cells. (B) (i) Confocal microscopy was used to confirm the colocalisation of NIS and PBF with CD63, shown in yellow. (ii) Confocal images of NIS, PBF and caveolin in COS-7 cells. Nuclei are visualised in blue with Hoechst 33342 stain in the merged images. Scale bars: 20 µM.

(Fig. 5Biii). Notably, unlike WT PBF, none of the mutants colocalised with CD63 (Fig. 5Biv), strongly suggesting they were not expressed within late endosomes.

PBF, NIS and iodide uptake

We next examined the colocalisation of WT and mutant PBF with NIS. HA-tagged WT PBF and the three mutants were each transiently transfected into COS-7 cells along with NIS-MYC. Localisation of WT PBF and the mutants (Fig. 6Ai) was as described previously (Fig. 5Ai). Whilst NIS showed intense staining within intracellular vesicles in the presence of WT PBF, it remained predominantly membranous when coexpressed with each of the mutants (Fig. 6Aii). Merged images demonstrated again WT PBF colocalisation with NIS in intracellular vesicles (Fig. 6Aiii). M1 showed strong colocalisation with NIS at the cell membrane, but not intracellularly, whereas M2 and M3 failed to significantly colocalise with NIS (Fig. 6Aiii).

Finally, we investigated the effect of altered PBF localisation upon endogenous NIS activity. We therefore used FRTL-5 thyroid cells, which show significant endogenous iodide uptake (Kogai et al., 1997; Riedel et al., 2001; Schmutzler et al., 1997; Spitzweg et al., 1999) and show colocalisation of NIS and PBF (Fig. 1). We first confirmed that FRTL-5 cells express endogenous PBF (supplementary material Fig. S1). Subsequently, we manipulated PBF expression through transient transfection of WT and mutant PBF constructs. Immunofluorescence analyses established that the localisation of WT and mutant PBF was consistent with that observed in COS-7 cells (Fig. 6B): WT PBF was apparent in intracellular vesicles, M1 localised to the membrane, and M2 and M3 localised to the ER. Iodide-uptake experiments were then performed. Data from FRTL-5 cells were normalised to iodide uptake in VO controls, which gave a mean count of 1029 c.p.m. after incubation with 0.05 µCi ^{125}I for 1 hour. WT PBF repressed iodide uptake into FRTL-5 cells by 39.4±5% (P<0.001; n=10) compared with VO control (Fig. 6C). By contrast, all three deletion mutants of PBF, which do not localise within intracellular vesicles in COS-7 or FRTL-5 cells, lost the ability to inhibit NIS activity (M1, 104.3±13%; M2, 89.2±11%; M3, 109.6±14%; P=NS compared with VO control) (Fig. 6C).

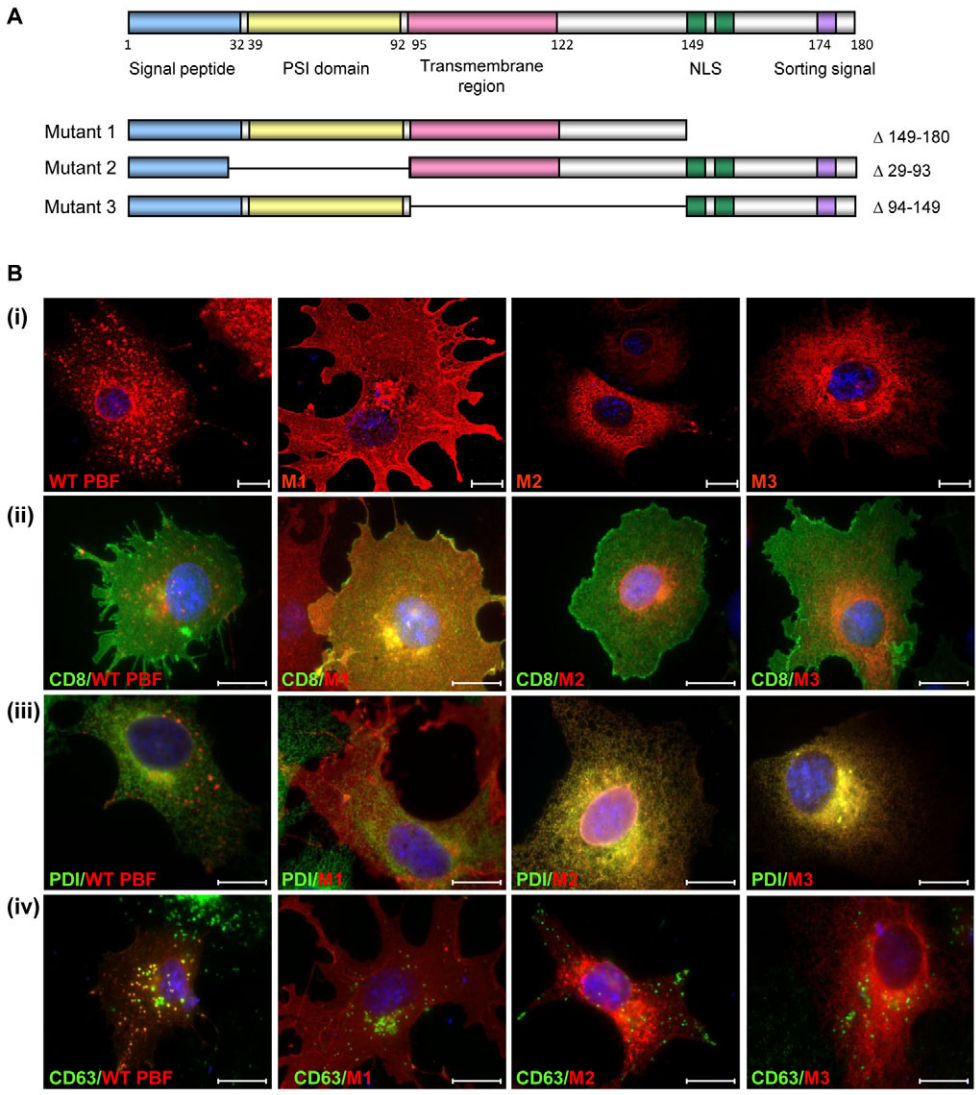

Fig. 5. Localisation of PBF deletion mutants. (A) Putative functional domains of WT PBF, as well as three deletion mutants M1, M2 and M3. NLS, nuclear localisation signal. Site-directed mutagenesis was used to delete the C-terminal 30 amino acids (149-180) for M1. M2 had a deletion of amino acids 29-93 and M3 lacked amino acids 94-149, containing the potential transmembrane domain. (B) (i) Confocal images demonstrating the localisation of each of the mutant PBF proteins compared with wild-type PBF in COS-7 cells. M1 is predominantly in the cell membrane whereas M2 and M3 appear to be in the endoplasmic reticulum. (ii) Coexpression of CD8 confirmed the presence of M1 in the plasma membrane. (iii) Endogenous PDI staining verified endoplasmic reticulum expression of M2 and M3. (iv) Intracellular expression of WT and mutated PBF with CD63 in COS-7 cells. Unlike the WT, none of the mutants show significant colocalisation with CD63. Scale bars: 20 μM.

Taken together, these data support the hypothesis that PBF and NIS colocalise within late endosomes, and that upregulation of PBF redistributes NIS away from the plasma membrane into these organelles, a mechanism that significantly represses cellular iodide uptake.

Discussion

The regulation of membrane transport proteins is an intricate process, and NIS regulation is characteristically complex. As an integral membrane glycoprotein which mediates active iodide transport into thyroid cells, NIS acts as the crucial first step in thyroid hormone biosynthesis (Boelaert and Franklyn, 2003; Dohan et al., 2003). The ability of the thyroid to accumulate iodide has provided an effective means for therapeutic doses of radioiodine to target and destroy iodide-transporting differentiated thyroid cancers and their metastases. However, most thyroid tumours exhibit reduced iodide uptake and a number of mRNA (Lazar et al., 1999; Park et al., 2000; Ringel et al., 2001; Ryu et al., 1999; Smanik et al., 1997; Ward et al., 2003) and protein (Caillou et al., 1998; Faggiano et al., 2007; Gerard et al., 2003; Jhiang et al., 1998; Trouttet-Masson et al., 2004) studies have reported decreased NIS expression in thyroid cancers, suggesting that the reduction in iodide uptake is due to a transcriptional effect.

By contrast, several other studies have shown either normal, or even increased levels of NIS mRNA (Arturi et al., 1998; Luciani et al., 2003; Saito et al., 1998; Tanaka et al., 2000) or protein (Dohan et al., 2001; Saito et al., 1998; Wapnir et al., 2003) expression in thyroid cancer. However, immunohistochemical analyses have detected NIS protein that was not located predominantly in the basolateral membrane, as found in normal thyroid tissue, but was principally in the cytoplasm (Castro et al., 1999b; Dohan et al., 2001; Wapnir et al., 2003). This suggests that the reduction in iodide uptake in thyroid cancer is at least partially attributable to altered NIS trafficking and subcellular localisation, which might therefore be more relevant than expression levels per se. Understanding the factors regulating NIS localisation and activity in thyroid tumours is thus important in improving radioiodine delivery to those tumours that fail to uptake radioiodine effectively.

At present, little is known about the regulation of NIS trafficking. In addition to stimulating cAMP-mediated NIS expression, TSH is also required for post-translational regulation of NIS (Riedel et al., 2001). Studies using FRTL-5 cells have

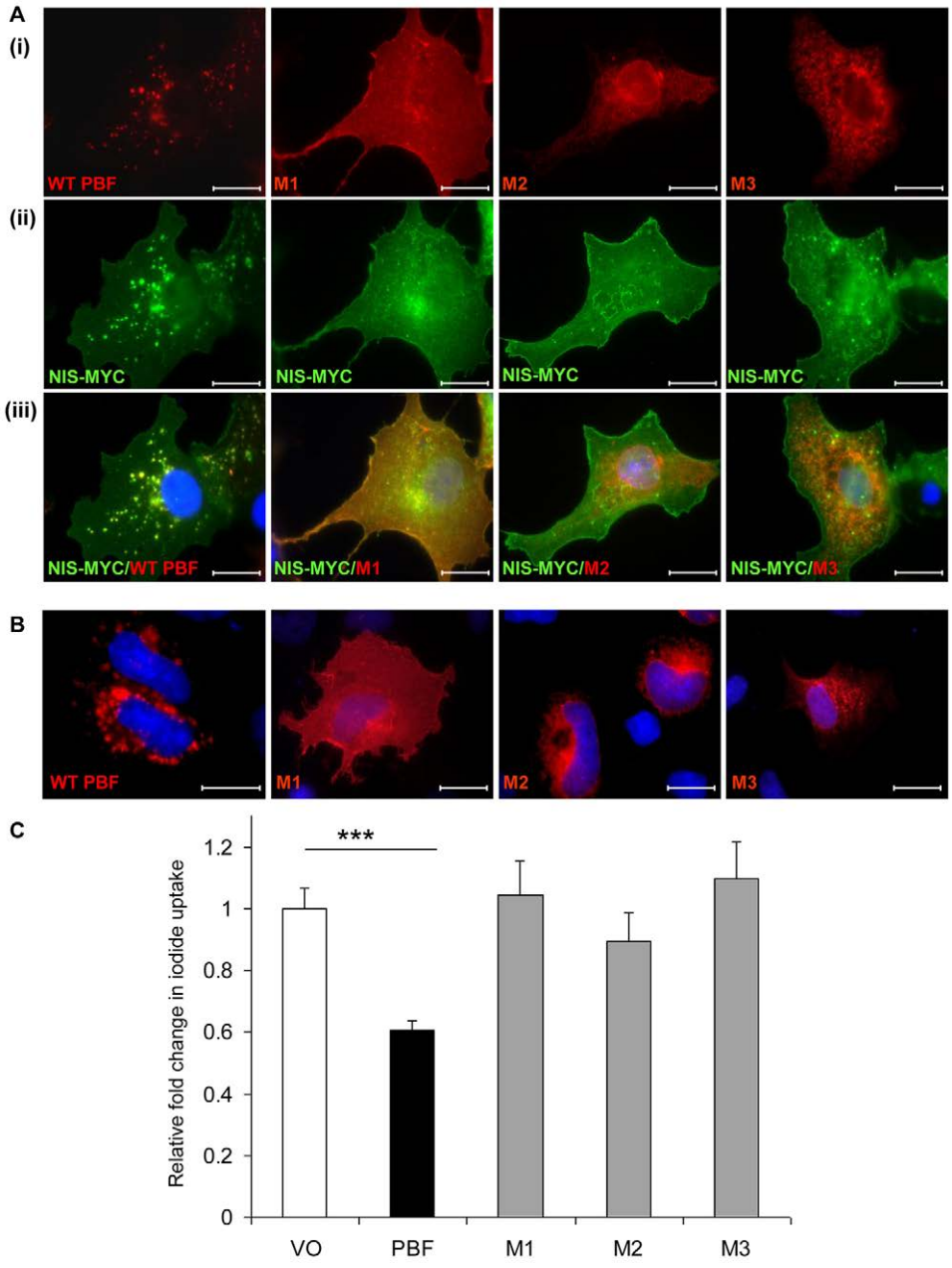

Fig. 6. The effect of PBF on NIS function. (A) Examination of the subcellular localisation of WT and mutated HA-tagged PBF in COS-7 cells (i), Myc-tagged NIS (ii) and colocalisation (iii). WT PBF predominantly colocalises with NIS within late endosomes. M1 colocalises with NIS at the cell membrane, whereas M2 and M3 fail to show any significant colocalisation with NIS. (B) Confocal images demonstrating the localisation of WT and mutant PBF in FRTL-5 cells. Scale bars: 20 μM. (C) Iodide-uptake studies in rat thyroid FRTL-5 cells transfected with WT PBF and mutants M1, M2 and M3. Graph shows c.p.m. values normalised to that of the VO control. ***P<0.001.

alluded to a mechanism by which NIS is located in the plasma membrane of thyroid cells in the presence of TSH, but is redistributed into intracellular vesicles upon TSH withdrawal. TSH is thus required for either the targeting of NIS to the plasma membrane or its retention there (Kaminsky et al., 1994; Kogai et al., 1997; Riedel et al., 2001). NIS is a phosphoprotein that has demonstrated different patterns of phosphorylation in FRTL-5 cells maintained in the presence or absence of TSH (Riedel et al., 2001). Phosphorylation of the C-terminus has been proposed to influence plasma membrane targeting of NIS (Dohan et al., 2005). However, although a number of phosphorylated residues have been confirmed, none has been shown to affect NIS cell membrane trafficking (Vadysirisack et al., 2007). A recent study assessing NIS regulation in breast cancer demonstrated that phosphatidylinositol-3 kinase (PI3K) activation interferes with cell-surface trafficking and function of all-*trans* retinoic acid and hydrocortisone (tRAH)-induced endogenous NIS, as well as transiently expressed exogenous NIS, in the MCF-7 human mammary carcinoma cell line (Knostman et al., 2007).

In the present study, we have assessed a potential role for PBF in the post-translational regulation of NIS activity, given its ability to repress iodide uptake. Although NIS was expressed at the cell surface, it was also present in intracellular vesicles reminiscent of those previously described (Kaminsky et al., 1994; Riedel et al., 2001). Similarly to NIS, PBF is also a predicted integral membrane glycoprotein (Yaspo et al., 1998). PBF was predominantly located in similar vesicular structures to NIS, and was also apparent at the plasma membrane. Our description of PBF localisation differs from a previous report (Chien and Pei, 2000), which did not describe vesicular staining. In common with this earlier study, we did observe a degree of nuclear localisation. However, our current and previous (Stratford et al., 2005) investigations into PBF suggest that the

protein is highly expressed in the cytoplasm. Validation of our antibody assessment of PBF localisation within intracellular vesicles is provided in supplementary material Fig. S2.

Given that PBF and NIS demonstrated strong colocalisation within such vesicles, we investigated whether PBF could bind NIS in vitro using pull-down and coimmunoprecipitation assays. GST-tagged PBF consistently pulled down [^{35}S]-labelled NIS, and PBF-HA coprecipitated with NIS-MYC in COS-7 cells, indicating that the proteins can interact. Critically, increased expression of PBF in COS-7 cells was accompanied by reduced plasma membrane expression of NIS, as determined through cell-surface biotinylation assays. This was in agreement with our immunofluorescent microscopy studies, which suggested an increased vesicular localisation of NIS in response to augmented PBF expression. Thus, NIS and PBF colocalise, bind each other, and PBF is able to alter the subcellular localisation of NIS. The physiological relevance of this phenomenon is a direct one. PBF is overexpressed in differentiated thyroid cancers (Stratford et al., 2005), which as a consequence would be expected to have a lower ability to uptake iodide, and hence a poorer response to radioiodine treatment. To test this hypothesis, it would therefore be interesting in future studies to assess PBF and NIS expression and localisation in a large series of differentiated thyroid tumours and to relate this to clinical outcome.

To investigate the vesicles in which PBF and NIS colocalised, we assessed CD63 staining. CD63 is a tetraspanin involved in protein trafficking and is located in a number of intracellular structures, including late endosomes and lysosomes, in addition to the cell membrane. At the C-terminus, CD63 has a YxxΦ motif, a tyrosine-based sorting signal, which has been shown to interact with adaptor protein (AP) complexes, thereby linking trafficking of CD63 to clathrin-dependent pathways (Berditchevski and Odintsova, 2007). We determined that both PBF and NIS showed a strong degree of colocalisation with CD63. Based on these findings, the presence of a YxxΦ motif at the C-terminus of PBF, and the fact that neither PBF nor NIS colocalises with caveolin-1, a regulator of caveolae-dependent lipid trafficking and endocytosis, we propose that PBF and NIS are indeed enriched within late endosomes, and use a clathrin-pit-mediated mechanism of internalisation.

NIS has a long half-life, estimated at 3-5 days (Riedel et al., 2001), and a hence a mechanism of post-translational regulation of activity would allow cells to respond to, and regulate their need for, iodide uptake over a much shorter timeframe. Indeed, we observed significant internalisation of NIS within 48 hours of PBF transfection. Membrane vesicles, which have been reported to contain NIS, were enriched for plasma membrane content, suggesting an endocytosis-mediated pathway of NIS regulation (Kaminsky et al., 1994). Our data shed new light on this mechanism, in that we have identified a protein that appears to significantly modulate this process.

A final strand of supporting evidence that supports our hypothesis came from iodide uptake studies in rat thyroid FRTL-5 cells. The protein structure of PBF is very poorly understood, and hence we constructed three PBF mutants, lacking the C-terminal YxxΦ motif (M1), a putative signal peptide and the putative PSI domain (M2), and the potential transmembrane region (M3). All three mutants lost vesicular enrichment, and failed to colocalise significantly with CD63 or with NIS. Iodide-uptake assays in FRTL-5 cells complemented our previous finding in human primary thyroid cells that PBF represses iodide uptake (Boelaert et al., 2007). The magnitude of effect was ~40%, which contrasts with our conservative estimate of transfection efficiency of 15-25%. This suggests either that we might be underestimating transfection efficiency by focusing only on strongly fluorescent GFP expression, or that other mechanisms exist (e.g. paracrine regulation of surrounding cell function). However, this is beyond the scope of the present investigation. In contrast to WT PBF, all three mutants failed to significantly influence iodide uptake compared with the control. This suggests that PBF requires endosomal entry to modulate NIS localisation and function. When the protein structure of PBF is resolved, it will be important to perform more subtle mutation analysis, investigating point mutations targeting specific and characterised domains, allowing us to elucidate this mechanism further.

One caveat to these studies is that because it is not known what regulates PBF, we are unable to manipulate its endogenous expression, and hence have used a largely exogenous system in COS-7 cells. Furthermore, immunofluorescence for native NIS expression is technically challenging in FRTL-5 cells. For this reason, most studies of NIS in the literature have focused on COS-7 cell manipulations. Indeed, in our hands, NIS was entirely functional in COS-7 cells, yielding extremely similar iodide uptake to that previously reported by Zhang and co-workers (Zhang et al., 2005).

Overall, the clinical relevance of PBF repression of NIS activity relates to its likely influence upon the efficacy of radioiodine therapy. The ability of the thyroid to accumulate iodide provides the basis for radioiodine ablation of iodide-transporting differentiated thyroid cancers and their metastases. Taken together, we propose that through downregulation of NIS via alteration of its subcellular localisation, increased PBF could fundamentally influence the prognosis of differentiated thyroid cancers, at least in part, through affecting their sensitivity to ablative radioiodine therapy.

Materials and Methods

Plasmids and mutagenesis

The full-length human NIS cDNA was kindly provided by John Morris (Mayo Graduate School of Medicine, Mayo Clinic, Rochester, MN) (Castro et al., 1999a). This was inserted into the *Eco*RI and *Xho*I restriction sites of the pcDNA3.1+ vector (Invitrogen, Carlsbad, CA) and simultaneously tagged on the 3′ end with either the HA epitope using the forward primer, 5′-GCC GAA TTC CCA CCA TGG AGG CCG TGG AGA CC-3′ and reverse primer, 5′-CGG CTC GAG TCA AGC GTA GTC TGG GAC GTC GTA TGG GTA GAG GTT TGT CTC CTG CTG G-3′ (NIS-HA), or the Myc epitope using the same forward primer, and the reverse primer, 5′-CGG CTC GAG TCA GGA TCC CAG GTC CTC CTC GGA AAT CAG CTT CTG CTC AAG GTT TGT CTC CTG CTG G-3′ (NIS-MYC).

Plasmids containing the full-length PBF cDNA with (PBF-HA) and without (PBF) a HA tag have previously been described (Stratford et al., 2005). Three deletion mutants of PBF were created by mutating the PBF-HA plasmid using the QuikChange Site-Directed Mutagenesis Kit (Stratagene, Cambridge, UK) using the following primers: M1_forward, 5′-GAGAGGCGGATACGGCAGGAGGAATACCCATAC-GACGTCCCAGACTAC-3′; M1_reverse, 5′-GTAGTCTGGGACGTCGTATG-GGTATTCCTCCTGCCGTATCCGCCTCTC-3′; M2_forward, 5′-CTCCTGCT-GCTCATCCCGAACTTTGAGGCGCTGATC-3′; M2_reverse, 5′-GATCAGCGC-CTCAAAGTTCGGGATGAGCAGCAGGAG-3′; M3_forward, 5′-GCTGGG-GAGTTTGTTGGGTGCGGAGAGCAGAGATGAAGAC-3′; M3_reverse, 5′-GTCTTCATCTCTGCTCTCCGCACCCAACAAACTCCCCAGC-3′.

Additionally, cDNA encoding CD8 was kindly provided by Barbara Reaves (Department of Biology and Biochemistry, University of Bath, UK) (James et al., 2008).

Cell lines and transient transfection

FRTL-5 cells are a nontransformed rat thyroid cell line, which were grown in modified Coon's F-12 medium as described (Ambesi-Impiombato et al., 1980) (Gibco, Paisley, Scotland). The medium was supplemented with TSH (300 mU/l), insulin (100 μg/l), penicillin (10^5 U/l), streptomycin (100 mg/l) and 5% fetal bovine serum (FBS).

The COS-7 African Green monkey kidney epithelial cell line was maintained in DMEM medium (Gibco) supplemented with 10% FBS, penicillin (10^5 U/l) and

streptomycin (100 mg/l). The H1299 non-small cell lung carcinoma cell line was maintained in RPMI 1640 medium (Gibco) supplemented with 10% FBS, sodium pyruvate (1 mM), glucose (3.5 g/l), HEPES (10 mM), penicillin (10^5 U/l) and streptomycin (100 mg/l).

Cells were transfected using Fugene 6 reagent (Roche, Indianapolis, IN) following the manufacturer's instructions at a 3:1 reagent:DNA ratio. For iodide-uptake assays, immunofluorescence staining, coimmunoprecipitation assays and cell-surface biotinylation assays, cells were seeded in 24-well plates, six-well plates with sterile coverslips, T25 flasks or T75 flasks, respectively, and transfected with 0.5 μg, 2 μg, 5 μg or 15 μg DNA after 24 hours.

The pMax-GFP plasmid (Amaxa, Cologne, Germany) was used to determine the transfection efficiency of FRTL-5 cells. Routinely, transfection efficiency was between 15 and 25% in FRTL-5 cells (see supplementary material Fig. S3).

Immunofluorescence staining

Medium was removed 48 hours after transfection, and cells were washed with phosphate-buffered saline (PBS). Cells were fixed for 20 minutes at room temperature in 0.1 M phosphate buffer (pH 7.4) containing 2% paraformaldehyde, 2% glucose and 0.02% sodium azide. After rinsing twice in PBS, cells were permeabilised in 100% chilled methanol for 10 minutes and then blocked with 10% newborn calf serum (NCS) in PBS for 30 minutes at room temperature.

Incubation with primary antibody was performed at room temperature for 1 hour in 1% BSA. The following antibodies were used: rabbit polyclonal anti-HA (Y-11) antibody (Santa Cruz Biotechnology, Santa Cruz, CA), mouse monoclonal anti-HA.11 antibody (Covance Research Products, Emeryville, CA), rabbit polyclonal anti-PBF antibody (made by Eurogentec, Seraing, Belgium) for our laboratory using the full-length PBF protein as an epitope), mouse monoclonal anti-human CD8 antibody (UCHT4; Ancell Corporation, Bayport, MN), mouse monoclonal anti-protein disulphide isomerase (PDI) antibody (Stressgen, San Diego, CA), mouse monoclonal anti-CD63 antibody (kindly provided by Fedor Berditchevski, School of Cancer Sciences, University of Birmingham, Birmingham, UK), mouse monoclonal anti-Myc-Tag (9B11) antibody (Cell Signaling Technology, Danvers, MA), and rabbit anti-caveolin (kindly provided by Melissa Westwood, University of Manchester, UK).

Cells were rinsed three times with PBS before a further 1 hour incubation with the secondary antibodies, Alexa-Fluor 488-conjugated goat anti-mouse IgG and Alexa-Fluor-594-conjugated goat anti-rabbit IgG (Invitrogen) at 1:250 in 1% BSA, with 1% NCS and Hoechst 33342 stain for nuclei (1:1000). Finally, cells were rinsed with PBS three times and coverslips mounted onto slides using Dako Fluorescent Mounting Solution (Dako, Glostrup, Denmark).

Conventional microscopy was performed using a 100× objective on a Zeiss Axioplan fluorescent microscope (Zeiss, Germany). A Zeiss confocal LSM 510 microscope with a 63× objective was used to perform confocal microscopy.

In vitro transcription: translation and glutathione-S-transferase (GST) pull-down assays

The TNT Coupled Reticulocyte Lysate System (Promega, Madison, WI) was used to express protein from the NIS-HA plasmid following the manufacturer's instructions. The following reaction components were assembled: 50 μl TNT Rabbit Reticulocyte Lysate, 4 μl TNT Reaction Buffer, 2 μl amino acid mixture (minus methionine; 1 mM), 4 μl L-α-[^{35}S]methionine, 1 μl RNasin Ribonuclease Inhibitor (40 U/μl), 2 μg plasmid DNA, 2 μl TNT RNA Polymerase (T7) and 29 μl nuclease-free water. The reaction was incubated at 30°C for 2 hours.

PBF was expressed as a fusion protein with glutathione-S-transferase (GST) from a pGEX plasmid (Amersham) as described previously (Turnell et al., 2000). Along with a GST-only control, 20 μg GST-tagged PBF protein were combined with 10 μl L-α-[^{35}S]methionine-labelled NIS protein and incubated for 1 hour on ice. Following the addition of 400 μl low-salt buffer (50 mM Tris-HCl pH 7.4, 150 mM NaCl, 1% NP-40), 40 μl of packed glutathione agarose beads were added to each reaction, which was subsequently incubated with end-over-end mixing using a rotator for 90 minutes at 4°C. After washing with the low-salt buffer, bound GST-PBF protein was eluted with 40 μl of 25 mM glutathione in 50 mM Tris-HCl, pH 8, on ice for 1 hour. The protein samples were then analysed by SDS-PAGE, using a 12% acrylamide gel, along with 1 μl L-α-[^{35}S]methionine-labelled NIS protein in 20 μl Laemmli sample buffer with 5% (v/v) β-mercaptoethanol, used as a control demonstrating 10% input. Following electrophoresis, the gel was fixed and stained. The gel was then immersed in Amplify Fluorographic Reagent (Amersham Biosciences, Little Chalfont, Buckinghamshire, UK) to increase the sensitivity of signal detection, dried at 65°C for 2 hours and, finally exposed to autoradiographic film at –20°C.

Coimmunoprecipitation assays

COS-7 cells in T25 flasks were transiently transfected with either NIS-MYC and pCI-neo (VO), PBF-HA and pcDNA3.1+ (VO) or NIS-MYC and PBF-HA. Cells were harvested in 500 μl RIPA buffer (50 mM Tris-HCl, pH 7.4, 150 mM NaCl, 1% v/v Igepal CA-630, 6 mM sodium deoxycholate, 1 mM EDTA) containing protease inhibitor cocktail (Sigma, Poole, Dorset, UK). After a brief sonication step, cell lysates were centrifuged at 15,700 ***g*** for 20 minutes and transferred to a clean Eppendorf. Each lysate was incubated with 12.5 μl mouse monoclonal anti-Myc-Tag (9B11) antibody at 4°C overnight with end-over-end rotation. Following the addition of 25 μl packed beads prepared from Protein-G-Sepharose 4 Fast Flow (Amersham), the samples were incubated for a further 2 hours at 4°C with end-over-end rotation. An antibody-only control consisting of 12.5 μl anti-Myc antibody and 25 μl packed beads in 500 μl RIPA buffer was also established. Protein-G-Sepharose beads were centrifuged and, following the removal of any unbound protein, washed four times with 500 μl RIPA buffer. Bound protein was eluted in 50 μl Laemmli Sample Buffer (Bio-Rad Laboratories, Hercules, CA) containing 5% (v/v) β-mercaptoethanol and 1% (w/v) SDS at 37°C for 30 minutes.

Proteins were separated by SDS-PAGE using a 15% acrylamide gel and transferred to polyvinylidene difluoride membrane. The membrane was blocked with 5% milk in TBS containing 0.025% Tween 80 and PBF-HA protein was probed with rabbit polyclonal anti-HA (Y-11) antibody at a concentration of 1:1000 in blocking buffer. Following incubation with Protein-G-HRP (Bio-Rad), the antigen-antibody complexes were detected using the ECL-Plus chemiluminescence detection system (Amersham). Total protein cell lysate (20 μg) taken before the coimmunoprecipitation steps was also separated by SDS-PAGE using 7.5% and 15% acrylamide gels to probe for NIS-MYC and PBF-HA, respectively. PBF-HA was probed in the same way as the coimmunoprecipitation samples and NIS-MYC detected with mouse anti-Myc antibody at a concentration of 1:1000 with 650 ng/ml HRP-conjugated polyclonal rabbit anti-mouse immunoglobulins (Dako) as secondary antibody. β-actin expression was assessed as a loading control for each protein.

The reciprocal experiment was performed in the same way by precipitating PBF-HA with 12.5 μl mouse monoclonal anti-HA.11 antibody (Covance Research Products) and probing for coimmunoprecipitated NIS-MYC with mouse monoclonal anti-Myc-Tag (9B11) antibody.

Cell-surface biotinylation

In each of four T75 flasks, NIS-HA and either pCI-neo (VO) or PBF plasmids were transiently transfected into COS-7 cells. 48 hours after transfection, the Cell Surface Protein Isolation Kit (Pierce, Rockford, IL) was used as recommended to biotinylate and isolate membrane-associated proteins. Briefly, cells were rinsed with PBS and exposed to EZ-Link Sulfo-NHS-SS-Biotin for 30 minutes at 4°C. This biotinylation reagent labels primary amines in extracellular regions of membrane-bound proteins. A quenching solution was added to prevent further biotinylation and the cells from each set of four flasks were scraped into solution and combined. Cells were rinsed with Tris-buffered saline (TBS) and lysed in buffer containing protease inhibitor cocktail (Sigma). Cells were disrupted by intermittent sonication and vortexing during a 30 minute incubation on ice. The lysate was centrifuged and 100 μl of the supernatant was retained as whole cell lysate.

Immobilised Neutravidin gel was applied to a column and washed with wash buffer. The remaining cell lysate was transferred to the column and incubated with end-over-end mixing using a rotator for 1 hour at room temperature to allow the biotinylated proteins within the lysate to bind the avidin-coated beads. Any unbound proteins were removed from the column by centrifugation, and the beads were rinsed thoroughly with wash buffer containing protease inhibitors. SDS-PAGE sample buffer (62.5 mM Tris-HCl, pH 6.8, 1% SDS, 10% glycerol) containing 50 mM DTT was added to the column and incubated for 1 hour at room temperature with end-over-end mixing to release protein bound to the avidin beads. The isolated membrane proteins were then eluted from the column by centrifugation.

The membrane protein fractions were analysed by immunoblotting. Trace amounts of bromophenol blue were added to 40 μl of each fraction which were denatured through incubation at 37°C for 30 minutes. Proteins were separated by SDS-PAGE using a 12% acrylamide gel and NIS protein was probed with mouse monoclonal anti-HA.11 antibody at a concentration of 1:1000, followed by secondary antibody, 650 ng/ml HRP-conjugated polyclonal rabbit anti-mouse immunoglobulins (Dako). Membranes were subsequently re-probed with mouse monoclonal anti-flotillin-1 antibody (BD Biosciences, Franklin Lakes, NJ) at 1:1000 to determine equal protein loading. Experiments were carried out on three separate occasions, and scanning densitometry used to quantify mean changes in expression versus flotillin controls.

Iodide-uptake assays

Iodide-uptake assays were undertaken to assess endogenous NIS function. 24 hours after transfection with either VO, PBF, M1, M2 or M3 plasmids, NaI with a final concentration of 10^{-6} moles/l and 0.05 μCi ^{125}I was added directly to FRTL-5 cell medium in each well. After 1 hour of incubation at 37°C to allow uptake of ^{125}I into the cells, medium was removed and cells were washed rapidly with Hank's balanced salt solution (HBSS) to remove unincorporated iodide. Cells were lysed in 200 μl of 2% SDS and the radioactivity of the lysate was counted for 1 minute in a gamma counter.

Exogenous NIS function in COS-7 cells was also assessed following the transient transfection of NIS-HA cDNA. 48 hours after transfection, cells were incubated with NaI with a final concentration of 10^{-5} moles/l and 0.15 μCi ^{125}I and iodide uptake determined in a similar manner to the FRTL-5 cells.

This work was supported by the Medical Research Council, UHB Charities and the Get-A-Head Charity. We thank John Morris (Mayo Graduate School of Medicine, Rochester, MN), Fedor Berditchevski

(School of Cancer Sciences, University of Birmingham, Birmingham, UK), Melissa Westwood (University of Manchester, UK) and Barbara Reaves (Department of Biology and Biochemistry, University of Bath, UK) for the kind provision of cDNAs, antibodies and expertise. Deposited in PMC for release after 6 months.

References

Ambesi-Impiombato, F. S., Parks, L. A. and Coon, H. G. (1980). Culture of hormone-dependent functional epithelial cells from rat thyroids. *Proc. Natl. Acad. Sci. USA* **77**, 3455-3459.

Arturi, F., Russo, D., Schlumberger, M., du Villard, J. A., Caillou, B., Vigneri, P., Wicker, R., Chiefari, E., Suarez, H. G. and Filetti, S. (1998). Iodide symporter gene expression in human thyroid tumors. *J. Clin. Endocrinol. Metab.* **83**, 2493-2496.

Berditchevski, F. and Odintsova, E. (2007). Tetraspanins as regulators of protein trafficking. *Traffic* **8**, 89-96.

Boelaert, K. and Franklyn, J. A. (2003). Sodium iodide symporter: a novel strategy to target breast, prostate, and other cancers? *Lancet* **361**, 796-797.

Boelaert, K., McCabe, C. J., Tannahill, L. A., Gittoes, N. J., Holder, R. L., Watkinson, J. C., Bradwell, A. R., Sheppard, M. C. and Franklyn, J. A. (2003). Pituitary tumor transforming gene and fibroblast growth factor-2 expression: potential prognostic indicators in differentiated thyroid cancer. *J. Clin. Endocrinol. Metab.* **88**, 2341-2347.

Boelaert, K., Smith, V. E., Stratford, A. L., Kogai, T., Tannahill, L. A., Watkinson, J. C., Eggo, M. C., Franklyn, J. A. and McCabe, C. J. (2007). PTTG and PBF repress the human sodium iodide symporter. *Oncogene* **26**, 4344-4356.

Caillou, B., Troalen, F., Baudin, E., Talbot, M., Filetti, S., Schlumberger, M. and Bidart, J. M. (1998). Na^+/I^- symporter distribution in human thyroid tissues: an immunohistochemical study. *J. Clin. Endocrinol. Metab.* **83**, 4102-4106.

Castro, M. R., Bergert, E. R., Beito, T. G., McIver, B., Goellner, J. R. and Morris, J. C. (1999a). Development of monoclonal antibodies against the human sodium iodide symporter: immunohistochemical characterization of this protein in thyroid cells. *J. Clin. Endocrinol. Metab.* **84**, 2957-2962.

Castro, M. R., Bergert, E. R., Beito, T. G., Roche, P. C., Ziesmer, S. C., Jhiang, S. M., Goellner, J. R. and Morris, J. C. (1999b). Monoclonal antibodies against the human sodium iodide symporter: utility for immunocytochemistry of thyroid cancer. *J. Endocrinol.* **163**, 495-504.

Chien, W. and Pei, L. (2000). A novel binding factor facilitates nuclear translocation and transcriptional activation function of the pituitary tumor-transforming gene product. *J. Biol. Chem.* **275**, 19422-19427.

De la Vieja, A., Ginter, C. S. and Carrasco, N. (2004). The Q267E mutation in the sodium/iodide symporter (NIS) causes congenital iodide transport defect (ITD) by decreasing the NIS turnover number. *J. Cell Sci.* **117**, 677-687.

De la Vieja, A., Ginter, C. S. and Carrasco, N. (2005). Molecular analysis of a congenital iodide transport defect: G543E impairs maturation and trafficking of the Na+/I-symporter. *Mol. Endocrinol.* **19**, 2847-2858.

Dohan, O., Baloch, Z., Banrevi, Z., Livolsi, V. and Carrasco, N. (2001). Rapid communication: predominant intracellular overexpression of the Na(+)/I(-) symporter (NIS) in a large sampling of thyroid cancer cases. *J. Clin. Endocrinol. Metab.* **86**, 2697-2700.

Dohan, O., De la Vieja, A., Paroder, V., Riedel, C., Artani, M., Reed, M., Ginter, C. S. and Carrasco, N. (2003). The sodium/iodide Symporter (NIS): characterization, regulation, and medical significance. *Endocr. Rev.* **24**, 48-77.

Dohan, O., Ginter, C. S. and Carrasco, N. (2005). Role of the NIS (Na+/I- symporter) carboxy terminus in iodide transport. *Thyroid* **15**, S48.

Faggiano, A., Caillou, B., Lacroix, L., Talbot, M., Filetti, S., Bidart, J. M. and Schlumberger, M. (2007). Functional characterization of human thyroid tissue with immunohistochemistry. *Thyroid* **17**, 203-211.

Gerard, A. C., Daumerie, C., Mestdagh, C., Gohy, S., De Burbure, C., Costagliola, S., Miot, F., Nollevaux, M. C., Denef, J. F., Rahier, J. et al. (2003). Correlation between the loss of thyroglobulin iodination and the expression of thyroid-specific proteins involved in iodine metabolism in thyroid carcinomas. *J. Clin. Endocrinol. Metab.* **88**, 4977-4983.

Heaney, A. P., Nelson, V., Fernando, M. and Horwitz, G. (2001). Transforming events in thyroid tumorigenesis and their association with follicular lesions. *J. Clin. Endocrinol. Metab.* **86**, 5025-5032.

James, S. R., Franklyn, J. A., Reaves, B. J., Smith, V. E., Chan, S. Y., Barrett, T. G., Kilby, M. D. and McCabe, C. J. (2008). Monocarboxylate transporter 8 (MCT8) in neuronal cell growth. *Endocrinology* **150**, 1961-1969.

Jhiang, S. M., Cho, J. Y., Ryu, K. Y., DeYoung, B. R., Smanik, P. A., McGaughy, V. R., Fischer, A. H. and Mazzaferri, E. L. (1998). An immunohistochemical study of Na^+/I^- symporter in human thyroid tissues and salivary gland tissues. *Endocrinology* **139**, 4416-4419.

Kaminsky, S. M., Levy, O., Salvador, C., Dai, G. and Carrasco, N. (1994). Na(+)-I-symport activity is present in membrane vesicles from thyrotropin-deprived non-I(-)-transporting cultured thyroid cells. *Proc. Natl. Acad. Sci. USA* **91**, 3789-3793.

Knostman, K. A., McCubrey, J. A., Morrison, C. D., Zhang, Z., Capen, C. C. and Jhiang, S. M. (2007). PI3K activation is associated with intracellular sodium/iodide symporter protein expression in breast cancer. *BMC Cancer* **7**, 137.

Kogai, T., Endo, T., Saito, T., Miyazaki, A., Kawaguchi, A. and Onaya, T. (1997). Regulation by thyroid-stimulating hormone of sodium/iodide symporter gene expression and protein levels in FRTL-5 cells. *Endocrinology* **138**, 2227-2232.

Kogai, T., Taki, K. and Brent, G. A. (2006). Enhancement of sodium/iodide symporter expression in thyroid and breast cancer. *Endocr. Relat. Cancer* **13**, 797-826.

Lazar, V., Bidart, J. M., Caillou, B., Mahe, C., Lacroix, L., Filetti, S. and Schlumberger, M. (1999). Expression of the Na^+/I^- symporter gene in human thyroid tumors: a comparison study with other thyroid-specific genes. *J. Clin. Endocrinol. Metab.* **84**, 3228-3234.

Luciani, P., Buci, L., Conforti, B., Tonacchera, M., Agretti, P., Elisei, R., Vivaldi, A., Cioppi, F., Biliotti, G., Manca, G. et al. (2003). Expression of cAMP response element-binding protein and sodium iodide symporter in benign non-functioning and malignant thyroid tumours. *Eur. J. Endocrinol.* **148**, 579-586.

Mazzaferri, E. L. and Kloos, R. T. (2001). Clinical review 128: Current approaches to primary therapy for papillary and follicular thyroid cancer. *J. Clin. Endocrinol. Metab.* **86**, 1447-1463.

Park, H. J., Kim, J. Y., Park, K. Y., Gong, G., Hong, S. J. and Ahn, I. M. (2000). Expressions of human sodium iodide symporter mRNA in primary and metastatic papillary thyroid carcinomas. *Thyroid* **10**, 211-217.

Riedel, C., Levy, O. and Carrasco, N. (2001). Post-transcriptional regulation of the sodium/iodide symporter by thyrotropin. *J. Biol. Chem.* **276**, 21458-21463.

Ries, L. A. G., Melbert, D., Krapcho, M., Stinchcomb, D. G., Howlander, N., Horner, M. J., Mariotto, A., Miller, B. A., Feuer, E. J., Altekruse, S. F. et al. (2008). *SEER Cancer Stat. Rev. 1975-2005*.

Ringel, M. D., Anderson, J., Souza, S. L., Burch, H. B., Tambascia, M., Shriver, C. D. and Tuttle, R. M. (2001). Expression of the sodium iodide symporter and thyroglobulin genes are reduced in papillary thyroid cancer. *Mod. Pathol.* **14**, 289-296.

Ryu, K. Y., Senokozlieff, M. E., Smanik, P. A., Wong, M. G., Siperstein, A. E., Duh, Q. Y., Clark, O. H., Mazzaferri, E. L. and Jhiang, S. M. (1999). Development of reverse transcription-competitive polymerase chain reaction method to quantitate the expression levels of human sodium iodide symporter. *Thyroid* **9**, 405-409.

Saez, C., Martinez-Brocca, M. A., Castilla, C., Soto, A., Navarro, E., Tortolero, M., Pintor-Toro, J. A. and Japon, M. A. (2006). Prognostic significance of human pituitary tumor-transforming gene immunohistochemical expression in differentiated thyroid cancer. *J. Clin. Endocrinol. Metab.* **91**, 1404-1409.

Saito, T., Endo, T., Kawaguchi, A., Ikeda, M., Katoh, R., Kawaoi, A., Muramatsu, A. and Onaya, T. (1998). Increased expression of the sodium/iodide symporter in papillary thyroid carcinomas. *J. Clin. Invest.* **101**, 1296-1300.

Schmutzler, C., Winzer, R., Meissner-Weigl, J. and Kohrle, J. (1997). Retinoic acid increases sodium/iodide symporter mRNA levels in human thyroid cancer cell lines and suppresses expression of functional symporter in nontransformed FRTL-5 rat thyroid cells. *Biochem. Biophys. Res. Commun.* **240**, 832-838.

Smanik, P. A., Liu, Q., Furminger, T. L., Ryu, K., Xing, S., Mazzaferri, E. L. and Jhiang, S. M. (1996). Cloning of the human sodium lodide symporter. *Biochem. Biophys. Res. Commun.* **226**, 339-345.

Smanik, P. A., Ryu, K. Y., Theil, K. S., Mazzaferri, E. L. and Jhiang, S. M. (1997). Expression, exon-intron organization, and chromosome mapping of the human sodium iodide symporter. *Endocrinology* **138**, 3555-3558.

Spitzweg, C., Joba, W., Morris, J. C. and Heufelder, A. E. (1999). Regulation of sodium iodide symporter gene expression in FRTL-5 rat thyroid cells. *Thyroid* **9**, 821-830.

Stratford, A. L., Boelaert, K., Tannahill, L. A., Kim, D. S., Warfield, A., Eggo, M. C., Gittoes, N. J., Young, L. S., Franklyn, J. A. and McCabe, C. J. (2005). Pituitary tumor transforming gene binding factor: a novel transforming gene in thyroid tumorigenesis. *J. Clin. Endocrinol. Metab.* **90**, 4341-4349.

Tanaka, K., Otsuki, T., Sonoo, H., Yamamoto, Y., Udagawa, K., Kunisue, H., Arime, I., Yamamoto, S., Kurebayashi, J. and Shimozuma, K. (2000). Semi-quantitative comparison of the differentiation markers and sodium iodide symporter messenger ribonucleic acids in papillary thyroid carcinomas using RT-PCR. *Eur. J. Endocrinol.* **142**, 340-346.

Trouttet-Masson, S., Selmi-Ruby, S., Bernier-Valentin, F., Porra, V., Berger-Dutrieux, N., Decaussin, M., Peix, J. L., Perrin, A., Bournaud, C., Orgiazzi, J. et al. (2004). Evidence for transcriptional and posttranscriptional alterations of the sodium/iodide symporter expression in hypofunctioning benign and malignant thyroid tumors. *Am. J. Pathol.* **165**, 25-34.

Turnell, A. S., Grand, R. J., Gorbea, C., Zhang, X., Wang, W., Mymryk, J. S. and Gallimore, P. H. (2000). Regulation of the 26S proteasome by adenovirus E1A. *EMBO J.* **19**, 4759-4773.

Vadysirisack, D. D., Chen, E. S., Zhang, Z., Tsai, M. D., Chang, G. D. and Jhiang, S. M. (2007). Identification of in vivo phosphorylation sites and their functional significance in the sodium iodide symporter. *J. Biol. Chem.* **282**, 36820-36828.

Van Sande, J., Massart, C., Beauwens, R., Schoutens, A., Costagliola, S., Dumont, J. E. and Wolff, J. (2003). Anion selectivity by the sodium iodide symporter. *Endocrinology* **144**, 247-252.

Wapnir, I. L., van de Rijn, M., Nowels, K., Amenta, P. S., Walton, K., Montgomery, K., Greco, R. S., Dohan, O. and Carrasco, N. (2003). Immunohistochemical profile of the sodium/iodide symporter in thyroid, breast, and other carcinomas using high density tissue microarrays and conventional sections. *J. Clin. Endocrinol. Metab.* **88**, 1880-1888.

Ward, L. S., Santarosa, P. L., Granja, F., da Assumpcao, L. V., Savoldi, M. and Goldman, G. H. (2003). Low expression of sodium iodide symporter identifies aggressive thyroid tumors. *Cancer Lett.* **200**, 85-91.

Yaspo, M. L., Aaltonen, J., Horelli-Kuitunen, N., Peltonen, L. and Lehrach, H. (1998). Cloning of a novel human putative type Ia integral membrane protein mapping to 21q22.3. *Genomics* **49**, 133-136.

Zhang, Z., Liu, Y. Y. and Jhiang, S. M. (2005). Cell surface targeting accounts for the difference in iodide uptake activity between human Na^+/I^- symporter and rat Na+/I-symporter. *J. Clin. Endocrinol. Metab.* **90**, 6131-6140.